Understanding the Reactivity of Ruthenium(II) Complexes: Kinetics and Mechanistic Studies

By

Gershom K. Mutua

Submitted in partial fulfilment of the academic requirements of Doctor of Philosophy

in Chemistry

School of Chemistry and Physics

College of Agriculture, Engineering and Science

Pietermaritzburg

South Africa

March 2019

Preface

The research work contained in this thesis was undertaken and completed by the candidate while based in the Discipline of Chemistry, School of Chemistry and Physics of the College of Agriculture, Engineering and Science, University of KwaZulu-Natal, Pietermaritzburg Campus, South Africa. The research work was financially supported by the University of KwaZulu-Natal.

This work has not been submitted in any form to another university and, except where the work of others is acknowledged in the text, the results reported are due to investigations by the candidate.

Supervisor: Dr. Allen Mambanda

Signed: _____ Date: _____

Co-Supervisor: Prof. Deogratius Jaganyi

Signed: _____ Date: _____

Declaration 1: Plagiarism

I, **Gershom Kyalo Mutua**, declare that:

(i) the research work reported in this thesis, except where otherwise indicated or acknowledged, is my original work;

(ii) this thesis has not been submitted in full or in part for any degree or examination to any other university;

(iii) this thesis does not contain other persons' data, pictures, graphs or other information, unless specifically acknowledged as being sourced from other persons;

(iv) this thesis does not contain other persons' writing, unless specifically acknowledged as being sourced from other researchers. Where other written sources have been quoted, then:

a) their words have been re-written but the general information attributed to them has been referenced;

b) where their exact words have been used, their writing has been placed inside quotation marks, and referenced;

(v) this thesis is primarily a collection of material, prepared by myself, prepared in form of manuscripts for publication or communicated as posters and/ oral presentations at conference meetings. Additional supporting material has been included as appendices to this thesis;

(vi) this thesis does not contain text, graphics or tables copied and pasted from the Internet, unless specifically acknowledged, and the source being detailed in the thesis and in the references sections.

Name: Gershom Kyalo Mutua

Signed: 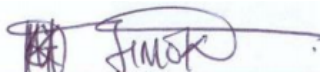 Date: March 26th 2019

Declaration 2: Publications

Gershom Kyalo Mutua, Allen Mambanda and Deogratius Jaganyi* (2018), *The role of bridging ligand on the reactivity of η^6-arene ruthenium(II) complexes: Kinetics and Mechanistic studies*. Submitted to New Chemistry Journal. ID NJ-ART-07-2018-003765

Gershom Kyalo Mutua, Allen Mambanda and Deogratius Jaganyi, *The role of bridging ligand on substitution of η^6-arene ruthenium(II) complexes*, Paper presented at the 9th International Conference of Kenya Chemical Society from 9th to 12th May 2017 at the United states International University, Nairobi, Kenya .

The following manuscripts are ready for submission;

a. **Gershom Kyalo Mutua**, Allen Mambanda and Deogratius Jaganyi, *The role of π-extension of the auxiliary ligand on the reactivity of ruthenium(II) terpyridyl complexes: Kinetic and Mechanistic studies.*

b. **Gershom Kyalo Mutua,** Allen Mambanda and Deogratius Jaganyi, *The influence of π-back-bonding and trans-effect on the reactivity of ruthenium(II) complexes: Kinetic and Mechanistic studies.*

c. **Gershom Kyalo Mutua,** Allen Mambanda and Deogratius Jaganyi, *Kinetic and Mechanistic Studies of η^6-p-Cymene ruthenium(II) complexes with α,α'-diimine bridging ligands.*

Name: Gershom Kyalo Mutua

Signed: _____ Date: _____

Dedication

This thesis is dedicated to my wife Beatrice Chepng'eno and our son Lloyd Musau for their endless love, encouragement and unconditional support.

Abstract

Kinetic and mechanistic studies of four sets of octahedral ruthenium(II) complexes were performed to establish the influence of the coordinated ligand systems on the reactivity of the complexes. The rate of substitution of the aqua or chloro ligands by biorelevant nucleophiles of different steric demands (thiourea, *N,N*-dimethylthiourea and *N,N,N',N'*-tetramethylthiourea) was investigated under *pseudo*-first order conditions as a function of nucleophile concentration and temperature using stopped flow or ultraviolet-visible spectrophotometry. Computational studies using density functional theory were carried out to gain insight into the structural and electronic properties of the complexes.

In the work reported in Chapter Three, the effect of π-conjugation of the auxiliary ligand on the substitution reactivity of mono aqua terpyridine-based ruthenium(II) complexes was investigated. The results obtained show that there is a positive correlation between the π-surface area of the bidentate (N^N) auxiliary ligands and reactivity of the complexes. This is attributable to an upsurge in π-acceptor ability of auxiliary ligand as its π-conjugation increases which facilitates effective π-back-donation of electron density from the metal centre to the ligands. Consequently, the complexes become more electrophilic thereby promoting faster nucleophilic attack on the metal centre. This is supported by computational results and measured p*K*a values. It was established that when the denticity of the auxiliary ligand is changed from one to two, the reactivity reduces due to an increase in steric hindrance around the metal centre.

In Chapter Four, the influence of π-back-bonding and *trans*-effect on the reactivity of mononuclear ruthenium(II) complexes with two chloro leaving groups is reported. It was established that increase in aromatic area of the ligands enhance the simultaneous substitution of the chloro ligands. This is due to increase in π-back-donation of electron density from the

metal centre as the π-surface increase. Accordingly, the global electrophilicity of the complexes as well as the positive charge at the central metal are increased leading to enhanced reactivity as supported by the DFT-results. However, increased steric hindrance due to the two biquinoline ligands (complex **Ru-4**) retarded its reactivity. Complexes with methyl substituents were more reactive compared to those without. This enhancement in reactivity is attributed to positive σ-*trans*-effect of the ortho-positioned methyl groups. Furthermore, it was established that an increase in π-acceptor properties of the influencing ligand reduces the σ-*trans*-effect of the groups due to π-back-donation thereby reducing the reactivity.

In Chapter Five, six complexes (two mononuclear and four dinuclear) were investigated to establish the role of a rigid bridging ligand on the reactivity of *p*-cymene complexes towards ligand substitution. The results showed that the rate of the simultaneous substitution of the aqua ligands in the binuclear complexes decreased with increase in steric hindrance around the metal centres as well as decrease in electrophilicity of the complexes. The dinuclear complex (**Ru-3**) was more reactive than its related mononuclear complex (**Ru-2**) due to synergistic effects of the two metal centres which make the complex more electrophilic. The introduction of bipyridyl chelating ligand to *p*-cymene complex drastically reduces the reactivity due to increased steric hindrance around the metal centre as well as reduced electrophilicity.

In Chapter Six, the effect of the nature and length of a α,α'-diimine bridging ligand on the reactivity of ruthenium(II) *p*-cymene complexes was investigated. It was noted that the complex with no spacer between the α,α'-diimine moieties was the most reactive due to effective π-back-bonding of electrons from the metal centre to the α,α'-diimine moieties. As the flexibility of bridging ligand increases, the steric hindrance in the vicinity of the metal centre decreases increasing the reactivity of the complexes in the same order. In addition, the xylyl spacer (**Ru-4**) forms two V-shaped curvatures that promote the reactivity through the cage effect.

In all the reactions, the activation parameters ($\Delta H^{\neq} > 0$, $\Delta S^{\neq} < 0$) support an associative mechanism. The crystal structures of $[Ru(terpy)(bipy)Tu](ClO_4)_2$ and *trans*-$[Ru(bipy)_2Tmtu)_2](ClO_4)_2$ reveal that the substitution products are stable and the oxidation state of the metal centre (+2) is maintained after reaction.

This study concludes that, the stereo-electronic properties of the ligand system around the metal centre play a key role in influencing the reactivity of ruthenium(II) complexes.

Acknowledgements

I express my sincere gratitude to my supervisors Dr. Allen Mambanda and Professor Deogratius Jaganyi for their guidance, encouragement and tremendous support throughout my study at the University of Kwazulu-Natal, South Africa.

Special gratitude to Professor William Shivoga and Dr. Francis Omoto of Masinde Muliro University of Science and Technology, Kenya for their role in fruition of the scholarship award to study at University of Kwazulu-Natal.

Special acknowledgements go to Mr. Craig Grimmer, Ms. Caryl Janse van Rensburg and Ms. Zimbini Ngcingina for their assistance in characterization of the ligands and complexes. I recognize Mr. Leigh Hunter and Mr. Sizwe Zamisa for their assistance in crystallographic analysis. I do sincerely thank Ms. Prudence Lubanyana, the technician in charge of Physical Chemistry and Mrs. Irene Ngubane for their assistance in time of need, mostly on short notice.

I am grateful for the support from the members of the Kinetic Group namely; Dr. Rajesh Bellam, Meshack Sitati, Rose Papo, Daniel Onunga, Moses Olusegun, Philisiwe Kunene and Lebogang Mphalele. My colleagues; Odwa Gonyela, Nassir Tajudeen, Grace Obi, Thandeka Tshabalala, Nontembeko Dube and Nadipha Botha.

My sincere and special gratitude goes to my wife Beatrice and our son Lloyd Musau for their enduring love and motivation. Be blessed abundantly. My parents, Timothy and Christine, my sibling Ordiliah, Reuben and Trace, thank you so much for your love and support in one way or another.

Lastly and most importantly I thank God for bestowing an enduring spirit throughout the study period.

Table of Contents

List of Tables

Chapter Two

Chapter Three

Chapter Four

Chapter Five

Chapter Six

List of Figures

Chapter One

Chapter Two

Chapter Three

Chapter Four

Chapter Five

Chapter Six

Chapter Seven

List of Schemes

Abbreviations

$\Delta H^{\neq}$	Activation enthalpy
$\Delta S^{\neq}$	Activation entropy
A	absorbance
Å	Angstrom
B3LYP	Hybrid Becke, 3-parameter, Lee-yang-Parr
CPCM	conductor-like polarizable continuum
DFT	density functional theory
DMSO	dimethyl sulfoxide
Dmtu	*N*,*N*-dimethylthiourea
DNA	deoxyribonucleic acid
ESI^+	electron spray ionization in positive mode
h	hour
HOMO	highest occupied molecular orbital
I	Ionic strength
K	kelvin
k_2	second order rate constant
k_{obs}	observed rate constant
LANL2DZ	Los Alamos National Laboratory 2 double ζ
LUMO	Lowest unoccupied molecular orbital
min	Minute(s)
NBO	Natural bond orbital
NMR	Nuclear Magnetic Resonance
Nu	Nucleophile
p*K*a	Acid dissociation constant

T	temperature
Tmtu	*N,N,N',N'*-tetramethylthiourea
TOF	Time of flight
Tu	thiourea

CHAPTER ONE

Introduction

1.1 Cancer

Cancer is a general term used to describe a group of related diseases that are characterized by abnormal multiplication of cells beyond their boundaries. The proliferation of the cells bear no relation to the physiological needs of the organ(s) affected.[1] It is caused by pathological failure in processes that control cell multiplication, differentiation and death.[2]

According to global statistics, in the year 2015 cancer was responsible for about 9 million deaths world-wide. A close scrutiny of this data showed that the most common types of cancer are; lung cancer (1.69 million deaths), liver cancer (788,000 deaths), colorectal cancer (774,000 deaths), stomach cancer (754,000 deaths) and breast cancer (571,000 deaths).[3] Of all the reported cancer cases, about 5-10% are attributed to genetic imperfections while the rest (90-95%) are caused by environmental and lifestyle factors.[4] Key human carcinogens are tobacco, asbestos, aflatoxin and ultraviolet light.[5]

Cancer is treated through surgery, radiotherapy and chemotherapy[6] with the choice of treatment depended on the location and grade of the tumour, stage of the disease and performance status of the patient.[7] Surgery is the most efficient treatment for localized tumours because it involves the total removal of the cancer cells from the patient. Radiotherapy and chemotherapy are complementary techniques because in each treatment regimen, not all the cancer cells are destroyed. For the treatment of metastatic cancer and tumours, a combination therapy is required.[8]

In chemotherapy, antineoplastic drugs are used for the destruction of cancerous cells and shrinkage of tumours. These drugs are classified according to their mechanism of action. The important classes are; antimetabolites, plant alkaloids, alkylating agents, antitumour

antibiotics, hormonal agents and topoisomerase inhibitors.[9] The most widely used metallodrugs are platinum-based complexes.

1.2 Platinum-Based Anticancer Agents

Platinum-based complexes have been used for several decades in cancer therapy with *cisplatin* (*cis*-diamminedichloroplatinum(II)) (Figure 1.1) being the most potent and widely used metallotherapeutic drug.[10]

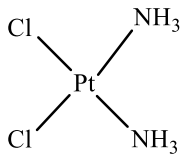

Figure 1.1: Molecular structure of *cisplatin*

In combination with other antineoplastics, *cisplatin* is used in the treatment of 50-70% of all lung, ovarian, bladder, testicular and lymphoma cancer cases.[11] Despite its extensive use in oncology, *cisplatin* is faced by serious drawbacks. Its use is restricted by dose limiting side-effects such as nephrotoxicity, neurotoxicity, ototoxicity and myelosuppression.[10] Besides, it is inactive against many cancer cell lines and metastases. Cancerous cells may also develop resistance to *cisplatin* therapy as a result of decreased drug uptake/increased drug elimination, degradation and or deactivation by thiol-based biomolecules as well as improved repair tolerance of the DNA-*cisplatin* adducts.[12]

Due to the aforementioned limitations, researchers are keen on delivering more effective and less toxic anticancer agents with reduced cross-resistance compared to the parent compounds.[13] After intensive research work involving synthesis of thousands of complexes, only two additional platinum(II) based complexes have entered global utilization as anticancer agents *viz*; carboplatin and oxaliplatin.[10-11]

Other complexes such as nedaplatin, lobaplatin and heptaplatin have been approved in Japan, China and North Korea, respectively.[10, 14] Structures of these complexes are shown in Figure 1.2.

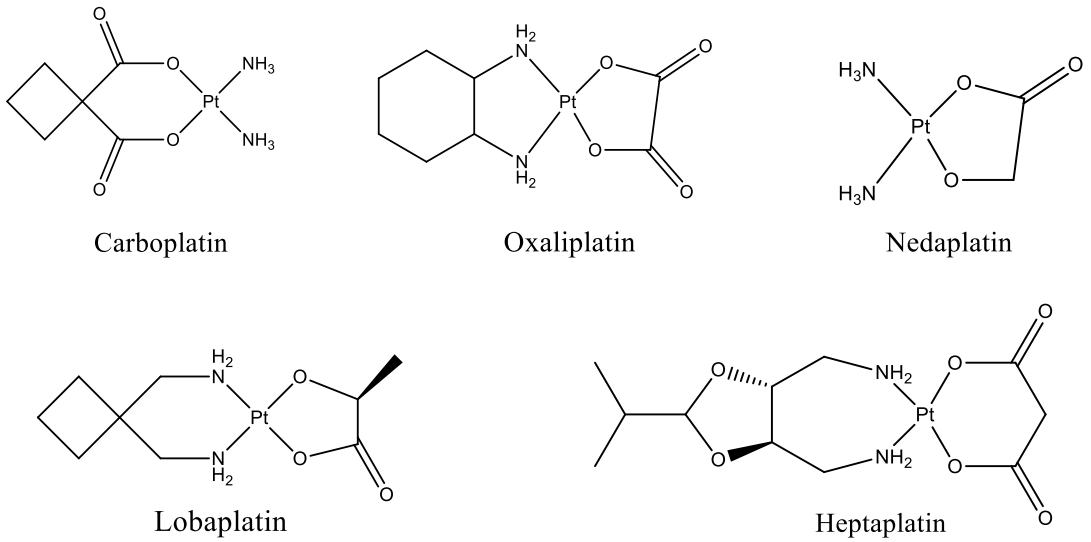

Figure 1.2: Structures of platinum(II) based metallotherapeutics used in cancer treatment

Notwithstanding their successful application in cancer treatment, these drugs are associated with side effects and other deficiencies just like *cisplatin*. For instance; thrombocytopenia is the dose-limiting toxicity for carboplatin, nedaplatin and lobaplatin[15] while oxaliplatin is restricted by its unpredictable sensory neuropathy.[16] The intrinsic and acquired resistance of tumoural cells to carboplatin and oxaliplatin reduces their efficacy occasionally causing treatment failure.[17] Moreover, most of the available platinum-based chemotherapeutics have limited spectrum of activity especially against metastatic tumours.[12, 18]

Due to the foregoing reasons, different strategies were considered in order to design and develop more efficient chemotherapeutic agents. These strategies involved ligand modification, development of multinuclear systems, variation of the coordination geometry and the use of non-platinum metal centres.[19]

Several non-platinum metal complexes such as gold, ruthenium, osmium, palladium, titanium and vanadium have been investigated for their anticancer properties.[20] Among them, ruthenium based complexes have emerged as the most attractive alternative to platinum based metallodrugs due to their unique and versatile biochemical properties.[18, 21]

1.3 Chemistry of Ruthenium

Ruthenium (Ru) is a transition metal belonging to the platinum group of elements with an atomic number of 44 and a relative atomic weight of 101.07 g/mol. It has melting and boiling points of 2310 and 3900 ℃, respectively. Ruthenium has a density of 12.45 g/cm^3 and exists in seven naturally occurring stable isotopes; ^{98}Ru (1.87%), ^{99}Ru (12.76%), ^{100}Ru (12.60%), ^{101}Ru (17.06%), ^{102}Ru (31.55%) and ^{104}Ru (18.62%). Its oxidation state ranges from -2 to +8 with +2, +3 and +4 being the most common.[22] Clinically, ruthenium complexes have shown impressive anticancer, immunosuppressing, antimicrobial, antibiotic and nitric oxide scavenging properties.[18]

1.4 Ruthenium Complexes as Potential Anticancer Agents

Ruthenium based complexes especially ruthenium(II) and (III) are well suited for medical application as anticancer metallotherapeutic agents due to their desirable properties.[23] As a result of their strong ligand field stabilization, these complexes adopt octahedral geometry[24] giving them a larger structural diversity relative to square planar platinum(II) complexes.[19, 24] In addition, the two additional coordination sites permit new modes of binding to intracellular targets compared to platinum(II) complexes.[25]

Another important attribute of ruthenium complexes is that they have various accessible oxidation states (II, III and IV) with low interconversion energy barrier at physiological conditions. Their ability to mimic iron in binding to biomolecules such as serum and transferrin make them less toxic to normal cells compared to the globally approved platinum-based

antineoplastic agents.[18, 26] These complexes have better selectivity for cancer cells further reducing their toxicity to the normal cells.[21] Furthermore, the cellular uptake of ruthenium complexes is enhanced due to their transferrin-binding abilities that lead to over-expression of protein receptors on the surfaces of cancerous cells.[26] Ruthenium complexes have similar ligand exchange rates as platinum complexes and have also shown excellent activity against some *cisplatin* resistance cancer cells.[21]

1.4.1 Development of Ruthenium Anticancer Complexes

Interests in anticancer properties of ruthenium complexes commenced when it was discovered that radio-ruthenium labelled compounds could be localized in tumour cells.[27] Among the first ruthenium complexes to be investigated was *fac*-[$RuCl_3(NH_3)_3$] (Figure 1.3) which was found to be active against *Escherichia coli* and sarcoma cell lines.[28] However, further clinical investigations on the complex was hampered by its poor aqueous solubility.[29]

Subsequent investigations focused on anionic complexes with better solubility and multiple chloro ligands.[30] Keppler and Rupp 1986, discovered that, ICR, KP 418 [(imidazolium)-*trans*-(bisimidazole)-tetrachlororuthenate(III)] (Figure 1.3) was highly active against murine leukemia and melanoma cancer cells. The tumour inhibiting ability of this complex was either better or comparable to those exhibited by *cisplatin*, cyclophosphamide and 5-fluorouracil.[23a] Moreover, it was active against acetoxymethyl-methylnitrosamine-induced colorectal cancer in rats,[31] a model with close semblance to colorectal cancer in human beings.[30] Further investigations on KP418 analogues led to the discovery that KP1019 (indazolium *trans*-[tetrachlorobis(indazole)ruthenate(III)]) (Figure 1.3), had exceptional activity against rat colon cancer recording up to 95% tumour reduction without any significant weight loss and mortality.[23b] To the dismay of the researchers, its low solubility hampered clinical trials.[30, 32] Instead, its sodium analogue, NKP-1339 (sodium *trans*-[tetrachlorobis(indazole)ruthenate(III)]) (Figure 1.3) has

been pursued for clinical trials due to its excellent solubility.[32] The high solubility also facilitated the application of large doses of the complex to patients.[30]

At the same time research interests in utilizing dimethyl sulfoxide (DMSO) as a ligand in ruthenium complexes grew because of its ability to bind to a metal centre through either S or O atoms depending on the stereo-electronic factors around the metal centre.[33] Coordinated DMSO combines the properties of being a fairly good π-acceptor and a good leaving group. It is therefore able to stabilize the metal centre as well as generate the active aqua species quite easily. Moreover, it imparts a good aqua solubility to complexes, making them diffuse easily though the cell membrane.[34]

A major break-through on DMSO-based ruthenium(II) complexes occurred when NAMI-A (imidazolium [*trans*-DMSO-imidazole-tetrachlororuthenate]) (Figure 1.3) was found to be efficacious against pulmonary metastases in several *in vivo* tumours models.[23c, 23d] The anti-metastatic activity of NAMI-A is grounded on cell adhesion and inhibition of cancer cell motility and invasiveness.[35] On the contrary, it was observed that NAMI-A has negligible activity towards primary tumour and had limited *in vitro* cytotoxicity.[23c, 23d] During clinical trials NAMI-A showed partial response in phase II causing failure of the trials.[36]

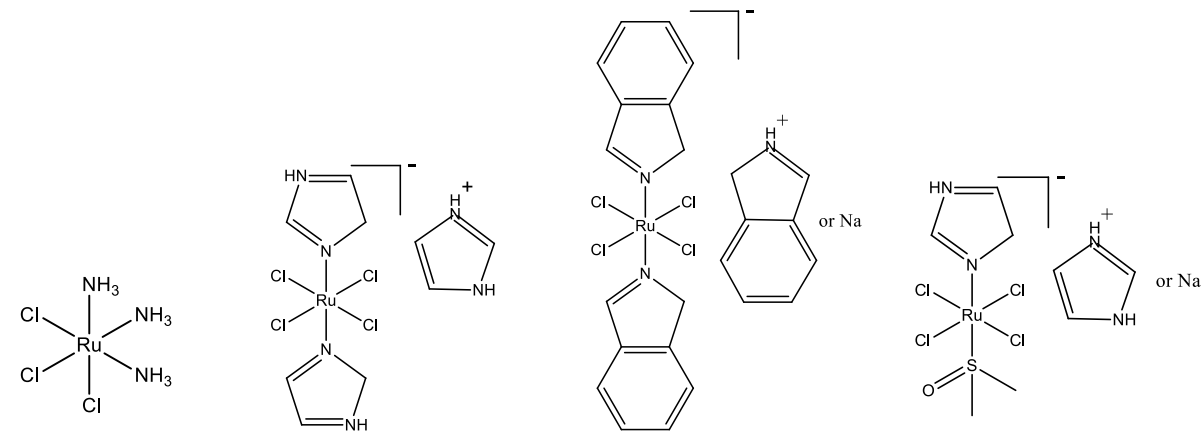

fac-[$RuCl_3(NH_3)_3$] ICR, KP418 KP1019/NKP-1339 NAMI/NAMI-A

Figure 1.3: Structures of tumour-inhibiting ruthenium(III) complexes

The ruthenium(III) anticancer complexes undergo *in vivo* reduction to the more reactive and cytotoxic ruthenium(II) and this has propelled research interest in the complexes of the latter oxidation state.[20a, 37]

1.4.2 Ruthenium(II) Complexes

The initial biological tests on ruthenium(II) complex, $RuCl_2(DMSO)_4$ showed a good activity against *Escherichia coli*.[38] Later both *trans* and *cis*-$RuCl_2(DMSO)_4$ (Figure 1.4) were found to have a good activity against primary tumour and metastases. Due to their stability to oxidation, these complexes were used as models to investigate interactions between ruthenium(II) complexes and DNA as well as oligonucleotides.[39]

Significant activity of ruthenium(II) complexes against numerous cancer cells was achieved with $[RuCl_2(azpy)_2]$ where azpy is 2-phenylazopyridine[23e] (Figure 1.4). It was found that the N-aromatic ligands present were able to stabilize the metal centre as well as increase the hydrophobic/intercalative interactions between the complex and DNA through non-covalent binding. In addition, the geometric effects of the aromatic ligands enhance protein binding.[24]

Other studies utilized η^6-arene moiety to stabilize the ruthenium metal centre at oxidation state of +2. Arene based complexes form the latest generation of ruthenium-based anticancer agents (*vide infra*).[40]

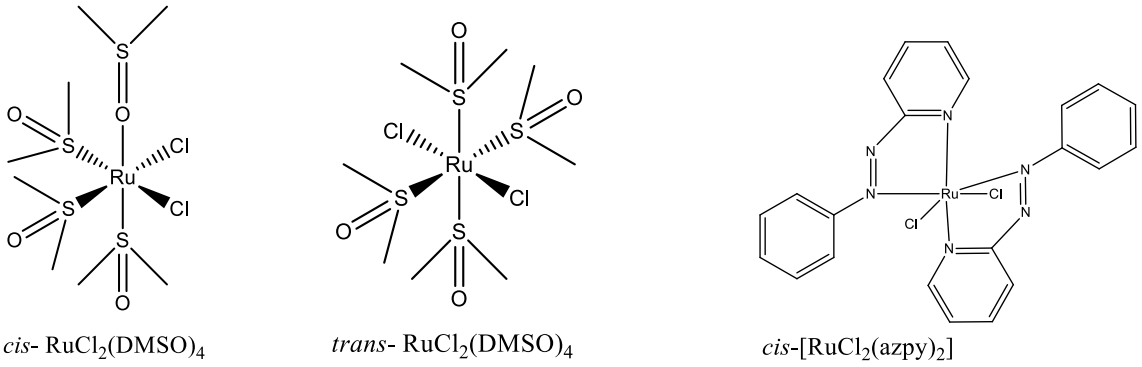

cis- $RuCl_2(DMSO)_4$ *trans*- $RuCl_2(DMSO)_4$ *cis*-$[RuCl_2(azpy)_2]$

Figure 1.4: Some ruthenium(II) complexes initially investigated

The major classes of ruthenium(II) anticancer agents are polypridyl and arene complexes.[41]

1.4.3 Ruthenium(II) Polypridyl Complexes

The diversity in size and flexibility of polypyridyl ligands confer different shapes and chirality to octahedral ruthenium complexes that can be utilized to achieve favorable DNA-binding properties.[41-42] Typical polypyridyl ligands include 2,2'-bipyridine, 1,10-phenanthroline, 2,2':6',2''-terpyridine and their substituted analogues; they readily form stable complexes with ruthenium metal ions.[20a]

Many ruthenium(II) complexes with nitrogen-based polypyridyl ligands have exhibited good activity in screening studies and are preferentially localized in tumour cells.[25] These complexes are considered as classical anticancer agents[41, 43] whose cytoxicity is positively correlated to the aromatic π-conjugated surface area of the coordinated ligands.[44] Likewise, a direct relationship between cytotoxicity and DNA binding has also been reported on these complexes.[25]

Ruthenium(II) polypyridyl complexes with one or multiple leaving group(s) are potent intercalators in addition to covalent coordination to DNA in two-step process. The first step is the replacement of the chloro ligand with an aqua ligand while the second step is binding to the DNA nucleobases through substitution of the labile aqua ligands.[25, 45]

Large number of monochloro terpyridine-based ruthenium(II) complexes; $Ru(terpy)(N\text{^}N)Cl]^+$ (where N^N is a bidentate ligand and terpy is unsubstituted/substituted 2,2':6',2'-terpyridine) have been studied.[46] For instance; complexes of the type [Ru(Cl-Ph-terpy)[1](L)Cl]Cl where L is phenanthroline or o-benzoquinonediimine have shown higher activity and selectivity compared to *cisplatin* against numerous cancer cell lines.[25, 47] Terpyridyl-based ruthenium(II)

[1] 4′-(4-chlorophenyl)-2,2′:6′,2″-terpyridine

complexes interact with DNA covalently through the guanine residues forming monofunctional adducts. Most of these complexes induce apoptosis of the cancer cells by activating mitochondrial apoptotic pathway while the others halt DNA replication.[25, 47]

Similarly, ruthenium(II) polypyridyl complexes with two chloro ligands have been evaluated for their oncological properties. For example; the chiral complex α-[Ru(azpy)$_2$Cl$_2$] showed excellent *in vitro* cytotoxicity against several cancer cells. It is more potent than *cisplatin* against breast and melanoma cancer cell lines.[23e] A series of dipyrido[3,2-a:2',3'-c]quinoxaline[2,3-b]quinoxaline based complexes with two labile chloro ligands have also shown good cytotoxicity against invasive and non-invasive human breast tumour cell lines.[48]

Other studies have also revealed that ruthenium(II) complexes with strain-inducing alkyl substituents are more cytotoxic compared to those with unsubstituted ligands.[49] Therefore, the electronic and steric properties of the ligand systems around the metal centre has a profound influence on the cytotoxicity of a complex.[25, 46-47]

1.4.4 Ruthenium(II) Arene Complexes

Interest in the utilization of *pseudo*-octahedral half-sandwich ruthenium(II) complexes as anticancer agents has vastly grown over the last two decades.[50] These complexes with a general formula [(η^6-arene)Ru(X)(Y)(Z) display a *pseudo*-octahedral geometry in which the π-bonded arene ligand occupy three coordination sites. The commonly used arene ligands are benzene, biphenyl, *para*-cymene and dihydroanthracene. The other three remaining coordination sites (X,Y,Z) in *fac*-position offer diverse coordination modes that can be utilized to design customized complexes. The sites X and Y can be occupied by two unidentate ligands or one bidentate ligand while Z is a leaving group usually a halogen.[51] The arene ligand influences the electron distribution of a complex, hence the nature of arene group affects the stability of the ruthenium(II) complexes.[52]

Arene-based ruthenium(II) complexes have exhibited excellent *in vivo* and *in vitro* cytotoxicity even in *cisplatin* resistant cells.[40b, 53] Leading active arene ruthenium(II) complexes are 1,3,5-triaza-7-phosphaadamantane-based complexes (RAPTA-T and RAPTA-C), RM175 and DW1/2 (Figure 1.5). For example; RAPTA-T has shown anti-metastatic and anti-invasive activity against mammary cancer cells[23f, 23g] while RAPTA-C exhibits broad anti-tumour efficacy by inhibiting cell growth.[23h]

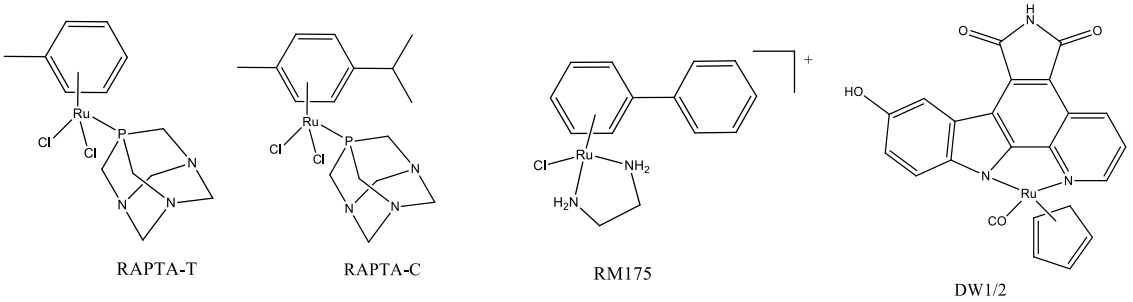

Figure 1.5: Some of the lead arene ruthenium(II) anticancer agents at preclinical trials

The cytoxicity of these complexes can be varied by changing the arene group and/or the chelating ligand.[54] It is documented that their cytotoxicity has a direct relationship with the π-surface area of the arene and/ or the chelating ligand.[55] Contrarily, changing the leaving group has no impact on cytoxicity because the complexes are activated by aquation.[56] Importantly, the cytotoxicity can be changed by increasing the number of metal centres linked together.[56-57]

Multinuclearity is an emerging approach in drug design and development to overcome chemo-resistant tumours.[57] Multinuclear ruthenium complexes mostly contain binuclear, trinuclear, tetranuclear or hexanuclear derivatives.[58] Among these systems, the binuclear complexes are well investigated for their anticancer properties.[59] It is established that they are more active than their mononuclear analogues due to synergistic effects. The length of the linker between the two metal centres has a positive correlation with the cytoxicity of a complex[53b, 60] because lipophilicity and cellular uptake increase with increase in length of the spacer.[53b,54,60a]

Therefore, the bridging ligand control the biological and pharmacological properties of these complexes as well as providing steric protection to the metal centres against biological non-target molecules.[61]

1.5 Potential Targets of Ruthenium(II) Complexes

Ruthenium(II) complexes enter the cells through either energy-depended and or energy-independent mechanisms such as active transport, passive diffusion and endocytosis.[62] The structural and electronic properties of ligands around the metal centre have influence on the target of the anticancer metallodrug.[63]

The main target of ruthenium(II)-based oncotherapeutics is the DNA.[63] Studies have shown that the DNA targeting metallodrugs are highly selective and effective in clinical utilization.[64] These complexes interact with DNA through either covalent or non-covalent binding. Covalent binding is irreversible and therefore the Ru-DNA adducts formed interferes with DNA replication. On the other hand, non-covalent binding occur through intercalation, groove and electrostatic binding.[65] Examples of ruthenium(II) compounds that bind to DNA are RAPTA-C and RM175.[65a, 66]

Apart from DNA, some ruthenium(II) complexes target protein especially protein kinases due to their three-dimensional structure and physicochemical properties. These complexes mimic staurosporine resulting in inhibition of protein kinases.[67] DW1/2 which acts on the glycogen synthase kinase is an example of protein kinase inhibiting agent.[68]

1.6 Need for Mechanistic Studies

In the search for more effective and less toxic non-platinum anticancer metallodrugs, ruthenium-based complexes have been considered as viable options due to their favourable properties.[18, 21] In drug design and development, a comprehensive understanding of the interactions between metal complexes and biomolecules is important.[69] A perusal of literature

reveal that there is lack of extensive kinetic and mechanistic information on ruthenium(II) complexes.[46c, 52b, 70] Therefore, it is important to establish structure-reactivity relationship for these complexes as affected by different ligand systems around the metal centre.

In biological systems, metallodrugs interact with DNA as well as other biomolecules including S-donor groups that have high affinity for metal centres such as glutathione and cysteine. These non-target molecules offer kinetic and thermodynamics competition to DNA binding and thus affect the distribution and efficacy of the metallodrug.[71] In this regard, studying the rate and mechanism of substitution reactions using bio-relevant nucleophiles are important in understanding the kinetics of these interactions between the complexes and molecules in biological systems.

Apart from activating the metal-based anticancer agents,[72] hydrolysis of the metal-choro bond enhance hydrophilicity and cellular uptake of metallodrug. The end result of this is increased anticancer efficacy.[72-73] Considering the importance of aquation, all the complexes investigated and discussed in Chapter **Three**, **Five** and **Six** were converted into their respective aqua species.

1.7 Aim of the Study

The aim of this study is to explore the kinetic and mechanistic behavior of model mononuclear and dinuclear ruthenium(II) complexes as influenced by different spectator ligands as a function of nucleophilic concentration and temperature. Bio-relevant thiol-based nucleophiles of varied steric requirements were used; thiourea (Tu), *N*,*N*-dimethylthiourea (Dmtu) and *N,N,N',N'*-tetramethylthiourea (Tmtu). These nucleophiles were used because of their biological importance, high solubility and nucleophilicity.[74] For instance; Tu combines the properties of thioether and thiolate and has been used as a protection agent to minimize

nephrotoxicity brought about by *cisplatin* treatment[71b] while Dmtu is utilized in cytoprotection of liver and kidney against mitochondrial damage caused by *cisplatin*.[75]

In chapter **Three** and **Four** ligand exchange kinetics and mechanism of mononuclear ruthenium(II) polypyridyl complexes is discussed. Chapter **Five** and **Six** focus on the effects of bridging ligand on the reactivity of binuclear ruthenium(II) arene complexes.

The specific objectives of this study were;

i. to investigate the role of π-extension of the auxiliary ligand on the reactivity of ruthenium(II) terpyridyl complexes: *A kinetic and mechanistic study*. The N/N^N auxiliary ligands used were pyridine (**Ru-2**), 2,2'-bipyridine (**Ru-2**), 2-(2-pyridyl)quinoline (**Ru-3**) and 2,2' biquinoline (**Ru-4**). This is presented in **Chapter Three**

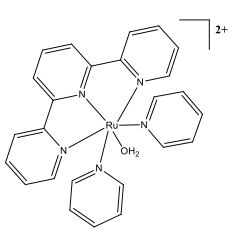

Ru-1

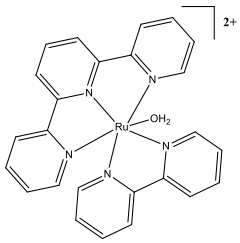

Ru-2

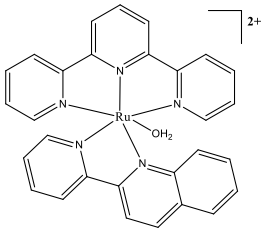

Ru-3

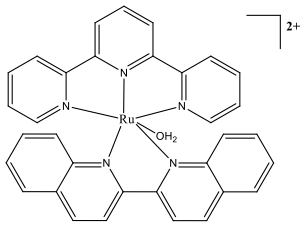

Ru-4

ii. to understand the influence of π-back-bonding and *trans*-effect on the reactivity of ruthenium(II) polypyridyl complexes with two chloro leaving groups. The spectator ligands used are pyridine (**Ru-1)**, 2,2'-bypridiyl (**Ru-2)**, 2,2'-biquinoline (**Ru-4**) 6,6-dimethyl-2,2'-bipyridyl (**Ru-5**), 2,9-dimethyl-1,10-phenanthroline (**Ru-6)**. **Ru-3** is a hybrid system with 2,2'-bypridiyl and 2,2'-biquinoline ligands. (**Chapter Four**)

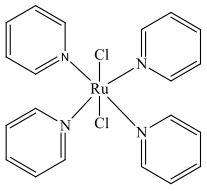

Ru-1

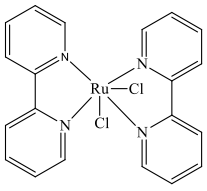

Ru-2

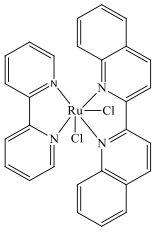

Ru-3

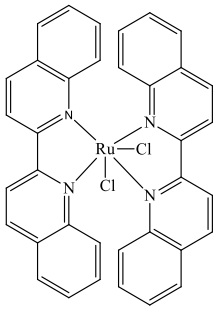

Ru-4

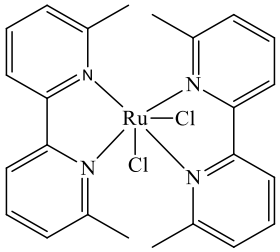

Ru-5

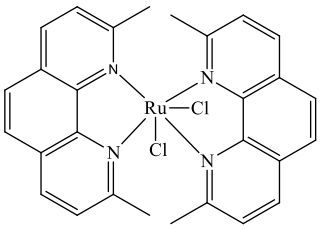

Ru-6

iii. to study the influence of bridging ligand on the substitution kinetics of *p*-cymene ruthenium(II) complexes. Two mononuclear and four dinuclear (with different bridging ligands) complexes were investigated. The bridging ligands used were; 2,2'-bipyrimidine (**Ru-3**), 2,3-*bis*(2-pyridyl)-pyrazine **(Ru-4)**, 2,3-*bis*(2-pyridyl)-quinoxaline **(Ru-5)** and 6,7-dimethyl-2,3-*bis*(2-pyridyl)quinoxaline **(Ru-6)**. (**Chapter Five**)

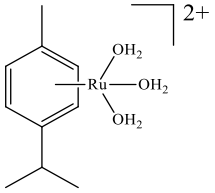

Ru-1

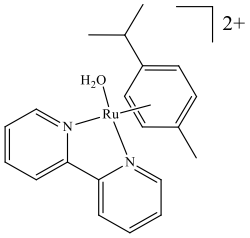

Ru-2

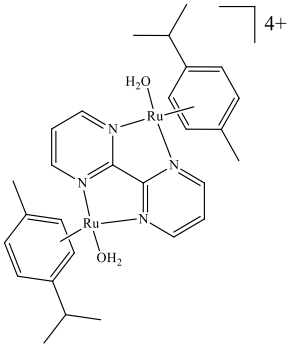

Ru-3

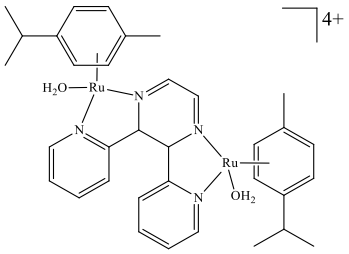

Ru-4

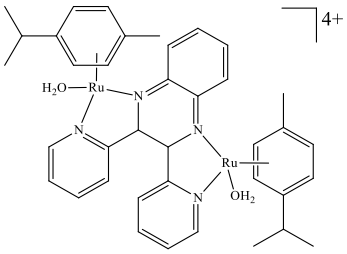

Ru-5

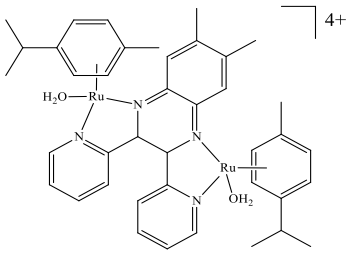

Ru-6

iv. to investigate the effect of hybrid N-N bridging ligand on the reactivity of η^6-*p*-cymene ruthenium(II) complexes. A series of four complexes with different spacers between the diimine moieties (no spacer (**Ru-1**), phenyl (**Ru-2**), biphenyl (**Ru-3**) and xylyl (**Ru-4**)) and invariant arene groups were studied. (**Chapter Six**)

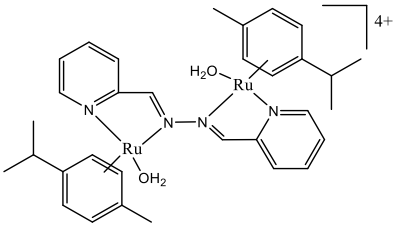

Ru-1

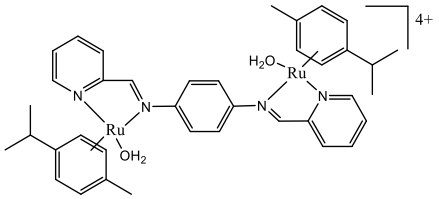

Ru-2

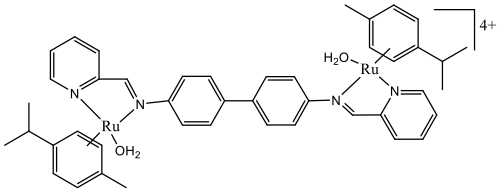

Ru-3

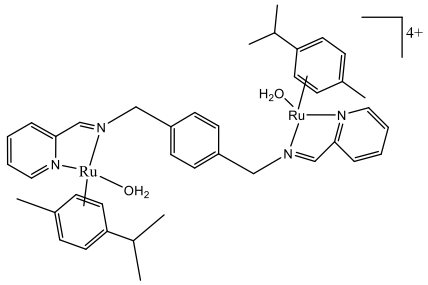

Ru-4

To gain an insight on the stability and structural properties of the substitution product formed, crystal structure of two substitution products were independently isolated and crystallographically analyzed. These crystals are discussed in chapter **Three** and **Four**.

To complement the experimental study on the complexes, computational studies using density functional theory (DFT) as implemented by Gaussian 09W suite of programs was done. The complexes were optimized using the hybrid Becke, 3-parameter, Lee-yang-Parr at the standard Los Alamos National Laboratory 2-double-ζ effective core potential.[76]

1.8 References

[1] S. Pichandi, P. Pasupathi, Y. Y. Rao, J. Farook, B. S. Ponnusha, A. Ambika, S. Subramaniyam, *International Journal of Biological & Medical Research* **2011**, *2*, 593-602.

[2] G. Cooper, in *The Development and Causes of Cancer* 2nd ed., USA: Sinauer Associates, Sunderland (MA), 2000, *https://www.ncbi.nlm.nih.gov/books/NBK9963/*, Accessed on 16.08.2018.

[3] W. H. Organization, in *Cancer Fact sheet*, 2017 *http://www.who.int/news-room/fact-sheets/detail/cancer*, Accessed on 16.08.2018.

[4] P. Anand, A. B. Kunnumakara, C. Sundaram, K. B. Harikumar, S. T. Tharakan, O. S. Lai, B. Sung, B. B. Aggarwal, *Pharmaceutical Research* **2008**, *25*, 2097-2116.

[5] G. P. Pfeifer, M. F. Denissenko, M. Olivier, N. Tretyakova, S. S. Hecht, P. Hainaut, *Oncogene* **2002**, *21*, 7435-7450.

[6] A. Recht, S. E. Come, I. C. Henderson, R. S. Gelman, B. Silver, D. F. Hayes, L. N. Shulman, J. R. Harris, *New England Journal of Medicine* **1996**, *334*, 1356-1361.

[7] J.-F. Bosset, M. Gignoux, J.-P. Triboulet, E. Tiret, G. Mantion, D. Elias, P. Lozach, J.-C. Ollier, J.-J. Pavy, M. Mercier, *New England Journal of Medicine* **1997**, *337*, 161-167.

[8] A. Urruticoechea, R. Alemany, J. Balart, A. Villanueva, F. Vinals, G. Capella, *Current Pharmaceutical Design* **2010**, *16*, 3-10.

[9] (a) B. A. Teicher, J. S. Lazo, A. C. Sartorelli, *Cancer Research* **1981**, *41*, 73-81; (b) G. Peters, C. Van der Wilt, C. Van Moorsel, J. Kroep, A. Bergman, S. Ackland, *Pharmacology & Therapeutics* **2000**, *87*, 227-253; (c) R. L. Noble, *Biochemistry and Cell Biology* **1990**, *68*, 1344-1351; (d) L. Gianni, L. Norton, N. Wolmark, T. M. Suter, G. Bonadonna, G. N. Hortobagyi, *Journal of Clinical Oncology* **2009**, *27*, 4798-4808; (e) E. Solary, R. Bertrand, K. Kohn, Y. Pommier, *Blood* **1993**, *81*, 1359-1368.

[10] N. J. Wheate, S. Walker, G. E. Craig, R. Oun, *Dalton Transactions* **2010**, *39*, 8113-8127.

[11] (a) P. J. Dyson, G. Sava, *Dalton Transactions* **2006**, 1929-1933; (b) S. Dasari, P. B. Tchounwou, *European Journal of Pharmacology* **2014**, *740*, 364-378.

[12] D. Wang, S. J. Lippard, *Nature Reviews Drug Discovery* **2005**, *4*, 307-320.

[13] D. Lebwohl, R. Canetta, *European Journal of Cancer* **1998**, *34*, 1522-1534.

[14] M. J. Clarke, P. J. Sadler, *Metallopharmaceuticals I: DNA Interactions, Vol. 1*, Springer Science & Business Media, Berlin Heidelberg, **2013**, pp. 47-53.

[15] (a) Y. Sasaki, T. Tamura, K. Eguchi, T. Shinkai, Y. Fujiwara, M. Fukuda, Y. Ohe, M. Bungo, N. Horichi, S. Niimi, *Cancer Chemotherapy and Pharmacology* **1989**, *23*, 243-246; (b) Q.-Q. Deng, X.-E. Huang, L.-H. Ye, Y.-Y. Lu, Y. Liang, J. Xiang, *Asian Pacific Journal of Cancer Prevention* **2013**, *14*, 413-417; (c) M. L. de Lemos, *Cancer Treatment Reviews* **1998**, *24*, 407-414.

[16] M. W. Saif, J. Reardon, *Therapeutics and Clinical Risk Management* **2005**, *1*, 249-258.

[17] (a) Z.-T. Cao, Z.-Y. Chen, C.-Y. Sun, H.-J. Li, H.-X. Wang, Q.-Q. Cheng, Z.-Q. Zuo, J.-L. Wang, Y.-Z. Liu, Y.-C. Wang, *Biomaterials* **2016**, *94*, 9-19; (b) D. J. Stewart, *Critical Reviews in Oncology/Hematology* **2007**, *63*, 12-31; (c) H. H. Hsu, M. C. Chen, R. Baskaran, Y. M. Lin, C. H. Day, Y. J. Lin, C. C. Tu, V. Vijaya Padma, W. W. Kuo, C. Y. Huang, *Journal of Cellular Physiology* **2018**, *233*, 5458-5467; (d) E. Martinez-Balibrea, A. Martínez-Cardús, A. Ginés, V. R. de Porras, C. Moutinho, L. Layos, J. L. Manzano, C. Bugés, S. Bystrup, M. Esteller, *Molecular Cancer Therapeutics* **2015**, *14*, 1-10.

[18] C. S. Allardyce, P. J. Dyson, *Platinum Metals Review* **2001**, *45*, 62-69.

[19] M. A. Jakupec, M. Galanski, V. B. Arion, C. G. Hartinger, B. K. Keppler, *Dalton Transactions* **2008**, 183-194.

[20] (a) T. Lazarević, A. Rilak, Ž. D. Bugarčić, *European Journal of Medicinal Chemistry* **2017**, *142*, 8-31; (b) I. Kostova, *Anti-Cancer Agents in Medicinal Chemistry (Formerly Current Medicinal Chemistry-Anti-Cancer Agents)* **2009**, *9*, 827-842; (c) R. J. Needham, C. Sanchez-Cano, X. Zhang, I. Romero-Canelón, A. Habtemariam, M. S. Cooper, L. Meszaros, G. J. Clarkson, P. J. Blower, P. J. Sadler, *Angewandte Chemie International Edition* **2017**, *56*, 1017-1020.

[21] E. S. Antonarakis, A. Emadi, *Cancer Chemotherapy and Pharmacology* **2010**, *66*, 1-9.

[22] D. R. Lide, *CRC Handbook of Chemistry and Physics, Internet Version* CRC Press, Boca Raton, **2006**, pp. 32-33.

[23] (a) B. Keppler, W. Rupp, *Journal of Cancer Research and Clinical Oncology* **1986**, *111*, 166-168; (b) B. Keppler, M. Henn, U. Juhl, M. Berger, R. Niebl, F. Wagner, in *Ruthenium and Other Non-Platinum Metal Complexes in Cancer Chemotherapy*, Springer, **1989**, pp. 41-69; (c) E. Alessio, G. Mestroni, A. Bergamo, G. Sava, *Current Topics in Medicinal Chemistry* **2004**, *4*, 1525-1535; (d) I. Bratsos, S. Jedner, T. Gianferrara, E. Alessio, *Chimia International Journal for Chemistry* **2007**, *61*, 692-697; (e) A. H. Velders, H. Kooijman, A. L. Spek, J. G. Haasnoot, D. de Vos, J. Reedijk, *Inorganic Chemistry* **2000**, *39*, 2966-2967; (f) R. F. Lee, S. Escrig, C. Maclachlan, G. W. Knott, A. Meibom, G. Sava, P. J. Dyson, *International Journal of Molecular Sciences* **2017**, *18*, 1869; (g) C. Scolaro, A. Bergamo, L. Brescacin, R. Delfino, M. Cocchietto, G. Laurenczy, T. J. Geldbach, G. Sava, P. J. Dyson, *Journal of Medicinal Chemistry* **2005**, *48*, 4161-4171;(h) S. Chatterjee, S. Kundu, A. Bhattacharyya, C. G. Hartinger, P. J. Dyson, *Journal of Biological Inorganic Chemistry* **2008**, *13*, 1149.

[24] M. J. Clarke, *Coordination Chemistry Reviews* **2002**, *232*, 69-93.

[25] O. Novakova, J. Kasparkova, O. Vrana, P. M. van Vliet, J. Reedijk, V. Brabec, *Biochemistry* **1995**, *34*, 12369-12378.

[26] M. Pongratz, P. Schluga, M. A. Jakupec, V. B. Arion, C. G. Hartinger, G. Allmaier, B. K. Keppler, *Journal of Analytical Atomic Spectrometry* **2004**, *19*, 46-51.

[27] S. C. Srivastava, L. F. Mausner, M. J. Clarke, in *Ruthenium and other Non-Platinum Metal Complexes in Cancer Chemotherapy*, Springer, **1989**, pp. 111-149.

[28] (a) M. Clarke, S. Bitler, D. Rennert, M. Buchbinder, A. Kelman, *Journal of Inorganic Biochemistry* **1980**, *12*, 79-87; (b) J. Durig, J. Danneman, W. Behnke, E. Mercer, *Chemico-Biological Interactions* **1976**, *13*, 287-294.

[29] M. Clarke, *Metal Ions in Biological Systems* **1980**, *11*, 231-283.

[30] R. Trondl, P. Heffeter, C. R. Kowol, M. A. Jakupec, W. Berger, B. K. Keppler, *Chemical Science* **2014**, *5*, 2925-2932.

[31] F. Garzon, M. Berger, B. Keppler, D. Schmähl, *Cancer Chemotherapy and Pharmacology* **1987**, *19*, 347-349.

[32] W. Peti, T. Pieper, M. Sommer, B. K. Keppler, G. Giester, *European Journal of Inorganic Chemistry* **1999**, *1999*, 1551-1555.

[33] E. Alessio, *Chemical Reviews* **2004**, *104*, 4203-4242.

[34] I. Bratsos, T. Gianferrara, E. Alessio, C. G. Hartinger, M. A. Jakupec, B. K. Keppler, *Bioinorganic Medicinal Chemistry* **2011**, 151-174.

[35] (a) G. Sava, F. Frausin, M. Cocchietto, F. Vita, E. Podda, P. Spessotto, A. Furlani, V. Scarcia, G. Zabucchi, *European Journal of Cancer* **2004**, *40*, 1383-1396; (b) F. Frausin, V. Scarcia, M. Cocchietto, A. Furlani, B. Serli, E. Alessio, G. Sava, *Journal of Pharmacology and Experimental Therapeutics* **2005**, *313*, 227-233; (c) A. Vacca, M. Bruno, A. Boccarelli, M. Coluccia, D. Ribatti, A. Bergamo, S. Garbisa, L. Sartor, G. Sava, *British Journal of Cancer* **2002**, *86*, 993-998.

[36] J. M. Rademaker-Lakhai, D. van den Bongard, D. Pluim, J. H. Beijnen, J. H. Schellens, *Clinical Cancer Research* **2004**, *10*, 3717-3727.

[37] (a) S. H. van Rijt, P. J. Sadler, *Drug Discovery Today* **2009**, *14*, 1089-1097; (b) M. J. Clarke, F. Zhu, D. R. Frasca, *Chemical Reviews* **1999**, *99*, 2511-2534.

[38] C. Monti-Bragadin, L. Ramani, L. Samer, G. Mestroni, G. Zassinovich, *Antimicrobial Agents and Chemotherapy* **1975**, *7*, 825-827.

[39] E. Alessio, G. Mestroni, G. Nardin, W. M. Attia, M. Calligaris, G. Sava, S. Zorzet, *Inorganic Chemistry* **1988**, *27*, 4099-4106.

[40] (a) C. S. Allardyce, P. J. Dyson, D. J. Ellis, S. L. Heath, *Chemical Communications* **2001**, 1396-1397; (b) R. E. Morris, R. E. Aird, P. del Socorro Murdoch, H. Chen, J. Cummings, N. D. Hughes, S. Parsons, A. Parkin, G. Boyd, D. I. Jodrell, *Journal of Medicinal Chemistry* **2001**, *44*, 3616-3621; (c) Y. V. Gopal, D. Jayaraju, A. K. Kondapi, *Biochemistry* **1999**, *38*, 4382-4388.

[41] W. Han Ang, P. J. Dyson, *European Journal of Inorganic Chemistry* **2006**, *2006*, 4003-4018.

[42] (a) S. S. née Kraft, C. Bischof, A. Loos, S. Braun, N. Jafarova, U. Schatzschneider, *Journal of Inorganic Biochemistry* **2009**, *103*, 1126-1134; (b) H. Huang, P. Zhang, Y. Chen, K. Qiu, C. Jin, L. Ji, H. Chao, *Dalton Transactions* **2016**, *45*, 13135-13145.

[43] T. Chen, Y. Liu, W.-J. Zheng, J. Liu, Y.-S. Wong, *Inorganic Chemistry* **2010**, *49*, 6366-6368.

[44] (a) U. Schatzschneider, J. Niesel, I. Ott, R. Gust, H. Alborzinia, S. Wölfl, *ChemMedChem: Chemistry Enabling Drug Discovery* **2008**, *3*, 1104-1109; (b) P. Čanović, A. R. Simović, S. Radisavljević, I. Bratsos, N. Demitri, M. Mitrović, I. Zelen, Ž. D. Bugarčić, *Journal of Biological Inorganic Chemistry* **2017**, *22*, 1007-1028.

[45] V. Brabec, O. Nováková, *Drug Resistance Updates* **2006**, *9*, 111-122.

[46] (a) A. Rilak, I. Bratsos, E. Zangrando, J. Kljun, I. Turel, Z. i. D. Bugarčić, E. Alessio, *Inorganic Chemistry* **2014**, *53*, 6113-6126; (b) D. Lazić, A. Arsenijević, R. Puchta, Ž. D. Bugarčić, A. Rilak, *Dalton Transactions* **2016**, *45*, 4633-4646; (c) M. M. Milutinović, S. K. Elmroth, G. Davidović, A. Rilak, O. R. Klisurić, I. Bratsos, Ž. D. Bugarčić, *Dalton Transactions* **2017**, *46*, 2360-2369.

[47] C. C. Cheng, W. L. Lee, J. G. Su, C. L. Liu, *Journal of the Chinese Chemical Society* **2000**, *47*, 213-220.

[48] J. P. Barolli, R. S. Corrêa, F. S. Miranda, J. U. Ribeiro, C. Bloch Jr, J. Ellena, V. Moreno, M. R. Cominetti, A. A. Batista, *Journal of the Brazilian Chemical Society* **2017**, *28*, 1879-1889.

[49] (a) J.-A. Cuello-Garibo, C. C. James, M. A. Siegler, S. Bonnet, *Chemistry Squared* **2017**, *1*, 1-19; (b) L. K. Filak, G. Mühlgassner, F. Bacher, A. Roller, M. Galanski, M. A. Jakupec, B. K. Keppler, V. B. Arion, *Organometallics* **2010**, *30*, 273-283; (c) M. Ganeshpandian, M. Palaniandavar, A. Muruganantham, S. K. Ghosh, A. Riyasdeen, M. A. Akbarsha, *Applied Organometallic Chemistry* **2018**, *32*, e4154; (d) Q.-P. Qin, T. Meng, M.-X. Tan, Y.-C. Liu, S.-L. Wang, B.-Q. Zou, H. Liang, *Medicinal Chemistry Communications* **2018**, *9*, 525-533.

[50] (a) L. Dale, J. Tocher, T. Dyson, D. Edwards, D. Tocher, *Anti-Cancer Drug Design* **1992**, *7*, 3-14; (b) P. J. Dyson, *Chimia International Journal for Chemistry* **2007**, *61*, 698-703.

[51] F. Wang, H. Chen, S. Parsons, I. D. Oswald, J. E. Davidson, P. J. Sadler, *Chemistry–A European Journal* **2003**, *9*, 5810-5820.

[52] (a) Y. K. Yan, M. Melchart, A. Habtemariam, P. J. Sadler, *Chemical Communications* **2005**, 4764-4776; (b) L. Dadci, H. Elias, U. Frey, A. Hoernig, U. Koelle, A. E. Merbach, H. Paulus, J. S. Schneider, *Inorganic Chemistry* **1995**, *34*, 306-315.

[53] (a) M. Melchart, P. J. Sadler, *Bioorganometallics: Biomolecules, Labeling, Medicine* **2006**, 39-64; (b) M.-G. Mendoza-Ferri, C. G. Hartinger, R. E. Eichinger, N. Stolyarova, K. Severin, M. A. Jakupec, A. A. Nazarov, B. K. Keppler, *Organometallics* **2008**, *27*, 2405-2407.

[54] S. Schäfer, I. Ott, R. Gust, W. S. Sheldrick, *European Journal of Inorganic Chemistry* **2007**, *2007*, 3034-3046.

[55] R. Aird, J. Cummings, A. Ritchie, M. Muir, R. Morris, H. Chen, P. Sadler, D. Jodrell, *British Journal of Cancer* **2002**, *86*, 1652-1657.

[56] M. G. Mendoza-Ferri, C. G. Hartinger, A. A. Nazarov, R. E. Eichinger, M. A. Jakupec, K. Severin, B. K. Keppler, *Organometallics* **2009**, *28*, 6260-6265.

[57] C. G Hartinger, A. D Phillips, A. A Nazarov, *Current Topics in Medicinal Chemistry* **2011**, *11*, 2688-2702.

[58] A. K. Singh, D. S. Pandey, Q. Xu, P. Braunstein, *Coordination Chemistry Reviews* **2014**, *270*, 31-56.

[59] H. Chen, J. A. Parkinson, O. Nováková, J. Bella, F. Wang, A. Dawson, R. Gould, S. Parsons, V. Brabec, P. J. Sadler, *Proceedings of the National Academy of Sciences* **2003**, *100*, 14623-14628.

[60] (a) A. Romerosa, T. Campos-Malpartida, C. Lidrissi, M. Saoud, M. Serrano-Ruiz, M. Peruzzini, J. A. Garrido-Cárdenas, F. García-Maroto, *Inorganic Chemistry* **2006**, *45*, 1289-1298; (b) M. Auzias, B. Therrien, G. Süss-Fink, P. Štěpnička, W. H. Ang, P. J. Dyson, *Inorganic Chemistry* **2008**, *47*, 578-583; (c) L. K. Batchelor, E. Păunescu, M. n. Soudani, R. Scopelliti, P. J. Dyson, *Inorganic Chemistry* **2017**, *56*, 9617-9633.

[61] S. D. Brown, K. D. Trotter, O. B. Sutcliffe, J. A. Plumb, B. Waddell, N. E. Briggs, N. J. Wheate, *Dalton Transactions* **2012**, *41*, 11330-11339.

[62] M. R. Gill, J. A. Thomas, *Chemical Society Reviews* **2012**, *41*, 3179-3192.

[63] (a) S. Balasubramanian, L. H. Hurley, S. Neidle, *Nature Reviews Drug Discovery* **2011**, *10*, 261; (b) N. Hosoya, K. Miyagawa, *Cancer Science* **2014**, *105*, 370-388.

[64] (a) K. Wu, W. Hu, Q. Luo, X. Li, S. Xiong, P. J. Sadler, F. Wang, *Journal of the American Society for Mass Spectrometry* **2013**, *24*, 410-420; (b) C. Tomasetti, L. Li, B. Vogelstein, *Science* **2017**, *355*, 1330-1334; (c) T. S. Kamatchi, N. Chitrapriya, S. K. Kim, F. R. Fronczek, K. Natarajan, *European Journal of Medicinal Chemistry* **2013**, *59*, 253-264.

[65] (a) H. Chen, J. A. Parkinson, R. E. Morris, P. J. Sadler, *Journal of the American Chemical Society* **2003**, *125*, 173-186; (b) L. Zeng, P. Gupta, Y. Chen, E. Wang, L. Ji, H. Chao, Z.-S. Chen, *Chemical Society Reviews* **2017**, *46*, 5771-5804.

[66] Z. Adhireksan, G. E. Davey, P. Campomanes, M. Groessl, C. M. Clavel, H. Yu, A. A. Nazarov, C. H. F. Yeo, W. H. Ang, P. Dröge, *Nature Communications* **2014**, *5*, 3462-3475.

[67] (a) E. Meggers, G. E. Atilla-Gokcumen, K. Gründler, C. Frias, A. Prokop, *Dalton Transactions* **2009**, 10882-10888; (b) J. Qin, R. Rajaratnam, L. Feng, J. Salami, J. S. Barber-Rotenberg, J. Domsic, P. Reyes-Uribe, H. Liu, W. Dang, S. L. Berger, *Journal of Medicinal Chemistry* **2014**, *58*, 305-314.

[68] J. É. Debreczeni, A. N. Bullock, G. E. Atilla, D. S. Williams, H. Bregman, S. Knapp, E. Meggers, *Angewandte Chemie International Edition* **2006**, *45*, 1580-1585.

[69] Ž. D. Bugarčić, J. Bogojeski, B. Petrović, S. Hochreuther, R. van Eldik, *Dalton Transactions* **2012**, *41*, 12329-12345.

[70] (a) F. Tiba, D. Jaganyi, A. Mambanda, *Journal of Coordination Chemistry* **2010**, *63*, 2542-2560; (b) M. Chrzanowska, A. Katafias, O. Impert, A. Kozakiewicz, A. Surdykowski, P. Brzozowska, A. Franke, A. Zahl, R. Puchta, R. van Eldik, *Dalton Transactions* **2017**, *46*, 10264-10280.

[71] (a) J. Reedijk, *Proceedings of the National Academy of Sciences* **2003**, *100*, 3611-3616; (b) J. Reedijk, *Chemical Reviews* **1999**, *99*, 2499-2510; (c) F. Wang, H. Chen, J. A. Parkinson, P. d. S. Murdoch, P. J. Sadler, *Inorganic Chemistry* **2002**, *41*, 4509-4523; (d) P. Pil, *Encyclopedia of Cancer* **1997**, *1*, 391-410.

[72] A. M. Pizarro, A. Habtemariam, P. J. Sadler, in *Medicinal Organometallic Chemistry*, Springer, **2010**, pp. 21-56.

[73] M. Li, L. Lai, Z. Zhao, T. Chen, *Chemistry–An Asian Journal* **2016**, *11*, 310-320.

[74] W. C. Schiessl, N. K. Summa, C. F. Weber, S. Gubo, C. Dücker-Benfer, R. Puchta, N. J. van Eikema Hommes, R. van Eldik, *Zeitschrift für Anorganische und Allgemeine Chemie* **2005**, *631*, 2812-2819.

[75] (a) N. A. G. dos Santos, N. M. Martins, C. Curti, M. d. L. P. Bianchi, A. C. dos Santos, *Chemico-Biological Interactions* **2007**, *170*, 177-186; (b) N. Santos, C. C. Bezerra, N. Martins, C. Curti, M. Bianchi, A. Santos, *Cancer Chemotherapy and Pharmacology* **2008**, *61*, 145-155.

[76] J. Li, L.-C. Xu, J.-C. Chen, K.-C. Zheng, L.-N. Ji, *The Journal of Physical Chemistry A* **2006**, *110*, 8174-8180.

CHAPTER TWO

Literature Review

2.1 Chemical Kinetics and Substitution Reactions

Chemical kinetics refer to the experimental investigation of rates of chemical reactions with the aim of inferring about the kinetic mechanisms involved.[1] A chemical transformation of a reactant to product occur through a series of elementary steps with a single transition state of definite and measurable life-time. The sequence of these elementary steps is referred to as the mechanism of the reaction.[2]

In a substitution reaction a coordinated ligand is replaced by another group from the environment through a process involving a brief alteration of the coordination number at the reaction centre due to bond breaking and formation. These reactions usually occur with retention of the oxidation state and coordination number of the central atom.[3] Initial substitution studies were done at a carbon centre and classified as either homolytic or heterolytic depending on the type of bond breaking that occurred between the reaction centre and the leaving group. In homolytic substitution, the electrons are shared equally between the reactive centre and the leaving group (*equation 2.1*) while in heterolytic reactions, the electrons are shared unequally. Heterolytic reactions are further divided into two; nucleophilic and electrophilic. In electrophilic heterolysis the electron pair remains at the reactive centre (*equation 2.2*) while in nucleophilic heterolysis the electron pair accompanies the leaving group (*equation 2.3*).[4]

$$M{:}Y \rightarrow M^{\cdot} + Y^{\cdot} \qquad 2.1$$

$$M{:}Y \rightarrow M{:}^{-} + Y^{+} \qquad 2.2$$

$$M{:}Y \rightarrow M^{+} + {:}Y^{-} \qquad 2.3$$

Nucleophilic substitutions are normally designated as either $S_N1$or S_N2 where S_N1 is first order nucleophilic substitution reaction while S_N2 is a bimolecular nucleophilic substitution reaction. [4] Although this classification satisfactorily describes substitution at carbon centre it is inadequate in describing reactions involving inorganic complexes.[3]

The foremost effort to study substitution reaction mechanisms of inorganic complexes were made by Langford and Gray.[5] They introduced the concept of stochiometric and intimate mechanism. The stochiometric mechanisms are concerned with the nature of intermediate formed and are divided into three distinct classes;

a. **Dissociative (D) mechanism**; involves a dissociative process with a recognizable intermediate of a lower coordination number than the starting reagent (*equation* 2.4).[5]

$$XM + Y \rightleftharpoons X, M, Y \rightarrow MY + X \qquad 2.4$$

The intermediate stays long enough to equilibrate with the environment before it interacts with the incoming nucleophile. The reaction is dependent on the nature of the leaving group and independent of the nature and concentration of the incoming group. In this mechanism, as the lability of the intermediate increases, its ability to discriminate incoming nucleophiles become more controlled by the concentrations such that the solvent will start dominating the substitution process.[3]

b. **Associative (A) mechanism**; involves an associative process with a recognizable intermediate with a higher coordination number than that of the starting reagent (*equation* 2.5).

$$XM + Y \rightleftharpoons XMY \rightarrow MY + X \qquad 2.5$$

In this mechanism there exists two transition states i.e. bond-making transition state and bond-breaking transition state. If the leaving and entering groups are chemically identical, the two transition states are energetically degenerate but if they are different one of them will occur at a higher energy than the other. The depth of the well in which

the intermediate sits is an indicator of the stability of the intermediate as well the extent of the differences between the two transition states.[3]

c. **The Interchange (I) mechanism**; involves an interchange process where the bond breaking and making process are either synchronous or occur within a pre-formed aggregate. No detectable intermediates are observed (*equation* 2.6).[3]

$$XM + Y \rightleftharpoons X \cdots M \cdots Y \rightarrow MY + X \qquad 2.6$$

In this mechanism, an outer-sphere complex is formed, then the leaving ligand moves from the inner coordination sphere to the outer coordination sphere. As this happens, the nucleophile moves from the outer-sphere to the inner coordination sphere of the complex.[6]

Intimate mechanisms are based on mode of activation involved and are classified into two; *viz*.

a. **A dissociatively activated (d) mechanism**. In this mechanism, in the rate determining transition state there is no direct interaction between the reaction centre and the incoming group.

b. **An associatively activated (a) mechanism**. In this mechanism, in the rate determining transition state there is a bonding between the reaction centre and the incoming group occur.

Interchange mechanism occurs between the two extreme mechanisms (dissociative and associative) and can either be associative interchange ($\boldsymbol{I_a}$) or dissociative interchange ($\boldsymbol{I_d}$).

In $\boldsymbol{I_a}$ mechanism, the reaction rate is more sensitive to the incoming group compared to the leaving group and for the $\boldsymbol{I_d}$ mechanism the reaction is more sensitive to the leaving group compared to the incoming group. Figure 2.1 and 2.2 illustrate the different mechanism through which a substitution reaction may occur.

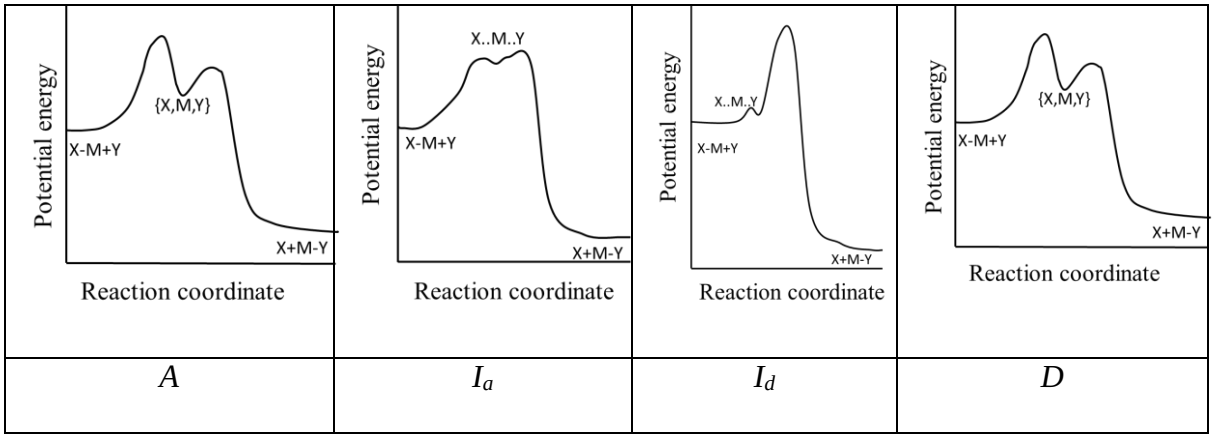

Figure 2.1: Reaction profiles diagrams for different mechanisms.[7]

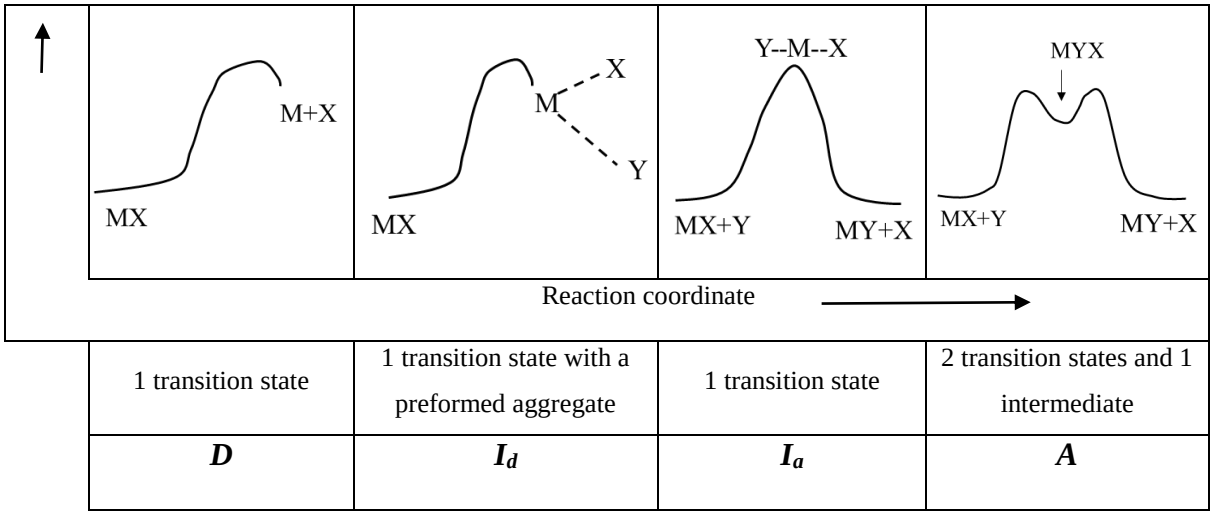

Figure 2.2: Energy profile diagrams showing transition states formed in different mechanisms[3]

2.2 Measurements of Rate Constants

Substitutions chemical reactions do not usually go to completion but tend to achieve an equilibrium. Therefore, the transformation of reactant to products can be expressed as shown in *equation* 2.7 or 2.8.

$$A + B \underset{k_{-2}}{\overset{k_2}{\rightleftharpoons}} C \qquad 2.7$$

or

$$ML_5X + Y \underset{k_{-2}}{\overset{k_2}{\rightleftharpoons}} ML_5Y + X \qquad 2.8$$

where; A is the metal complex (ML_5X), X is the leaving group; B is incoming nucleophile (Y) C is the product (ML_5Y), k_2 is the second order rate constant for the forward reaction, k_{-2} is the second order rate constant for the reverse reaction.

To conveniently follow a second order reaction, the concentration of one of the reactants is kept higher than the other to create a *pseudo*-first order condition.[8] In the present study, the concentration of the nucleophile B was at least 10 times higher with respect to each leaving group in the complex A. These concentrations can be expressed as $[B]_0 \gg [A]_0$

Rate of a chemical reaction is defined as the change in the concentration of a reactant or a product over time.[9] Therefore, the rate of transformation of A to C is as expressed in *equation* 2.9.

$$-\frac{d[A]}{dt} = -\frac{d[B]}{dt} = \frac{d[C]}{dt} = k_2[A]_t[B]_t - k_{-2}[C]_t \qquad 2.9$$

Taking into consideration the initial concentration of the metal complex, *equation* 2.9 can be simplified as shown in *equation* 2.10.

$$-\frac{d[A]}{dt} = -\frac{d[B]}{dt} = \frac{d[C]}{dt} = k_2[A]_t[B]_t - k_{-2}[A]_t - k_{-2}[A]_o \qquad 2.10$$

At time, *t*, the concentration of the three species can be expressed as shown in *equation* 2.11-2.12

$$[A]_t = [A]_0 - [C]_t \qquad 2.11$$

$$[C]_t = [A]_0 - [A]_t \qquad 2.11a$$

and

$$[B]_t = [B]_0 - [C]_t \qquad 2.12$$

At the equilibrium, the concentration of the three species are as shown in *equation* 2.13-2.14

$$[A]_e = [A]_0 - [C]_e \quad 2.13$$

$$[C]_e = [A]_0 - [A]_e \quad 2.13a$$

and

$$[B]_e = [B]_0 - [C]_e \quad 2.14$$

At the equilibrium, the rate of the forward reaction is equal to the rate of reverse reaction

$$-\frac{d[A]}{dt} = k_2[A]_e[B]_e - k_{-2}[C]_e = 0 \quad 2.15$$

Rearrangement of *equation* 2.15 gives

$$k_2[A]_e[B]_e = k_{-2}[C]_e \quad 2.16$$

Replacing $[C]_e$ in equation 2.16 with *equation* 2.13a gives

$$k_2[A]_e[B]_e = k_{-2}[A]_0 - k_{-2}[A]_e \quad 2.17$$

$$k_{-2}[A]_0 = k_2[A]_e[B]_e + k_{-2}[A]_e \quad 2.17a$$

Modifying *equation* 2.9 using *equation* 2.11a yields

$$-\frac{d[A]}{dt} = [A]_t[B]_t - k_{-2}([A]_0 - [A]_t) \quad 2.18$$

$$= k_2[A]_t[B]_t - k_{-2}[A]_0 + k_{-2}[A]_t \quad 2.18a$$

Substituting $k_{-2}[A]_0$ in *equation* 2.18a with *equation* 2.17a gives

$$-\frac{d[A]}{dt} = k_2[A]_t[B]_t - k_2[A]_e[B]_e - k_{-2}[A]_e + k_{-2}[A]_t \quad 2.19$$

Substituting $[B]_t$ and $[B]_e$ in *equation* 2.19 using *equations* 2.12 and 2.14, respectively results in

$$-\frac{d[A]}{dt} = k_2[A]_t([B]_0 - [C]_t) - k_2[A]_e([A]_0 - [C]_e) - k_{-2}[A]_e + k_{-2}[A]_t \quad 2.20$$

Under *pseudo*-first order conditions; $[B]_0 >> [A]_0$, *equation* 2.20 becomes

$$-\frac{d[A]}{dt} = (k_2[B]_0 + k_{-2})([A]_t - [A]_{eq}) \quad 2.21$$

Separating the variables in *equation* 2.21 and further integrating the resulting equation, gives

$$\int_{[A]_0}^{[A]_t} \frac{d[A]}{([A]_t - [A]_e)} = -(k_2[B]_0 + k_{-2}) \int_0^t dt \qquad 2.22$$

$$\ln\left(\frac{[A]_t - [A]_{eq}}{[A]_0 - [A]_{eq}}\right) = -(k_2[B]_0 + k_{-2})t \qquad 2.22a$$

$$= -k_{obs}t \qquad 2.22b$$

Therefore,

$$k_{obs} = k_2[B]_0 + k_{-2} \qquad 2.23$$

where; k_{obs} is the observed rate constant, $[B]_0$ is the initial nucleophilic concentration

To determine the second order rate constant (k_2), k_{obs} values obtained at different nucleophilic concentrations [Nu] are plotted against respective [Nu]. k_2 and k_{-2} values are obtained from the slope and y-intercept of the plot, respectively. Typical plots of k_{obs} versus [Nu] are shown in Figures 2.3 and 2.4. The relationship between k_{obs} and k_2 can be described by the rate law;

$$k_{obs} = k_2[\mathrm{Nu}] + k_{-2} \qquad 2.24$$

A plot with a zero y-intercept means that the forward reaction is irreversible (Figure 2.3) while one with an appreciable y-intercept imply a reverse reaction which may be due to solvotic pathway (Figure 2.4).[10]

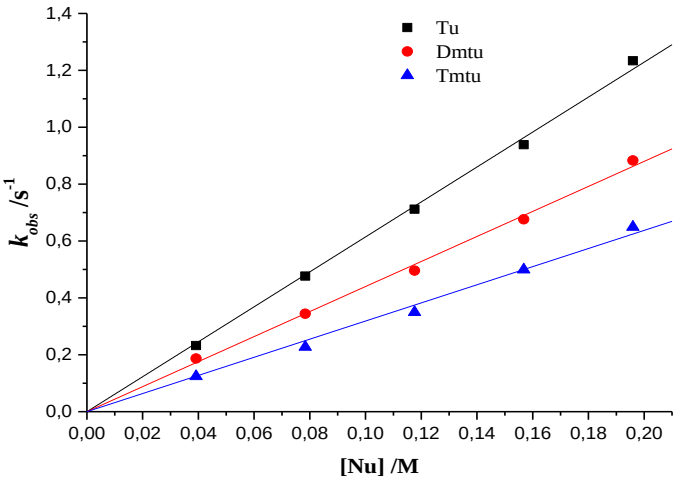

Figure 2.3: Plots of k_{obs} versus the concentration of thiourea nucleophiles for the substitution of aqua ligands in [(*p*-cymene)Ru(H_2O)$_3$]$^{2+}$

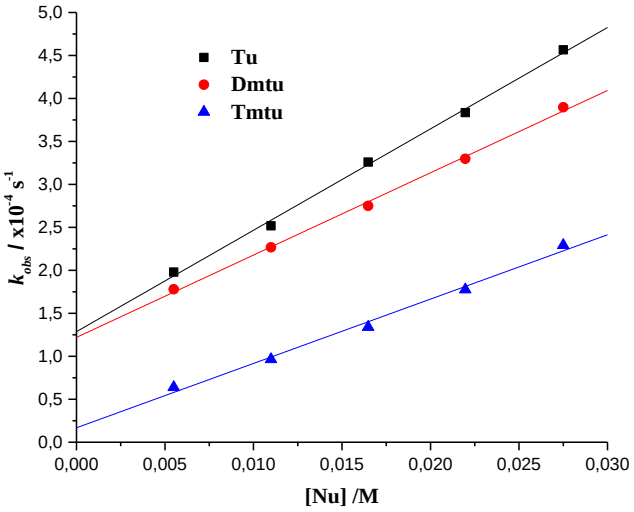

Figure 2.4: Plots of k_{obs} versus the concentration of thiourea nucleophiles for the substitution of the aqua ligand in [(*p*-cymene)Ru(2,2'-bipyrimidine)(H_2O)]$^{2+}$

2.3 Determination of Thermodynamic Parameters

Activation parameters are essential in inferring about the mechanism of a substitution chemical reaction.[9, 11] It is documented that the rate of substitution in octahedral ruthenium(II) complexes is positively correlated to the reaction temperature.[12] Temperature dependent k_2 values are employed in the calculation of $\Delta H^{\neq}$ (activation enthalpy) and $\Delta S^{\neq}$ (activation entropy) using the transition state theory. On the other hand, $\Delta V^{\neq}$ (activation volume) is determined by monitoring the k_2 values as the pressure of the reaction medium is varied.[9]

2.3.1 Determination of Activation Enthalpy ($\Delta H^{\neq}$) and Entropy ($\Delta S^{\neq}$)

According to the transition state theory, majority of chemical reactions proceed through a pre-equilibrium state between the reactants (A and B) and the activated complex ($A \cdots B^*$) as shown in *expression* 2.25.[13]

$$A + B \underset{}{\overset{K^{\#}}{\rightleftharpoons}} \{A\text{---}B\}^* \xrightarrow{k_2} C \qquad \text{(Activated Complex)} \qquad 2.25$$

The rate of reaction is written as;

$$-\frac{d[A]}{dt} = k_2\{A \cdots B\}^* = \frac{k_b \mathrm{T}}{h} K^{\neq}[A][B] \quad 2.26$$

where; k_b is Boltzmann constant; $1.3806 \times 10^{-23} JK^{-1}$

h is Planck's constant; $6.6261 \times 10^{-34} Js$

T is temperature; K

$K^{\neq}$ is equilibrium constant

Therefore, the second order rate constant, k_2 at a specific temperature is given by *equation* 2.27

$$k_2 = \frac{k_b \mathrm{T}}{h} K^{\neq} \quad 2.27$$

The Gibbs energy of activation ($\Delta G^{\neq}$) which consists of the entropy of activation ($\Delta S^{\neq}$) and enthalpy of activation ($\Delta H^{\neq}$) is given by *equation* 2.28

$$\Delta G^{\neq} = -\mathrm{RT}\ln K^{\neq} = \Delta H^{\neq} - \mathrm{T}\Delta S^{\neq} \quad 2.28$$

where; R is the gas constant; 8.3145 $JK^{-1}mol^{-1}$

Substituting *equation* 2.28 in *equation* 2.27 yields

$$k_2 = \frac{k_b \mathrm{T}}{h} e^{\left(-\frac{\Delta G^{\neq}}{RT}\right)} = e^{\left(-\frac{\Delta H^{\neq}}{RT}\right)} e^{\left(\frac{\Delta S^{\neq}}{R}\right)} \quad 2.29$$

Taking natural logarithm and rearranging *equation* 2.29 gives

$$\ln\left(\frac{k_2}{\mathrm{T}}\right) = -\frac{\Delta H^{\neq}}{\mathrm{R}} . \frac{1}{\mathrm{T}} + \left(\ln\frac{k_b}{h} + \frac{\Delta S^{\neq}}{\mathrm{R}}\right) \quad 2.30$$

Since $\ln\frac{k_b}{h} = 23.78$, *equation* 2.30 can be written as;

$$\ln\left(\frac{k_2}{\mathrm{T}}\right) = -\frac{\Delta H^{\neq}}{\mathrm{R}} . \frac{1}{\mathrm{T}} + \left(23.78 + \frac{\Delta S^{\neq}}{\mathrm{R}}\right) \quad 2.31$$

A plot of $\ln\left(\frac{k_2}{\mathrm{T}}\right)$ versus $\frac{1}{\mathrm{T}}$ is popularly known as the Eyring plot. The $\Delta H^{\neq}$ and $\Delta S^{\neq}$ values are calculated from the slope ($-\frac{\Delta H^{\neq}}{\mathrm{R}}$) and the y-intercept $\left(23.78 + \frac{\Delta S^{\neq}}{\mathrm{R}}\right)$, respectively. Typical Eyring plots obtained for the temperature range of 20 - 40℃ is shown in Figure 2.5.

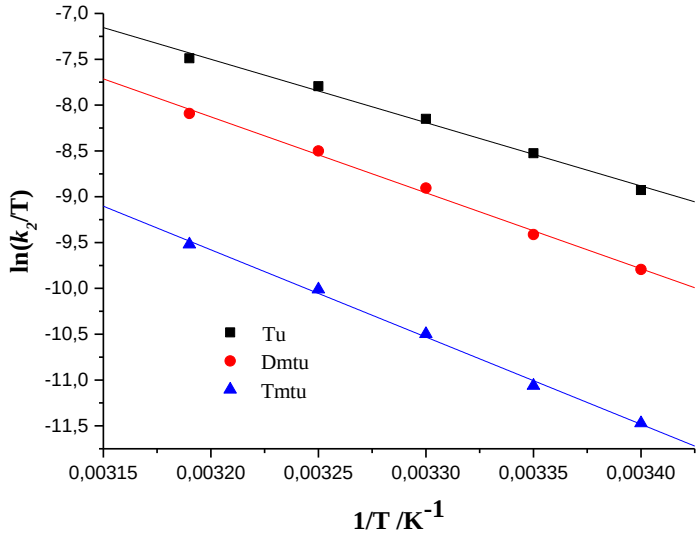

Figure 2.5: Eyring plots for the reaction of **Ru-4** (Chapter Five) with thiourea nucleophiles at different temperatures, pH = 2.0, *I* = 0.1 M $HClO_4/NaClO_4$

In a bimolecular reaction, the terms, $\Delta H^{\neq}$ and $\Delta S^{\neq}$ refer to the differences in enthalpy and entropy, respectively between the activated complex and the reactants.[6] Studies have shown that $\Delta H^{\neq}$values for associative reaction mechanisms are usually smaller compared to those for dissociative reaction mechanisms. In dissociative reactions, $\Delta H^{\neq}$ values indicate the strength of the dissociating bond. $\Delta S^{\neq}$ plays a pivotal role in the determination of the reaction mechanism. Any value of $\Delta S^{\neq} <$ -10 eu indicate an associative mechanism while any value $\Delta S^{\neq} >$ -10 eu indicate a dissociative reaction mechanism. It is difficult to interpret the mechanism for reactions with $-10 \geq \Delta S^{\neq} \leq 10$ eu values due to the contributions of solvent reorganization.[6, 9] Substitution reactions of ruthenium(II) arene and polypyridyl complexes have shown associative mechanisms as summarized in Table 2.1.

Table 2.1: Activation parameters obtained in the substitution studies of ruthenium(II) complexes

Complex	Nucleophile	$\Delta H^{\neq}$	$\Delta S^{\neq}$	Ref.
$[(\eta^6$-benzene)Ru(bipy)$(H_2O)]^{2+}$	Thiourea	68 ± 4	-31 ± 9	[11b]
$[(\eta^6$- *p*-cymene)Ru(bipy)$(H_2O)]^{2+}$	SCN^-	70 ± 3	-22 ± 7	[11b]
$[(\eta^6$-hmb) Ru(bipy)$(H_2O)]^{2+}$	Thiourea	66 ± 4	-34 ± 8	[11b]
$[(\eta^6$-*p*-cymene)Ru(pydc)Cl)$]^+$	G-5mp	22 ± 2	-193 ± 6	[13]
Ru(Cl-terpy)en$(H_2O)]^{2+}$	G-5mp	69 ± 3	-45 ± 10	[11c]
	L-histidine	44 ± 4	-145 ± 12	[14]
	L-cysteine	44 ± 1	-155 ± 3	[15]
Ru(Cl-terpy)dach$(H_2O)]^{2+}$	G-5mp	51 ± 3	-101 ± 9	[11c]
	L-cysteine	38 ± 4	-178 ± 12	[15]
	1,2,4-triazole	59 ± 5	-155 ± 14	[15]
$[Ru(bipy)_2(OH_2)(PPh_3)]^{2+}$	Acetonitrile	15± 1	-19 ± 3	[16]
$[Ru(bipy)_2(OH_2)(P(i\text{-}Pr)_3)]^{2+}$	Acetonitrile	11 ± 1	-25 ± 4	[16]
[*Cis*-Ru$(bipy)_2(OH_2)_2]^{2+}$	Dimethylglyoxime	59 ± 9	-122 ± 27	[17]
	α-Furil dioxime	70 ± 9	-99 ± 26	[17]

where; G-5mp is guanosine-5'-monophosphate, en is ethylene diamine, hmb is hexamethylbenzene, dach is *trans*-1,2-diamminocyclohexane, bipy is 2,2'-bipyridyl, $P(i\text{-}Pr)_3$ is tri-isopropylphosphine, PPh_3 is triphenylphosphine, Cl-terpy is 4′-chloro-2,2′:6′,2″-terpyridine, pydc is 2,3-pyridinedicarboxylato

2.3.2 Determination of Activation Volume ($\Delta V^{\neq}$)

Activation volume ($\Delta V^{\neq}$) is a complementary parameter to $\Delta H^{\neq}$ and $\Delta S^{\neq}$ in the assignment of the mechanism of a chemical reaction. It is more accurate compared to $\Delta S^{\neq}$ because of extrapolation of data. Activation volume describes the difference in compressibility between

the ground state and the transition state.[9] The relationship between pressure and volume is described by the *equation* 2.32

$$dG + SdT = VdP \tag{2.32}$$

Under isothermal conditions, the partial derivative of dG with respect to the pressure applied yields

$$\left(\frac{d(\Delta G^{\circ})}{dP}\right)_T = \Delta V^{\circ} \tag{2.33}$$

where; ΔV° is the change in partial molar volumes between the reactants and products

From *equation* 2.28 (*vide supra*) $\Delta G^{\neq} = -\mathrm{RTln}K^{\neq}$. Therefore, *equation* 2.33 can be written as

$$\left(\frac{d(-RTlnK^{\neq})}{dP}\right)_T = \Delta V^{\circ} \tag{2.34}$$

Equation 2.34 can be simplified further to give

$$\left(\frac{d(-RTlnK^{\neq})}{dP}\right)_T = \frac{-\Delta V^{\circ}}{RT} \tag{2.35}$$

Since the equilibrium constant, $K^{\neq} = \frac{k_2}{k_{-2}}$, *equation* 2.35 becomes

$$\left(\frac{d(\frac{k_2}{k_{-2}})}{dP}\right)_T = \frac{-\Delta V^{\circ}}{RT} \tag{2.36}$$

Simplifying equation 2.36 gives

$$\left(\frac{d(lnk_2}{dP}\right) - \left(\frac{d(lnk_{-2})}{dP}\right) = \frac{-\Delta V^{\circ}}{RT} \tag{2.37}$$

$$\left(\frac{d(lnk_2}{dP}\right) - = \frac{-\Delta V^{\circ}}{RT} + \left(\frac{d(lnk_{-2})}{dP}\right) \tag{2.37a}$$

Therefore,

$$\left(\frac{d(lnk_2}{dP}\right) = \frac{-\Delta V^{\neq}}{RT} \tag{2.38}$$

On integrating *equation* 2.38 from $P = 0$ to $P = P$ and from $k_2 = (k_{-2})_0$ to $k_2 = k_2$ gives

$$\ln k_2 = \ln(k_{-2})_0 - \frac{\Delta V^{\neq}}{RT}P \tag{2.39}$$

A plot of $\ln k_2$ against P yields a straight line graph whose y-intercept and slope is $\ln(k_{-2})_0$ and $-\frac{\Delta V^{\neq}}{RT}$, respectively. The $\Delta V^{\neq}$ for the forward reaction is obtained from the slope. The y-intercept, $(k_{-2})_0$ gives the compressibility coefficient of the medium. A negative value of $\Delta V^{\neq}$ indicates an associative mechanism while a positive value indicate that the reaction proceed through a dissociative mechanism.[19] The challenge with $\Delta V^{\neq}$ in describing the mechanism of a chemical reaction is that it reflects intrinsic volume change that occurs in the reactants as well as volume changes that occur due to the reorganization of the solvent medium.[6, 9]

2.4 Factors Affecting the Rate of Substitution in Transition Metal Complexes

The substitution kinetic behavior of a transition metal complex is influenced by the stereo-electronic factors around the metal centre, the inherent properties of the incoming nucleophile and the chemical characteristics of the reaction medium.[12a, 12b, 14-18] These factors are discussed (*vide infra*).

2.4.1 Effects of Spectator Ligands

A spectator ligand does not participate in a chemical reaction but influences the reactivity of the complex. In octahedral systems spectator ligands at *trans* and *cis* positions relative to the leaving group have profound effect on the reactivity of a complex.[6] These effects are referred to as *trans*-effects and *cis*-effects, respectively.[9]

2.4.1.1 *Trans*-Effects

Trans-effect (kinetic *trans*-effect) refers to the effect of a coordinated ligand on the rate of substitution of a ligand *trans* to it. It affects the properties of a complex at the ground state as well as at the transition state. *Trans*-influence (structural *trans*-effect) on the other hand is the effect of the *trans*-ligand on the ground state properties such as bond length and infrared stretching frequencies on a ligand *trans* to it.[9, 20] Depending on the influencing ligand, *trans*-effect is classified as either σ-*trans*-effect or π-*trans*-effect.

In divalent ruthenium complex, *trans*-$[Ru(NH_3)_4(L)H_2O]^{2+}$, σ-*trans*-effect was evaluated by studying the labilising power of ligand L on the aqua leaving group. The labilising effect was found to increase with increase in the σ-donor ability of the *trans*-ligand L in the order; $CO \sim N_2 \ll acn < isn^{2} < Cl^{-} \sim pyridine \sim H_2O < imN^{3} \sim NH_3 < OH^{-} < CN^{-} < SO_3^{2-} < imC^{4}$. This is attributed to ground state destabilization of the Ru-OH_2 bond. As the σ-donicity of the *trans*-ligand (L) increase, more electron density is contributed to the shared p_x orbital thus weakening the Ru-OH_2 bond. Consequently, the lability of the aqua ligand increases accordingly.[9, 21]

Increase in π-acceptor character in the influencing ligand reduces its σ-*trans*-effect. Likewise, a π-acceptor ligand coordinated at *cis*-position to the leaving group decreases the σ-*trans*-influence of a *trans*-ligand.[22] This occur because the σ-inductive effect is partially cancelled by the strong metal-ligand charge transfer associated with π-back-donation.[23]

When a π-acceptor ligand is coordinated at *trans*-position to the leaving group, it is found to enhance the rate of substitution of the leaving group. This effect is referred to π-*trans*-effect. The enhancement is attributed to π-back-bonding of electron density from the dπ orbital largely based on the metal centre to the dπ* orbital based on the ligand. This makes the metal centre deficient of electron density hence promoting facile nucleophilic attack.[10, 24] A ligand exerting strong π-*trans*-effect stabilizes the transition state by lowering its energy.[9]

2.4.1.2 *Cis*- Effects

Ligands *cis* to the leaving group have both electronic and steric effect on the metal centre. The electronic c*is*-effect operate in two ways. First, when a π-acceptor ligand is coordinated at *cis*

[2] isonicotinamide

[3] N-coordinated imidazole

[4] C-coordinated imidazole

position to the leaving group it interferes with the ground state charge distribution on the complex by withdrawing electron density from the metal centre through π-back-donation. This enhances the positive charge on the metal centre thus facilitating nucleophilic attack.[25] The π-*cis* effect is usually smaller in magnitude compared to π-*trans* effect because the metal orbitals are utilized in the transmission of the effect. Contrarily, a σ-donor ligand at *cis* position to the leaving group has little effect on the ground-state charge distribution. However, it stabilizes the transition state by delocalizing the charge donated to the metal centre by the incoming nucleophile.[26] The steric -*cis* effects are discussed under steric factors.

2.4.1.3 Steric Effects

Steric effects caused by coordinated ligands around a reaction centre can either be steric bulkiness or steric hindrance. Steric bulkiness is caused by mutual repulsion of electron densities brought about by congestion of groups around the reaction centre. The magnitude of the steric effect caused by steric bulkiness is positively corelated the size of the group(s) causing it. On the other hand, steric hindrance refers to the shielding of a reaction centre from direct attack by an incoming group. The steric hindrance experienced by the incoming group depends on the size of the coordinated group, spatial orientation of the group relative to both the metal centre and the leaving group.[27]

In reactions that proceed through an associative mechanism, an increase in steric hindrance reduces their rate of reaction. This is because the upsurge in steric crowding around the metal centre destabilizes the transition state hence slowing down the reactivity. This is referred to as steric retardation.[28] It is more pronounced when the steric-causing substituent is located at *cis*-position to the leaving group than at *trans*-position.[9] For dissociative-activated reactions, an increase in steric interactions enhance the rate of substitution through steric acceleration because the steric hindrance is relieved in the transition state.[28] Therefore, steric crowding

around the metal centre can be used in distinguishing the substitution mechanisms involved in a chemical reaction.[6, 9]

2.4.2 Effect of the Entering Nucleophile

The rate of substitution in a metal complex is affected by the nucleophilicity of the entering group. Nucleophilicity is defined as the kinetic ability of a nucleophile in a substitution process.[29] The sensitivity of a metal centre to the nucleophilicity of an incoming group is described by the nucleophilic discrimination factor.[9] The nucleophilicity of a ligand is affected by several factors;

i. **The basicity of the ligand**: Basicity is a thermodynamic term describing the ability of an electron-rich species to displace an equilibrium and is characterized by acidity constants (p*K*a).[30] There exist a positive relationship between the basicity and nucleophilicity of a ligand. For instance; imidazole is a better nucleophile than pyrazole as indicated by their p*K*a values of 7.00 and 2.52, respectively.[29] This is further supported by the higher second order rate constants (k_2) obtained for imidazole compared to pyrazole in the substitution of the chloro ligand in a series of platinum based complexes.[31]

ii. **Polarizability**: Polarizability of a molecule is defined as the relative tendency of its electron cloud to be distorted by an electric field.[29, 32] Electrons in small-sized atoms are less polarizable and therefore have a lower van der Waals attraction for a given surface area of contact. On the contrary, larger atoms possess more diffuse electron density hence more polarizable. Soft (polarizable) nucleophiles prefer soft substrates and vice versa.[33] Polarizable molecules such as thiourea, iodide and other unsaturated species are more nucleophilic than non-polarizable molecules.[34] Since most kinetic investigations are done in solution, polarizable nucleophiles have an edge over non-polarizable nucleophiles because they easily undergo charge reorganization.

For instance; for halogenic ions their polarizability decreases in the order; $I^- > Br^- > Cl^-$; a trend that parallels rates of nucleophilic substitution when used as entering groups.[35]

iii. **Oxidizability**: It is a measure of the reducing power of a nucleophile as determined by electrochemical methods. It is positively corelated to the nucleophilicity of a ligand and therefore the higher the oxidizability the better the nucleophile.[36]

iv. **Steric demands**: Steric demands of the incoming nucleophiles play a key role on the rate of substitution in metal complexes. For example; the rate of substitution of chloro/aqua ligands using sulfur-based nucleophiles usually follow the order; thiourea > dimethylthiourea > tetramethylthiourea in line with increasing steric bulkiness of the nucleophile. Similarly, 1,2-dimethyl-imidazole reacts slower than 1-methyl-imidazole. As the bulkiness of the nucleophile increases, the steric hindrance increases accordingly hampering attack on the metal centre.[31, 35b, 37] However, in some cases dimethylthiourea has been found to be more reactive than thiourea because of its higher basicity which overcompensates the increased steric hinderance.[12a, 35a, 37]

2.4.3 Effects of the Leaving Group

The effect of the leaving group on the rate of a substitution reaction is depended on its nucleofugacity (leaving ability). Nucleofugacity of a ligand depends on its inherent lability as well as the labilising effects exerted on it by other ligands in the system. In addition, the leaving ability is influenced by the nature of the metal centre and the incoming nucleophile.[3]

In a reaction proceeding through dissociative mechanism, the rate has a large dependence on the nature of the leaving group because the metal-leaving group bond is broken in the transition state. In associatively activated reactions, the effect hinges on the extent of the bond breaking at the transition state and therefore has a minor role in determining the rate of the reaction. Nucleofugacity of a chemical species has a negative relationship with *trans*-effect because

trans-effect depends on the strength of the bonding and therefore strongly bound ligands break off more slowly.[9]

Chelate effect is also an important factor in nucleofugacity. As illustrated in Table 2.2, the rate of substitution of bidentate ligands are lower compared to monodentate ligands because complexes with chelating ligands are more stable than those with monodentate ligands. For example, the rate of substitution of 2,2'-bipyridyl ligand is 10^5 slower than pyridine ligand.[9, 38]

Table 2.2: Effects of chelate on substitution in octahedral nickel complexes.[9]

Complex	k_1 (s^{-1})
$Ni(py)_2$	38.5
Ni(bipy)	3.8×10^{-4}
$Ni(NH_3)_2$	5.8
Ni(en)	0.27

where; py is pyridine, bipy is 2,2'-bipridyl and en is ethylene diamine

2.4.4 Effect of the Solvent

In most substitution reactions the solvent is in large excess relative to the reactants. This make its molecules to coordinate the metal centre and constantly dissociate to give room for other ligand(s). If the solvent is a potential ligand, it has the capability of dominating the substitution process. Therefore, in choosing a solvent to be used as a medium in kinetic studies, it is important to understand the coordinating ability of the solvent.[39]

As shown in Table 2.3, solvents with high coordinating power such as pyridine and dimethyl sulfoxide react with the metal centre through a ligand independent path. They easily displace the leaving group and bind strongly to the metal center making them unfit for kinetic studies.[40] Conversely, substitution reactions performed in solvents with low coordinating abilities, proceed exclusively by direct nucleophilic attack on the metal centre.[9, 41]

Table 2.3: Commonly used solvents and their coordinating ability index (a^{TM}) in transition metals[41]

Solvent	Coordinating ability index (a^{TM})
Pyridine	1.4
Dimethyl sulfoxide	0.3
1-Propanol	0.0
Water	-0.1
Dimethylformamide	-0.2
Ethane-1,2-diol	-0.2
Acetonitrile	-0.2
Methanol	-0.4
Ethanol	-0.5
Benzene	-0.7
Acetone	-1.0
Phenol	-1.4

2.4.5 The Oxidation State of Central Metal.

The oxidation state of the metal centre plays a key role in the rate of substitution of the leaving group. Ruthenium(II) complexes are more reactive compared to ruthenium(III) because ruthenium(III) is more inert and therefore less attractive for nucleophilic attack.[3, 42] This is illustrated in Table 2.4.

Table 2.4: First order rate constant for the aquation of ruthenium(II) and ruthenium(III) complexes, *trans*-$[MLCl_2]^{n+}$

L	Ru(II) k_1 (s^{-1})	Ru(III), k_1 (s^{-1})
$(NH_3)_4$	1.00	1.7×10^{-6}
$(en)_2$	0.35	4.2×10^{-6}
pEn	0.07	4.8×10^{-7}

where; M is Ru(II)/Ru(III), n is either 2/3, en is ethylene diamine, pEn is N1-N1'-(propane-1,3-diyl)bis(ethane-1,2-diamine)[42]

2.5 Techniques used in Kinetic and Mechanistic Studies

Experimental methods used in studying the kinetic behavior of a chemical reaction do so by monitoring the change in concentration of at-least one species in the reaction mixture over time. The suitability of a method in kinetic investigations is dictated by the time scale of the chemical reaction. The appropriate detection method is determined by the properties of the species being monitored. An excellent detection method should be highly specific to the species of interest and applicable over a wide range of concentrations.[36] Ultraviolet-visible spectrophotometry, nuclear magnetic resonance spectrophotometry and stopped-flow have been utilized to study substitution reactions of ruthenium(II) complexes.[12a, 12b, 15]

2.5.1 Ultraviolet-Visible Spectrophotometry

It is a highly sensitive analytical technique that is able to detect accurately concentrations in the range of 10^{-4} to 10^{-6} M.[6] It is suitable for kinetic studies of slow reaction; a reaction that takes at-least 16 minutes to complete.[43] It is based on the fact that chemical species containing π or non-bonding electrons are able to absorb ultraviolet or visible light which causes excitation of the electrons to higher molecular levels. These transitions include; $\sigma \rightarrow \sigma^*$ $\pi \rightarrow \pi^*$, $n \rightarrow \sigma^*$ and $n \rightarrow \pi^*$. The lower the energy gap between the frontier orbitals, the lower the energy of the absorbed light.[44]

A diagrammatic representation of a double beam ultraviolet-visible spectrophotometer is shown in Figure 2.6. Key component of ultraviolet-visible spectrophotometer are light sources (visible and ultraviolet), monochromator, reference and sample compartments, detector, data processor, display unit and temperature control unit.

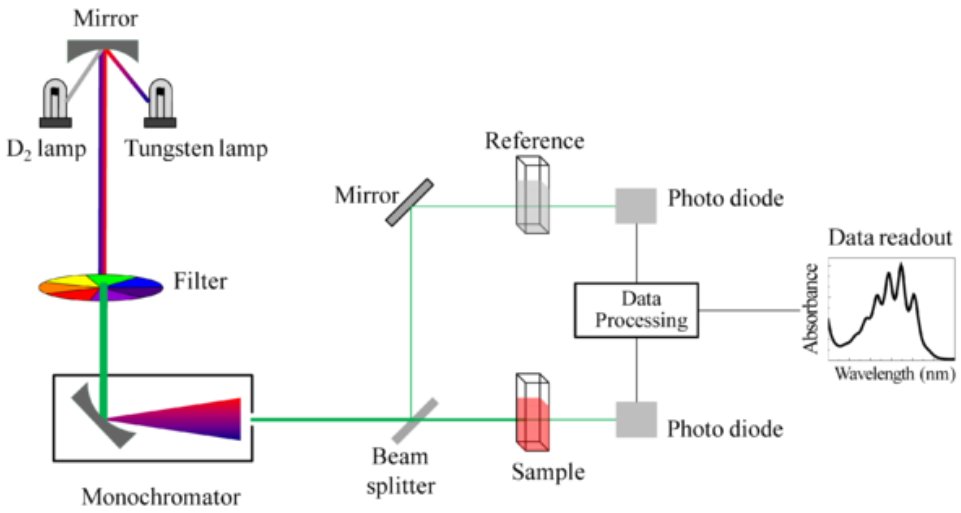

Figure 2.6: A diagram showing the components of a double beam ultraviolet-visible spectrophotometer.[45]

The visible light is supplied by a tungsten lamp while ultraviolet light source is a deuterium arc lamp with a quartz envelop.[46] The radiation from the light sources passes through a monochromator which produce a single wavelength beam. The monochromatic beam produced is split into two sub-beams; one passes through the reference cell while other passes through the sample cell before striking two harmonized detectors. Samples and reference solutions are usually analyzed in fused joint glass or quartz cells. The cell holder aligns the sample in the path of the beam of light to ensure reproducible and precise interaction.[47] The commonly used detectors are photo-diodes comprising of doped silicon strips in reverse bias. They are robust and have low power supply and control circuit demands.[48] Compared to a single beam, double beam spectrophotometers compensate for short term fluctuations in the intensity of the radiation produced. Therefore, they are well suited for continuous recording of the absorption spectra over time such as in kinetic studies.[47]

Ultraviolet-visible spectrophotometer works by measuring the amount of light transmitted (T) through the analyzed sample. Transmittance, a ratio of the intensity of transmitted light to that of the incident light is described by *equation* 2.40

$$T = \frac{I}{I_0} \quad 2.40$$

where; I_0 is the incident light intensity at a particular wavelength, λ

I is the transmitted light intensity at a particular wavelength, λ

The absorbance (A) is then calculated from the transmittance and displayed on the ultraviolet-visible spectrophotometer display unit. The relationship between transmittance and absorbance is shown in *equation* 2.41 and 2.41a

$$\mathrm{A} = -\log T \quad 2.41$$

$$= \log\left(\frac{I_0}{I}\right) \quad 2.41a$$

When the absorbance (A) of a reaction mixture is known, the time resolved concentration spectrum of the reaction can be determined using the Beer–Lambert–Bouguer law (*equation* 2.42)

$$A = \varepsilon \mathrm{cb} \quad 2.42$$

where; A is the absorbance,

ε is extinction coefficient, $\mathrm{Lmol^{-1}cm^{-1}}$

c is the concentration of the sample, M

b is the path length of the sample, cm (usually 1 cm)

Consider the first order reaction involving the conversion of reactant C to product D shown in *expression* 2.43

$$\mathrm{C} \xrightarrow{k_1} \mathrm{D} \quad 2.43$$

At initiation of the reaction, $t = 0$, the absorbance of the reaction mixture is given by

$$A_0 = \varepsilon_C[C]_0 + \varepsilon_D[D]_0 \quad 2.44$$

At any time, t, the absorbance of the reaction mixture becomes

$$A_t = \varepsilon_C[C]_t + \varepsilon_D[D]_t \quad 2.45$$

Upon completion of the reaction, the absorbance of the reaction mixture is given by

$$A_\infty = \varepsilon_D([C]_0 + \varepsilon_D[D]_0) \quad 2.46$$

where; $\varepsilon_C, \varepsilon_D$ are the molar absorptivity of species C and D, respectively

$[C]_0$ and $[D]_0$ are the initial concentration of species C and D, respectively.

The direct relationship between the concentration and optical absorbance as shown by the Beer–Lambert–Bouguer law (*equation* 2.42), allows the derivation of the rate law in terms of the physically measurable optical absorbance. When a reaction (*equation* 2.43) follows first order kinetics, the integrated rate law can either be expressed in terms of concentration or optical absorbance as shown in *equation* 2.47

$$ln\frac{[C]_0}{[C]_t} = \ln\left(\frac{A_0 - A_\infty}{A_t - A_\infty}\right) = k_{obs}t \quad 2.47$$

The time-resolved absorbance data, can therefore be directly used to determine the first order rate constant (k_{obs}).[28] This is achieved by fitting the data into an appropriate exponential function using non-linear square regression. Typical ultraviolet-visible spectra recorded during the substitution reaction of [(*p*-cymene)Ru(2,2'-bipyridyl)(H_2O)]$^{2+}$ with dimethylthiourea is shown in Figure 2.7. The inset shows a kinetic trace obtained at λ = 455 nm. The *pseudo*-first order rate constant (k_{obs}) was obtained by fitting the trace into a single exponential function.

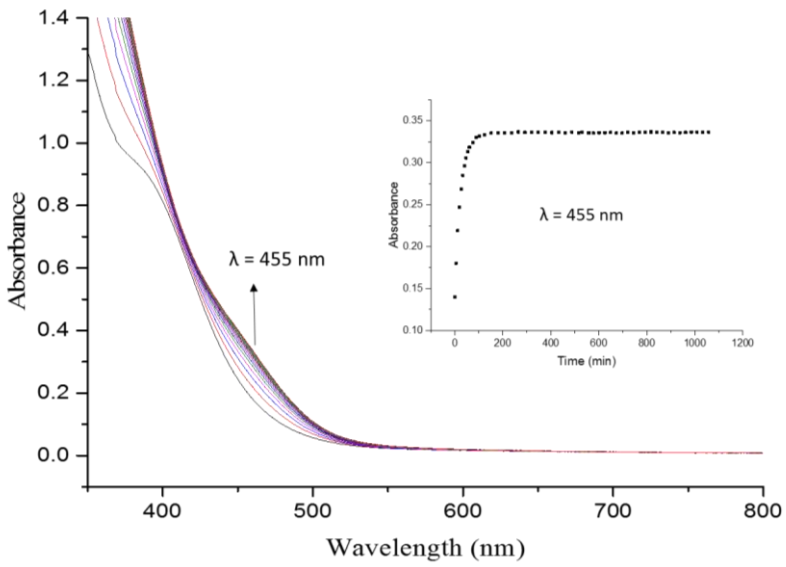

Figure 2.7: Ultraviolet-visible spectra for the reaction of [(p-cymene)Ru(2,2'-bipyridyl)$(H_2O)]^{2+}$ with dimethylthiourea. **Inset:** Kinetic trace at λ = 455 nm. Data is part of results reported in Chapter Five

Apart from kinetic studies, ultraviolet-visible spectrophotometry is used for acid-base titrations to determine acid dissociation constants (p*K*a values).[12a, 37] The change in absorbance is monitored as the acidity of the solution is varied. The absorbance-pH resolved data is fitted to an appropriate sigmoid equation to obtain the p*K*a values.

2.5.2 Stopped-Flow Technique

It is ideal for kinetic studies of rapid reactions whose half-life range between 10^0 to 10^3 s. It is designed to use very small sample volumes (~ 0.2 mL).[28] A schematic diagram of stopped flow apparatus is shown in Figure 2.8. A stopped flow analyzer works on the principle of fluid dynamics.[47] The reactants are usually placed in two separate thermally equilibrated drive syringes. A high pressure of about 800 KPa is applied to force the reactants into the mixing chamber where they are rapidly mixed in ~10^{-3} s.[28] The mixed solution immediately proceeds into the observation chamber eventually flowing into the stopping syringe. Once the stopping syringe is filled, the stopping block is activated and flow is abruptly stopped.[47]

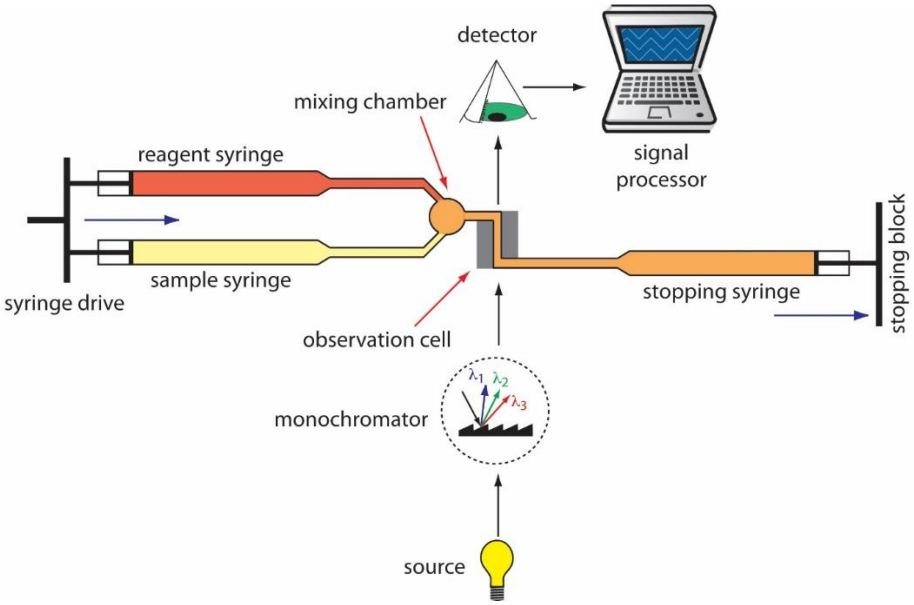

Figure 2.8: A diagram showing the components of a stopped-flow apparatus.[49]

The mixed solution is monitored and detected spectrophotometrically by light that passes through the observation chamber into the detector. Changes in absorbance caused by variation in the intensity of the transmitted light is promptly recorded as absorbance versus time trace.

The kinetic traces are processed and the first-order rate constants calculated by an online program. After the reaction is completed, the spent solution is ejected through a drain tube.[28] A typical stopped-flow kinetic trace for the reaction of [(*p*-cymene)Ru(H_2O)$_3$]$^{2+}$ with thiourea is shown in Figure 2.9.

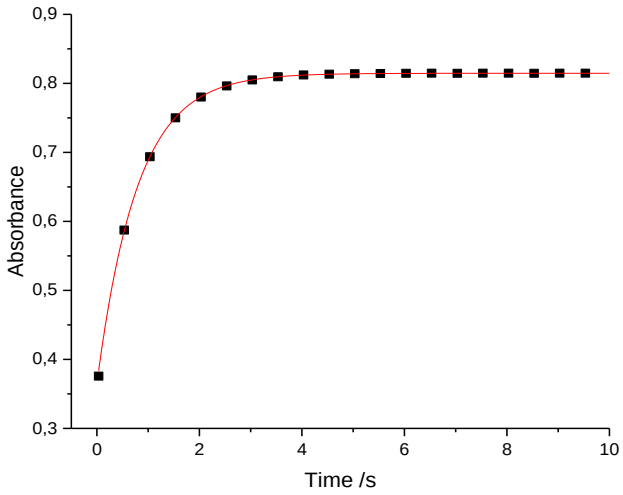

Figure 2.9: Stopped flow kinetic trace for reaction of [(*p*-cymene)Ru(H_2O)$_3$]$^{2+}$ with thiourea

2.6 References

[1] J. E. House, *Principles of Chemical Kinetics*, Elsevier Inc., USA, **2007**, pp. 1-30.

[2] T. Harris, M. Keshwani, in *Methods in Enzymology, Vol. 463*, Elsevier, **2009**, pp. 57-71.

[3] M. L. Tobe, J. Burgess, *Inorganic Reaction Mechanisms*, Addison Wesley Longman, New York, **1999**, pp. 19-20, 30-39, 70-112, 128-204.

[4] L. G. Arnaut, S. J. Formosinho, H. Burrows, *Chemical Kinetics: from Molecular Structure to Chemical Reactivity*, Elsevier, Amsterdam, The Netherlands, **2006**, pp. 273-294.

[5] C. H. Langford, H. B. Gray, *Ligand substitution processes*, WA Benjamin, Inc., New York, **1966**, pp. 1-90.

[6] D. Katakis, G. Gordon, *Mechanisms of Inorganic Reactions*, **1987**, pp. 58-128, 175-176, 198-210.

[7] D. Shriver, P. Atkins, C. Langford, *Inorganic Chemistry Oxford University Press*, 5th Edition ed., Oxford University Press, New York, **2010**.

[8] O. A. El Seoud, W. J. Baader, E. L. Bastos, *Encyclopedia of Physical Organic Chemistry* **2016**, 1-68.

[9] J. D. Atwood, *Inorganic and Organometallic Reaction Mechanisms*, 2nd ed., VCH Publishers, **1997**, pp. 1-18, 47-90.

[10] A. Hofmann, L. Dahlenburg, R. van Eldik, *Inorganic Chemistry* **2003**, *42*, 6528-6538.

[11] M. Twigg, in *Mechanisms of Inorganic and Organometallic Reactions*, Springer, **1989**, pp. 219-246.

[12] (a) F. Tiba, D. Jaganyi, A. Mambanda, *Journal of Coordination Chemistry* **2010**, *63*, 2542-2560; (b) L. Dadci, H. Elias, U. Frey, A. Hoernig, U. Koelle, A. E. Merbach, H. Paulus, J. S. Schneider, *Inorganic Chemistry* **1995**, *34*, 306-315; (c) A. Rilak, I. Bratsos, E. Zangrando, J. Kljun, I. Turel, Z. i. D. Bugarčić, E. Alessio, *Inorganic Chemistry* **2014**, *53*, 6113-6126.

[13] (a) S. Asperger, *Chemical Kinetics and Inorganic Reaction Mechanisms* Springer science, New York, **2003**, pp. 38-39, 105-106, 140-153; (b) H. Eyring, *The Journal of Chemical Physics* **1935**, *3*, 107-115; (c) M. G. Evans, M. Polanyi, *Transactions of the Faraday Society* **1935**, *31*, 875-894.

[14] A. Rilak, B. Petrović, S. Grgurić-Šipka, Ž. Tešić, Ž. D. Bugarčić, *Polyhedron* **2011**, *30*, 2339-2344.

[15] D. Lazić, A. Arsenijević, R. Puchta, Ž. D. Bugarčić, A. Rilak, *Dalton Transactions* **2016**, *45*, 4633-4646.

[16] A. Rilak, R. Puchta, Ž. D. Bugarčić, *Polyhedron* **2015**, *91*, 73-83.

[17] R. A. Leising, J. S. Ohman, K. J. Takeuchi, *Inorganic Chemistry* **1988**, *27*, 3804-3809.

[18] T. Das, B. Bera, A. Datta, A. Ghosh, *Transition Metal Chemistry* **2009**, *34*, 247-253.

[19] T. Swaddle, *Inorganic Chemistry* **1980**, *19*, 3203-3205.

[20] B. J. Coe, S. J. Glenwright, *Coordination Chemistry Reviews* **2000**, *203*, 5-80.

[21] J. A. Marchant, T. Matsubara, P. C. Ford, *Inorganic Chemistry* **1977**, *16*, 2160-2165.

[22] F. Hartley, *Chemical Society Reviews* **1973**, *2*, 163-179.

[23] T.-G. Appleton, H. Clark, L. Manzer, *Coordination Chemistry Reviews* **1973**, *10*, 335-422.

[24] D. Jaganyi, A. Hofmann, R. van Eldik, *Angewandte Chemie International Edition* **2001**, *40*, 1680-1683.

[25] U. Belluco, L. Cattalini, F. Basolo, R. G. Pearson, A. Turco, *Journal of the American Chemical Society* **1965**, *87*, 241-246.

[26] L. Cattalini, M. Martelli, *Inorganica Chimica Acta* **1967**, *1*, 189-192.

[27] (a) R. Romeo, D. Minniti, M. Trozzi, *Inorganic Chemistry* **1976**, *15*, 1134-1138; (b) R. Romeo, D. Minniti, M. Trozzi, *Inorganica Chimica Acta* **1975**, *14*, L15-L16; (c) R. Romeo, M. Tobe, M. Trozzi, *Inorganica Chimica Acta* **1974**, *11*, 231-236.

[28] R. G. Wilkins, *Kinetics and Mechanisms of Reactions of Transition Metal Complexes*, VCH Publishers, **1991**, pp. 87-158.

[29] A. Streitwieser, C. H. Heathcock, E. M. Kosower, P. J. Corfield, *Introduction to Organic Chemistry*, Macmillan New York, New York, **1992**, pp. 140-145, 166-169, 643.

[30] J. Harris, S. McManus, in *Nucleophilicity Advances in Chemistry Series, Vol. 215*, American Chemical Society, Washington, DC, Washington,DC, **1987**, pp. 1-20.

[31] (a) A. Shaira, D. Reddy, D. Jaganyi, *Dalton Transactions* **2013**, *42*, 8426-8436; (b) D. Reddy, K. J. Akerman, M. P. Akerman, D. Jaganyi, *Transition Metal Chemistry* **2011**, *36*, 593-602.

[32] M. Salanne, R. Vuilleumier, P. A. Madden, C. Simon, P. Turq, B. Guillot, *Journal of Physics: Condensed Matter* **2008**, *20*, 494207 (494208pp).

[33] R. G. Pearson, *Journal of the American Chemical Society* **1963**, *85*, 3533-3539.

[34] J. O. Edwards, R. G. Pearson, *Journal of the American Chemical Society* **1962**, *84*, 16-24.

[35] (a) D. Jaganyi, F. Tiba, O. Q. Munro, B. Petrović, Ž. D. Bugarčić, *Dalton Transactions* **2006**, 2943-2949; (b) P. Ongoma, D. Jaganyi, *Dalton Transactions* **2012**, *41*, 10724-10730.

[36] R. B. Jordan, *Reaction Mechanisms of Inorganic and Organometallic Systems*, 3rd ed., Oxford University Press, **2007**, pp. 422-455.

[37] A. Hofmann, D. Jaganyi, O. Q. Munro, G. Liehr, R. van Eldik, *Inorganic Chemistry* **2003**, *42*, 1688-1700.

[38] R. G. Wilkins, *Accounts of Chemical Research* **1970**, *3*, 408-416.

[39] M. L. Tobe, *Reaction Mechanisms in Inorganic Chemistry*, Thomas Nelson and sons **1972**, pp. 83-107.

[40] M. D. Hall, K. A. Telma, K.-E. Chang, T. D. Lee, J. P. Madigan, J. R. Lloyd, I. S. Goldlust, J. D. Hoeschele, M. M. Gottesman, *Cancer Research* **2014**, *74*, 1-10.

[41] R. Díaz-Torres, S. Alvarez, *Dalton Transactions* **2011**, *40*, 10742-10750.

[42] (a) C.-K. Poon, C.-M. Che, Y.-P. Kan, *Journal of the Chemical Society, Dalton Transactions* **1980**, 128-133; (b) C. K. Poon, D. A. Isabirye, *Journal of the Chemical Society, Dalton Transactions* **1977**, 2115-2120.

[43] D. Reddy, University of Kwazulu Natal (Pietermaritzburg), **2009**.

[44] C. Knowles, A. Knowles, *Practical Absorption Spectrometry: Ultraviolet Spectrometry Group*, Springer Science & Business Media, **2013**, pp. 6-19.

[45] A. M. Crasto, in *https://orgspectroscopyint.blogspot.com/p/basics-of-uv-visible-spectroscopy.html*, Accessed on 06.08.2018.

[46] G. Gauglitz, *Ultraviolet and Visible Spectroscopy*, Wiley-VCH Verlag GmbH & Co. KGaA, Weinheim, Germany, **2000**, pp. 552-576.

[47] D. A. Skoog, D. M. West, F. Holler, S. R. Crouch, *Fundamentals of Analytical Chemistry*, 8th ed., Thompson Learning, Singapore, **2004**, pp. 771-807, 892-900.

[48] H.-H. Perkampus, *UV-VIS Spectroscopy and its Applications*, Springer Science & Business Media, Berlin **2013**, pp. 10-24.

[49] D. Harvey, in *Image and Video exchange Forum*, *http://community.asdlib.org/imageandvideoexchangeforum/2013/08/04/instrumentation-for-kinetic-methods-of-analysis*, Accessed on 08.08.2018

CHAPTER THREE

The Role of π-Extension of the Auxiliary Ligand on the Reactivity of Ruthenium(II) Terpyridyl Complexes: Kinetic and Mechanistic studies

Abstract

Substitution kinetics of the aqua ligand in four mono-functional terpyridine-based ruthenium(II) complexes with different auxiliary ligands was investigated using biorelevant nucleophiles, *viz*; thiourea, *N*,*N*-dimethylthiourea and *N,N,N',N'*-tetramethylthiourea. Concentration and temperature dependence studies were done under *pseudo*-first order conditions using the ultraviolet-visible spectrophotometric technique. In all the reactions, the observed rates of substitution obeyed the rate law, $k_{obs} = k_2$[Nucleophile]. The reactivity of the complexes decreased in the order: **Ru-4** > **Ru-3** > **Ru-1** > **Ru-2**. This study has established that an increase in the π-conjugation of the N^N bidentate ligand accelerates the rate of substitution of the aqua ligand. This is accounted by increase in π-back-donation from the metal to the empty π* orbital of the ligands as the π-extension increases which also increases the electrophilicity of the complexes. The increased steric hindrance to the incoming nucleophile introduced by the bipyridyl ligand is responsible for the retarded reactivity of **Ru-2** as compared to **Ru-1** which has two separate *trans* pyridyl rings as auxiliary ligands. Therefore, the metal centre in **Ru-1** is more exposed to nucleophilic attack than in **Ru-2**. The results from DFT-calculations show that as the π-conjugation of the auxiliary ligand is increased from **Ru-1** to **Ru-4**, the energy separation between the frontier orbitals decrease. This enhances the chemical softness and electrophilicity of the complexes. Likewise, the p*K*a values of the complexes decrease from **Ru-1** to **Ru-4**, pointing out to increase in electrophilicity of the complexes in that order. Consequently, nucleophilic attack become facile from **Ru-1** to **Ru-4**.

The activation parameters ($\Delta H^{\neq} > 0$, $\Delta S^{\neq} < 0$) for all the complexes support an associative mechanism. The solid-state crystal structure of $[Ru(terpy)(bipy)Tu)](ClO_4)_2$ show that the thiourea ligand is coordinated to the metal centre via the S donor atom and the substitution product formed is stable; i.e. none of the coordinated ligands is induced to dechelate from the ruthenium(II) metal centre.

3.1 Introduction

Ruthenium based complexes are well suited for medical applications due to their rich and well-established coordination chemistry as well as their ability to exist in variable oxidation states (II, III, and IV) under physiological conditions.[1] They have been considered as viable alternatives to platinum based chemotherapeutic agents due to their superior activity against metastatic cancer of the colon, low toxicity to normal cells, high selectivity for cancer cells, ability to overcome resistance induced by platinum-based agents, high cellular uptake, and the ability to mimic iron in binding biomolecules.[1c, 2]

Polypyridyl ruthenium complexes form one of the most important classes of explored ruthenium-based anticancer agents.[3] Polypyridyl ruthenium complexes with labile chloro group(s) have been exploited due to their ability to bind to DNA in two-step process like *cisplatin*. The first step is the substitution of the chloro ligand(s) by aqua ligand(s) and the second step is nucleobase binding.[4] Since polypridyl ligands determine the shape and chirality of a complex, they can be utilized to achieve desired cellular uptake and DNA-binding properties of a complex. This is so because DNA binding affinity of their complex increases with increase in the aromatic π- surface area of ligands.[3, 5] Similarly, the cellular uptake and anticancer activities of antitumour agents are positively corelated to the π-surface of the complex.[6] Among the ruthenium polypyridyl complexes, terpyridine coordinated complexes have shown high cytotoxicity against different human tumour cell lines and potential of being anticancer agents.[4a, 5b, 7]

Literature is available detailing the effects of peripheral substituents and π-conjugation on the terpyridine framework on the reactivity of metal complexes especially square planar platinum(II) complexes.[8] These investigations have shown that electron withdrawing substituents accelerate the displacement of the labile ligand by making the complex more electrophilic while electron donating groups have an opposite effect.[8a-c]

On the other hand, the effect of π-conjugation on the reactivity of terpyridine based metal complexes depend on its location on the terpyridine framework. For instance; a quinoline moiety at the lateral position in square planar platinum(II) complexes dampens the reactivity by destabilizing the LUMO.[8] Contrarily, a phenyl ring placed between the terminal and central pyridine rings in the terpyridine backbone increases the π-acceptor ability of the ligand system hence accelerating the displacement of the labile ligand.[8d] However, there is limited information on the effects of π-conjugation on the reactivity of octahedral terpyridine based ruthenium(II) systems. In addition, the role of auxiliary ligands on the reactivity of these octahedral complexes is not well established.[7d, 9].

Most metallodrugs are delivered intravenously into biological fluids where they encounter an array of biomolecules which play critical roles in their distribution, in particular the ultimate concentration reaching the DNA, the anticancer target site. Intercellular molecules which may interact with metallodrugs include sulfur-based compounds such as cysteine and glutathione.[10] These anticipated interactions can be tuned by a careful choice of the chelating ligands around the metal center.

Taking into consideration the biomedical and pharmaceutical applications of terpyridine,[11] this study utilizes it as the backbone ligand to investigate and understand the effect of π-extension of the auxiliary ligand on the reactivity of octahedral ruthenium(II) complexes. The study was conducted under *pseudo*-first order conditions using bio-relevant nucleophiles *viz*: thiourea, *N,N*-dimethylthiourea and *N,N,N',N'*-tetramethylthiourea. The rigid auxiliary N/N^N ligands used are; pyridine (**Ru-1**), 2,2'-bipyridine (**Ru-2**), 2-(2-pyridyl)quinoline (**Ru-3**) and 2,2' biquinoline (**Ru-4**). The studied complexes are shown in Figure 3.1.

Hydrolysis of Ru-Cl bond is an important step in the activation of metal based anticancer agents in their interaction with DNA.[12] Furthermore, it promotes cellular uptake of metallodrugs effectively enhancing their efficacy.[13] Noting, the importance of this process, all the complexes studied herein were converted into their respective aqua species.

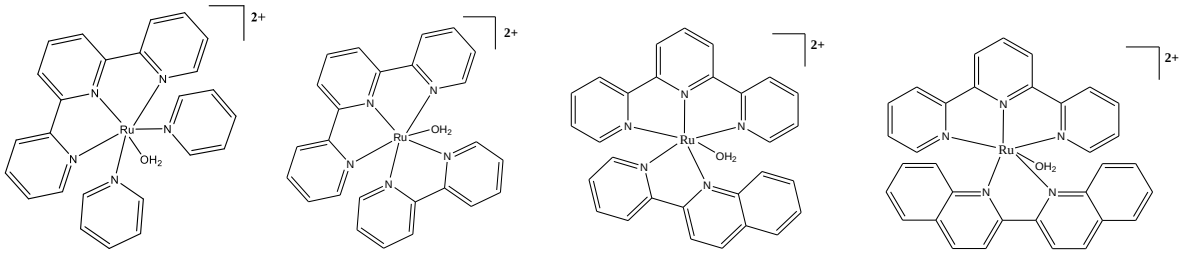

Ru-1 **Ru-2** **Ru-3** **Ru-4**

Figure 3.1: Structures of investigated ruthenium(II) complexes

Neutral thiourea nucleophiles were chosen because of their biological importance, high solubility and nucleophilicity.[14] The use of thiourea in drug delivery[10a] and its high affinity for metal ions such as ruthenium(II), motivated the investigation of the solid-state structure of the product formed when it substitutes the aqua ligand from the ruthenium(II) complexes. To gain an in-depth understanding of the electronic and structural properties of the complexes, computational studies using density functional theory was also done.

3.2 Experimental

3.2.1 Materials and Procedures

All the syntheses were performed under dry N_2 atmosphere using standard Schlenk techniques. $RuCl_3.3H_2O$, 2,2':6',2'-terpyridine (terpy) (98%), anhydrous pyridine (99.8%), 2,2'-bipyridyl (bipy) (99%), 2,2'-biquinoline (98%), NH_4PF_6 (≥ 99%), LiCl (≥ 99%), $NaBF_4$ (98%), $HClO_4$ (70 wt % solution), HCl (37%), NaOH (≥ 97%), $AgClO_4$ (99%), $NaClO_4.H_2O$ (98%), triphenylphosphine (99%), triethylamine (≥ 99.5%), Tu (≥ 99%), Dmtu (99%) and Tmtu (98%) were supplied by Sigma-Aldrich. 2-(2-pyridyl)quinoline was synthesized according to a

published literature method[15] (Supplementary Information, SI 3.1). Organic solvents were purchased from Merck (Pty) and used without further purification. Deionized water was used throughout the study.

3.2.2 Synthesis of the Complexes

The complexes were synthesized according to published literature methods.[16]

Trichloro(2,2':6',2''-terpyridyl)ruthenium(III): Equimolar amounts of $RuCl_3.3H_2O$ (262 mg, 1.0 mmol) and 2,2':6',2''-terpyridine (233 mg, 1.0 mmol) in 60 mL absolute ethanol were refluxed with vigorous stirring for 4 h. After cooling to ambient temperature, the fine brown powder formed was filtered off, washed with ethanol (3 × 30 mL) and diethyl ether (3 × 30 mL). The product was then dried under reduced pressure. Yield (86%). The complex was used as a precursor in the synthesis of all the other complexes without further purification or characterization.

***Trans*-chloro*bis*(pyridine)(2,2':6',2''-terpyridyl)ruthenium(II) hexaflourophosphate:** A mixture of trichloro(2,2':6',2''-terpyridyl)ruthenium(III) (200 mg, 0.45 mmol), triphenylphosphine (472 mg, 18 mmol) and triethylamine (1 mL) in 40 mL of chloroform was refluxed for 3 h to obtain a violet solution. After cooling the solution to room temperature, 30 mL of absolute ethanol was added and the resulting solution concentrated to about 10 mL. The violet solids obtained were filtered off and re-dissolved in minimum volume of warm chloroform/ethanol (1:1) mixture and precipitated by diethyl ether as a dark violet solid. The solid was further dissolved in 50 mL of pyridine and refluxed for 2 h after which the solution was evaporated to dryness. The residue was thereafter dissolved in 30 mL of water from which salt of pure complex was precipitated by addition of a saturated solution of NH_4PF_6. The product was filtered off and washed with diethyl ether and dried under vacuum. Yield (168 mg, 56%). *Anal. Calc.* for $C_{25}H_{21}ClN_5PF_6Ru$; C, 44.62; H, 3.15; N, 10.41. *Found*: C, 44.38; H, 3.21; N, 10.28. ^{1}H NMR (400 MHz, DMSO-d_6): δ (ppm) = 9.19 (d, 2H), 8.66 (m, 4H), 8.15 (t,

2H), 8.01 (t, 1H), 7.93 (d, 4H), 7.86 (t, 2H), 7.60 (t, 2H), 7.09 (t, 4H). ^{13}C NMR (400 MHz, DMSO-d_6): δ (ppm) = 160.9, 158.9, 152.7, 152.2, 137.9, 137.4, 132.5, 129.2, 125.1, 124.7, 124.1. ESI-MS (*m/z*): 528.00 (M^+).

(2,2'-Bipyridyl)chloro(2,2':6',2"-terpyridyl)ruthenium(II) chloride: In 40 mL absolute ethanol/water (75-25%) solvent mixture, trichloro(2,2':6',2''-terpyridyl)ruthenium(III) (400 mg, 0.91 mmol), 2,2-bipyridine (142 mg, 0.91 mmol), LiCl (212 mg, 5 mmol) and trimethylamine (1 mL) were refluxed for 4 h. The obtained solution was filtered while hot and the volume of the filtrate reduced to about 10 mL. After chilling the solution at 4℃ for 48 h, the solid formed was filtered off and washed with 3 M HCl (2 × 10 mL), acetone (30 mL), and copious amount of diethyl ether and dried under vacuum. Yield: 352 mg (69%). *Anal*. *Calc*. for $C_{25}H_{19}Cl_2N_5Ru.2H_2O$; C, 50.26; H, 3.88; N, 11.72. *Found*: C, 49.91; H, 3.97; N, 11.64. ^{1}H NMR (400 MHz, DMSO-d_6): δ (ppm) = 10.11 (d, 1H), 8.94 (d, 1H), 8.84 (d, 2H), 8.71 (d, 2H), 8.66 (d, 1H), 8.38 (t, 1H), 8.24 (t, 1H), 8.08 (t, 1H), 8.00 (t, 2H), 7.79 (t, 1H), 7.63 (d, 2H), 7.40 (t, 2H),7.33 (d, 1H), 7.10 (t, 1H). ^{13}C NMR (400 MHz, DMSO-d_6): δ (ppm) = 158.9, 158.8, 157.9, 156.2, 152.4, 152.3, 152.0, 137.5, 137.1, 136.0, 134.3, 127.9, 127.4, 126.9, 124.2, 123.9, 123.2. ESI-MS (TOF) (*m/z*): 526.04 (M^+).

***Proximal*-Chloro(2-(2-pyridinyl)quinoline)(2,2':6',2''-terpyridyl)ruthenium(II) chloride**: In 40 mL absolute ethanol/water (75-25%) solvent mixture, trichloro(2,2':6',2''-terpyridyl)ruthenium(III) (200 mg, 0.45 mmol), 2-(2-pyridinyl)quinoline (93 mg, 0.45 mmol), LiCl (19 mg, 0.45 mmol) and trimethylamine (0.1 mL) were refluxed for 5 h. The resulting purple solution was filtered while hot to remove unreacted materials and the filtrate concentrated to about 5 mL. The cooled concentrated solution was refrigerated for 48 h after which the purple precipitate which formed was filtered off. The product was washed with 3 M HCl (0.1 mL), acetone (2.5 mL) and diethyl ether (10 mL). Yield: (230 mg, 71%). *Anal*. *Calc*. for $C_{29}H_{21}ClN_5PF_6Ru.H_2O$; C, 47.13; H, 3.14; N, 9.48. *Found*: C, 47.02; H, 3.45; N, 9.37. ^{1}H

NMR (500 MHz, Cd_3Od-d_4): δ (ppm) = 10.65 (d, 1H), 9.03 (d, 1H), 8.93-8.85 (m, 4H), 8.75 (d, 2H), 8.36 (d, 1H), 8.29 (t, 1H), 8.04 (t, 2H), 7.94-7.87 (m, 5H), 7.76 (d, 1H), 7.38 (t, 2H), 7.23 (t, 1H). ^{13}C NMR (500 MHz, Cd_3Od-d_4): δ (ppm) = 160.2, 159.0, 158.9, 157.2, 152.9, 151.6, 151.0, 138.3, 137.3, 135.2, 131.0, 129.8, 129.0, 128.4, 127.2, 125.9, 125.0, 123.7, 122.6, 118.9. ESI-MS (TOF) (*m/z*): 576.5 (M^+).

(2,2'-Biquinoline)chloro(2,2':6',2"-terpyridyl)ruthenium(II) hexafluorophosphate: Equimolar amounts of trichloro(2,2':6',2''-terpyridyl)ruthenium(III) (200 mg, 0.45 mmol), 2,2'-biquinoline (115.3 mg, 0.45 mmol) together with LiCl (20 mg, 0.47 mmol) and trimethylamine (0.1 mL) in 40 mL absolute ethanol/water (75-25%) solvent mixture were refluxed for 5 h. The resultant solution was filtered while hot to remove insoluble by-products and unreacted materials. About 5 mL of aqueous saturated solution of $NaBF_4$ was added to the filtrate and the resulting solution refrigerated overnight. The solution was re-filtered, reduced to about 10 mL and the solids that appeared filtered off. The solids were then dissolved in methanol/dichloromethane (10-90%) solvent mixture and flushed through an alumina column, where the front purple-blue band was collected. An equal volume of toluene was added to the extract and the resultant solution concentrated to about 5 mL. The solid which formed was filtered off, washed with toluene and diethyl ether and dried under vacuum. Yield: (198 mg, 57%). *Anal*. *Calc*. for $C_{33}H_{23}ClN_5PF_6Ru$; C, 51.40; H, 3.01; N, 9.08. *Found*: C, 51.78; H, 3.21; N, 8.95. ^1H NMR (400 MHz, Cd_3od-d_4): δ (ppm) = 9.90 (d, 1H), 9.11 (d, 1H), 9.01 (d, 1H), 8.82(d, 1H), 8.76 (d, 2H), 8.60 (d, 2H), 8.37 (d, 2H), 8.28 (t, 1H), 8.02-7.84 (m, 8H), 7.53 (t, 1H), 7.42 (t, 2H), 6.94 (d, 1H). ^{13}C (400 MHz, Cd_3od-d_4): δ (ppm) = 161.8, 159.3, 159.0, 156.1, 152.5, 151.8, 151.1, 138.3, 137.4, 136.9, 136.3, 135.4, 130.7, 130.3, 129.6, 129.0, 128.5, 128.3, 127.5, 127.0, 123.5, 122.5, 120.2, 119.1. ESI-MS (TOF) (*m/z*): 626.06 (M^+).

3.2.3 Physical Measurements and Instrumentation

Bruker Avance DPX III 400/500 MHz spectrometer fitted with 5 mm probe was used to record mono-dimensional NMR spectra of the complexes at 30 ℃. All the chemical shifts were expressed in parts per million (ppm) and referenced to trimethylsilane. Mass spectra were recorded in the positive mode on an electrospray ionization time of flight Micromass spectrometer. Sample MS and NMR spectra are presented in the Supplementary Information (Figures SI 3.9-3.19). Elemental analyses of C, H, and N of the complexes were done by Thermo Scientific Flash 2000 analyzer. Agilent technologies Cary 100 Series ultraviolet-visible spectrophotometer equipped with a temperature control unit (accuracy of ± 0.05 ℃) was used for acid-base titrations and monitoring the kinetics of the reactions. Jenway 4330 pH/conductivity meter with a 4.5 mm micro-electrode was used to determine the pH of the aqueous complexes. Before use, the pH meter was calibrated with three standard buffer solutions; pH 4.0, 7.0 and 10.0. OriginPro 9.1® program was used to fit and analyze the acid-base titration data of the aqua complexes and kinetic data from their reactions.[17]

3.2.4 Crystallography

Suitable crystals of [Ru(terpy)(bipy)Tu)]$(ClO_4)_2$ were obtained by reacting **Ru-2** with excess thiourea in a minimum volume of 0.1 M $HClO_4$/$NaClO_4$ aqueous medium for 4 days at room temperature. The solution was then allowed to crystallize by slow evaporation of the solvent. X-ray diffraction structure of the substituted product was determined by Bruker Smart Apex II diffractometer coupled with Oxford Instruments Cryojet nitrogen jet system at 100 K. The crystal was illuminated with a monochromatic MoKα1 (λ = 0.71073 Å) radiation and the resulting diffraction intensities recorded using the ω-2θ scan mode at a theta range of 1.896 < θ < 27.450°. The crystal structure was solved by Shelxs program package supported by Olex2 for windows using direct methods.[18] It was then refined by ShelXL refinement package using full matrix least squares on F^2 on all the observed reflections.[19]

3.2.5 Aquation of the Complexes

Aqua solutions of the complexes were prepared by reacting known amounts of the chloro complexes with equivalent amounts of $AgClO_4$ in 0.01 M $HClO_4$ solution. All the reactions were carried out in the dark at 50 ℃ for 48 h. The solutions were thereafter cooled to room temperature and allowed to stand for 2 h. The grey AgCl precipitate therein was filtered off using 0.2 μM Millipore filtration discs to afford the stock solutions of the ruthenium(II) complexes.[20] The filtrates were refrigerated at 4 ℃ until use. They were diluted appropriately for p*K*a titrations and kinetic studies.

3.2.6 Spectrophotometric Determination of pKa of the Aqua Complexes

p*K*a titration of the aqua complexes with NaOH was done from pH 2-13 at 25 ℃. In all the experiments, large volumes of the complex solutions (500 mL) were used to avoid dilution effects and absorbance corrections.[21] From pH 2 to 3 and 10-13, finely crushed NaOH granules were carefully added to the complex solution while for the other pH range, varying concentrations of dilute NaOH solutions were used. After each addition of the base, the complex solution was stirred for about 2 min preceding pH measurement and respective spectrum recording. About 0.6 mL aliquots were used for pH measurements and discarded thereafter to avoid *in situ* contamination of the titration solution while the aliquots used for absorbance measurements were returned back to the solution. A confirmatory reverse pH titration was done using $HClO_4$ solutions in place of NaOH.

3.2.7 Kinetic Measurements

Both complex and nucleophile solutions were maintained at pH 2.0 and 0.1 M $HClO_4/NaClO_4$ ionic strength. The concentration of the aqua complexes used were; **Ru-1** (0.421 mM), **Ru-2** (0.159 mM), **Ru-3** (0.467 mM), **Ru-4** (0.310 mM). The nucleophile solutions were always prepared shortly before use.

Kinetic studies were performed under *pseudo*-first order conditions in which the concentration of the nucleophile was at least 10 folds higher than the concentration of the metal complex. The ultraviolet-visible spectral changes resulting from the reactions were recorded from 900/800-200 nm wavelength range to establish a suitable wavelength at which to monitor the kinetic reactions. Concentration dependence studies were performed at a constant temperature of 298 K while the temperature dependence reactions were studied from 298 to 318 K at an interval of 5 K.

All the reactions (both concentration and temperature depended) were initiated by mixing equal volumes (0.9 mL) of the complex and nucleophile in a tandem cuvette thermostated in a cell compartment. The results recorded herein are an average of no less than three independent runs.

3.2.8 Computational Modelling

Computational calculations were performed using density functional theory (DFT) method executed by Gaussian 09W suite of programs.[22] The structures were optimized using the hybrid Becke, 3-parameter, Lee-Yang-Parr at the standard LANL2DZ basis set.[23] DFT utilizes physically observable electron density over a wave-function in the determination of the optimized properties of a molecule or a compound. It is applicable in compounds with a large number of electrons because electron densities are always three dimensional irrespective of the number of electrons involved.[24] LANL2DZ exploits relativistic effective core potentials to account for the effect of inner core 28 electrons ([Ar]$3d^{10}$) in ruthenium.[25] To factor in the influence of the solvent used, the systems were fully optimized in aqua media using conductor-like polarizable continuum implicit solvent model.[26] The calculations were done at a singlet spin ground state and at an overall charge of +2. Electronic chemical potential (μ), chemical hardness (η), chemical softness (σ) and global electrophilicity indices (ω) for the complexes were calculated as described in literature.[27] Natural bonding orbitals (NBO) was used to determine atomic charges in the complexes.

3.3 Results

3.3.1 Acid-Base Equilibrium of the Aqua Complexes

The p*K*a values of the H_2O molecule coordinated to ruthenium were determined by plotting absorbance at a specific wavelength as a function of pH. The plot was then fitted into a sigmoid function (i).

$$y = A_2 + (A_1 - A_2)/(1+ \exp((x - x_0)/dx) \quad \text{i}$$

Typical ultraviolet-visible spectra obtained for the titration of **Ru-3** with NaOH is shown in Figure 3.2. The inset shows a plot of absorbance versus pH at λ = 252 nm. Additional spectra are presented in the Supplementary Information (Figures SI 3.5 and 3.6).

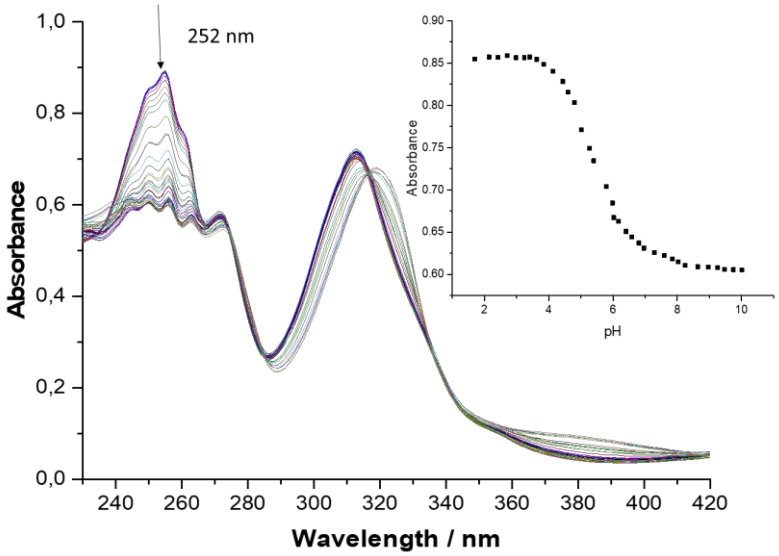

Figure 3.2: Ultraviolet-visible spectra of **Ru-3** complex recorded as a function of pH in the range 2–13 at 298 K. **Inset**: A plot of absorbance versus pH at λ = 252 nm

The p*K*a values were 9.81 ± 0.03 (**Ru-1**), 9.74 ± 0.02 (**Ru-2)**, 9.40 ± 0.03 (**Ru-3)** and 8.78 ± 0.02 **(Ru-4)**. These values compare favourably with those reported in literature.[9b, 16d] Noteworthy, the acidity constants have a negative relationship with the π-conjugation of the auxiliary ligands; an indication of an increase in the π-acceptor ability of the ligands and electrophilicity of the complexes as π-surface of auxiliary ligand is extended.[21, 28]

As the π-acceptor character of the auxiliary ligand increases, the withdrawal of electrons from the metal centre is enhanced leaving it depleted of negative charge. This makes the aqua ligand more acidic.[12] At a pH of 2.0, all the complexes exist entirely as aqua, therefore an ideal pH for the kinetic investigations.

3.3.2 Computational Results

Computational optimization and calculations were carried out to give an insight into the electronic and structural properties of the complexes. DFT-optimized structures of the complexes are shown in Table 3.1 and a summary of selected parameters is presented in Table 3.2. Figure 3.3 shows typical numbering of the atoms in the complexes. In all the complexes, the tridentate terpyridine ligand is bonded meridionally due to steric constraints. The complexes have a distorted octahedral geometry in which Ru-N1 and Ru-N3 bond lengths are dissimilar, with the Ru-N2 being significantly shorter. This is attributed to steric constraints imposed on the terpyridine ligand on coordination to a metal centre.[7d] Consequently, the N1-Ru-N3 angle deviates markedly from the expected 180º to range from 158.51 to 159.89º

In **Ru-1**, as expected the two pyridine rings are *trans* to each other and *cis* to the leaving group. In the other complexes, the N^N bidentate chelating ligand is anchored in such a way that one arm of the bidentate ligand is *cis* while the other is *trans* to the leaving group. Besides, it is coordinated asymmetrically to the metal centre as indicated by the slight longer Ru-N4 bond compared to the Ru-N5 bond (Table 3.2). This elongation is attributed to inter-ligand steric repulsions.[29] To gauge the deviation from optimal octahedral geometry, the angle N2-Ru-N5 was used. The bidentate chelating ligand in **Ru-2, Ru-3** and **Ru-4** is tilted away from the terpyridine plane as indicated by the obtuse nature of the angle. The highest deviation is recorded in **Ru-4** which is attributed to increased steric repulsion between the two ligands as a result of large π-surface area of the biquinoline ligand.[9b]

Table 3.1: DFT-optimized structures of the frontier molecular orbitals for the complexes

COMPLEX	HOMO	LUMO	PLANARITY
Ru-1	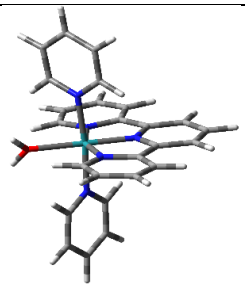	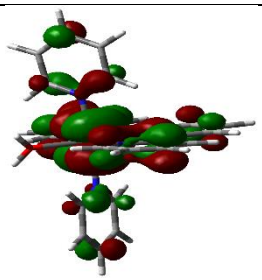	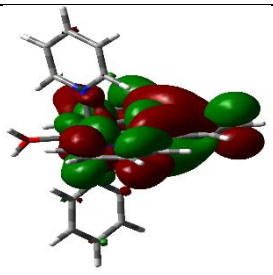	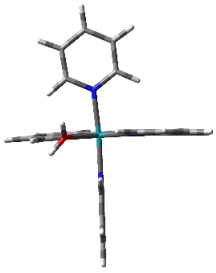
Ru-2	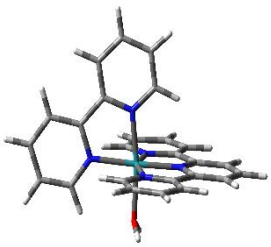	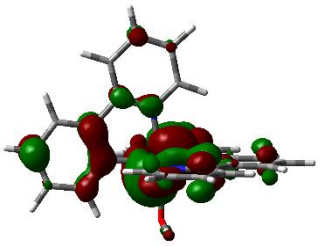	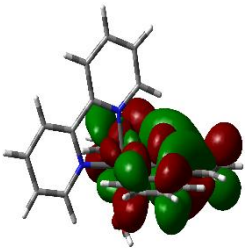	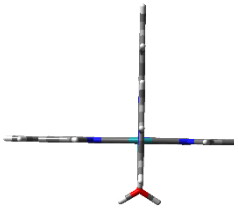
Ru-3	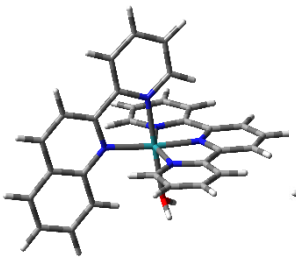	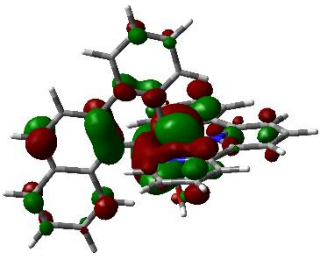	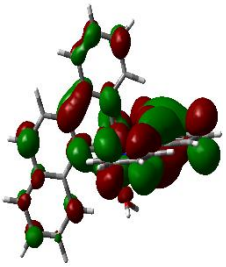	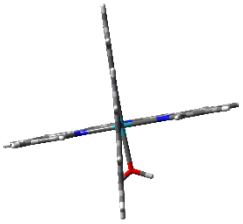
Ru-4	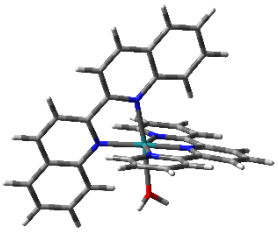	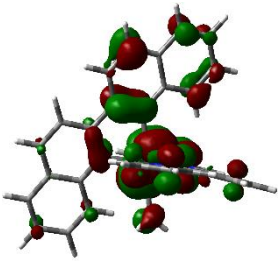	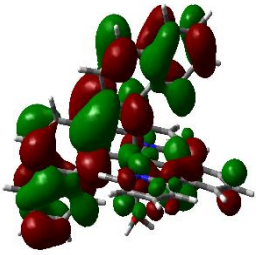	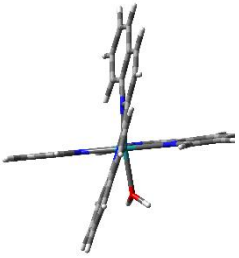

From the optimized structures in Table 3.1, the HOMO is largely based on the ruthenium metal centre for all the complexes. For complexes **Ru-1** and **Ru-2**, the LUMO is entirely based on the terpyridine ligand. On extending the π-conjugation of the auxiliary ligand, the contribution of the bidentate ligand to the LUMO increases accordingly with the 2,2'-biquinoline ligand in **Ru-4** recording the greatest contribution. Indeed, in **Ru-4**, the LUMO is largely based on the 2,2'-biquinoline ligand. Consequently, the LUMO energy is lowered as one moves from **Ru-1** to **Ru-4**.

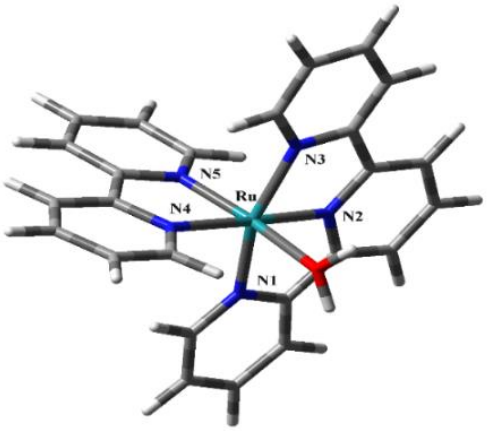

Figure 3.3: Molecular structure of **Ru-2** showing typical atomic labelling in the complexes

Table 3.2: Summary of selected computational data for the studied complexes

Complex	**Ru-1**	**Ru-2**	**Ru-3**	**Ru-4**
HOMO-LUMO energy / eV				
HOMO	-6.094	-6.102	-6.137	-6.111
LUMO	-2.845	-2.862	-2.943	-3.147
$\Delta E_{HOMO-LUMO}$	3.249	3.240	3.194	2.964
NBO charge (Ru)	0.370	0.373	0.378	0.375
Chemical potential (μ) / eV	-4.470	-4.482	-4.453	-4.629
Chemical hardness (η) /eV	1.625	1.620	1.597	1.482
Chemical softness (σ) / eV^{-1}	0.615	0.617	0.626	0.675
Electrophilicity index (ω) / eV	6.148	6.200	6.385	7.229
Dipole moment / D	2.998	3.178	6.399	6.552
Bond Length / Å				
Ru-N1	2.106	2.104	2.103	2.100
Ru-N3	2.108	2.104	2.106	2.118
Ru-N2	1.964	2.001	1.997	2.006
Ru-N5		2.054	2.044	2.100
Ru-N4	2.130	2.090	2.168	2.123
Ru-OH_2	2.217	2.173	2.223	2.193
Bond angle / º				
N2-Ru-OH_2	179.27	89.84	83.26	81.19
N1-Ru-N3	159.89	158.53	158.81	158.51
N2-Ru-N5		98.50	96.23	103.36

It is observed that, the planarity of the terpyridine ligand remain unaffected as the auxiliary ligand is changed. Conversely, the auxiliary ligand suffers distortion from planarity as the number of rings increase, with the highest distortion observed in the 2,2'-biquinoline ligand where the dihedral angle between the two quinolinyl moiety planes is 14.79º compared to 5.26º between the quinolinyl and pyridyl planes in **Ru-3** (Figure SI 3.7 and 3.8, Supplementary Information). In **Ru-2** no substantial distortion of the bipyridyl ligand was observed.

3.3.3 Kinetics Results

The substitution kinetics of coordinated aqua ligand in the four complexes was investigated with three thiourea based nucleophiles under *pseudo*-first order conditions. The substitution reactions were monitored spectrophotometrically by following change in absorbance of the spectra at a selected wavelength as a function of time. Typical spectra obtained for the reaction of **Ru-1** with Dmtu is shown in Figure 3.4.

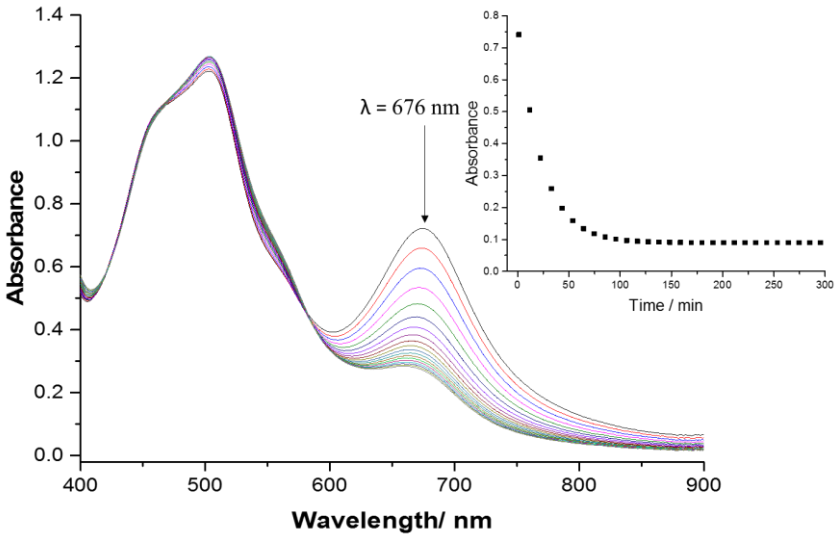

Figure 3.4: Ultraviolet-visible spectra for the reaction of **Ru-1 (**0.421 mM) with Dmtu (42.1 mM) at 298 K, pH = 2.0, *I* = 0.1 M $HClO_4/NaClO_4$. **Inset**: A kinetic trace at λ = 676 nm

Kinetic traces taken at the suitable wavelength were fitted into a single exponential decay function to generate *pseudo*-first order rate constants (k_{obs}) using equation (ii). [30]

Tables SI 3.1- 3.4 (Supplementary Information) show k_{obs} obtained and respective nucleophile concentrations.

$$A_t = A_o + (A_o - A_\infty)\exp(-k_{obs}t) \quad \text{(ii)}$$

where; A_o = absorbance at the initiation of the reaction, A_t = absorbance at time t, and A_∞ = absorbance at the end of the reaction.

The k_{obs} values obtained were plotted against nucleophile concentrations. A linear dependence of k_{obs} on nucleophile concentration was exhibited in all the complexes. No evidence for reverse or solvotic reaction was observed. Representative plots of k_{obs} versus nucleophile concentration obtained for **Ru-1** is shown in Figure 3.5. Additional plots of k_{obs} versus nucleophile concentration are presented in the Supplementary Information (Figures SI 3.1 and 3.2). The slope of the graph gave the second order rate constant (k_2); the values obtained are collected in Table 3.3. All the concentration dependent reactions can be described by equation (iii).

$$k_{obs} = k_2[\text{Nucleophile}] \quad \text{(iii)}$$

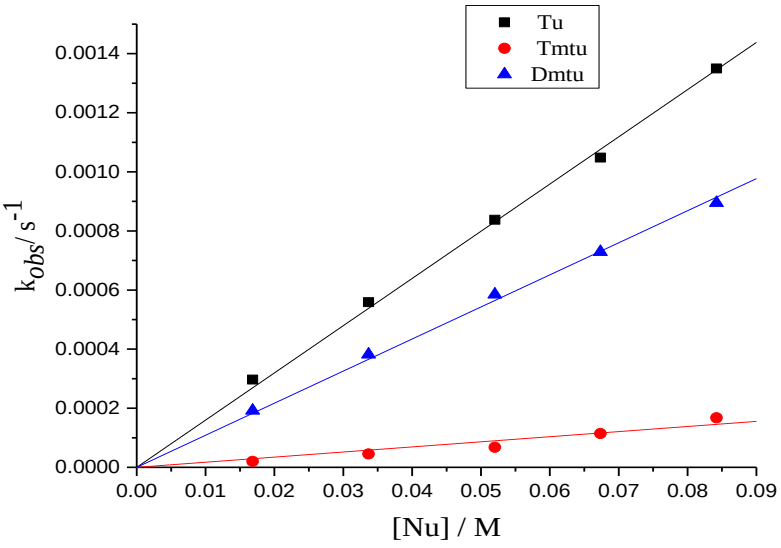

Figure 3.5: Dependence of k_{obs} on concentration of thiourea nucleophiles for the substitution of the aqua ligands in **Ru-1** at 298 K, pH = 2.0, I = 0.1 M $HClO_4/NaClO_4$

To determine the thermodynamic parameters of the substitution process, the reaction temperature was varied systematically from 298 to 318 at an interval of 5 K. Activation parameters ($\Delta H^{\neq}$ and $\Delta S^{\neq}$) were calculated using the Eyring equation (iv).[30]

$$\ln\left(\frac{k_2}{T}\right) = -\frac{\Delta H^{\neq}}{R}.\frac{1}{T} + \left(23.78 + \frac{\Delta S^{\neq}}{R}\right) \qquad \text{(iv)}$$

Typical Eyring plots obtained for **Ru-3** are shown in Figure 3.6 and the values of $\Delta H^{\neq}$ and $\Delta S^{\neq}$obtained are collected in Table 3.3. Additional Eyring plots, $\ln\left(\frac{k_2}{T}\right)$ and respective $\frac{1}{T}$ values are presented in the Supplementary Information (Figures SI 3.3-3.4 and Tables SI 3.5-8, respectively).

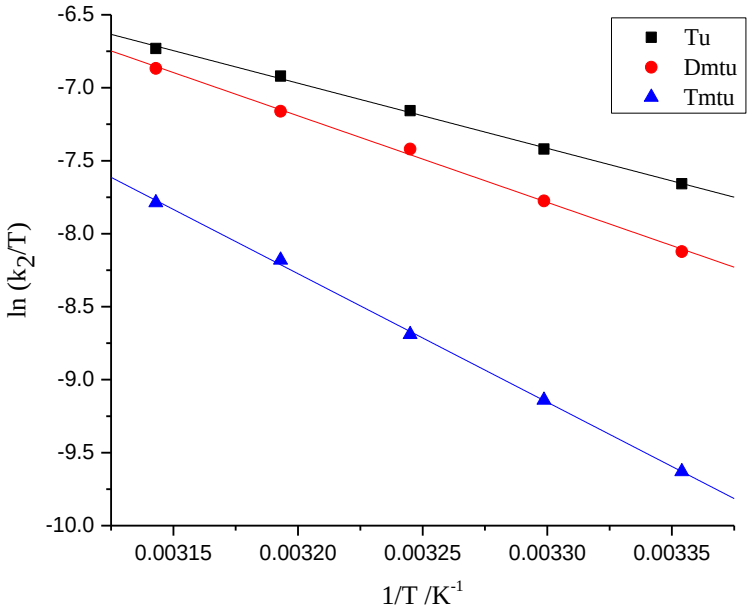

Figure 3.6: Eyring plots for the reaction of **Ru-3** with thiourea nucleophiles, pH = 2.0, *I* = 0.1 M $HClO_4/NaClO_4$

Table 3.3: Second order rate constants (k_2) and activation parameters ($\Delta H^{\neq}$ and $\Delta S^{\neq}$) for the displacement of aqua ligand by thiourea nucleophiles

Complex	Nu	k_2 (10^{-2} M^{-1} s^{-1})	$\Delta H^{\neq}$ (kJ mol^{-1})	$\Delta S^{\neq}$ (J mol^{-1} K^{-1})
Ru-1	**Tu**	1.60 ± 0.02	46 ± 1	-126 ± 3
	Dmtu	1.09 ± 0.01	54 ± 2	-102 ± 6
	Tmtu	0.17 ± 0.01	63 ± 3	-82 ± 9
Ru-2	**Tu**	0.06 ± 0.01	72 ± 2	-63 ± 8
	Dmtu	0.12 ± 0.01	69 ± 2	-71 ± 8
	Tmtu	0.05 ± 0.01	84 ± 2	-26 ± 8
Ru-3	**Tu**	13.85 ± 0.26	37 ± 1	-137 ± 3
	Dmtu	7.65 ± 0.19	49 ± 3	-101 ± 8
	Tmtu	0.34 ± 0.03	73 ± 2	-34 ± 6
Ru-4	**Tu**	21.97 ± 0.40	42 ± 2	-117 ± 7
	Dmtu	35.03 ± 0.30	40 ± 2	-119 ± 7
	Tmtu	3.67 ± 0.16	57 ± 2	-79 ± 5

3.3.4 Product Analysis: Crystal structure of $[Ru(terpy)(bipy)Tu)](ClO_4)_2$

The x-ray crystallographic data obtained reveal vital information about the structure of the complex. Ellipsoidal molecular structure of the complex is shown in Figure 3.7. Selected crystallographic and structure refinement parameters are collected in Table 3.4. Important interatomic distances and angles of the crystal structure and DFT-optimized minimum energy structure of the complex are presented in Table 3.5. Further information about the crystal structures may be accessed at CCDC refcode, NIGHOD.

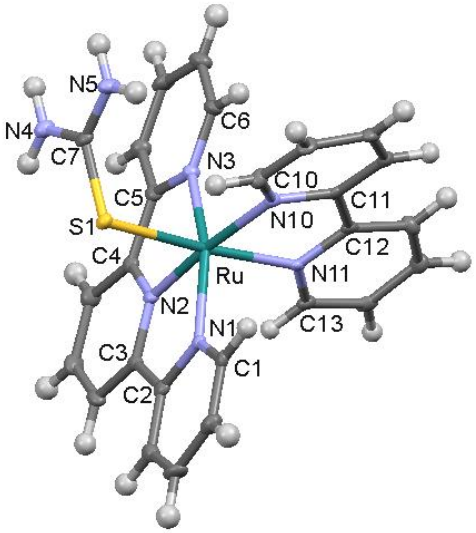

Figure 3.7: Displacement ellipsoid plotted at 50% probability showing the crystal structures of $[Ru(terpy)(bipy)Tu)](ClO_4)_2$ (counterions omitted for clarity)

The complex crystallizes with two ClO_4^- ions as counterions, an indication that the oxidation state (+2) of the metal centre is maintained after reaction with the thiourea nucleophile. The complex adopts slightly distorted octahedral geometry in which all the Ru-N(terpyridine) bond lengths are typical of terpyridine based ruthenium systems.[5b, 7d, 9a, 16d, 31] The Ru-N2 bond is slightly shorter compared to the Ru-N1 and Ru-N3 bonds. This phenomenon has been reported in other complexes and is attributed to steric and geometric constraints imposed on the terpyridine ligand upon coordination to a metal centre. Consequently, the terpyridine's bite angle is restricted to 159.31º, a deviation from the idealized angle of 180º.[31]

The terpyridine ligand is slightly twisted as shown by an average tilt angle of 2.71º between the central and terminal pyridines. The thiourea ligand is coordinated to the metal centre via the S-donor atom with the Ru-S bond length within the reported range for Ru-Tu bonds (2.304 – 2.427 Å).[32] The bipyridyl ligand is asymmetrically coordinated to the metal centre with the Ru-N bond *cis* to the Tu (Ru-N10) slightly longer than the one at *trans* position (Ru-N11). The difference in length is attributed to inter-ligand steric repulsions.[29] The two pyridyl rings of the bipyridyl ligand are non-planar, with a dihedral angle of 11.89º between them.

Table 3.4: Crystallographic data and structure refinement parameters

Parameters	**Data**
Empirical formula	$C_{26}H_{23}Cl_2N_7O_8RuS$
Formula weight / $gmol^{-1}$	765.54
Crystal system	Monoclinic
Space group	P 21/c
a /Å	9.281(15)
b /Å	26.211(4)
c /Å	11.930(2)
α /°	90
β /°	99.206(4)
γ /°	90
Volume /$Å^3$	2864.5(8)
Z	4
Density (Calc) /gcm^{-3}	1.775
Absorption coefficient /mm^{-1}	0.871
F(000)	1544
Crystal size / mm^3	0.56 ×0.160 ×0.140
Goodness-of-fit on F^2 /%	99.3
Index ranges	-11<=h<=11, -34<=k<=33,-15<=l<=15
Final R indices [I>2σ(I)]	$R1$ = 0.0543, wR_2 = 0.1181
R indices (all data)	$R1$ = 0.0711, wR_2 = 0.1274

The planes RuN1N2N3N10 and RuS1N2N10N11 are near orthogonal to each other with a dihedral angle of 84.93º. This distortion from ideal octahedral geometry is ascribed to constraints caused by the bite angles of terpyridine and bipyridyl ligands. The crystal packing of the complex is dominated by van der Waals forces. The bond lengths and angles compare well with those of the DFT-optimized structure thus benchmarking favourably the DFT theoretical calculations as applied in the aqua complexes.

Table 3.5: Selected bond lengths and bond angles for [Ru(terpy)(bipy)Tu)]$(ClO_4)_2$

Bond Length /Å		
Bond	**Crystal**	**DFT**
Ru-S1	2.430(11)	2.476
Ru-N1	2.066(4)	2.113
Ru-N2	1.965(3)	1.997
Ru-N3	2.088(3)	2.105
Ru-N10	2.087(3)	2.112
Ru-N11	2.074(3)	2.073
Bond Angle /º		
Bond Angle	**Crystal**	**DFT**
N2-Ru-N1	79.89(14)	79.20
N2-Ru-N3	79.42(14)	79.38
N1-Ru-N3	159.31(13	158.29
N2-Ru-S1	90.69(10)	88.57
N3-Ru-S1	94.74(9)	92.99
N1-Ru-S1	85.31(9)	87.05
N10-Ru-S1	95.92(9)	96.18
N11-Ru-S1	173.89(9)	171.79

3.4 Discussion

The rate of displacement of the aqua ligand from the complexes by Tu was used as a representative to discuss the trend in the reactivity of the complexes. The marked differences in reactivity of the complexes observed is due to stereo-electronic effects of the ligands around the metal centre, largely attributable to the auxiliary ligand(s) because the meridionally coordinated π-acceptor terpyridine is present in all the complexes. **Ru-1** has two coordinated pyridine rings as auxiliary ligands which are moderate π-acceptors/weak σ-donors.[33] The rest of the complexes have N^N bidentate ligands in which the aqua labile ligand lie in the plane of the ruthenium centre and the bidentate ligand. This makes the bidentate ligand exert an in-plane

effects on the aqua group.[34] The π-conjugation of the auxiliary ligand increase sequentially as one moves from **Ru-2** to **Ru-4.**

Based on the extent of π-conjugation the trend in reactivity should follow the order; **Ru-1 < Ru-2** < **Ru-3** < **Ru-4** due to enhanced electronic communication and systematic increase in π-acceptor properties of the auxiliary ligand brought by the bipyridyl ligand in **Ru-2** and successive extension of the π-conjugation of the bidentate ligand from **Ru-2** to **Ru-4**.[21, 33, 35] However, **Ru-1** is ≈ 27 times more reactive than **Ru-2**. This is because the bipyridyl ligand in **Ru-2** introduces significant steric hindrance to the incoming nucleophile compared to the two separate pyridyl rings in **Ru-1**. Since the reaction proceeds through an associative mechanism, the steric hindrance posed in **Ru-2** limits the formation of the transition complex by retarding the incoming nucleophile from swiftly attacking the metal centre.[7d] The Ru-OH_2 bond is significantly shorter in **Ru-2** (2.173 Å) compared to **Ru-1** (2.217 Å). Therefore, the H_2O ligand in **Ru-2** is more strongly bound compared to **Ru-1** making its displacement harder. [7d, 9a]

The mappings of the molecular orbitals in Table 3.1 show that the contribution of the auxiliary ligand to the LUMO increases with increase in the π-conjugation of the auxiliary ligand. Increasing the aromatic surface of the auxiliary ligand leads to successive stabilization of the LUMO as shown by the decrease of its energy.[21, 36] As a result, the HOMO-LUMO gap narrows and the interaction between the frontier orbitals increases from **Ru-1** to **Ru-4.** This also increases the electron affinity of the complexes in the same order as it becomes easier for π-back donation of electron density from the metal centre to the ligand. Therefore, the rate of substitution of the aqua ligand is accelerated as conjugation of the auxiliary ligand increases.

Furthermore, as the π-surface area of the auxiliary ligand increases, the ability of the complexes to stabilize the entering electron density becomes more effective by spreading it over the extended aromatic system.[21] As a result, an increase in π-conjugation is correlated by a

systematic increase in the electronic chemical softness (σ) found in the DFT-calculated data. While the electronic chemical potentials (μ) of the complexes do not correlate well with the reactivity trend observed owing to its improper behavior,[37] it plays an important role in combination with chemical hardness (η) to determine the global electrophilicity index (ω) of a system, a more superior parameter in describing the propensity of a system to accept electrons.[38] This is because it measures both the ability to acquire an additional electronic charge as well as the resistance of the system to exchange the acquired electronic charge with the environment.[39] Thus, it describes the overall charge of a complex.[27c] The calculated ω values corelate positively to the reactivity trend observed except for **Ru-1**, whose anomalous reactivity is earlier discussed (*vide supra*). Of the studied complexes, **Ru-4** is the strongest electrophile and therefore as expected is the most reactive.[37]

One notes that **Ru-4** is only marginally more reactive than **Ru-3**, despite its larger extended π-surface and electrophilicity index.[21] This is attributed to increased steric hindrance brought about by the 2,2'-biquinoline ligand. Its optimized structure assumes an out of plane banana-curvatured conformation as shown in Table 3.1.The inter-ligand steric interactions between the terpyridine and the biquinoline ligand are increased by the large in-plane size of the latter[40] as depicted by the significant increase in N2-Ru-N5 angle by ≈ 7º compared to **Ru-3**. Consequently, the spatial access to the metal centre is restricted for easy approach of the nucleophile. From the DFT-optimized structures it is observed that the dihedral angle between the two planes of the quinolinyl moieties in **Ru-4** is 14.79º compared to 5.26º between the planes of pyridyl and quinolinyl moieties in **Ru-3** (Supplementary Information, Figure SI 3.7-3.8).The substantial distortion of planarity of the 2,2'-biquinoline ligand compromises its π-back-bonding property leading to a less positive metal centre.[9b, 40a, 41] This is evidenced by the slightly lower NBO charge on the ruthenium metal centre in **Ru-4.** The lower charge can also be as a result of somewhat significant σ-donicity of the 2,2'-biquinoline ligand towards the

metal centre since it has both σ-donor and π-acceptor properties.[41] The overall effect is a reduced reactivity.

Redox potentials and absorption electronic transitions have been used occasionally as measures of electrophilicity of metal based complexes.[8d, 27c] For example; when the auxiliary ligand is changed from 2,2'-bipyridyl to 2,2'-biquinoline, the first reduction potential shifts to a more positive value because the π* orbital energy is lowered and thus stabilized.[16e, 42] The reduction in potential validate the fact that the π-acceptor properties of the auxiliary ligand increases with increase in π-delocalization. Similarly, the characteristic metal to ligand charge transfer (MLCT) absorption band is bathochromic shifted as the auxiliary ligand is changed from 2,2'-bipyridyl to 2,2'-biquinoline.[16d, 42c] This is in line with the reduction in the HOMO-LUMO gap as π-conjugation of the coordinated ligand increases. Thus, the electron withdrawing capability of the ligands is expected to increase from 2,2'-bipyridyl to 2,2'-biquinoline. This argument supports the observed trend from **Ru-2** to **Ru-4**, is as a result of increase in π-surface of the auxiliary ligands from **Ru-2** to **Ru-4** which increases the electrophilicity of the complexes in the same order.

Further to this, a negative correlation was observed between spectrophotometrically determined p*K*a values and the aromatic surface of the coordinated auxiliary ligands of the ruthenium(II) complexes. Acidity of the aqua labile ligands increase from **Ru-1** to **Ru-4.** This is due to increase in the strength of π-acceptor ability of the ligands which enhances the withdrawal of electron density from the metal centre.[12, 21] Moreover, the dipole moments of the complexes increases from **Ru-1** to **Ru-4**, further indicating an upsurge in π-withdrawing properties of the ligands.[43] The trend in the theoretically computed electrophilicity indices together with the p*K*a values affirms that as the π-surface area of the bidentate ligand increases the electrophilicity of the metal complexes increases likewise leading to the observed increase in reactivity from **Ru-2** to **Ru-4**.

Theoretically, the reactivity of the three nucleophiles should follow the trend Tu > Dmtu > Tmtu due to increasing bulkiness of the nucleophile. However, in **Ru-2** and **Ru-4**, the more sterically demanding Dmtu reacts faster than the unhindered Tu. The explanation for this is that the inductive effect brought by the methyl substituents in Dmtu overcompensates the steric effect.[21, 44]

The negative values for $\Delta S^{\neq}$ obtained suggest an associatively activated substitution process dominated by bond-making with the incoming nucleophile. The negative activation entropy also imply a more ordered transition state compared to the starting reactants and the final products.[45] Associative mechanism of activation has recently been reported in other terpyridine based ruthenium(II) complexes.[7d, 9a]

3.5 Conclusion

The study has established that the reactivity of terpyridine based ruthenium(II) complexes with N/N^N auxiliary ligand(s) is strongly depended on the intrinsic stereo-electronic properties of the auxiliary ligands. In complexes **Ru-2** to **Ru-4,** the reactivity is controlled by the π-acceptor character of the bidentate ligand which increases with increase in π-conjugation. As the π-conjugation increases, the complexes become more electrophilic and consequently more reactive. The lower reactivity of **Ru-2** compared to **Ru-1** is attributed to significant steric hindrance caused by the bipyridyl ligand compared to the two *trans* pyridyl ligands in **Ru-1**. Results obtained from the DFT-calculations show that, steady stabilization of the LUMO and diminution of the HOMO-LUMO gap occur as the π-surface area of the auxiliary ligand is extended from **Ru-1** to **Ru-4** leading to enhanced electrophilicity of the complexes. Likewise, the p*K*a values of the complexes decrease from **Ru-1** to **Ru-4** implying that the acidity of the coordinated aqua ligand increases accordingly because of reduced electron density at the metal centre. Therefore, both DFT results and p*K*a values support the trend in reactivity observed except in **Ru-1** where low steric hindrance around the metal centre makes it more reactive than

Ru-2. The mode of activation in these complexes is associative. The solid state crystal structure of [Ru(terpy)(bipy)Tu)]$(ClO_4)_2$ show that terpyridine ruthenium(II) thiourea complexes are stable and the thiourea is coordinated to the metal centre via the S-donor atom.

3.6 References

[1] (a) C. G. Hartinger, M. A. Jakupec, S. Zorbas-Seifried, M. Groessl, A. Egger, W. Berger, H. Zorbas, P. J. Dyson, B. K. Keppler, *Chemistry & Biodiversity* **2008**, *5*, 2140-2155; (b) S. Leijen, S. A. Burgers, P. Baas, D. Pluim, M. Tibben, E. van Werkhoven, E. Alessio, G. Sava, J. H. Beijnen, J. H. Schellens, *Investigational New Drugs* **2015**, *33*, 201-214; (c) C. S. Allardyce, P. J. Dyson, *Platinum Metals Review* **2001**, *45*, 62-69.

[2] (a) A. Bergamo, G. Sava, *Dalton Transactions* **2011**, *40*, 7817-7823; (b) M. Pongratz, P. Schluga, M. A. Jakupec, V. B. Arion, C. G. Hartinger, G. Allmaier, B. K. Keppler, *Journal of Analytical Atomic Spectrometry* **2004**, *19*, 46-51.

[3] W. Han Ang, P. J. Dyson, *European Journal of Inorganic Chemistry* **2006**, *2006*, 4003-4018.

[4] (a) O. Novakova, J. Kasparkova, O. Vrana, P. M. van Vliet, J. Reedijk, V. Brabec, *Biochemistry* **1995**, *34*, 12369-12378; (b) V. Brabec, O. Nováková, *Drug Resistance Updates* **2006**, *9*, 111-122.

[5] (a) S. S. née Kraft, C. Bischof, A. Loos, S. Braun, N. Jafarova, U. Schatzschneider, *Journal of Inorganic Biochemistry* **2009**, *103*, 1126-1134; (b) H. Huang, P. Zhang, Y. Chen, K. Qiu, C. Jin, L. Ji, H. Chao, *Dalton Transactions* **2016**, *45*, 13135-13145.

[6] (a) F. Giannini, L. E. Paul, J. Furrer, B. Therrien, G. Süss-Fink, *New Journal of Chemistry* **2013**, *37*, 3503-3511; (b) Y. Mulyana, D. K. Weber, D. P. Buck, C. A. Motti, J. G. Collins, F. R. Keene, *Dalton Transactions* **2011**, *40*, 1510-1523.

[7] (a) C. C. Cheng, W. L. Lee, J. G. Su, C. L. Liu, *Journal of the Chinese Chemical Society* **2000**, *47*, 213-220; (b) M. M. Milutinović, Ž. D. Bugarčić, R. Wilhelm, *New Journal of Chemistry* **2018**; (c) K. Karidi, A. Garoufis, A. Tsipis, N. Hadjiliadis, H. den Dulk, J. Reedijk, *Dalton Transactions* **2005**, 1176-1187; (d) M. M. Milutinović, S. K. Elmroth, G.

Davidović, A. Rilak, O. R. Klisurić, I. Bratsos, Ž. D. Bugarčić, *Dalton Transactions* **2017**, *46*, 2360-2369.

[8] (a) D. Reddy, D. Jaganyi, *Dalton Transactions* **2008**, 6724-6731; (b) D. Reddy, K. J. Akerman, M. P. Akerman, D. Jaganyi, *Transition Metal Chemistry* **2011**, *36*, 593-602; (c) D. Jaganyi, K. L. D. Boer, J. Gertenbach, J. Perils, *International Journal of Chemical Kinetics* **2008**, *40*, 808-818; (d) P. Ongoma, D. Jaganyi, *Dalton Transactions* **2012**, *41*, 10724-10730; (e) A. Shaira, D. Jaganyi, *Journal of Coordination Chemistry* **2014**, *67*, 2843-2857; (f) A. Mambanda, D. Jaganyi, in *Advances in Inorganic Chemistry, Vol. 70*, Elsevier, **2017**, pp. 243-276.

[9] (a) M. Chrzanowska, A. Katafias, O. Impert, A. Kozakiewicz, A. Surdykowski, P. Brzozowska, A. Franke, A. Zahl, R. Puchta, R. van Eldik, *Dalton Transactions* **2017**, *46*, 10264-10280; (b) F. Tiba, D. Jaganyi, A. Mambanda, *Journal of Coordination Chemistry* **2010**, *63*, 2542-2560.

[10] (a) J. Reedijk, *Chemical Reviews* **1999**, *99*, 2499-2510; (b) R. Zee-Cheng, C. Cheng, *Methods and Findings in Experimental and Clinical Pharmacology* **1989**, *11*, 439-529.

[11] (a) B. Deka, A. Bhattacharyya, S. Mukherjee, T. Sarkar, K. Soni, S. Banerjee, K. K. Saikia, S. Deka, A. Hussain, *Applied Organometallic Chemistry* **2018**; (b) K. Becker, C. Herold-Mende, J. J. Park, G. Lowe, R. H. Schirmer, *Journal of medicinal chemistry* **2001**, *44*, 2784-2792; (c) E. I. Ikitimur-Armutak, K. Sonmez, K. Akgun-Dar, G. Sennazli, A. Kapucu, F. Yigit, V. T. Yilmaz, E. Ulukaya, *Anticancer Research* **2015**, *35*, 1491-1497; (d) J.-W. Liang, Y. Wang, K.-J. Du, G.-Y. Li, R.-L. Guan, L.-N. Ji, H. Chao, *Journal of Inorganic Biochemistry* **2014**, *141*, 17-27.

[12] A. M. Pizarro, A. Habtemariam, P. J. Sadler, in *Medicinal Organometallic Chemistry*, Springer, **2010**, pp. 21-56.

[13] M. Li, L. Lai, Z. Zhao, T. Chen, *Chemistry–An Asian Journal* **2016**, *11*, 310-320.

[14] W. C. Schiessl, N. K. Summa, C. F. Weber, S. Gubo, C. Dücker-Benfer, R. Puchta, N. J. van Eikema Hommes, R. van Eldik, *Zeitschrift für Anorganische und Allgemeine Chemie* **2005**, *631*, 2812-2819.

[15] Q. Zhao, S. Liu, M. Shi, C. Wang, M. Yu, L. Li, F. Li, T. Yi, C. Huang, *Inorganic Chemistry* **2006**, *45*, 6152-6160.

[16] (a) B. P. Sullivan, J. M. Calvert, T. J. Meyer, *Inorganic Chemistry* **1980**, *19*, 1404-1407; (b) H. F. Suen, S. Wilson, M. Pomerantz, J. L. Walsh, *Inorganic Chemistry* **1989**, *28*, 786-791; (c) K. J. Takeuchi, M. S. Thompson, D. W. Pipes, T. J. Meyer, *Inorganic Chemistry* **1984**, *23*, 1845-1851; (d) M. Hirahara, T. Hakamata, A. B. League, M. Z. Ertem, K. Takahashi, S. Nagai, K. Inaba, H. Yamazaki, K. Saito, T. Yui, *European Journal of Inorganic Chemistry* **2015**, *2015*, 3892-3903; (e) C. A. Bessel, J. A. Margarucci, J. H. Acquaye, R. S. Rubino, J. Crandall, A. J. Jircitano, K. J. Takeuchi, *Inorganic Chemistry* **1993**, *32*, 5779-5784.

[17] OriginPro9.1, OriginLab Corporation, One Roundhouse Plaza, Suite 303, Northampton, MA 01060, United States, 2014 1800-969-7720. *www.OriginLab.com.*

[18] O. V. Dolomanov, L. J. Bourhis, R. J. Gildea, J. A. Howard, H. Puschmann, *Journal of Applied Crystallography* **2009**, *42*, 339-341.

[19] G. M. Sheldrick, *Acta Crystallographica Section C: Structural Chemistry* **2015**, *71*, 3-8.

[20] Ž. D. Bugarčić, B. V. Petrović, R. Jelić, *Transition Metal Chemistry* **2001**, *26*, 668-671.

[21] A. Hofmann, D. Jaganyi, O. Q. Munro, G. Liehr, R. van Eldik, *Inorganic Chemistry* **2003**, *42*, 1688-1700.

[22] M. Frisc, G. Trucks, H. Schlegel, G. Scuseria, M. Robb, J. Cheeseman, G. Scalmani, V. Barone, B. Mennucci, G. Petersson, *Gaussian Inc, Wallingford* **2010**.

[23] J. Li, L.-C. Xu, J.-C. Chen, K.-C. Zheng, L.-N. Ji, *The Journal of Physical Chemistry A* **2006**, *110*, 8174-8180.

[24] V. Gupta, *Principles and Applications of Quantum Chemistry*, Elsevier Inc., London, UK, **2015**, pp. 156-175.

[25] M. Okamura, M. Yoshida, R. Kuga, K. Sakai, M. Kondo, S. Masaoka, *Dalton Transactions* **2012**, *41*, 13081-13089.

[26] M. Cossi, G. Scalmani, N. Rega, V. Barone, *The Journal of Chemical Physics* **2002**, *117*, 43-54.

[27] (a) R. G. Parr, L. v. Szentpaly, S. Liu, *Journal of the American Chemical Society* **1999**, *121*, 1922-1924; (b) R. G. Pearson, *Inorganica Chimica Acta* **1992**, *198*, 781-786; (c) I. M. Wekesa, D. Jaganyi, *Dalton Transactions* **2014**, *43*, 2549-2558; (d) R. G. Pearson, *Journal of Molecular Structure: THEOCHEM* **1992**, *255*, 261-270.

[28] A. F. Peacock, A. Habtemariam, S. A. Moggach, A. Prescimone, S. Parsons, P. J. Sadler, *Inorganic Chemistry* **2007**, *46*, 4049-4059.

[29] C. R. Hecker, P. E. Fanwick, D. R. McMillin, *Inorganic Chemistry* **1991**, *30*, 659-666.

[30] J. D. Atwood, *Inorganic and Organometallic Reaction Mechanisms*, 2nd edition ed., VCH Publishers, **1997**, pp. 1-18, 47-90.

[31] J. L. Walsh, R. McCracken, A. T. McPhail, *Polyhedron* **1998**, *17*, 3221-3226.

[32] (a) P. Vijayan, P. Viswanathamurthi, P. Sugumar, M. N. Ponnuswamy, J. G. Malecki, K. Velmurugan, R. Nandhakumar, M. D. Balakumaran, P. T. Kalaichelvan, *Applied Organometallic Chemistry* **2017**, *31*, 1-23; (b) G. Douglas, K. W. Muir, A. Patel, D. Richens, *Acta Crystallographica Section C: Crystal Structure Communications* **1991**, *47*, 1394-1397;(c) D. P. Fairlie, W. A. Wickramasinghe, K. A. Byriel, H. Taube, *Inorganic Chemistry* **1997**, *36*, 2242-2243.

[33] S. J. Dougan, M. Melchart, A. Habtemariam, S. Parsons, P. J. Sadler, *Inorganic Chemistry* **2006**, *45*, 10882-10894.

[34] M. H. V. Huynh, J. Smyth, M. Wetzler, B. Mort, P. K. Gong, L. M. Witham, D. L. Jameson, D. K. Geiger, J. M. Lasker, M. Charepoo, *Angewandte Chemie* **2001**, *113*, 4601-4605.

[35] (a) D. Jaganyi, A. Hofmann, R. van Eldik, *Angewandte Chemie International Edition* **2001**, *40*, 1680-1683; (b) Y.-Z. Hu, G. Zhang, R. P. Thummel, *Organic letters* **2003**, *5*, 2251-2253; (c) D. Reddy, D. Jaganyi, *Transition Metal Chemistry* **2006**, *31*, 792-800.

[36] K. Hanson, L. Roskop, P. I. Djurovich, F. Zahariev, M. S. Gordon, M. E. Thompson, *Journal of the American Chemical Society* **2010**, *132*, 16247-16255.

[37] C. A. Mebi, *Journal of Chemical Sciences* **2011**, *123*, 727-731.

[38] P. K. Chattaraj, D. R. Roy, *Chemical Reviews* **2007**, *107*, PR46-PR74.

[39] H. Ben El Ayouchia, H. Anane, M. L. El Idrissi Moubtassim, L. R. Domingo, M. Julve, S.-E. Stiriba, *Molecules* **2016**, *21*, 1434

[40] (a) A. Spek, A. Gerli, J. Reedijk, *Acta Crystallographica Section C: Crystal Structure Communications* **1994**, *50*, 394-397; (b) B. A. Johnson, H. Agarwala, T. A. White, E. Mijangos, S. Maji, S. Ott, *Chemistry-A European Journal* **2016**, *22*, 14870-14880.

[41] J. D. Knoll, B. A. Albani, C. B. Durr, C. Turro, *The Journal of Physical Chemistry A* **2014**, *118*, 10603-10610.

[42] (a) N. Yoshikawa, J. Sakamoto, T. Matsumura-Inoue, H. Takashima, K. Tsukahara, N. Kanehisa, Y. Kai, *Analytical Sciences* **2004**, *20*, 711-716; (b) M. Heijden, P. M. Van Vliet, J. G. Haasnoot, J. Reedijk, *Journal of the Chemical Society, Dalton Transactions* **1993**, 3675-3679; (c) H.-W. Tseng, R. Zong, J. T. Muckerman, R. Thummel, *Inorganic Chemistry* **2008**, *47*, 11763-11773.

[43] D. P. Rillema, A. J. Cruz, C. Moore, K. Siam, A. Jehan, D. Base, T. Nguyen, W. Huang, *Inorganic Chemistry* **2012**, *52*, 596-607.

[44] Ž. D. Bugarčić, J. Bogojeski, B. Petrović, S. Hochreuther, R. van Eldik, *Dalton Transactions* **2012**, *41*, 12329-12345.

[45] (a) T. Das, B. Bera, A. Datta, A. Ghosh, *Transition Metal Chemistry* **2009**, *34*, 247-253; (b) M. A. A. K.Ghosh, B. K.Bera, S. Mallick, S. Mondal, P. Karmakar, *Inorganic Chemistry: An Indian Journal* **2010**, *5*, 176-183.

SI 3 Supplementary Information

SI 3.1 Synthesis of 2-(2-pyridyl)quinoline

5 mL of saturated ethanolic solution of NaOH was added to a mixture of 2-aminobenzadehyde (250 mg, 2.65 mmol) and 2-acetylpyridine (250 mg, 2.65 mmol) in ethanol, and the mixture was refluxed for 12 h. After cooling the solution to ambient temperatures, the precipitate was filtered off under vacuum and purified by recrystallization from dichloromethane. White crystalline solid was obtained. Yield: 273 mg (65%). *Anal*. *Calc*. for $C_{14}H_{10}N_2$; C, 81.53; H, 4.89; N, 13.58. *Found*: C, 81.49; H, 4.97; N, 13.38. ^{1}H NMR (400 MHz, acetone-d_6): δ (ppm) = 8.73 (t, 2H), 8.68 (d, 1H), 8.46 (d, 1H), 8.16 (d, 1H), 7.99 (t, 2H), 7.82 (t, 1H), 7.62 (t, 1H), 7.48 (t, 1H). ^{13}C NMR (500 MHz, acetone-d_6): δ (ppm) = 156.0, 149.2, 147.9, 136.9, 136.7, 129.6, 128.4, 127.8, 126.8, 124.3, 121.2, 118.6. ESI-MS (TOF) (*m/z*): 207 (M)

SI 3.2 Average k_{obs} for the substitution of aqua ligands in the investigated complexes

Table SI 3.1: Average k_{obs} (s^{-1}) for the reaction of **Ru-1** (0.421 mM) with thiourea nucleophiles

[Nu] /M	**Tu** (λ = 676 nm)	**Dmtu** ((λ = 676 nm)	**Tmtu** ((λ = 675 nm)
	k_{obs} /s^{-1}	k_{obs} /s^{-1}	k_{obs} /s^{-1}
0.0842	1.35×10^{-3}	8.95×10^{-4}	1.68×10^{-4}
0.0674	1.05×10^{-3}	7.29×10^{-4}	1.14×10^{-4}
0.0520	8.38×10^{-4}	5.85×10^{-4}	6.79×10^{-5}
0.0337	5.59×10^{-4}	3.82×10^{-4}	4.51×10^{-5}
0.0168	2.97×10^{-4}	1.92×10^{-4}	2.01×10^{-5}

Table SI 3.2: Average k_{obs} (s^{-1}) for the reaction of **Ru-2** (0.1594 mM) with thiourea nucleophiles

[Nu] /M	**Tu** ((λ = 676 nm) k_{obs} /s^{-1}	**Dmtu** ((λ = 676 nm) k_{obs} /s^{-1}	**Tmtu** ((λ = 675 nm) k_{obs} /s^{-1}
0.0797	4.96×10^{-5}	9.41×10^{-5}	4.15×10^{-5}
0.0638	3.87×10^{-5}	7.58×10^{-5}	3.33×10^{-5}
0.0478	2.95×10^{-5}	5.51×10^{-5}	2.52×10^{-5}
0.0319	2.06×10^{-5}	3.87×10^{-5}	1.61×10^{-5}
0.0159	1.05×10^{-5}	1.92×10^{-5}	8.52×10^{-6}

Table SI 3.3: Average k_{obs} (s^{-1}) for the reaction of **Ru-3** (0.467 mM) with thiourea nucleophiles

[Nu] /M	**Tu** (λ = 722 nm) k_{obs} /s^{-1}	**Dmtu** (λ = 717 nm) k_{obs} /s^{-1}	**Tmtu** (λ = 680 nm) k_{obs} /s^{-1}
0.0467	6.29×10^{-3}	3.64×10^{-3}	1.42×10^{-4}
0.0374	5.31×10^{-3}	2.87×10^{-3}	1.25×10^{-4}
0.0280	4.06×10^{-3}	1.96×10^{-3}	1.09×10^{-4}
0.0187	2.52×10^{-3}	1.57×10^{-3}	8.97×10^{-5}
0.0093	1.24×10^{-3}	5.81×10^{-4}	4.41×10^{-5}

Table SI 3.4: Average k_{obs} (s^{-1}) for the reaction of **Ru-4** (0.310 mM) with thiourea nucleophiles

[Nu] /M	**Tu** ((λ = 699 nm) k_{obs} /s^{-1}	**Dmtu** ((λ = 700 nm) k_{obs} /s^{-1}	**Tmtu** ((λ = 700 nm) k_{obs} /s^{-1}
0.03095	7.02×10^{-3}	1.08×10^{-2}	1.06×10^{-3}
0.02476	5.44×10^{-3}	8.85×10^{-3}	8.92×10^{-4}
0.01857	3.82×10^{-3}	6.45×10^{-3}	7.61×10^{-4}
0.01236	2.58×10^{-3}	4.25×10^{-3}	5.39×10^{-4}
0.00618	1.31×10^{-3}	1.99×10^{-3}	2.50×10^{-4}

SI 3.3 Average $\ln\left(\frac{k_2}{T}\right)$ values for the substitution of aqua ligands in the investigated complexes

Table SI 3.5: Average $ln\left(\frac{k_2}{T}\right)$ for the reaction of **Ru-1** with thiourea nucleophiles

T/ K	$\frac{1}{T}$ /K^{-1}	$\ln\left(\frac{k_2}{T}\right)$ **Tu**	$\ln\left(\frac{k_2}{T}\right)$ **Dmtu**	$\ln\left(\frac{k_2}{T}\right)$ **Tmtu**
298.15	0.00335	-9.796	-10.094	-11.466
303.15	0.00330	-9.538	-9.804	-11.071
308.15	0.00325	-9.246	-9.417	-10.646
313.15	0.00319	-8.953	-9.038	-10.176
318.15	0.00314	-8.625	-8.772	-9.913

Table SI 3.6: Average $ln\left(\frac{k_2}{T}\right)$ obtained for the reaction of **Ru-2** with thiourea nucleophiles

T/ K	$\frac{1}{T}$ /K^{-1}	$\ln\left(\frac{k_2}{T}\right)$ **Tu**	$\ln\left(\frac{k_2}{T}\right)$ **Dmtu**	$\ln\left(\frac{k_2}{T}\right)$ **Tmtu**
298.15	0.00335	-12.75	-12.32	-13.29
303.15	0.00330	-12.41	-11.97	-12.71
308.15	0.00325	-11.88	-11.46	-12.19
313.15	0.00319	-11.42	-10.98	-11.61
318.15	0.00314	-10.95	-10.63	-11.16

Table SI 3.7: Average $ln\left(\frac{k_2}{T}\right)$ for the reaction of **Ru-3** with thiourea nucleophiles

T/ K	$\frac{1}{T}$ /K^{-1}	$\ln\left(\frac{k_2}{T}\right)$ **Tu**	$\ln\left(\frac{k_2}{T}\right)$ **Dmtu**	$\ln\left(\frac{k_2}{T}\right)$ **Tmtu**
298.15	0.00335	-7.66	-8.12	-9.63
303.15	0.00330	-7.42	-7.78	-9.14
308.15	0.00325	-7.16	-7.42	-8.69
313.15	0.00319	-6.92	-7.16	-8.18
318.15	0.00314	-6.73	-6.87	-7.79

Table SI 3.8: Average $ln\left(\frac{k_2}{T}\right)$ for the reaction of **Ru-4** with thiourea nucleophiles

T/ K	$\frac{1}{T}$ /K^{-1}	$\ln\left(\frac{k_2}{T}\right)$ **Tu**	$\ln\left(\frac{k_2}{T}\right)$ **Dmtu**	$\ln\left(\frac{k_2}{T}\right)$ **Tmtu**
298.15	0.00335	-7.279	-6.755	-8.89
303.15	0.00330	-7.095	-6.427	-8.56
308.15	0.00325	-6.782	-6.273	-8.15
313.15	0.00319	-6.437	-5.960	-7.81
318.15	0.00314	-6.261	-5.712	-7.43

SI 3.4 Typical plots of k_{obs} versus nucleophile concentration for the substitution aqua ligands by thiourea nucleophiles

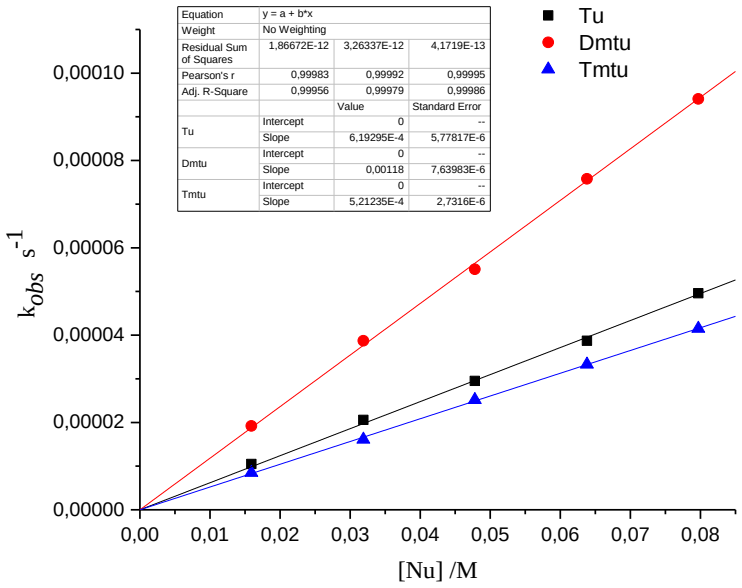

Figure SI 3.1: Dependence of k_{obs} on concentration of incoming thiourea nucleophiles for the substitution of the aqua ligand in **Ru-2** at 298 K, pH = 2.0, I = 0.1 M $HClO_4/NaClO_4$

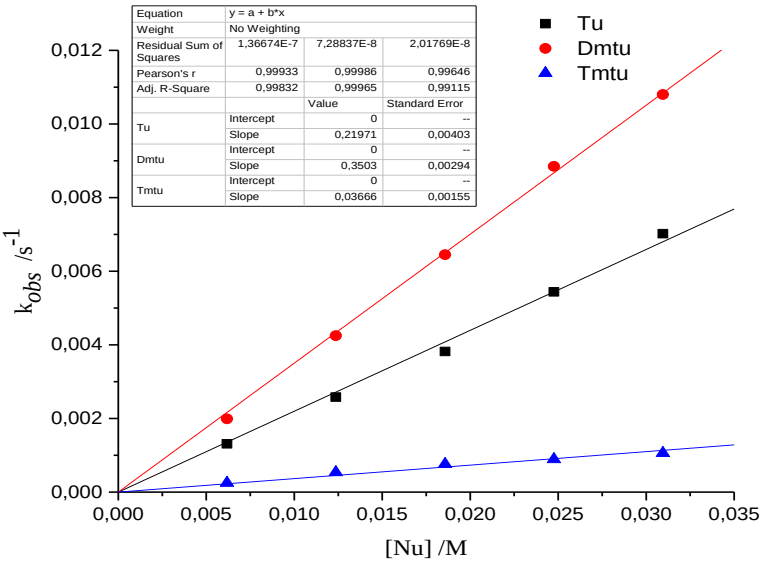

Figure SI 3.2: Dependence of k_{obs} on concentration of incoming thiourea nucleophiles for the substitution of the aqua ligand in **Ru-4** at 298 K, pH = 2.0, I = 0.1 M $HClO_4/NaClO_4$

SI 3.5 Typical Eyring plots obtained for the complexes

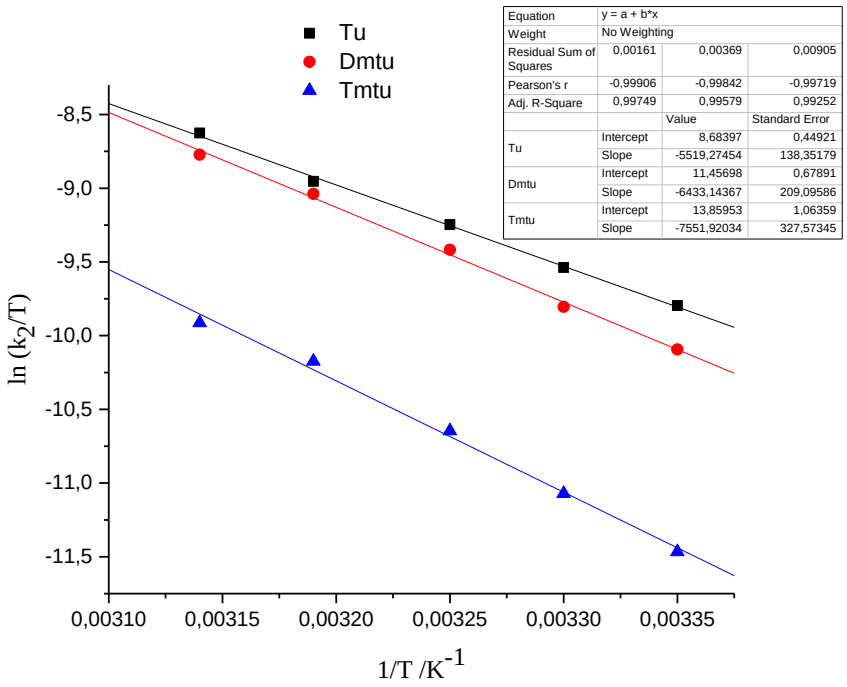

Figure SI 3.3: Eyring plots for the reaction of **Ru-1** with thiourea nucleophiles, pH = 2.0, I = 0.1 M $HClO_4/NaClO_4$

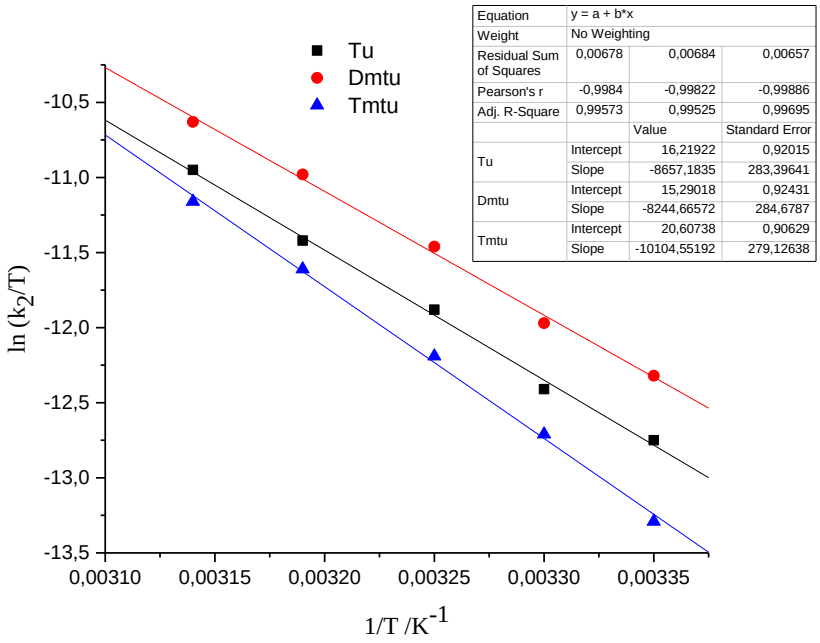

Equation	y = a + b*x		
Weight	No Weighting		
Residual Sum of Squares	0,00678	0,00684	0,00657
Pearson's r	-0,9984	-0,99822	-0,99886
Adj. R-Square	0,99573	0,99525	0,99695
		Value	Standard Error
Tu	Intercept	16,21922	0,92015
	Slope	-8657,1835	283,39641
Dmtu	Intercept	15,29018	0,92431
	Slope	-8244,66572	284,6787
Tmtu	Intercept	20,60738	0,90629
	Slope	-10104,55192	279,12638

Figure SI 3.4: Eyring plots for the reaction of **Ru-2** with thiourea nucleophiles, pH = 2.0, *I* = 0.1 M $HClO_4/NaClO_4$

SI 3.6 Typical ultraviolet-visible Spectra for p*K*a titrations of the complexes

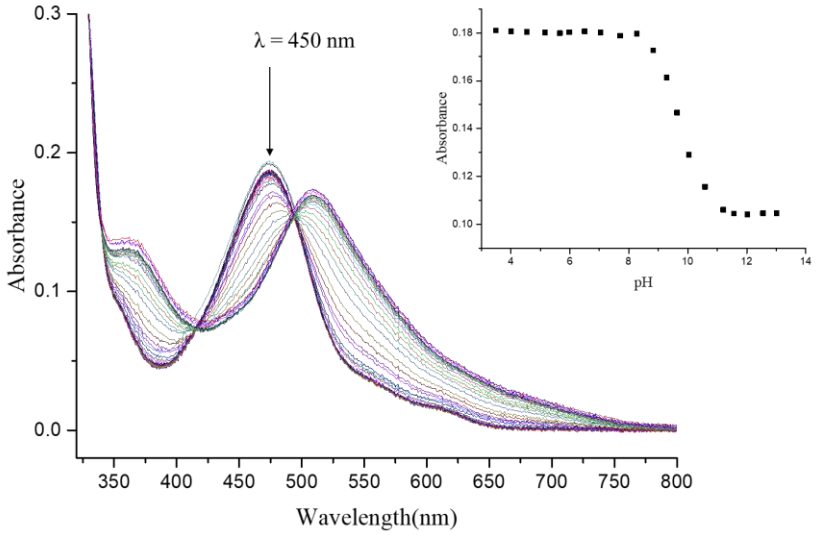

Figure SI 3.5: Ultraviolet-visible spectra of **Ru-2** recorded as a function of pH in the range 2–13 at 298 K. **Inset**: A plot of absorbance versus pH at λ = 450 nm

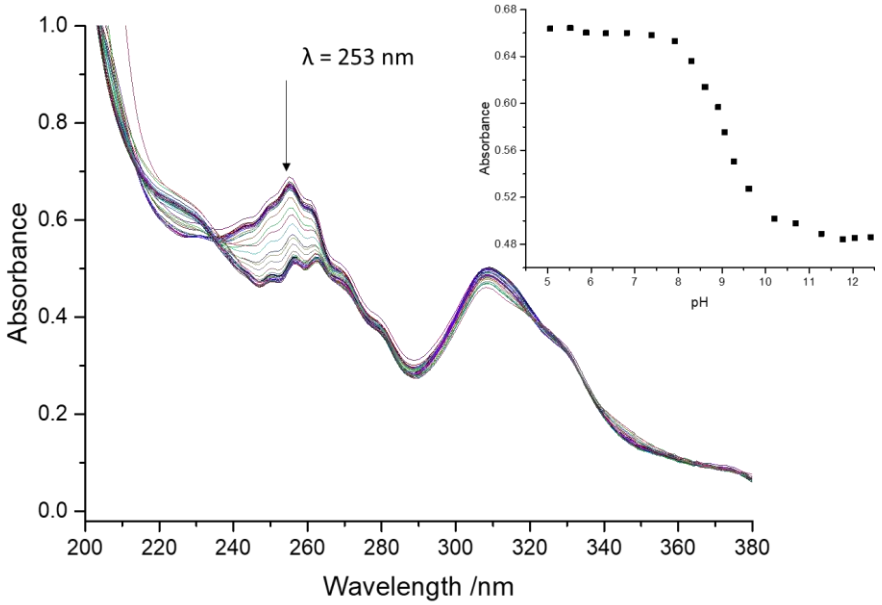

Figure SI 3.6: Ultraviolet-visible spectra of **Ru-4** complex recorded as a function of pH in the range 2–13 at 298 K. **Inset**: A plot of absorbance versus pH at λ = 253 nm

SI 3.7 Additional DFT-optimized structures of the studied complexes

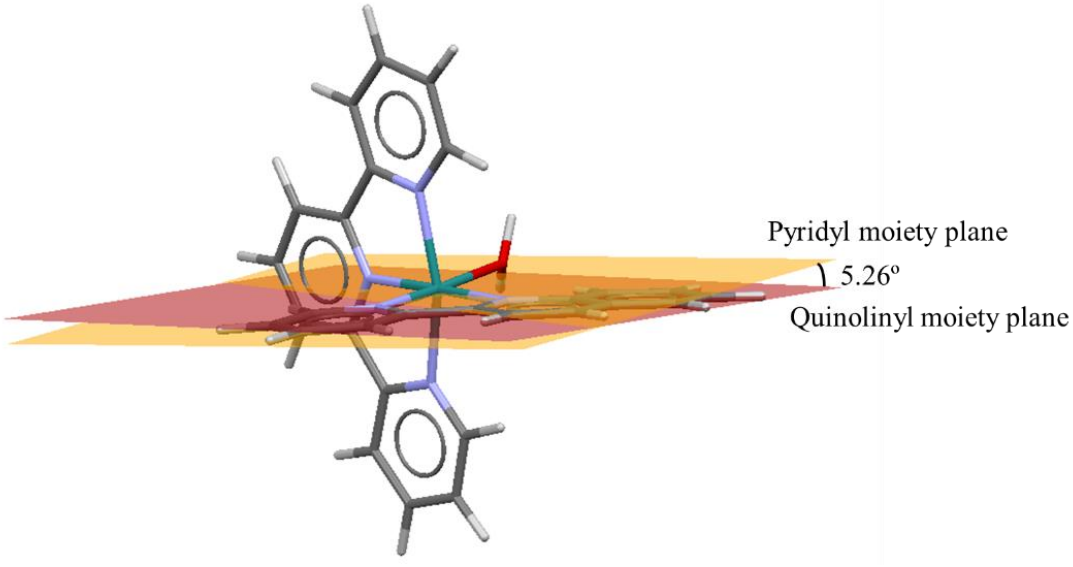

Figure SI 3.7: DFT-optimized structure of **Ru-3** showing the dihedral angle between the planes of the pyridyl and quinolinyl moieties

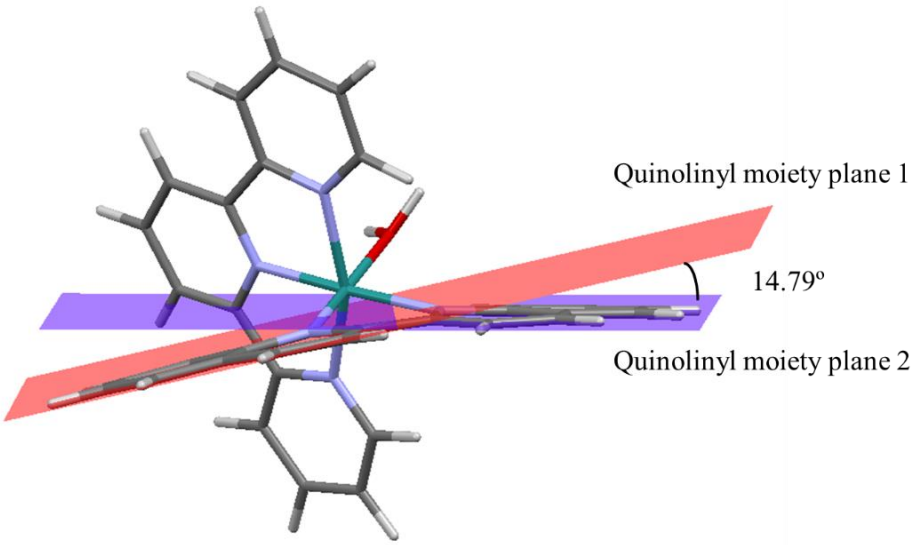

Figure SI 3.8: DFT-optimized structure of **Ru-4** showing the dihedral angle between the planes of the quinolinyl moieties

SI 3.8 Samples of MS, ^{1}H and ^{13}C NMR spectra for compounds

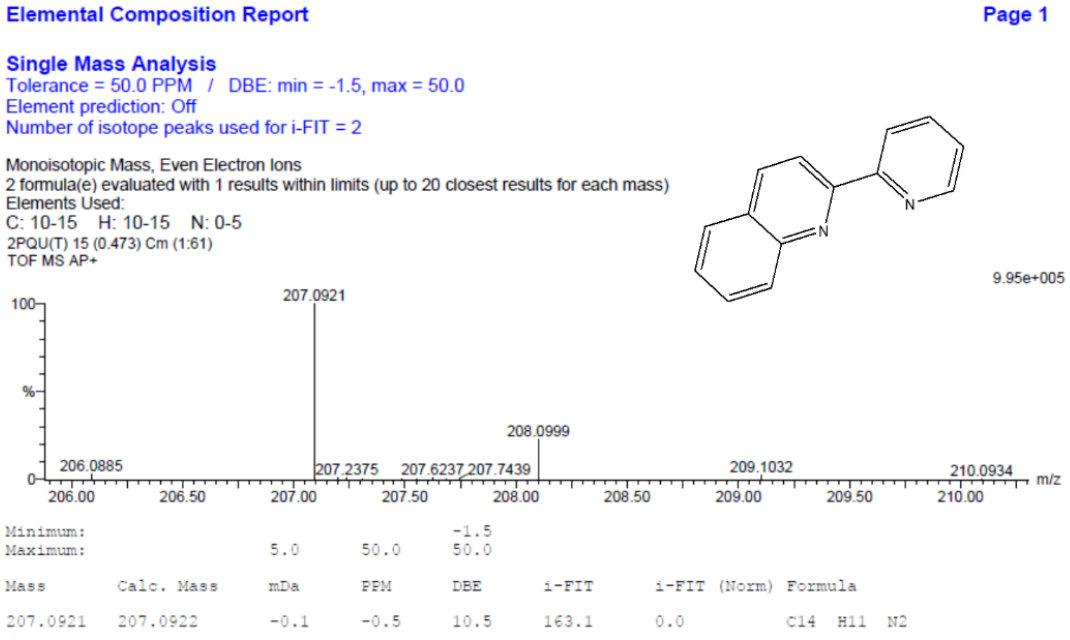

Figure SI 3.9: ESI-MS (TOF) spectrum of 2-(2-pyridyl)quinoline

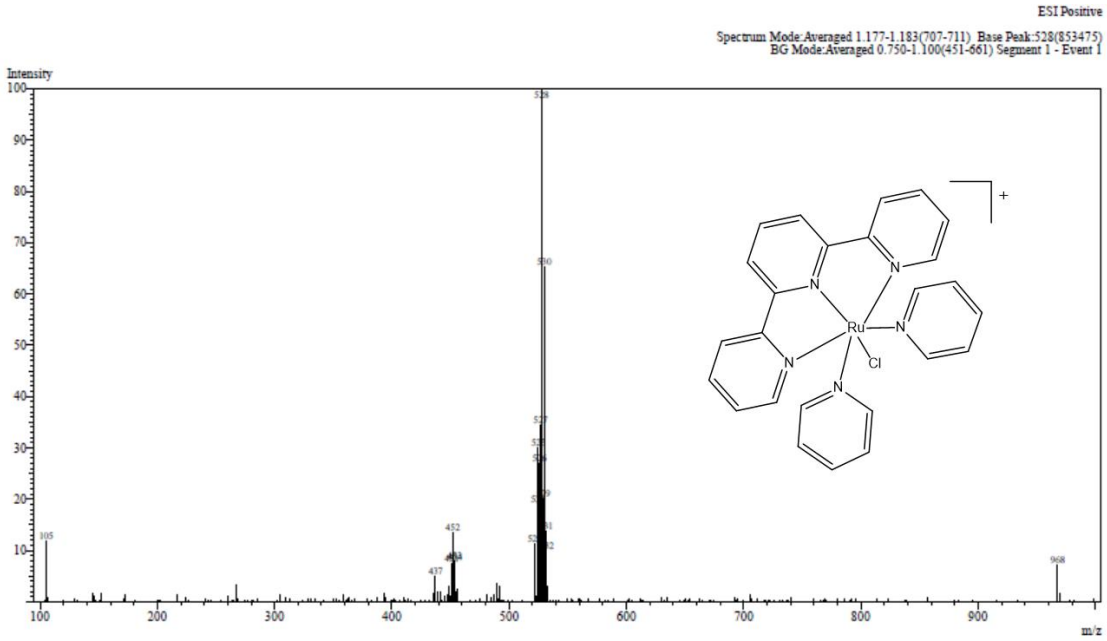

Figure SI 3.10: ESI-LCMS spectrum of *trans*-chlorobis(pyridine)(2,2':6',2''-terpyridyl) ruthenium(II) hexaflourophosphate

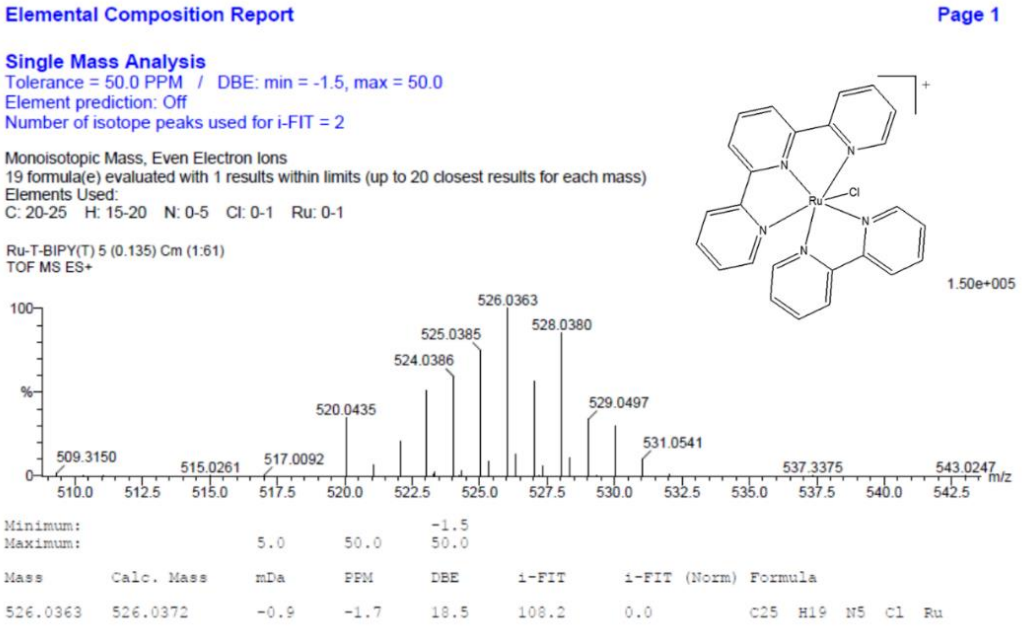

Figure SI 3.11: ESI-MS (TOF) spectrum of (2,2'-bipyridyl)chloro(2,2':6',2''-terpyridine) ruthenium(II) chloride

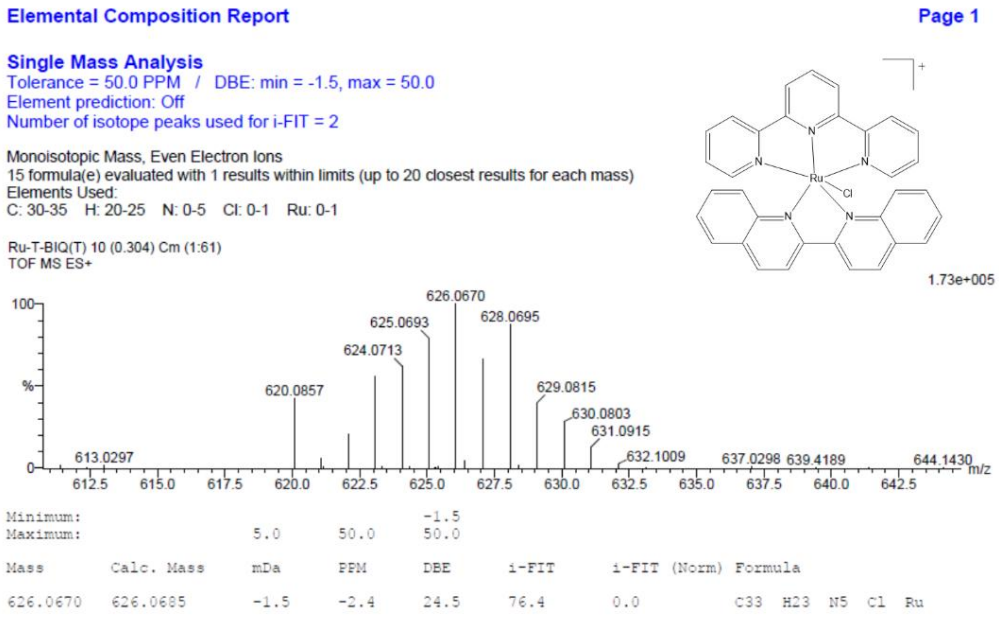

Figure SI 3.12: ESI-MS (TOF) spectrum of (2,2'-Biquinoline)chloro(2,2':6',2''-terpyridine) ruthenium(II) hexafluorophosphate

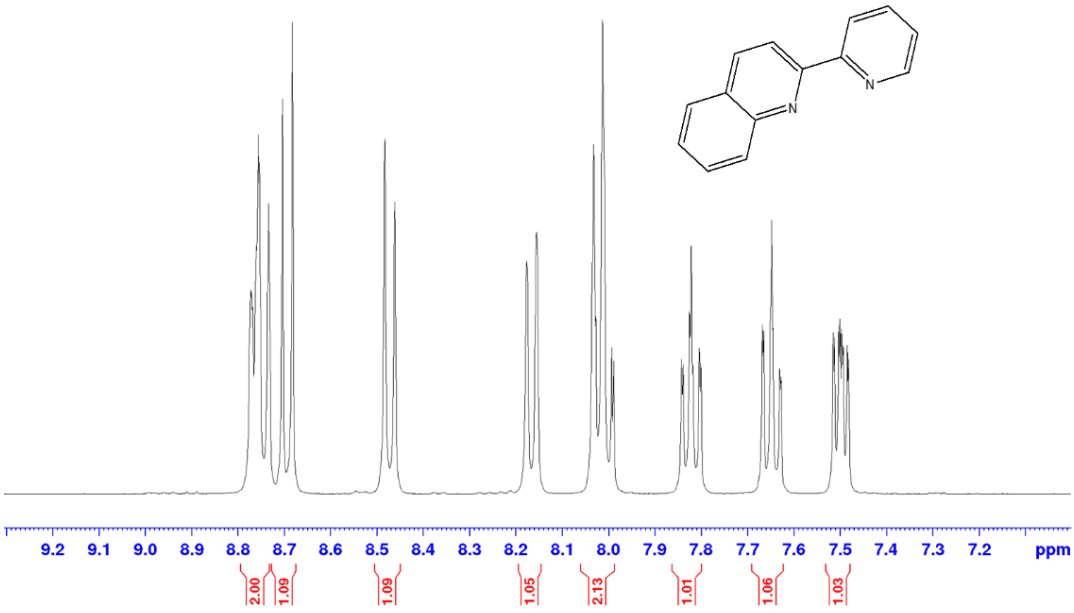

Figure SI 3.13: ^{1}H NMR (400 MHz, acetone-d_6) spectrum of 2-(2-pyridinyl)quinoline

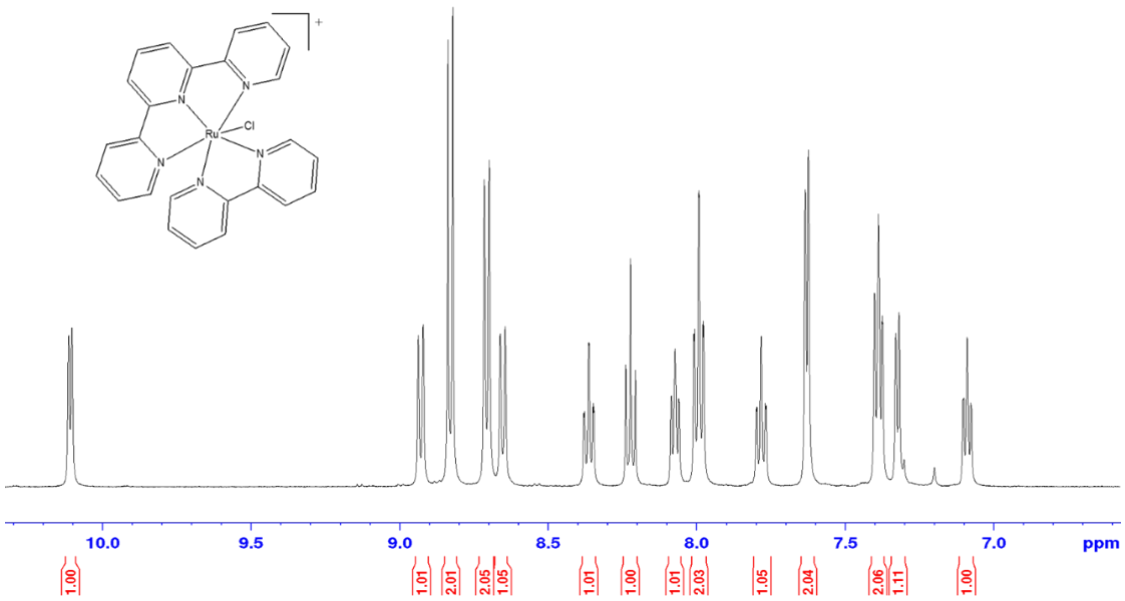

Figure SI 3.14: ^{1}H NMR (400 MHz, DMSO-d_6) spectrum of (2,2'-Bipyridyl)chloro(2,2':6',2''-terpyridyl)-ruthenium(II) chloride

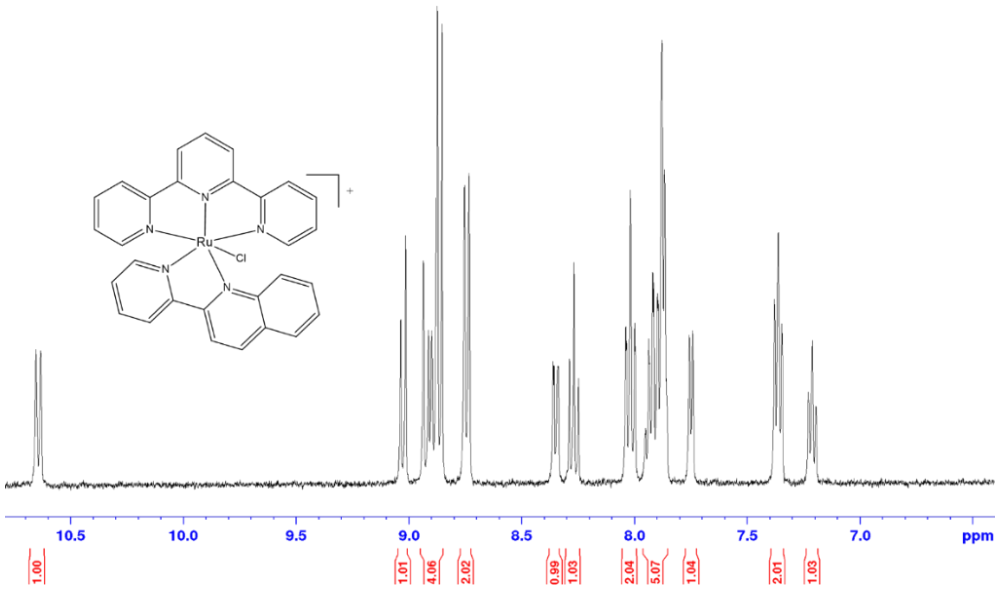

Figure SI 3.15: ^{1}H NMR (500 MHz, Cd_3Od-d_4) spectrum of *Proximal*-Chloro(2-(2-pyridinyl)quinoline)(2,2':6',2''-terpyridyl)ruthenium(II) chloride

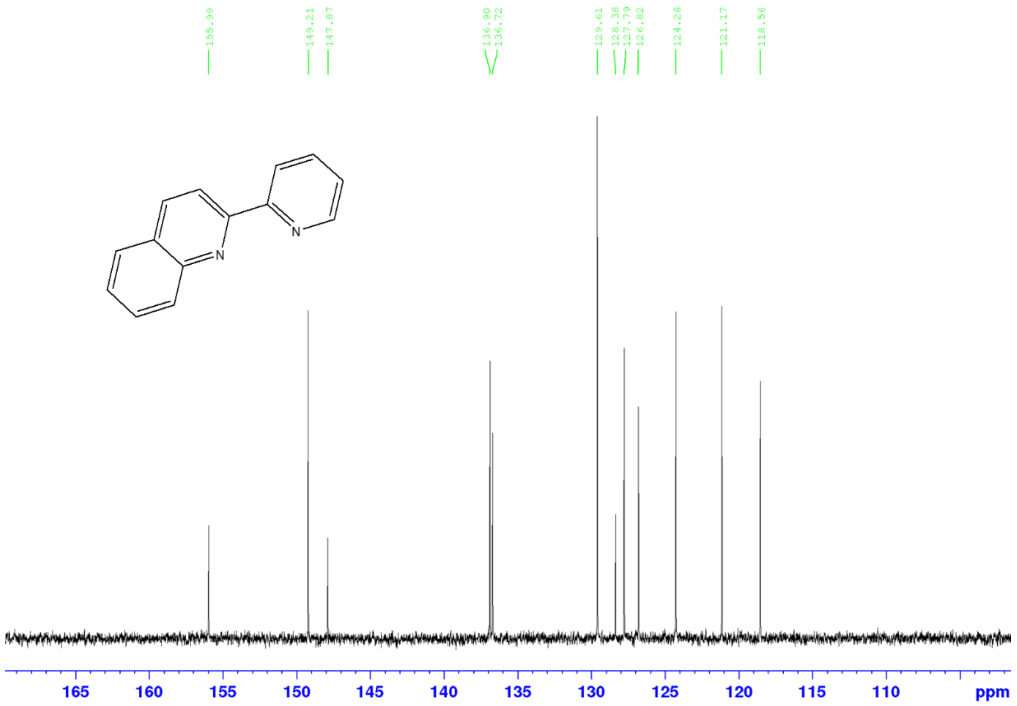

Figure SI 3.16: ^{13}C NMR (400 MHz, acetone-d_6) spectrum of 2-(2-pyridinyl)quinoline

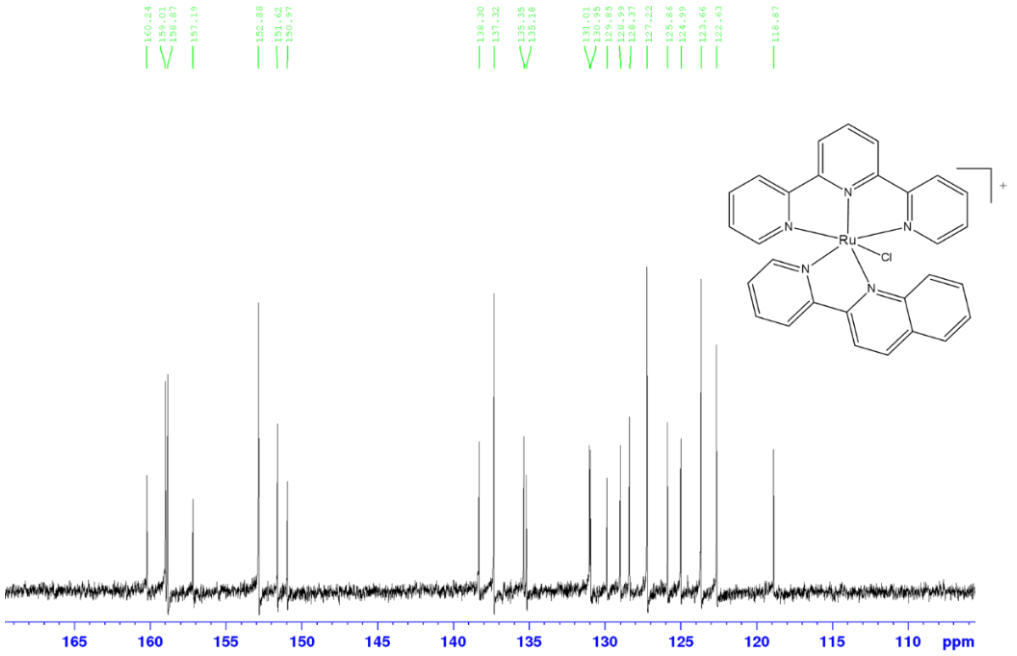

Figure SI 3.17: ^{13}C NMR (500 MHz, Cd_3Od-d_4) spectrum of *Proximal*-Chloro(2-(2-pyridinyl)quinoline)(2,2':6',2"-terpyridyl)ruthenium(II) chloride

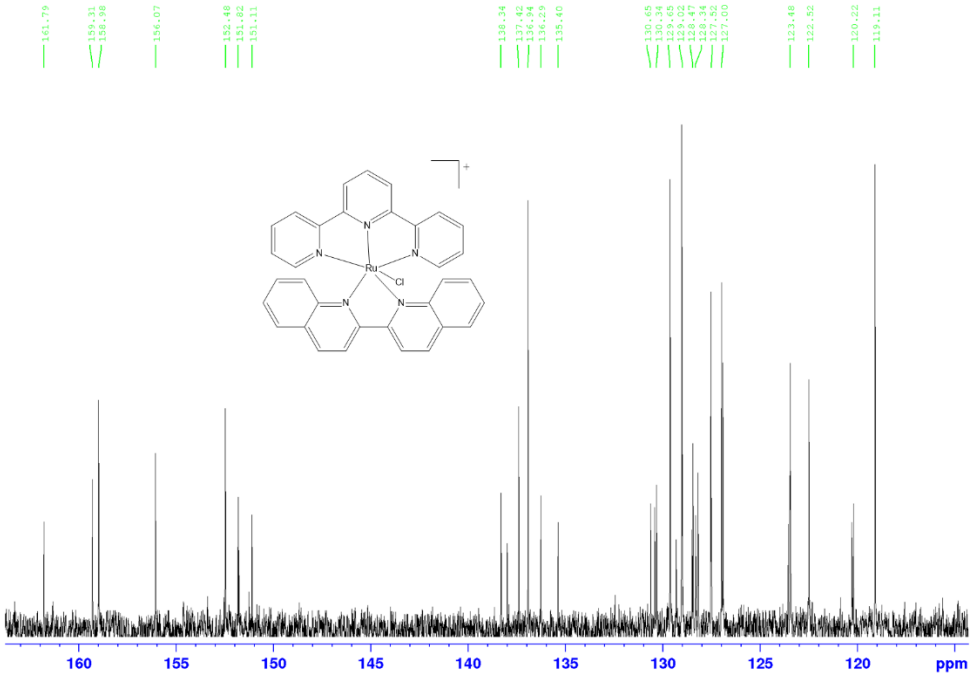

Figure SI 3.18: ^{13}C NMR (400 MHz, Cd_3Od-d_4) spectrum of (2,2'-Biquinoline)chloro(2,2':6',2''-terpyridine)ruthenium(II) hexafluorophosphate

CHAPTER FOUR

The Role of π-Back-Bonding and *Trans*-Effect on the Reactivity of Ruthenium (II) Complexes: Kinetic and Mechanistic studies

Abstract

Substitution kinetics of the chloro ligands in a series of six ruthenium(II) polypridyl complexes by three thiourea nucleophiles (thiourea, *N,N*-dimethylthiourea and *N,N,N',N'*-tetramethylthiourea) was investigated as a function of concentration and temperature under *pseudo*-first order conditions using ultraviolet-visible spectrophotometric techniques. The simultaneous substitution of the coordinated chloro ligands in all the complexes obeyed the rate law, $k_{obs} = k_2$[Nucleophile]. The complexes were grouped into two with the trend in reactivity decreasing in the order; **Ru-3** > **Ru-4** > **Ru-2** > **Ru-1** and **Ru-5** > **Ru-6** > **Ru-2.** This trend in reactivity is attributed to the concerted effects of stereo-electronic properties of the coordinated spectator ligands. When the denticity of the ligands is changed from one (**Ru-1**) to two (**Ru-2**), and the π-conjugated surface area of the complexes successively increased from **Ru-2** to **Ru-4**, the energy separation between the frontier orbitals reduces. Therefore, as one moves from **Ru-1** to **Ru-4**, the electrophilicity of complexes increase due to improved π-back-bonding of electron density from the dπ orbital largely based on the metal centre to the π* orbitals of the spectator ligands. This accordingly increases susceptibility of the metal centre to facile nucleophilic attack. However, despite the higher electrophilicity index and narrower HOMO-LUMO gap, the reactivity of **Ru-4** is lower than that of **Ru-3**. This is attributed to increased steric hindrance around the metal centre caused by the banana shaped curvatures formed by the two 2,2'-biquinoline ligands which restricts the space around the metal centre. The higher reactivity observed in **Ru-5** and **Ru-6** compared to **Ru-2** is ascribed to σ *trans*-

effect brought about by the dimethyl-substituted chelating ligands therein which causes ground state labilisation of the Ru-Cl bonds. This is shown by the more elongated Ru-Cl bonds in **Ru-5** (2.594 Å) and **Ru-6** (2.590 Å) compared to **Ru-2** (2.566 Å). Replacement of the 2,2'-bipyridyl backbone with a stronger π-acceptor 1,10-phenanthroline reduces the *trans*-effect through metal-ligand charge transfer hence the lower reactivity observed in **Ru-6** compared to **Ru-5**. The activation parameters ($\Delta H^{\neq} > 0$, $\Delta S^{\neq} < 0$) obtained in all the complexes support an associative mechanism of activation. As proven by the crystal structure of the product, the stereochemistry of the complex and oxidation state (+2) of the metal centre are maintained after reaction with *N*,*N*,*N*,*N*-tetramethylthiourea. Moreover, it proves that no dechelation of the coordinated spectator ligands occur, an indication of stability of the final product.

4.1 Introduction

Ruthenium(II) and (III) based complexes are considered viable options in the design of anticancer drugs because they exhibit similar reactivity profiles with respect to ligand substitution as platinum(II).[1] They also have attractive properties such as; high selectivity for cancer cells, high cellular uptake, low systemic toxicity, and ability to mimic the role of iron binding functions with biomolecules.[2] The fact that ruthenium(III) complexes are activated by *in vivo* reduction to more reactive and cytotoxic ruthenium(II) complexes, has enhanced anticancer research interests in the latter.[1, 3] The divalent complexes provide an array of diverse coordination modes such as covalent binding, groove binding, insertion and intercalation.[4] Moreover, it is documented that, apart from their main target, the DNA, they also interact with DNA topoisomerase and mitochondria.[5]

Polypyridyl based complexes form an important class of potential anticancer ruthenium complexes[6] whose cytoxicity is positively correlated to the aromatic π-conjugated surface area of the coordinated ligands.[7] Numerous studies have also shown that complexes with strain-inducing methyl substituents are more cytotoxic compared to those with unsubstituted ligands.[7c, 8]

Effects of π-conjugation on the substitution kinetics of transition metal complexes has been comprehensively investigated especially on square planar platinum(II) complexes.[9] It is established that extended π-conjugation may enhance or retard a substitution reaction depending on its position relative to the leaving group as well as the nature of the organic moiety therein. For instance; in square planar platinum(II) complexes, pyridyl rings at *cis/trans* position accelerates the rate of substitution by increasing the electrophilicity of the complex while a quinoline moiety placed at the lateral position retards the reactivity by destabilizing the LUMO. [9a-c] On the other hand, available information show that electron withdrawing substituents on the aromatic ligand framework generally enhance the reactivity of complexes while electron donating groups have an

opposite effect.[9b] The former withdraws electron density from metal centres while the latter donates electrons to the metal centre. However, in some cases, electron donating substituents have been reported to enhance reactivity compared to complexes with unsubstituted ligands due to strong *trans*-effects.[10] Based on these facts, the role of π-conjugation and substituent groups on reactivity of complexes remain unexhausted especially in octahedral ruthenium complexes.

Examination of the substitution kinetics of mononuclear complexes with two labile groups reveal that, the labile ligands can either be substituted simultaneously or consecutively depending on the nature of the coordinated spectator ligand. Complexes with asymmetrical ligands experience two substitution steps while those with symmetrical ligands may experience a single or two substitution steps depending on the nucleophile used.[9d, 10b, 11] Therefore, there is need for further research on complexes with two leaving groups especially for those with octahedral geometries.

Taking into account, the ever-growing interest in utilization of ruthenium complexes as alternative or complementary anticancer metallodrugs, it is important to establish the structure-reactivity relationships of these complexes. The present study investigates and reports on the effect of different ligands on the reactivity of the ruthenium(II) complexes with two leaving groups. The spectator ligands judiciously selected for the synthesis of the complexes were pyridine, 2,2'-bypridiyl (bipy), 6,6-dimethyl-2,2'-bipyridyl, 2,9-dimethyl-1,10-phenanthroline and 2,2'-biquinoline (Figure 4.1). The ligands offer a range of electronic and structural properties. In complex **Ru-1**, the two chloro ligands are *trans* to each other while in the other complexes the two chloro ligands are coordinated in *cis* fashion. Complex **Ru-3** has a hybrid ligand system, a 2,2'-bypridiyl and 2,2'-biquinoline. Bio-relevant thiourea nucleophiles of varied steric demands were used; thiourea (Tu), *N*,*N*-dimethylthiourea (Dmtu) and *N,N,N',N'*-tetramethylthiourea (Tmtu).

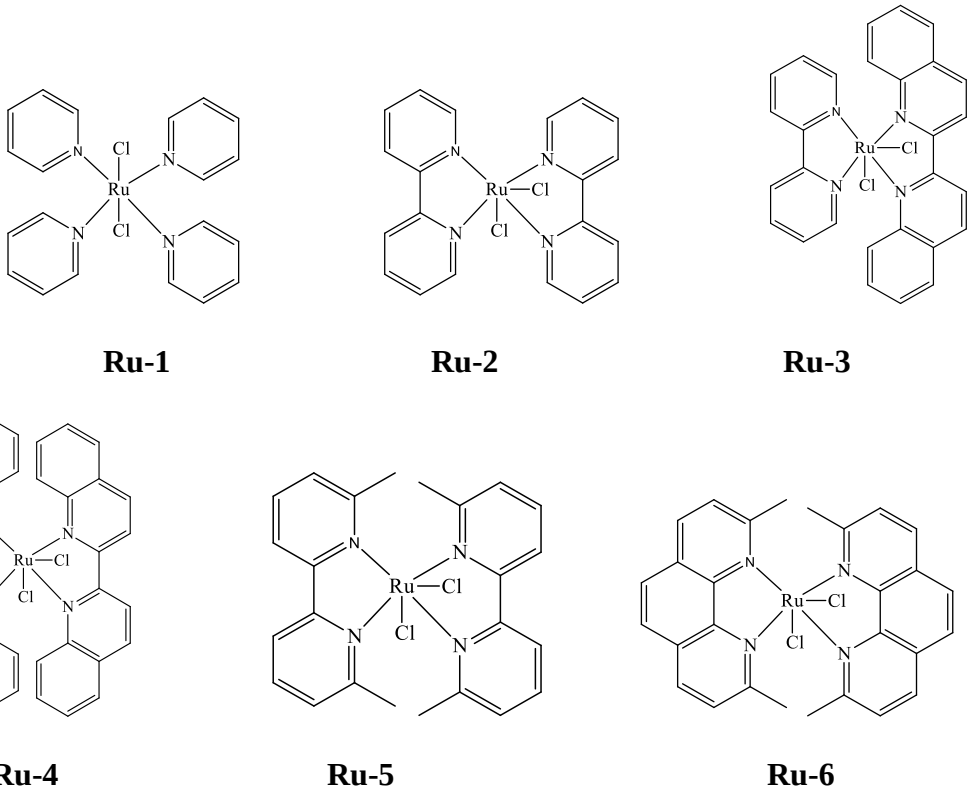

Figure 4.1: Structures of the investigated ruthenium(II) complexes

In addition to the experimental studies, computational investigations were performed using density functional theory to gain in-depth insight of the intrinsic electronic and structural properties of the complexes. To further understand the interaction of these divalent ruthenium complexes with the sulfur-donor nucleophiles, an independent study was carried out to crystallographically characterize a solid-state crystal structure of a substitution product formed.

4.2 Experimental

4.2.1 Materials and Procedures

All the syntheses were performed under inert atmosphere of dry oxygen-free dinitrogen using standard Schlenk-ware techniques. Dichloro(*p*-cymene)ruthenium(II) dimer (97%), LiCl (≥ 99%),

$LiCF_3SO_3$ (≥ 99%), $RuCl_3.3H_2O$, NH_4PF_6 (≥ 99%), 2,2'-bipyridyl (99%), anhydrous pyridine (99.8%), 6,6'-dimethyl-2,2'-bipyridyl (98%), 2,9-dimethyl-1,10-phenanthroline (≥ 98%), 2,2'-biquinoline (98%), Tu (≥ 99%), Dmtu (99%) and Tmtu (98%) were supplied by Sigma-Aldrich/Merck (Pty). Organic solvents were purchased from Merck (Pty) and used without further purification. Modulab deionized water was used where necessary.

4.2.2 Synthesis of the Complexes

The complexes were synthesized according to published literature methods.[12]

(2,2'-bipyridyl)chloro(η^6-*p*-cymene)ruthenium(II) hexaflourophosphate: In 25 mL of methanol, a mixture of 2, 2'-bipyridyl (59.0 mg, 0.38 mmol) and dichloro(*p*-cymene)ruthenium(II) dimer) (100.0 mg, 0.16 mmol) was stirred at room temperature for 2 h. Afterwards, 5 mL of methanol containing NH_4PF_6 (57.0 mg, 0.35 mmol) was added into the solution and the resulting mixture stirred for further 1 h. The orange precipitate which was formed was filtered off, washed with chilled methanol and diethyl ether. The product was purified by recrystallization from methanolic solution of the complex. Shiny yellow crystalline solid was obtained. Yield: 164.0 mg (90%). *Anal. Calc*. for $C_{20}H_{22}ClN_2PF_6Ru$; C, 42.00; H, 3.88 N, 4.90. *Found*: C, 42.27; H, 3.84; N, 4.87. ^{1}H NMR (400 MHz, acetone-d_6): δ (ppm) = 9.62 (d, 2H), 8.62 (d, 2H), 8.32 (td, 2H), 7.82 (m, 2H), 6.25 (d, 2H), 6.00 (d, 2H), 2.67 (hept, 1H), 2.33 (s, 3H), 1.11 (d, 6H). ESI-MS (TOF) (*m/z*): 427.05 (M^+). This precursor complex was used in the synthesis of **Ru-3**.

***Trans*-Dichlorotetrapyridineruthenium(II) (Ru-1):** $RuCl_3.3H_2O$ (500 mg, 1.91 mmol) dissolved in 25 mL of ethanol-water (60-40% v/v) solvent system was refluxed for 4 h. The deep blue solution obtained was cooled to ambient temperature, 30 mL of anhydrous pyridine added and the resultant solution refluxed for 0.5 h. The solution was then concentrated to about 10 mL and the orange crystalline solid filtered off, washed with chilled water (3 × 10 mL) and diethyl

ether (3 × 30 mL) and dried under vacuum. Orange shiny crystalline solid was obtained. Yield: 640 mg (70%). *Anal. Calc for* $C_{20}H_{20}Cl_2N_4Ru$: C, 49.19; H, 4.13; N, 11.47. *Found*: C, 49.08; H, 3.98; N, 11.14. ^{1}H NMR (500 MHz, DMSO-d_6): δ (ppm) = 8.43 (d, 2H), 7.75 (t, 1H), 7.20 (d, 2H). LC-MS-ES$^+$ m/z: 488 (M).

***cis*-bis(2,2'-Bipyridyl)dichlororuthenium(II) (Ru-2):** A mixture of $RuCl_3.3H_2O$ (340 mg, 1.49 mmol), 2,2'-bipyridyl (468 mg, 3.00 mmol), and LiCl (420 mg, 0.10 mmol) in 30 mL of N,N-dimethylformamide were refluxed for 8 h. After cooling the solution to ambient temperature, 125 mL of acetone was added and the resultant solution kept in a refrigerator at -4 ℃ for 12 h. The dark brown crystalline solid formed was filtered off and washed with water (3 × 25 mL) followed by diethyl ether (3 × 30 mL), and then dried under vacuum. Dark brown crystals were obtained. Yield: 289 mg (40%). *Anal. Calc. for* $C_{20}H_{16}Cl_2N_4Ru.2H_2O$: C, 49.60; H, 3.33; N, 11.57; *Found*: C, 49.57; H, 3.41; N, 11.60. ^{1}H NMR (500 MHz, DMSO-d_6): δ (ppm) = 9.98 (d, 2H), 8, 63 (d, 2H), 8.47 (d, 2H), 8.05 (t, 2H), 7.75 (t, 2H), 7.66 (t, 2H), 7.51 (d, 2H), 7.09 (t, 2H). ESI-MS (TOF) (*m/z*): 449.01 (M^+).

***cis*-(2,2'-Bipyridyl)(2,2'-biquinoline)dichlororuthenium(II) (Ru-3):** A mixture of (2,2'-bipyridyl)-chloro(η^6-*p*-cymene)ruthenium(II) hexaflourophosphate (311 mg, 0.505 mmol), 2,2'-biquinoline (142 mg, 0.55 mmol) and LiCl (156 mg, 3.65 mmol) in 2 mL *N,N*-dimethylformamide was refluxed for 3 h. Upon cooling to room temperature, 50 mL of acetone was added. The dark green precipitate obtained was filtered off and rinsed with 15 mL of water and 15 mL of diethyl ether and dried under vacuum. Green product was obtained. Yield (208 mg, 62%). *Anal. Calc. for* $C_{28}H_{20}Cl_2N_4Ru$: C, 57.54; H, 3.45; N, 9.59; *Found*: C, 57.18; H, 3.53; N, 9.25. ^{1}H NMR (400 MHz, DMSO-d_6): δ (ppm) = 9.75 (t, 2H), 8.74 (m, 2H), 8.62 (d, 1H), 8.57 (d, 1H), 8.25 (d, 1H),

8.18 (d, 1H), 8.09 (t, 1H), 7.91 (d, 1H), 7.75-7.71 (m, 4H), 7.53 (d, 1H) 7.42 (t, 1H);, 7.10 (t, 2H), 6.98 (d,1H). ESI-MS (TOF) (*m/z*): 549.04 (M^+)

***cis*-bis(2,2'-biquinoline)dichlororuthenium(II) (Ru-4):** A mixture of $RuCl_3.3H_2O$ (180 mg, 0.67 mmol), 2,2-biquinoline (370 mg, 1.5 mmol) and LiCl (87 mg, 2.1 mmol) in 6 mL *N,N*-dimethylformamide was refluxed for 6 h. The mixture was then allowed to cool to ambient temperature and pipetted dropwise to 500 mL of stirring water. The precipitate which formed was filtered off and re-dissolved in 5 mL of dichloromethane and filtered again. To the filtrate, 50 mL of water was added and the green precipitate formed filtered off, washed with copious amount of water and rinsed with diethyl ether and dried under vacuum. Green precipitate was obtained. Yield (206 mg, 45%). *Anal. Calc. for* $C_{36}H_{24}Cl_2N_4Ru.2H_2O$: C, 60.00; H, 3.92; N, 7.78; *Found*: C, 59.64; H, 4.15; N, 7.61. ^{1}H NMR (400 MHz, DMSO-d_6): δ (ppm) = 9.10-9.07 (m, 2H), 9.03 (d, 3H), 8.83 (d, 2H), 8.60 (d, 2H), 8.34 (d, 2H), 8.21(d, 4H), 8.10 (d, 3H), 7.97-7.93 (m, 2H), 7.88 (t, 2H), 7.71 (t, 2H). ESI-MS (TOF) (*m/z*): 649.07 (M^+).

***cis*-bis(6,6'-dimethyl-2,2'-bipyridyl)dichlororuthenium(II) (Ru-5):** A mixture of $RuCl_3.3H_2O$ (250 mg, 0.95 mmol), 6,6'-dimethyl-2,2'-bipyridyl (375 mg, 2 mmol) and LiCl (550 mg, 13 mmol) in 10 mL of ethane-1,2-diol were refluxed at 140℃ for 3 h. The mixture was then allowed to cool to ambient temperature and 7 mL of water added. The crystalline product obtained was filtered off, washed with 10 mL of cold water and dried under a stream of nitrogen. Yield (301 mg, 52%). *Anal. Calc. for* $C_{24}H_{24}Cl_2N_4Ru$: C, 53.34; H, 4.48; N, 10.37; *Found*: C, 53.73; H, 4.65; N, 10.25. ^{1}H NMR (400 MHz, Cd_3Od-d_4): δ (ppm) = 8.24 (dd, 2H), 8.02 (d, 4H), 7.73 (m, 2H), 7.62 (t, 2H), 7.23 (dd, 2H), 2.49-1.83 (m, 12H). ESI-MS (TOF) (*m/z*): 505.07 (M^+).

***cis*-bis(2,9-dimethyl-1,10-phenanthroline)dichlororuthenium(II) (Ru-6):** A mixture of $RuCl_3.3H_2O$ (250 mg, 0.95 mmol), 2,9-dimethyl-1,10-phenanthroline (425 mg, 2 mmol) and LiCl

(625 mg, 15 mmol) in 10 mL of ethane-1,2-diol were refluxed at 150℃ for 6 h. The mixture was then allowed to cool to room temperature and 5 mL of water added. The crystalline product obtained was filtered off, washed with 5 mL chilled water and dried under a stream of nitrogen. Purple solid. Yield (482 mg, 85 %). *Anal. Calc. for* $C_{28}H_{24}Cl_2N_4Ru.H_2O$: C, 55.45; H, 4.32; N, 9.24; *Found*: C, 55.11; H, 4.48; N, 9.42. ^{1}H NMR (400 MHz, Cd_3Od-d_4): δ (ppm) = 8.37 (d, 4H), 8.01 (s, 2H), 7.80 (br, 2H), 7.57 (d, 2H), 7.24 (br, 2H), 3.09 (s, 6H), 1.87 (s, 6H). ESI-MS (TOF) (*m/z*): 553.07 (M^+).

4.2.3 Physical Measurements and Instrumentation

^{1}H NMR spectra of the complexes were recorded at 303 K on Bruker Avance DPX III 400/500 MHz spectrometer. Chemical shifts expressed in parts per million (δ) were referenced to $Si(CH_3)_4$ internal standard. Mass spectra were recorded in the positive mode after electrospray ionization and mass analysis on a Time of flight (TOF) of Waters Micromass LCT Premier spectrometer. Samples of NMR and MS spectral data are presented in Supplementary Information (Figures SI 4.8-4.15**)**. Elemental composition (C, H, and N) of the synthesized compounds were carried out using Thermo Scientific Flash 2000 analyzer. Kinetic studies were performed using Cary 100 Series ultraviolet-visible spectrophotometer attached to a thermoelectric cell temperature controller (Agilent technologies) with an accuracy of ± 0.05 °C. Kinetic data was processed using OriginPro 9.1®[13]

4.2.4 Kinetic Measurements

Both complex and nucleophile solutions were prepared in methanol and maintained at an ionic strength of 0.1 M LiCl/$LiCF_3SO_3$. The concentration of the complexes used were; **Ru-1** (0.40 mM), **Ru-2** (0.31 mM) **Ru-3** (0.184 mM), **Ru-4** (0.142 mM), **Ru-5** (0.100 mM) and **Ru-6** (0.100 mM). All the nucleophile solutions were prepared shortly before use. All substitution studies were

performed under *pseudo*-first order conditions in which the concentration of the nucleophile was at least 20 folds higher than the concentration of the complex. The reactions were initiated by mixing equal volumes of thermally equilibrated complex and nucleophile in tandem cuvettes. ultraviolet-visible spectral changes resulting from the reactions were recorded from 800 nm to 200 nm wavelength range and followed by monitoring the change in absorbance at an appropriate wavelength as a function of time. Concentration dependence reactions were performed at a constant temperature of 25℃ while the temperature dependence reactions were studied from 25 to 45℃ at an interval of 5℃. The results recorded herein are an average of at least three reproducible independent runs.

4.2.5 Computational Modelling

Computational calculations were performed using density functional theory (DFT) method as executed by Gaussian 09W program.[14] The structures were optimized using the hybrid 3-parameter B3LYP at the standard LANL2DZ basis set.[15] In DFT, the total energy is expressed in terms of physically observable three dimensional electron density over wave-function and therefore applicable to these systems with large number of electrons.[16] LANL2DZ utilizes relativistic effective core potentials (ECP) to account for the effect of inner core 28 electrons ([Ar]$3d^{10}$) in Ru.[17] The influence of the methanol solvent was evaluated using single point conductor-like polarizable continuum implicit solvent model (CPCM).[18] All the calculations were done at neutral charge singlet spin ground state settings. GaussView 5.0 program was used to visualize the optimized minimum energy structures of the complexes.[14] Electronic chemical potential (μ), chemical softness (σ) and global electrophilicity indices (ω) for the complexes were calculated as per literature methods.[19] Natural bonding orbitals (NBO) was used to determine localized atomic charges in the complexes. [14]

4.2.6 Crystallographic Substitution Product Analysis

An independent crystallographic structural determination of the substitution product of ruthenium(II) with Tmtu was used to understand the structural properties of the substitution products formed between ruthenium(II) complexes and thiourea nucleophiles. Crystals of the substitution product *trans*-$[Ru(bipy)_2Tmtu)_2](ClO_4)_2$, $C_{30}H_{40}Cl_2N_8O_8RuS_2$ were obtained by reacting *trans*-$[Ru(bipy)_2H_2O)_2](ClO_4)_2$ with excess Tmtu in 0.1 M $HClO_4/NaClO_4$ aqueous medium for 48 h at room temperature. The solution was left to crystalize at room temperature by slow evaporation of the solvent. After several weeks, crystals suitable for x-ray diffraction were obtained. The molecular structure of the complex was determined by Bruker Smart Apex II diffractometer equipped with Oxford Instruments Cryojet cooling system. A graphite-monochromated MoKα1 (λ = 0.71073 Å) radiation was used and the crystallographic data collected at 100 K using a 30 W Incoatec micro-focus source and ω-2θ scan mode. The theta range utilized for data collection was 1.839 to 27.779º. The molecular structure obtained was solved by SHELXS program suite supported by Olex2 for windows using direct methods.[20] Refinement of the structure was done using ShelXL package applying full matrix least squares on F^2 on all the observed reflections.[21]

4.3 Results

4.3.1 Computational Results

Computational optimization of the complexes was carried out to gain an insight into the spatial relationships of the coordinated ligand systems as well as the electronic properties of the complexes. Mappings of the frontier orbitals of the complexes are presented in Table 4.1 and 4.2 while key computational data is summarized in Table 4.3. From the minimum energy structures of the complexes we observed that in **Ru-1**, the two chloro ligands are *trans*-disposed with respect

to each other and all the pyridyl rings are perfectly *cis* to them. In addition, the *trans* pyridyl rings are twisted away from each to alleviate steric interactions between α-hydrogen atoms of proximate *cis* pyridyl rings. In complexes **Ru-2** to **Ru-6**, the two chloro ligands are coordinated in *cis* fashion such that one arm of each bidentate ligand is *trans* while the other is *cis* to the chloro ligands. In **Ru-1**, all the Ru-N bond lengths are equal while in the rest of the complexes they are unequal due to inter-ligand steric repulsions.[22]

Table 4.1: Mappings of the frontier orbitals of complexes **Ru-1**, **Ru-2** and **Ru-3**

	Ru-1	**Ru-2**	**Ru-3**
	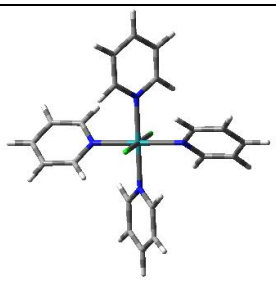	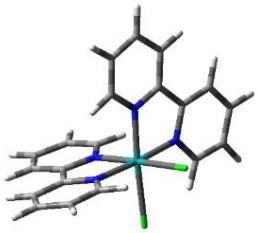	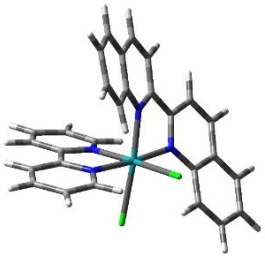
LUMO	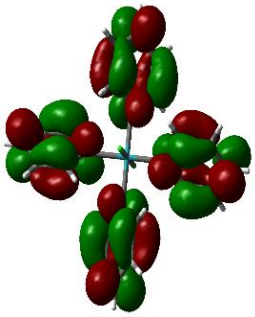	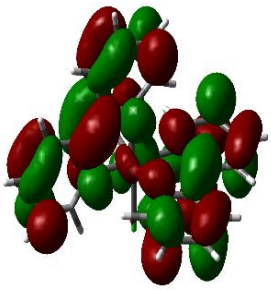	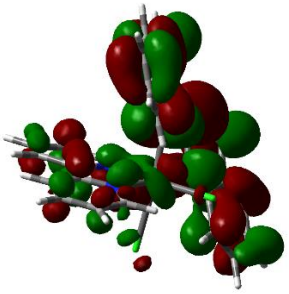
HOMO	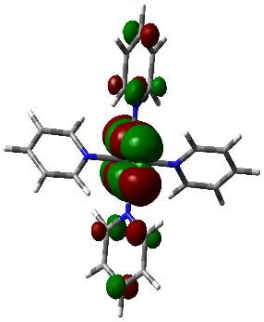	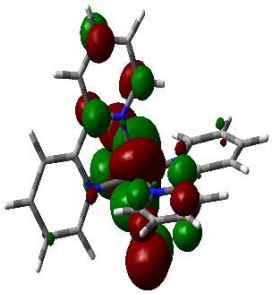	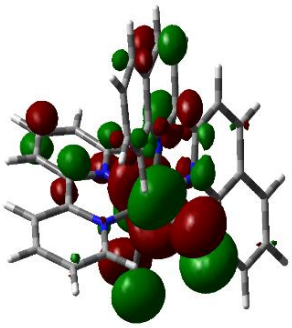

Table 4.2: Mappings of the frontier orbitals of complexes **Ru-4, Ru-5** and **Ru-6**

	Ru-4	**Ru-5**	**Ru-6**
	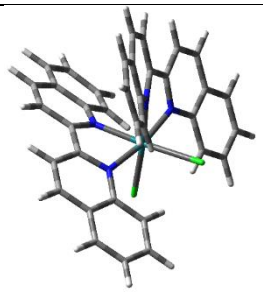	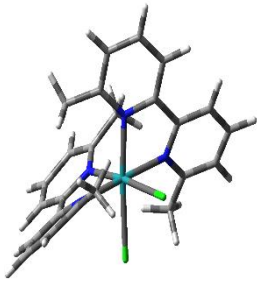	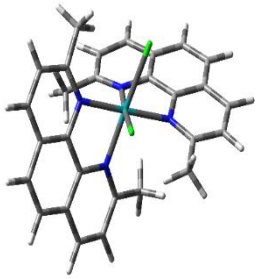
LUMO	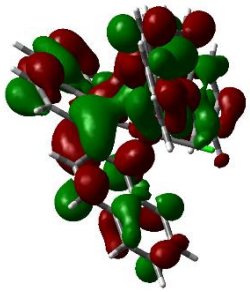	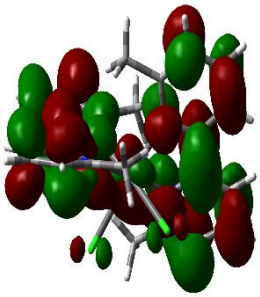	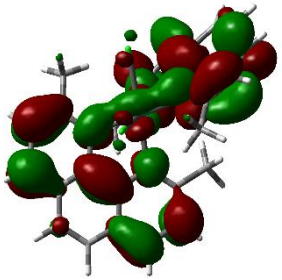
HOMO	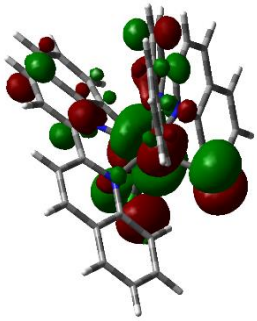	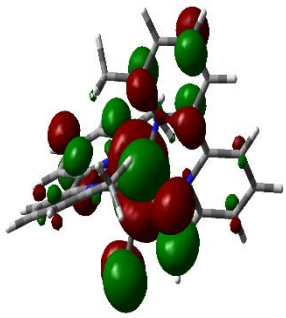	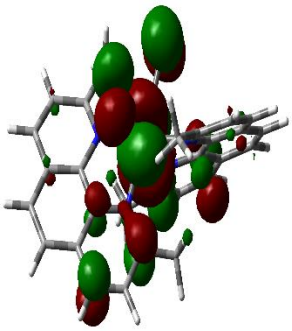

From the frontier orbital diagrams, the highest occupied molecular orbital (HOMO) in all the complexes is largely based on the metal centre and chloro groups. Additionally, for complexes **Ru-2** to **Ru-6**, the pyridyl rings *trans* to the chloro groups have a small contribution. On the other hand, the lowest unoccupied molecular orbital (LUMO) is largely localized on the N-based ligand systems. In **Ru-3**, the contribution of 2,2'-bipyridyl ligand to the LUMO is lower compared to its benzo-analogue 2,2'-biquinoline due to differences in the extended π-surface area.

Table 4.3: Selected computational data obtained for the studied complexes

Complex	Ru-1	Ru-2	Ru-3	Ru-4	Ru-5	Ru-6
HOMO-LUMO Energy / eV						
HOMO	-5.128	-5.263	-5.301	-5.325	-5.213	-5.261
LUMO	-1.430	-2.382	-2.869	-3.074	-2.195	-2.259
$\Delta_{HOMO-LUMO}$	3.698	2.881	2.432	2.251	3.018	3.002
Chemical potential (μ) / eV	-3.279	-3.823	-4.085	-4.200	-3.704	-3.760
Chemical softness (σ) / eV^{-1}	0.270	0.347	0.411	0.444	0.331	0.333
Electrophilicity index(ω) / eV	2.907	5.072	6.862	7.835	4.546	4.710
NBO charges (Ru)	0.101	0.110	0.117	0.121	0.102	0.106
Bond Length / Å						
Ru-$N_{trans\ to\ Cl}$		2.050	2.071_{bipy} 2.088_{biq}	2.087	2.082	2.090
Ru-$N_{Cis\ to\ Cl}$	2.112	2.080	2.089_{bipy} 2.116_{biq}	2.123	2.126	2.138
Ru-Cl	2.547	2.566	2.556_{tbipy}[5] 2.568_{tbiq}[6]	2.570	2.594	2.590

A positive relationship was observed between the π-conjugated area and the extent of planarity distortion of the coordinated ligands. For example; in **Ru-3**, the two quinolinyl moieties of the 2,2'-biquinoline ligand form a dihedral angle of 19.06º compared to 9.27º between the pyridyl moiety planes of the bipyridyl ligand therein. In **Ru-4**, the two quinolinyl moiety planes form a dihedral angle of 24.43º. Figures showing these planes are presented in the Supplementary Information (Figure SI 4.5 - 4.7).

Computational results documented in Table 4.3 show that increase in denticity of ligand system from one to two and subsequent progressive increase in π-conjugation stabilizes the energies of

[5] *t-bpy-* the chloro is *trans* to N of Bpy
[6] *t-biq-* the chloro is *trans* to N of Biq

the frontier orbitals. This is illustrated by the decrease in molecular orbital energies as one moves from **Ru-1** to **Ru-4**. On the other hand, introduction of methyl substituents on the bidentate ligands destabilizes the LUMO and causes elongation of the Ru-Cl bonds. The global electrophilicity indices (ω) and chemical softness (σ) of the complexes have a positive correlation with the π-conjugated surface area of the ligand systems; they increase from **Ru-1** to **Ru-4**. Comparing complexes **Ru-2**, **Ru-5** and **Ru-6**, magnitude of these chemical descriptors decreases on introduction of methyl substituents on the ligands, but with the extension of the π-conjugation from **Ru-5** to **Ru-6** a slight increase is observed.

4.3.2 Kinetic Results

The rate of substitution of the coordinated chloro ligands in six complexes by biorelevant thiourea nucleophiles was investigated under *pseudo*-first order conditions at a constant ionic strength of 0.1 M $LiCl/LiCF_3SO_3$. The reactions were monitored spectrophotometrically by following change in absorbance of the spectra at an appropriate wavelength as a function of time. Typical spectra obtained for the reaction of **Ru-2** with Tu is displayed in Figure 4.2. The inset shows a kinetic trace taken at $\lambda = 506$ nm.

Kinetic traces taken at the suitable wavelength were fitted into non-linear least square fit to generate *pseudo*-first order rate constants (k_{obs}) using equation (i).[23]

$$A_t = A_o + (A_o - A_\infty)\exp(-k_{obs}t) \qquad \text{(i)}$$

where; A_o = absorbance at the onset of the reaction, A_t = absorbance at time t, and A_∞ = absorbance at the end of the reaction.

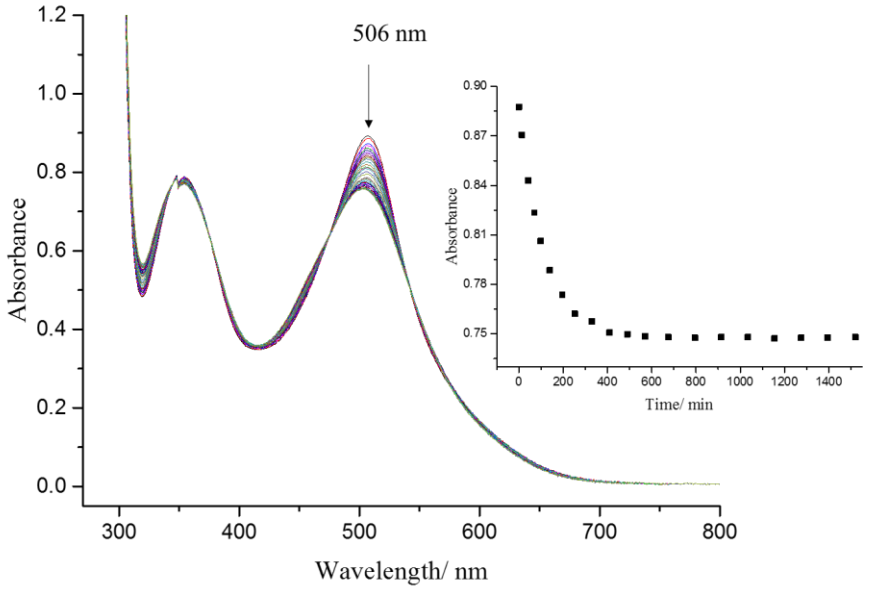

Figure 4.2: Time-resolved ultraviolet-visible spectra for the reaction of **Ru-2** (0.31 mM) with Tu (62.1 mM) in methanol at 298 K, I = 0.1 M LiCl/$LiCF_3SO_3$. **Inset**: A kinetic trace at λ = 506 nm

All the k_{obs} values were found to increase linearly with nucleophile concentration as shown in Figure 4.3. Additional plots of k_{obs} versus nucleophile concentration are presented in the Supplementary Information (Figures SI 4.1- 4.2). k_{obs} values obtained and respective nucleophile concentration are summarized in Supplementary Information (Table SI 4.1-4.6).

The second order rate constant (k_2) was obtained from the slope of the graph of k_{obs} versus nucleophile concentration. The k_2 values are tabulated in Table 4.4. Zero y-intercept were observed in all the plots and therefore the relationship between k_{obs} and nucleophile concentration can be described by equation (ii).

$$k_{obs} = k_2[\text{Nucleophile}] \qquad \text{(ii)}$$

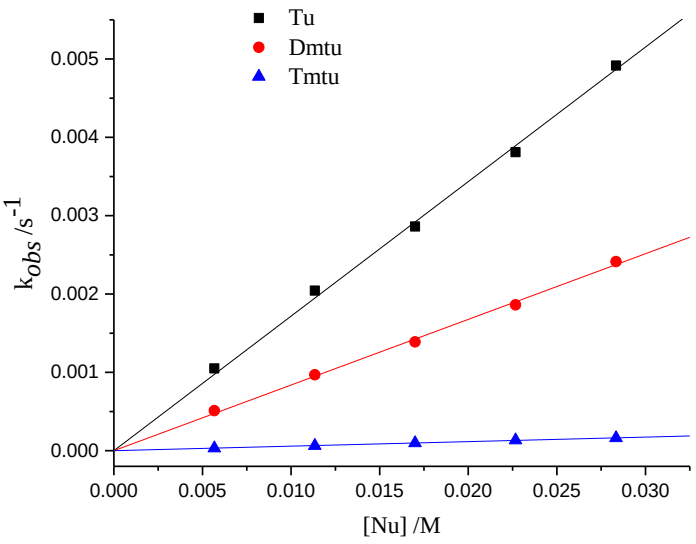

Figure 4.3: Dependence of k_{obs} on concentration of thiourea nucleophiles for the substitution of the chloro ligands in **Ru-4** in methanol at 298 K, I = 0.1 M LiCl/$LiCF_3SO_3$

To determine the thermodynamic parameters of the substitution process, the reaction temperature was varied systematically from 298 to 318 K at an interval of 5 K. Thermal activation parameters ($\Delta H^{\neq}$ and $\Delta S^{\neq}$) were calculated using the Eyring equation (iii).[23]

$$\ln\left(\frac{k_2}{T}\right) = -\frac{\Delta H^{\neq}}{R}.\frac{1}{T} + \left(23.78 + \frac{\Delta S^{\neq}}{R}\right) \qquad \text{(iii)}$$

Exemplary Eyring plots obtained for the reactions of **Ru-5** are shown in Figure 4.4 and the values for $\Delta H^{\neq}$ and $\Delta S^{\neq}$ obtained are summarized in Table 4.4. Additional Eyring plots and $\ln\left(\frac{k_2}{T}\right)$ and respective $\frac{1}{T}$ values are presented in the Supplementary Information (Figures SI 4.3-4.4 and Tables SI 4.7-4.12).

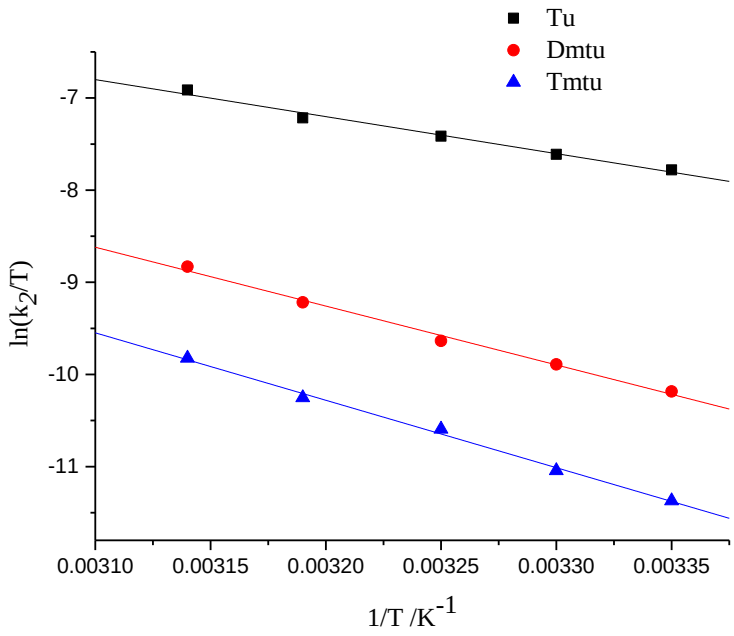

Figure 4.4: Eyring plots for the reaction of **Ru-5** with thiourea nucleophiles at *I* = 0.1 M LiCl/$LiCF_3SO_3$ and temperature range of 298-318 K

Table 4.4: Second order rate constants (k_2) and activation parameters for the displacement of chloro ligands by thiourea nucleophiles

Complexes	Nu	k_2 /× 10^{-2} M^{-1} s^{-1}	$\Delta H^{\neq}$ / kJ mol^{-1}	$\Delta S^{\neq}$/ J mol^{-1} K^{-1}
Ru-1	Tu	0.006 ± 0.00	81 ± 2	-55 ± 7
	Dmtu	Too slow	-	-
	Tmtu	Too slow	-	-
Ru-2	Tu	0.23 ± 0.01	78 ± 2	-32 ± 6
	Dmtu	0.15 ± 0.01	75 ± 3	-46 ± 9
	Tmtu	0.08 ± 0.01	83 ± 3	-25 ± 8
Ru-3	Tu	34.59 ± 0.25	57 ± 2	-64 ± 5
	Dmtu	30.67 ± 0.26	60 ± 1	-55 ± 3
	Tmtu	6.06 ± 0.08	74 ± 1	-19 ± 3
Ru-4	Tu	17.18 ± 0.20	57 ± 3	-69 ± 8
	Dmtu	8.38 ± 0.09	71 ± 2	-27 ± 5
	Tmtu	0.58 ± 0.01	79 ± 2	-22 ± 8
Ru-5	Tu	123.27 ± 1.03	33 ± 2	-150 ± 7
	Dmtu	12.00 ± 0.19	53 ± 2	-105 ± 6
	Tmtu	3.39 ± 0.03	61 ± 2	-89 ± 7
Ru-6	Tu	96.54 ± 1.69	42 ± 2	-104 ± 7
	Dmtu	8.08 ± 0.09	54 ± 3	-85 ± 9
	Tmtu	2.96 ± 0.05	61 ± 2	-67 ± 7

4.3.3 Product Analysis: Crystal Structure of *trans*-$[Ru(bipy)_2(Tmtu)_2](ClO_4)_2$

X-ray crystallographic structure of the Tmtu substituted complex at 50% probability ellipsoids is shown in Figure 4.5. Selected crystallographic and structure refinement parameters are collected in Table 4.5 while important bond lengths and angles are presented in Table 4.6. The crystal structure and related information may be accessed at CDCC refcode, TEVWUP.

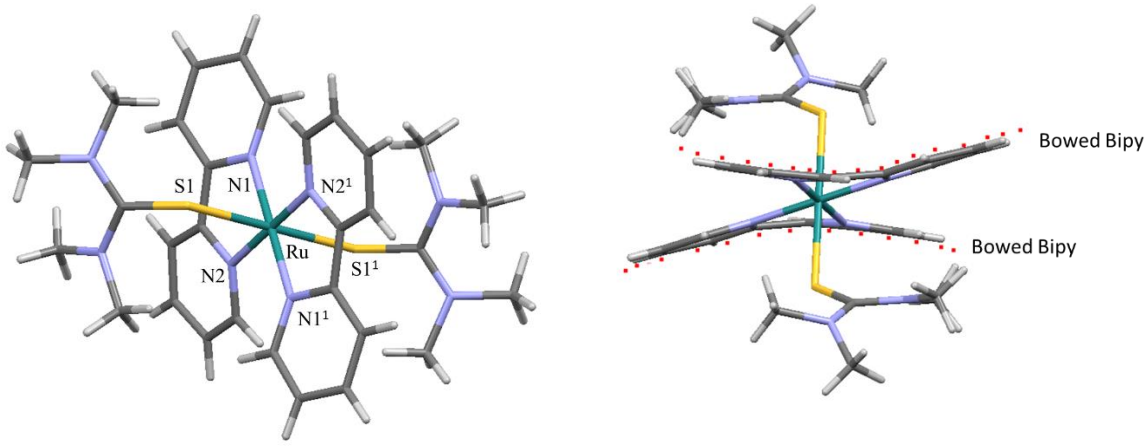

Figure 4.5: Molecular structure of *trans*-$[Ru(bipy)_2(Tmtu)_2](ClO_4)_2$ at 50% probability ellipsoid at different orientation (counterions have been omitted for clarity)

The crystal structure consists of a discrete $[Ru(bipy)_2(Tmtu)_2]^{2+}$ cation and two ClO_4^- counterions. The ruthenium(II) metal is located at a crystallographic inversion centre with equivalent ligands *trans*-disposed with respect to each other. It is noteworthy that the bipyridyl ligands are bowed in opposite direction. This makes the two α-hydrogen atoms of one 2,2'-bipyridyl ligand to be displaced to the same side of the RuN1-N2-$N1^1$-$N2^1$ plane while those on the other bipyridyl ligand displaced on the opposite direction. The bowed conformation of the 2,2'-bipyridyl ligands cause a dihedral angle of 157.76º between the individual pyridyl moieties. This reduces inter-ligand steric interactions between the proximate pairs of α-hydrogen atoms on the 2,2'-bipyridyl ligands.[24] The configuration gives an inter-ligand α-hydrogen separation distance of 2.119 Å. Another important observation is that the bipyridyl ligands are bowed away from the methyl groups of the N,N,N,N-tetramethyl thiourea ligands, this further reduces steric interactions between the two sets of ligands. The two Ru-S bonds are equal and comparable with other Ru-S bonds reported in literature for 2,2'-bipyridyl based systems.[25] The crystal packing of the complex is dominated by van der Waals forces with no classical intra and or inter molecular hydrogen bonding interactions.

Table 4.5: Selected crystallographic data and structure refinement parameters

Parameters	*trans*-$[Ru(bipy)_2(Tmtu)_2](ClO_4)_2$
Empirical formula	$C_{30}H_{40}Cl_2N_8O_8RuS_2$
Formula weight	876.79
Crystal system	Triclinic
Space group	P-1
Unit cell dimensions	
a / Å	8.5741(12)
b / Å	9.9984(12)
c / Å	12.672(2)
α /°	107.967(7)
β /°	109.489(8)
γ /°	97.336(5)
Volume / $Å^3$	941.4(2)
Z	1
Density (calculated) / Mg/m^3	1.547
Absorption coefficient / mm^{-1}	0.727
Crystal size / mm^3	0.330 x 0.240 x 0.110
Index ranges	-11<=h<=7
	-13<=k<=13
	-16<=l<=16
Goodness-of-fit on F^2	1.036
Final R indices [I>2σ(I)]	*R1* = 0.0347, w*R2* = 0.0757
R indices (all data)	*R1* = 0.0420, w*R2* = 0.0792

Table 4.6: Selected bond lengths and bond angles for *trans*-$[Ru(bipy)_2(Tmtu)_2](ClO_4)_2$

Bond Length	/ Å	**Bond Angle**	/ º
Ru-N1	2.083(2)	N1-Ru-N1[1]	180.00
Ru-N2	2.082(2)	N2-Ru-N2[1]	180.00
Ru-S1	2.402(6)	S1-Ru-S1[1]	180.00
Ru-N1[1]	2.083(2)	N1-Ru-S1	86.40(6)
Ru-N2[1]	2.082(2)	N1[1]-Ru-S1	93.60(6)
Ru-S1[1]	2.402(6)	N1-Ru-S1[1]	93.60(6)
		N1[1]-Ru-S1[1]	86.40(6)
		N2-Ru-S1	98.20(6)
		N2[1]-Ru-S1	81.80(6)
		N2-Ru-S1[1]	81.80(6)
		N2[1]-Ru-S1[1]	98.20(6)
		N1-Ru-N2	77.51(9)
		N1[1]-Ru- N2[1]	77.51(9)

To understand the effect of substitution on the structure of the complex, the crystal structure of product, *trans*-$[Ru(bipy)_2(Tmtu)_2](ClO_4)_2$ was compared to that of the reactant *trans*-$[Ru(bipy)_2(OH_2)_2](ClO_4)_2$ (Figure 4.6). Selected bond lengths and angles of the reactant are shown in Table 4.7. Additional information is given in the Supplementary Information (Table SI 4.13).

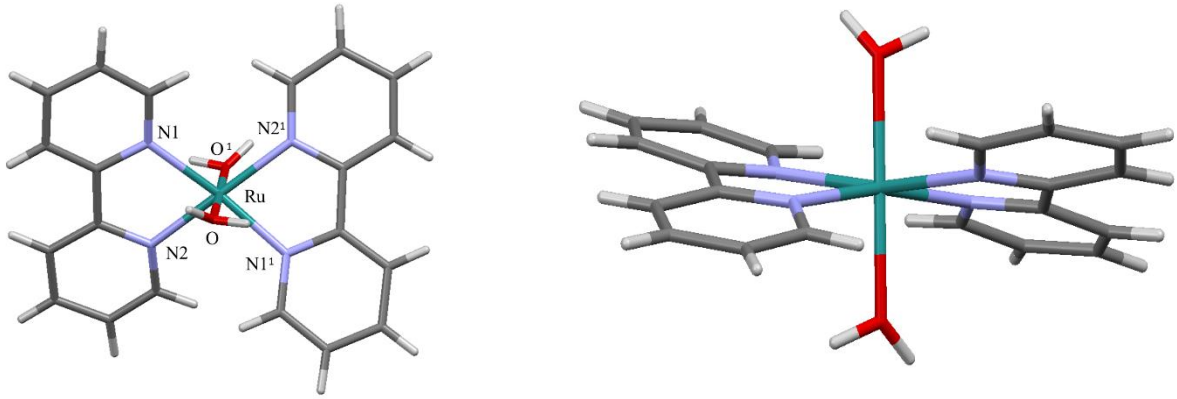

Figure 4.6: Molecular structure of *trans*-$[Ru(bipy)_2(H_2O)_2](ClO_4)_2$ at 50% probability ellipsoids at different orientations (counterions have been omitted for clarity)

Table 4.7: Selected bond lengths and bond angles for *trans*-$[Ru(bipy)_2(H_2O)_2](ClO_4)_2$

Bond Length	/ Å	**Bond Angle**	/ º
Ru-N1	2.095(18)	N1-Ru-$N1^1$	167.97
Ru-$N1^1$	2.078(18)	N2-Ru-$N2^1$	167.97
Ru-N2	2.078(18)	O-Ru-O^1	178.85
Ru-$N2^1$	2.095(18)	N1-Ru-O	83.00
Ru-O	2.003(14)	$N1^1$-Ru-O	85.24(7)
Ru-O^1	2.003(14)	N1-Ru-O^1	96.30(7)
		$N1^1$-Ru-O^1	95.49(7)
		N2-Ru-O	95.49(7)
		$N2^1$-Ru-O	96.30(7)
		N2-Ru-O^1	85.24(7)
		$N2^1$-Ru-O^1	83.00(7)
		N1-Ru-N2	77.66(7)
		$N1^1$-Ru-$N2^1$	77.66(7)

The major difference between the two crystal structures is the conformation of the 2,2'-bipyridyl bidentate ligands. While in *trans*-$[Ru(bipy)_2(Tmtu)_2](ClO_4)_2$ the 2,2'-bipyridyl ligands are bowed, in *trans*-$[Ru(bipy)_2(OH_2)_2](ClO_4)_2$ the 2,2'-bipyridyl ligands are twisted in the opposite direction with minimal distortion on their individual planarity. In the twisted conformation, the pyridyl moieties are not distorted to alleviate inter-ligand steric interactions between the α-hydrogen atoms.[26] The inter-ligand steric interactions between the bulky Tmtu and bipyridyl ligands is partly responsible for the bowed conformation of the bipyridyl ligands in *trans*-$[Ru(bipy)_2(Tmtu)_2](ClO_4)_2$. These two forms of distortion have been reported in other complexes.[26-27]

The average Ru-N bond lengths of 2.083 Å and 2.087 Å, in *trans*-$[Ru(bipy)_2(Tmtu)_2](ClO_4)_2$ and *trans*-$[Ru(bipy)_2(OH_2)_2](ClO_4)_2$, respectively are comparable. The N1-Ru-N2 bite angle of 77.51º

and 77.63º in *trans*-[Ru(bipy)$_2$(Tmtu)$_2$](ClO$_4$)$_2$ and *trans*-[Ru(bipy)$_2$(OH$_2$)$_2$](ClO$_4$)$_2$, respectively are typical of ruthenium 2,2'-bipyridyl complexes.[24, 28]

From the crystal structures obtained, it is unequivocal that the oxidation state of +2 and the stereochemistry of the divalent ruthenium complex are maintained after reaction with Tmtu. The substitution product *trans*-[Ru(bipy)$_2$(Tmtu)$_2$](ClO$_4$)$_2$ formed is stable i.e. the coordinated bidentate ligands do not dechelate from the ruthenium metal centre, an indication of stability of the product.

4.4 Discussion

This study investigated the effect of different ligand systems on the reactivity of low spin d_6 ruthenium(II) complexes. A simultaneous substitution of the two chloro ligands was observed in all the complexes, an indication that two leaving groups in each complex are in similar chemical environment.[11a, 11d] The reactivity of these divalent complexes is controlled by the concerted stereo-electronic effects of all the spectator ligands therein.

Due to variation in ligand architecture across the studied complexes, the reactivity of **Ru-1, Ru-2, Ru-3** and **Ru-4** is first compared. Using Tu as a representative nucleophile the reactivity decreased in the order; **Ru-3** (0.34 M^{-1} s^{-1}) > **Ru-4** (0.17 M^{-1} s^{-1}) > **Ru-2** (0.002 M^{-1} s^{-1}) > **Ru-1** (6.0×10^{-5} M^{-1} s^{-1}). This trend in reactivity can be rationalized in terms of electronic and steric factors associated with the coordinated aromatic ligands. It is important to mention that in **Ru-1**, the two chloro ligands are coordinated in *trans*-fashion while in the other complexes *viz*; **Ru-2, Ru-3** and **Ru-4** the labile ligands are coordinated in *cis*-fashion and therefore the steric hindrance around the metal centre is least in **Ru-1**.

Foremost, changing denticity of the ligand from one to two i.e. replacing the four pyridyl ligands in **Ru-1** with two bipyridyl ligands (**Ru-2)** and changing the stereochemistry of the complex from *trans* to *cis* enhanced the reactivity by ~ 40 folds notwithstanding the increased steric hindrance. When two pyridyl moieties combine to form a 2,2'-bipyridyl, the π-surface area increases enhancing electronic communication. In addition, an in-phase combination of the two LUMOs occur leading to an increased stabilization of the resultant LUMO. This makes 2,2'-bipyridyl a stronger π-acceptor than pyridine.[23] A concomitant increase in the aromatic π-surface area occurs as the conjugation of bidentate ligands is systematically increased from **Ru-2** to **Ru-4.** This accordingly, strengthens the π-acceptor ability of the ligands as demonstrated by the enhanced stabilization of the frontier orbitals and diminution of the HOMO-LUMO energy separation of complexes at ground state.[9a, 9b] Likewise, the localized positive charge on the metal centres show an upward trend as one moves from **Ru-1** to **Ru-4** due to increased ability of the ligands to withdraw electron density from the metal centre through π-back-bonding. Consequently, the overall charge of the complex as described by the global electrophilicity indices increases in the same order. As a result, the susceptibility to substitution of the coordinated chloro ligands increases accordingly.[9a, 9c]

When the aromatic area of a coordinated ligand is extended, its ability to stabilize the entering electron density at the metal centre increases making it possible for the complex to accept more electron density from the environment i.e. it stabilizes the transition state.[9a] This is indicated by the steady decrease in electronic chemical potential from **Ru-1** to **Ru-4**.[19b, 29] Since electronic chemical potential has a negative relationship with the reactivity of a system, the reactivity is expected to be accelerated in that order. Similarly, the chemical softness of the systems increase from **Ru-1** to **Ru-4** implying that resistance to electronic transfer reduces accordingly.[30]

Reported literature electrochemical results show that the reduction potential peak shift to more positive values as one moves from **Ru-2 to Ru-4**[31], supporting the trend of calculated quantum chemical descriptors. Therefore, the reactivity of complexes **Ru-1, Ru-2** and **Ru-3** is chiefly controlled by electronic properties, even though there is an increase in steric hindrance.

Despite the computational results predicting otherwise, the rate of substitution of the chloro ligands in **Ru-4** is slower than in **Ru-3.** This is so because the 2,2'-biquinoline ligand forms a banana shaped curvature around the centre of coordination and features substantial buckling due to limited space around the metal centre.[12a, 32] Therefore, the steric hinderance in vicinity of the metal centre is more pronounced in **Ru-4** due to the presence of two 2,2'-biquinoline ligands. Consequently, the space around the metal centre is more crowded thus limiting facile nucleophilic attack.[32]

Based on the electronic chemical potential, global electrophilicity indices as well as chemical softness one would predict the reactivity of the second set of complexes to decrease in the order; **Ru-2** > **Ru-6** > **Ru-5**. However, the observed trend in reactivity was the opposite. With respect to Tu as the entering group, the order in reactivity is; **Ru-5** (1.23 M^{-1} s^{-1}) > **Ru-6** (0.97 M^{-1} s^{-1}) > **Ru-2** (0.002 M^{-1} s^{-1}). Compared to **Ru-2**, the higher reactivity observed in complexes **Ru-5** and **Ru-6** is attributed to net σ *trans*-effect due to the dimethyl-substituted chelating ligands therein. The methyl groups enhance σ-donicity of the bidentate ligands though positive σ-inductive effect.[33] Thus, they contribute more electron density to the shared *p* orbital (p_x) weakening the Ru-Cl bonds through ground state destabilization. The overall effect of this is ground-state labilisation of the coordinated chloro ligands.[23, 34] The *trans*-influence is portrayed on the Ru-Cl bond lengths which are 2.566 Å (**Ru-2**), 2.594 Å (**Ru-5**) and 2.590 Å (**Ru-6**).

On the other hand, the methyl groups in **Ru-5** and **Ru-6** causes substantial amount of steric hindrance around the metal centres compared to **Ru-2**.[12f] However, the effect of steric retardation is overshadowed by the strong *trans*-effect henceforth the reactivity is accelerated by at least 400 folds. A similar observation was made on terpyridine based ruthenium(II) complexes in which complexes with dimethyl substituted ligands showed a faster reactivity compared to those with unsubstituted ligands.[35]

When the 2,2'-bipyridyl backbone is replaced by a more π-conjugated phenanthroline backbone, the π-acceptor properties of the ligand increase as shown by the electrophilicity index of 4.710 in **Ru-6** compared to 4.564 in **Ru-5**.[36] Likewise, the localized charges on the ruthenium metal centres as shown by the NBO charge show a similar trend. Corroborating these computed descriptors is reported electronic properties of the two complexes by Collin and Sauvage, 1986. The metal ligand charge transfer (MLCT) of the type Ru $d\pi \rightarrow \pi^*$ of **Ru-6** is red-shifted by 20 nm compared to **Ru-5**.[12f] Therefore, the substantial π-acceptor properties of the ligand system in **Ru-6** compromises the σ *trans*-effect thereof. This occurs because the σ-inductive effect is partially cancelled by metal-ligand charge drift associated with π back-donation.[37]

A comparative assessment of π-back-bonding and σ-*trans*-effect on rates of substitution was made by comparing the reactivity of complexes **Ru-2**, **Ru-4** and **Ru-5**. The assumption is that the π-effect experienced in **Ru-2** is common to all. The π-effect increases from increases from **Ru-2** to **Ru-4** while σ-effect is increased from **Ru-2** to **Ru-5**. The ratio in reactivity with Tu as the incoming nucleophile is 1 (**Ru-2)**: 75 **(Ru-4)**: 536 **(Ru-5)** and therefore it is clear that σ *trans*-effect due to the four methyl groups on the 2,2'-bipyridyl backbone is stronger in enhancing reactivity of ruthenium(II) complexes compared to π-back-donation. This can be explained by the fact that once

electron density is donated to the shared *p* orbital, the Ru-Cl bonds experience differential weakening leading to labilisation of chloro ligands.[34a, 34b]

As determined by in-plane cone angles, the quantitative sizes of 6,6'-dimethyl-2,2'-bipyridyl and 2,2'-biquinoline ligands are comparable and therefore steric hindrance around the metal centres in **Ru-4** and **Ru-5** are somewhat similar.[35] Similar findings have been reported in literature on terpyridine based complexes.[35]

The reactivity of the three nucleophiles follow the order; Tu > Dmtu > Tmtu according to the steric bulkiness of the nucleophile. As the bulkiness increases, the approach towards the metal centre is retarded causing transition state destabilization hence slowing down the reactivity.[38]

The negative values for $\Delta S^{\neq}$ for all the reactions suggest an associative mechanism in the activation of the substituting process where the rupture of Ru-Cl bonds and the formation of Ru-Nucleophile bonds are concerted. As a result of bimolecularity, the number of unbound molecules in the transition state decreases leading to a significant drop in the activation entropy.[11c] The sensitivity of the reactivity of the metal complexes on the steric bulkiness of incoming nucleophiles further supports an associative mechanism.[11c]

4.5 Conclusions

The simultaneous substitution of the two chloro ligands in ruthenium(II) polypyridyl complexes is controlled by the stereo-electronic properties of the coordinated spectator ligands. Increase in ligand denticity from one to two and extension of the π-conjugated surface area of the coordinated ligands accelerates the reactivity of complexes. This is due to increase in electrophilicity of the complexes as a result of enhanced π-back-donation as shown by the DFT-calculated parameters. The study has also established that strong σ-*trans* effect is responsible for the enhancement of the

reactivity of complexes with dimethyl-substituted ligand systems compared to that with unsubstituted ligands. In addition, an increase in π-acceptor ability of the dimethyl-substituted ligands reduces the *trans*-effect dampening the reactivity of the complex. The substitution reactions proceed through an associative mechanism.

The substitution reactions of ruthenium(II) polypyridyl complexes occur with retention of stereochemistry of the complexes and the oxidation state (+2) of the metal centre. The substitution products formed are stable and, in this respect, can potentially act as a reservoir for metallodrugs in biological systems before their covalent interactions with DNA.

4.6 References

[1] S. H. van Rijt, P. J. Sadler, *Drug Discovery Today* **2009**, *14*, 1089-1097.

[2] (a) M. Pongratz, P. Schluga, M. A. Jakupec, V. B. Arion, C. G. Hartinger, G. Allmaier, B. K. Keppler, *Journal of Analytical Atomic Spectrometry* **2004**, *19*, 46-51; (b) C. S. Allardyce, P. J. Dyson, *Platinum Metals Review* **2001**, *45*, 62-69; (c) G. Sava, S. Zorzet, C. Turrin, F. Vita, M. Soranzo, G. Zabucchi, M. Cocchietto, A. Bergamo, S. DiGiovine, G. Pezzoni, *Clinical Cancer Research* **2003**, *9*, 1898-1905.

[3] M. J. Clarke, F. Zhu, D. R. Frasca, *Chemical Reviews* **1999**, *99*, 2511-2534.

[4] (a) A. Astarina, M. J. Chow, W. H. Ang, *Australian Journal of Chemistry* **2012**, *65*, 1271-1276; (b) A. C. Komor, J. K. Barton, *Chemical Communications* **2013**, *49*, 3617-3630.

[5] (a) X. Chen, J.-H. Wu, Y.-W. Lai, R. Zhao, H. Chao, L.-N. Ji, *Dalton Transactions* **2013**, *42*, 4386-4397; (b) K.-J. Du, J.-Q. Wang, J.-F. Kou, G.-Y. Li, L.-L. Wang, H. Chao, L.-N. Ji, *European Journal of Medicinal Chemistry* **2011**, *46*, 1056-1065; (c) C. Tan, S. Wu, S. Lai, M. Wang, Y. Chen, L. Zhou, Y. Zhu, W. Lian, W. Peng, L. Ji, *Dalton Transactions* **2011**, *40*, 8611-8621; (d) C. Qian, J.-Q. Wang, C.-L. Song, L.-L. Wang, L.-N. Ji, H. Chao, *Metallomics* **2013**, *5*, 844-854.

[6] (a) W. Han Ang, P. J. Dyson, *European Journal of Inorganic Chemistry* **2006**, *2006*, 4003-4018; (b) T. Chen, Y. Liu, W.-J. Zheng, J. Liu, Y.-S. Wong, *Inorganic Chemistry* **2010**, *49*, 6366-6368.

[7] (a) F. Giannini, L. E. Paul, J. Furrer, B. Therrien, G. Süss-Fink, *New Journal of Chemistry* **2013**, *37*, 3503-3511; (b) Y. Mulyana, D. K. Weber, D. P. Buck, C. A. Motti, J. G. Collins, F. R. Keene, *Dalton Transactions* **2011**, *40*, 1510-1523; (c) M. Ganeshpandian, M. Palaniandavar, A. Muruganantham, S. K. Ghosh, A. Riyasdeen, M. A. Akbarsha, *Applied Organometallic Chemistry* **2018**, *32*, e4154.

[8] (a) J.-A. Cuello-Garibo, C. C. James, M. A. Siegler, S. Bonnet, *Chemistry Squared* **2017**, *1*, 1-19; (b) L. K. Filak, G. Mühlgassner, F. Bacher, A. Roller, M. Galanski, M. A. Jakupec, B. K. Keppler, V. B. Arion, *Organometallics* **2010**, *30*, 273-283.

[9] (a) A. Hofmann, D. Jaganyi, O. Q. Munro, G. Liehr, R. van Eldik, *Inorganic Chemistry* **2003**, *42*, 1688-1700; (b) A. Mambanda, D. Jaganyi, in *Advances in Inorganic Chemistry, Vol. 70*, Elsevier, **2017**, pp. 243-276; (c) I. M. Wekesa, D. Jaganyi, *Dalton Transactions* **2014**, *43*, 2549-2558; (d) R. Bellam, J. Deogratius, A. Mambanda, R. S. Robinson, *New Journal of Chemistry* **2018**, *42*, 12557-12569.

[10] (a) T. R. Papo, D. Jaganyi, *Journal of Coordination Chemistry* **2015**, *68*, 794-807; (b) W. M. Mthiyane, A. Mambanda, D. Jaganyi, *International Journal of Chemical Kinetics* **2018**, *50*, 531-543.

[11] (a) G. Kinunda, D. Jaganyi, *Transition Metal Chemistry* **2016**, *41*, 235-248; (b) W. M. Mthiyane, A. Mambanda, D. Jaganyi, *Transition Metal Chemistry* **2017**, *42*, 739-751; (c) T. Das, B. Bera, A. Datta, A. Ghosh, *Transition Metal Chemistry* **2009**, *34*, 247-253; (d) W. P. Asman, D. Jaganyi, *International Journal of Chemical Kinetics* **2017**, *49*, 545-561.

[12] (a) T. A. Grusenmeyer, B. A. McClure, C. J. Ziegler, J. J. Rack, *Inorganic Chemistry* **2010**, *49*, 4466-4470; (b) B. A. Albani, C. B. Durr, C. Turro, *The Journal of Physical Chemistry A* **2013**, *117*, 13885-13892; (c) L. Colina-Vegas, W. Villarreal, M. Navarro, C. R. de Oliveira,

A. E. Graminha, P. I. d. S. Maia, V. M. Deflon, A. G. Ferreira, M. R. Cominetti, A. A. Batista, *Journal of Inorganic Biochemistry* **2015**, *153*, 150-161; (d) D. Ooyama, Y. Miura, Y. Kanazawa, F. S. Howell, N. Nagao, M. Mukaida, H. Nagao, K. Tanaka, *Inorganica chimica acta* **1995**, *237*, 47-55; (e) B. Sullivan, D. Salmon, T. Meyer, *Inorganic Chemistry* **1978**, *17*, 3334-3341; (f) J. Collin, J. P. Sauvage, *Inorganic Chemistry* **1986**, *25*, 135-141.

[13] OriginPro9.1, OriginLab Corporation, One Roundhouse Plaza,Suite 303, Northampton, MA 01060, United States, 2014 1800-969-7720. *www.OriginLab.com.*

[14] M. Frisc, G. Trucks, H. Schlegel, G. Scuseria, M. Robb, J. Cheeseman, G. Scalmani, V. Barone, B. Mennucci, G. Petersson, *Gaussian Inc, Wallingford* **2010**.

[15] J. Li, L.-C. Xu, J.-C. Chen, K.-C. Zheng, L.-N. Ji, *The Journal of Physical Chemistry A* **2006**, *110*, 8174-8180.

[16] V. Gupta, *Principles and Applications of Quantum Chemistry*, Elsevier Inc., London, UK, **2015**, pp. 156-175.

[17] M. Okamura, M. Yoshida, R. Kuga, K. Sakai, M. Kondo, S. Masaoka, *Dalton Transactions* **2012**, *41*, 13081-13089.

[18] M. Cossi, G. Scalmani, N. Rega, V. Barone, *The Journal of Chemical Physics* **2002**, *117*, 43-54.

[19] (a) R. G. Parr, L. v. Szentpaly, S. Liu, *Journal of the American Chemical Society* **1999**, *121*, 1922-1924; (b) R. G. Pearson, *Inorganica Chimica Acta* **1992**, *198*, 781-786.

[20] O. V. Dolomanov, L. J. Bourhis, R. J. Gildea, J. A. Howard, H. Puschmann, *Journal of Applied Crystallography* **2009**, *42*, 339-341.

[21] G. M. Sheldrick, *Acta Crystallographica Section C: Structural Chemistry* **2015**, *71*, 3-8.

[22] C. R. Hecker, P. E. Fanwick, D. R. McMillin, *Inorganic Chemistry* **1991**, *30*, 659-666.

[23] J. D. Atwood, *Inorganic and Organometallic Reaction Mechanisms*, 2nd edition ed., VCH Publishers, **1997**, pp. 1-18, 47-90.

[24] (a) N. R. Weathers, R. C. Sadoski, B. Durham, A. W. Cordes, *Acta Crystallographica Section C: Crystal Structure Communications* **1997**, *53*, 1047-1049; (b) P. Klüfers, A. Zangl, *Acta Crystallographica Section E: Structure Reports Online* **2007**, *63*, m3088-m3088.

[25] M. K. Smith, J. A. Gibson, C. G. Young, J. A. Broomhead, P. C. Junk, F. R. Keene, *European Journal of Inorganic Chemistry* **2000**, *2000*, 1365-1370.

[26] A. Cordes, B. Durham, P. Swepston, W. Pennington, S. Condren, R. Jensen, J. Walsh, *Journal of Coordination Chemistry* **1982**, *11*, 251-260.

[27] (a) P. Bonneson, J. L. Walsh, W. Pennington, A. Cordes, B. Durham, *Inorganic Chemistry* **1983**, *22*, 1761-1765; (b) H. Endres, H. Keller, W. Moroni, D. Nöthe, V. Dong, *Acta Crystallographica Section B* **1978**, *34*, 1823-1827.

[28] (a) J. Małecki, M. Jaworska, R. Kruszynski, R. Gil-Bortnowska, *Polyhedron* **2005**, *24*, 1445-1453; (b) H. Jude, P. S. White, D. M. Dattelbaum, R. C. Rocha, *Acta Crystallographica Section E: Structure Reports Online* **2008**, *64*, m1388-m1389.

[29] R. G. Pearson, *Journal of Molecular Structure: THEOCHEM* **1992**, *255*, 261-270.

[30] C. A. Mebi, *Journal of Chemical Sciences* **2011**, *123*, 727-731.

[31] (a) S. A. Kubow, M. E. Marmion, K. J. Takeuchi, *Inorganic Chemistry* **1988**, *27*, 2761-2767; (b) N. Yoshikawa, J. Sakamoto, T. Matsumura-Inoue, H. Takashima, K. Tsukahaba, N. Kanehisa, Y. Kai, *Analytical Sciences* **2004**, *20*, 711-716.

[32] A. Spek, A. Gerli, J. Reedijk, *Acta Crystallographica Section C: Crystal Structure Communications* **1994**, *50*, 394-397.

[33] F. Tiba, D. Jaganyi, A. Mambanda, *Journal of Coordination Chemistry* **2010**, *63*, 2542-2560.

[34] (a) P. D. Lyne, D. M. P. Mingos, *Journal of the Chemical Society, Dalton Transactions* **1995**, 1635-1643; (b) E. Shustorovich, M. Porai-Koshits, Y. A. Buslaev, *Coordination Chemistry Reviews* **1975**, *17*, 1-98; (c) B. J. Coe, S. J. Glenwright, *Coordination Chemistry Reviews* **2000**, *203*, 5-80.

[35] C. A. Bessel, J. A. Margarucci, J. H. Acquaye, R. S. Rubino, J. Crandall, A. J. Jircitano, K. J. Takeuchi, *Inorganic Chemistry* **1993**, *32*, 5779-5784.

[36] S. R. Maqsood, N. Islam, S. Bashir, B. Khan, A. H. Pandith, *Journal of Coordination Chemistry* **2013**, *66*, 2308-2315.

[37] T.-G. Appleton, H. Clark, L. Manzer, *Coordination Chemistry Reviews* **1973**, *10*, 335-422.

[38] G. K. Rauth, D. Das, C. Sinha, K. Bag, A. Mahapatra, *Transition Metal Chemistry* **2002**, *27*, 639-645.

SI 4 Supplementary Information

SI 4.1 Average observed rate constants (k_{obs}) for the substitution of chloro ligands

Table SI 4.1: Average k_{obs} (s^{-1}) for the reaction of **Ru-1** (0.807 mM) with thiourea nucleophiles

[Nu] /M	**Tu** ((λ = 508 nm) k_{obs} /s^{-1}
0.3228	4.842×10^{-6}
0.2581	3.834×10^{-6}
0.1938	2.994×10^{-6}
0.1292	1.972×10^{-6}
0.0649	8.362×10^{-7}

Table SI 4.2: Average k_{obs} (s^{-1}) for the reaction of **Ru-2** (0.311 mM) with thiourea nucleophiles

[Nu] /M	**Tu** (λ = 508 nm) k_{obs} /s^{-1}	**Dmtu** (λ = 506 nm) k_{obs} /s^{-1}	**Tmtu** (λ = 508 nm) k_{obs} /s^{-1}
0.0621	1.427×10^{-4}	9.283×10^{-5}	4.667×10^{-5}
0.0497	1.155×10^{-4}	7.183×10^{-5}	3.823×10^{-5}
0.0373	9.035×10^{-5}	5.567×10^{-5}	2.867×10^{-5}
0.0249	6.152×10^{-5}	3.915×10^{-5}	2.033×10^{-5}
0.0124	3.046×10^{-5}	2.038×10^{-5}	1.011×10^{-5}

Table SI 4.3: Average k_{obs} (s^{-1}) for the reaction of **Ru-3** (0.184 mM) with thiourea nucleophiles

[Nu] /M	**Tu** (λ = 590 nm)	**Dmtu** (λ = 650 nm)	**Tmtu** (λ = 590 nm)
	k_{obs} /s^{-1}	k_{obs} /s^{-1}	k_{obs} /s^{-1}
0.01841	6.42×10^{-3}	5.71×10^{-3}	1.091×10^{-3}
0.01473	5.06×10^{-3}	4.47×10^{-3}	8.863×10^{-4}
0.01104	3.86×10^{-3}	3.42×10^{-3}	7.044×10^{-4}
0.00736	2.44×10^{-3}	2.15×10^{-3}	4.590×10^{-4}
0.00368	1.24×10^{-3}	1.13×10^{-3}	2.212×10^{-4}

Table SI 4.4: Average k_{obs} (s^{-1}) for reaction of **Ru-4** (0.142 mM) with thiourea nucleophiles

[Nu] /M	**Tu** (λ = 609 nm)	**Dmtu** (λ = 600 nm)	**Tmtu** (λ = 562 nm)
	k_{obs} /s^{-1}	k_{obs} /s^{-1}	k_{obs} /s^{-1}
0.02840	4.917×10^{-3}	2.413×10^{-3}	1.621×10^{-4}
0.02267	3.810×10^{-3}	1.862×10^{-3}	1.347×10^{-4}
0.01700	2.861×10^{-3}	1.389×10^{-3}	9.833×10^{-5}
0.01134	2.043×10^{-3}	9.684×10^{-4}	6.264×10^{-5}
0.00567	1.050×10^{-3}	5.110×10^{-4}	3.096×10^{-5}

Table SI 4.5: Average k_{obs} (s^{-1}) for the reaction of **Ru-5** (0.10 mM) with thiourea nucleophiles

[Nu] /M	**Tu** (λ = 520 nm)	**Dmtu** (λ = 520 nm)	**Tmtu** (λ = 520 nm)
	k_{obs} /s^{-1}	k_{obs} /s^{-1}	k_{obs} /s^{-1}
0.010	0.01216	1.230×10^{-3}	3.430×10^{-4}
0.008	0.00989	9.568×10^{-4}	2.652×10^{-4}
0.006	0.00748	6.756×10^{-4}	2.046×10^{-4}
0.004	0.00517	4.842×10^{-4}	1.356×10^{-4}
0.002	0.00246	2.286×10^{-4}	6.834×10^{-5}

Table SI 4.6: Average k_{obs} (s^{-1}) for the reaction of **Ru-6** (0.10 mM) with thiourea nucleophiles

[Nu]/M	**Tu** (λ = 520 nm) k_{obs} /s^{-1}	**Dmtu** (λ = 520 nm) k_{obs} /s^{-1}	**Tmtu** (λ = 520 nm) k_{obs} /s^{-1}
0.010	0.00941	8.134×10^{-4}	2.897×10^{-4}
0.008	0.00764	6.458×10^{-4}	2.393×10^{-4}
0.006	0.00616	4.645×10^{-4}	1.883×10^{-4}
0.004	0.00408	3.333×10^{-4}	1.124×10^{-4}
0.002	0.00197	1.723×10^{-4}	6.214×10^{-5}

SI 4.2 Average $\ln\left(\frac{k_2}{T}\right)$ values for the substitution of chloro ligands

Table SI 4.7: Average $\ln\left(\frac{k_2}{T}\right)$ for the reaction of **Ru-1** with thiourea nucleophiles

T /K	$\frac{1}{T}$ /K^{-1}	$\ln\left(\frac{k_2}{T}\right)$ **Tu**
298.15	0.00335	-15.417
303.15	0.00330	-14.838
308.15	0.00325	-14.359
313.15	0.00319	-13.817
318.15	0.00314	-13.353

Table SI 4.8: Average $ln\left(\frac{k_2}{T}\right)$ for the reaction of **Ru-2** with thiourea nucleophiles

T /K	$\frac{1}{T}$ /K^{-1}	$\ln\left(\frac{k_2}{T}\right)$ **Tu**	$\ln\left(\frac{k_2}{T}\right)$ **Dmtu**	$\ln\left(\frac{k_2}{T}\right)$ **Tmtu**
298.15	0.00335	-11.692	-12.204	-12.868
303.15	0.00330	-11.143	-11.626	-12.424
308.15	0.00325	-10.692	-11.262	-11.852
313.15	0.00319	-10.142	-10.728	-11.217
318.15	0.00314	-9.695	-10.245	-10.813

Table SI 4.9: Average $ln\left(\frac{k_2}{T}\right)$ for the reaction of **Ru-3** with thiourea nucleophiles

T /K	$\frac{1}{T}$ /K^{-1}	$\ln\left(\frac{k_2}{T}\right)$ **Tu**	$\ln\left(\frac{k_2}{T}\right)$ **Dmtu**	$\ln\left(\frac{k_2}{T}\right)$ **Tmtu**
298.15	0.00335	-6.748	-6.897	-8.446
303.15	0.00330	-6.475	-6.571	-8.032
308.15	0.00325	-6.069	-6.206	-7.622
313.15	0.00319	-5.672	-5.738	-7.009
318.15	0.00314	-5.342	-5.409	-6.589

Table SI 4.10: Average $ln\left(\frac{k_2}{T}\right)$ for the reaction of **Ru-4** with thiourea nucleophiles

T /K	$\frac{1}{T}$ /K^{-1}	$\ln\left(\frac{k_2}{T}\right)$ **Tu**	$\ln\left(\frac{k_2}{T}\right)$ **Dmtu**	$\ln\left(\frac{k_2}{T}\right)$ **Tmtu**
298.15	0.00335	-7.480	-8.202	-10.903
303.15	0.00330	-7.123	-7.780	-10.344
308.15	0.00325	-6.703	-7.348	-9.871
313.15	0.00319	-6.412	-6.782	-9.297
318.15	0.00314	-6.012	-6.428	-8.893

Table SI 4.11: Average $ln\left(\frac{k_2}{T}\right)$ for the reaction of **Ru-5** with thiourea nucleophiles

T /K	$\frac{1}{T}$ /K^{-1}	$\ln\left(\frac{k_2}{T}\right)$ **Tu**	$\ln\left(\frac{k_2}{T}\right)$ **Dmtu**	$\ln\left(\frac{k_2}{T}\right)$ **Tmtu**
298.15	0.00335	-7.780	-10.184	-11.371
303.15	0.00330	-7.612	-9.891	-11.043
308.15	0.00325	-7.414	-9.635	-10.594
313.15	0.00319	-7.216	-9.217	-10.252
318.15	0.00314	-6.913	-8.831	-9.824

Table SI 4.12: Average $ln\left(\frac{k_2}{T}\right)$ for the reaction of **Ru-6** with thiourea nucleophiles

T /K	$\frac{1}{T}$ /K^{-1}	$\ln\left(\frac{k_2}{T}\right)$ **Tu**	$\ln\left(\frac{k_2}{T}\right)$ **Dmtu**	$\ln\left(\frac{k_2}{T}\right)$ **Tmtu**
298.15	0.00335	-5.671	-8.256	-9.159
303.15	0.00330	-5.336	-7.907	-8.716
308.15	0.00325	-5.098	-7.513	-8.336
313.15	0.00319	-4.864	-7.210	-7.904
318.15	0.00314	-4.563	-6.873	-7.598

SI 4.3 Typical plots of k_{obs} versus nucleophile concentration for the reaction of the complexes with thiourea nucleophiles

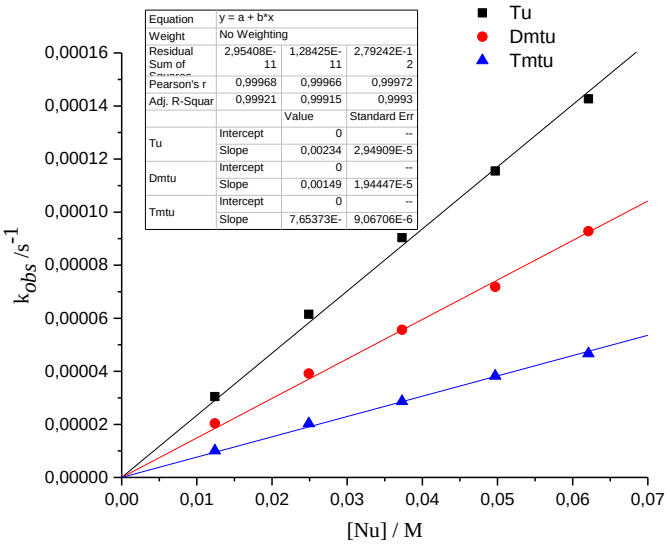

Figure SI 4.1: Dependence of k_{obs} on concentration of thiourea nucleophiles for the substitution of the chloro ligands in **Ru-2** in methanol at 298 K, I = 0.1 M LiCl/$LiCF_3SO_3$

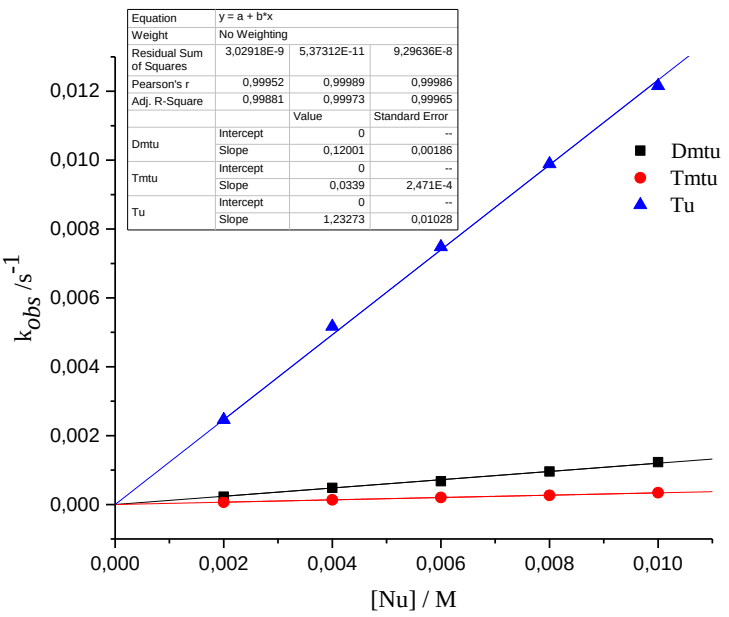

Figure SI 4.2: Dependence of k_{obs} on concentration of thiourea nucleophiles for the substitution of the chloro ligands in **Ru-5** in methanol at 298 K, I = 0.1 M LiCl/$LiCF_3SO_3$

SI 4.4 Typical Eyring plots obtained for the complexes

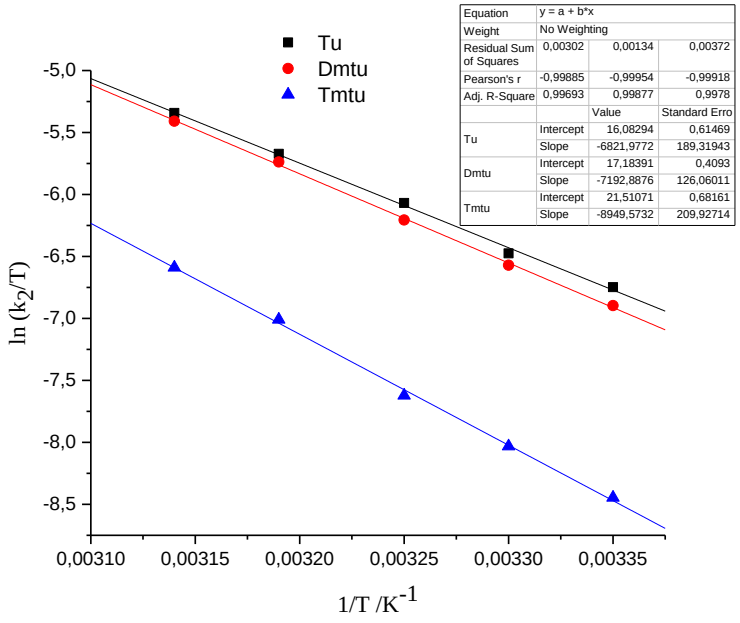

Figure SI 4.3: Eyring plots for the reaction of **Ru-3** with thiourea nucleophiles at I = 0.1 M LiCl/$LiCF_3SO_3$ and temperature range of 298-318 K

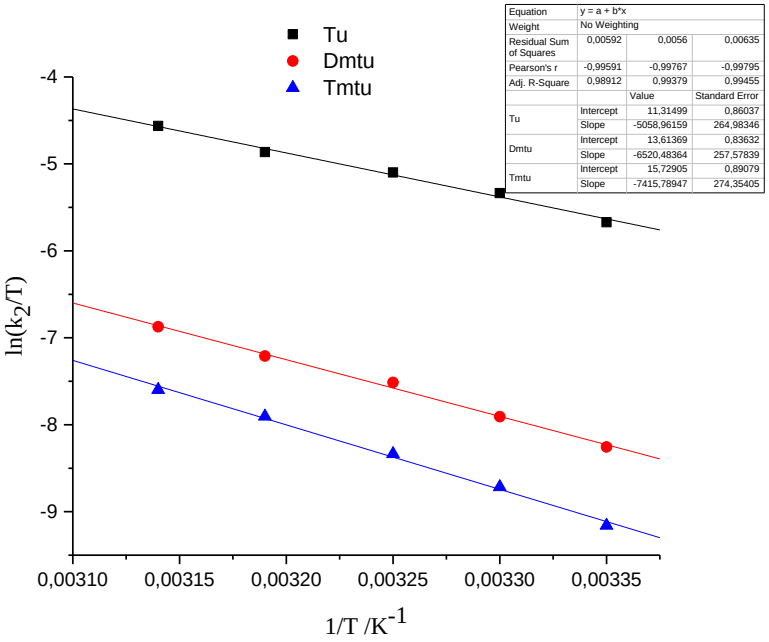

Figure SI 4.4: Eyring plots for the reaction of **Ru-6** with thiourea nucleophiles at I = 0.1 M LiCl/$LiCF_3SO_3$ and temperature range of 298-318 K

SI 4.5 Additional DFT-optimized structures of the investigated complexes

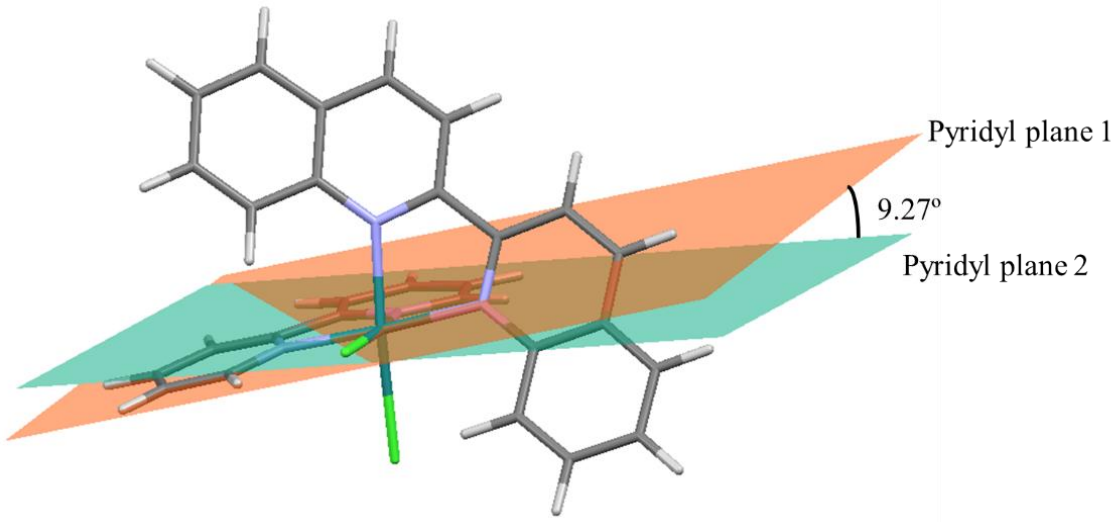

Figure SI 4.5: DFT-optimized structure of **Ru-3** showing the dihedral angle between the planes of the pyridyl moieties

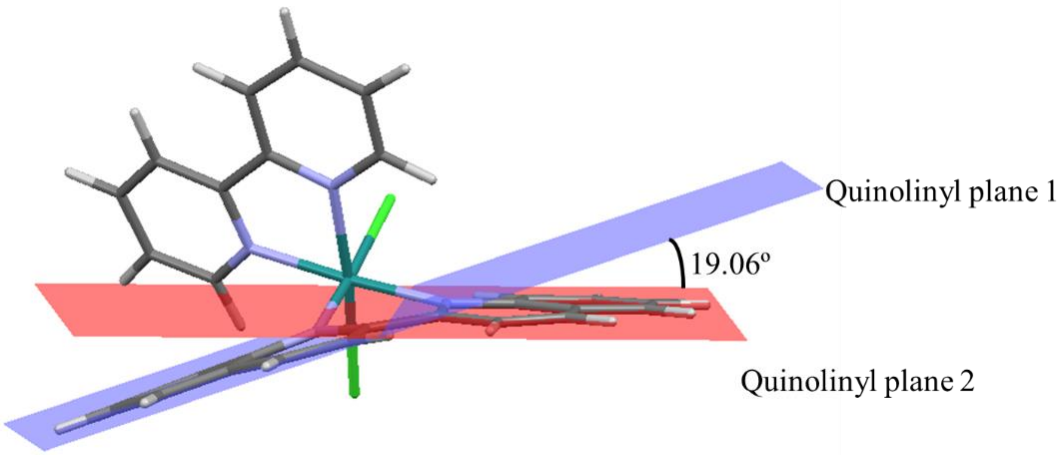

Figure SI 4.6: DFT-optimized structure of **Ru-3** showing the dihedral angle between the planes of the quinolinyl moieties

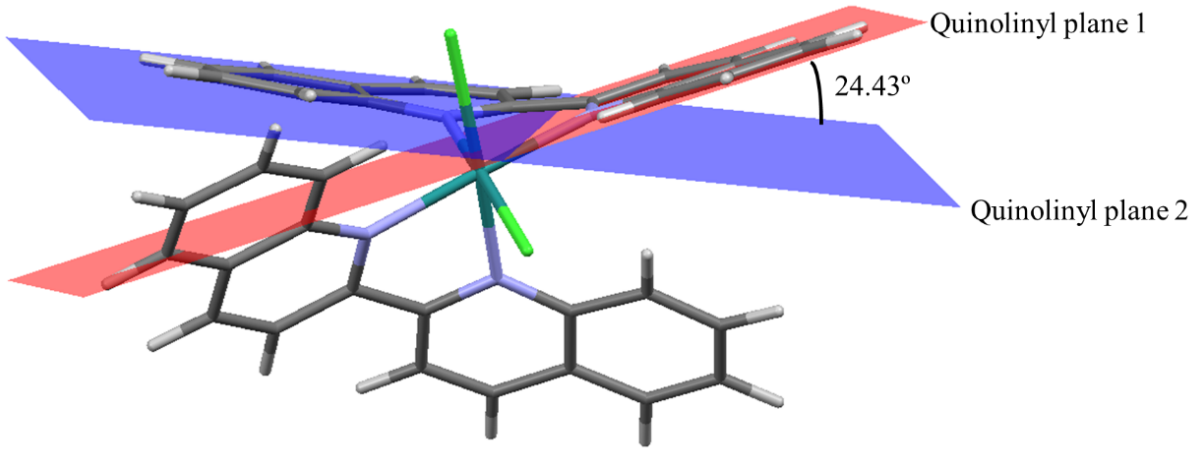

Figure SI 4.7: DFT-optimized structure of **Ru-4** showing the dihedral angle between the planes of the quinolinyl moieties

SI 4.6 Crystallographic data for *trans*-$[Ru(bipy)_2(H_2O)_2](ClO_4)_2$

Table SI 4.13: Selected crystallographic data and structure refinement parameters

Parameters	***trans*-$[Ru(bipy)_2(H_2O)_2](ClO_4)_2$**
Formula	$C_{20}H_{20}Cl_2N_4O_{10}Ru$
Formula Weight	648.36
Crystal System	Trigonal
Space Group	$P3_221$
Unit Cell dimensions	
a /Å	10.773(7)
b /Å	10.773(7)
c /Å	16.956(13)
α /°	90
β /°	90
γ /°	120
Volume /Å^3	1704.2(3)
Z	3
Density (calculated) /gcm^{-3}	1.895
Absorption coefficient /mm^{-1}	0.993
Crystal Size /mm^3	0.32×0.26×0.14
Wavelength /Å	0.71073
Radiation type	MoK$_\alpha$
Θ_{min}/°	2.183
Θ_{max}/°	27.535
Measured Refl.	9620
Independent Refl.	2612
wR_2 (all data)	0.0380
wR_2	0.0379
R_1 (all data)	0.0147
R_1	0.0145

SI 4.7 Samples of MS and ^{1}H NMR spectra for the investigated complexes

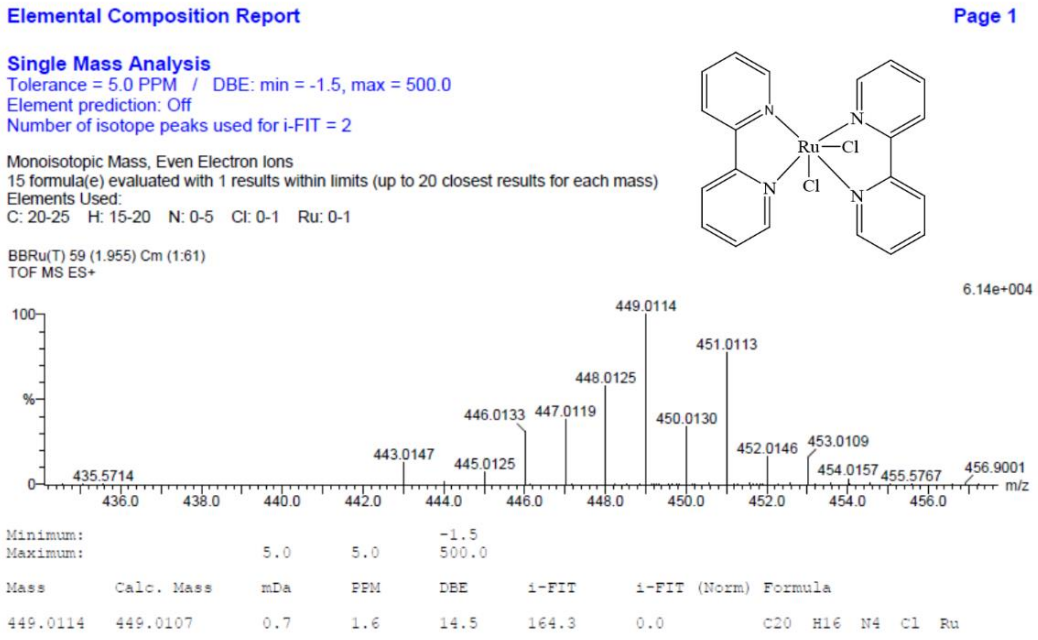

Figure SI 4.8: ESI-MS (TOF) spectrum for **Ru-2**

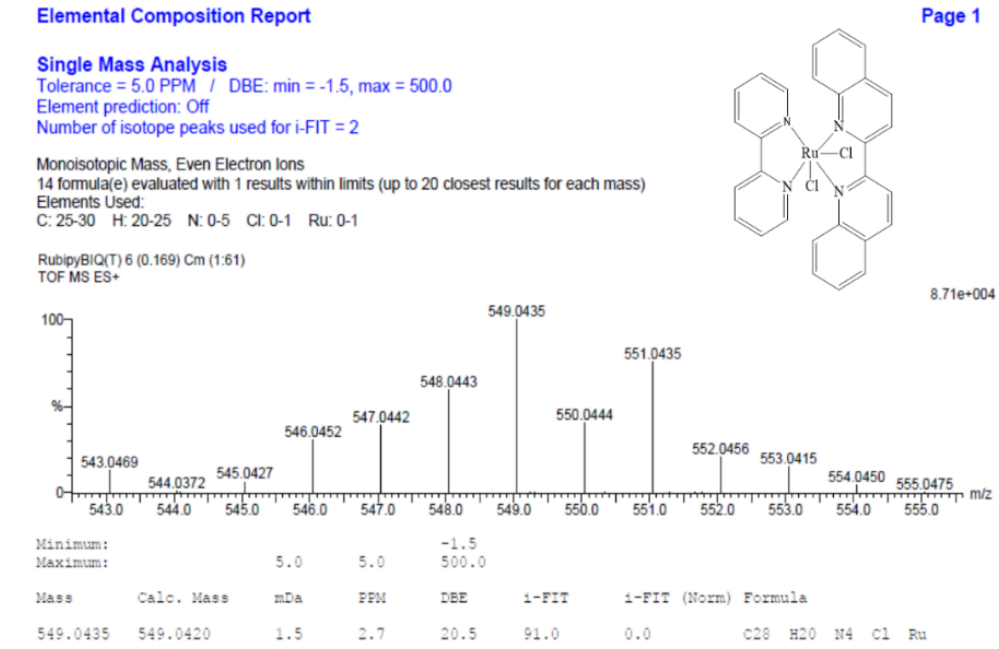

Figure SI 4.9: ESI-MS (TOF) spectrum for **Ru-3**

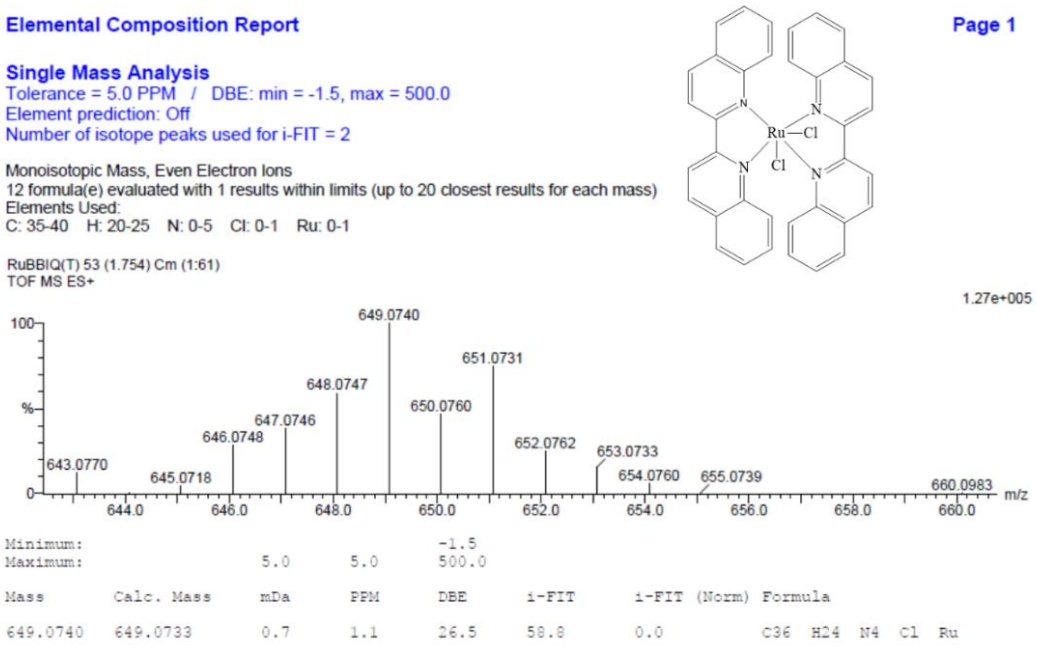

Figure SI 4.10: ESI-MS (TOF) spectrum for **Ru-4**

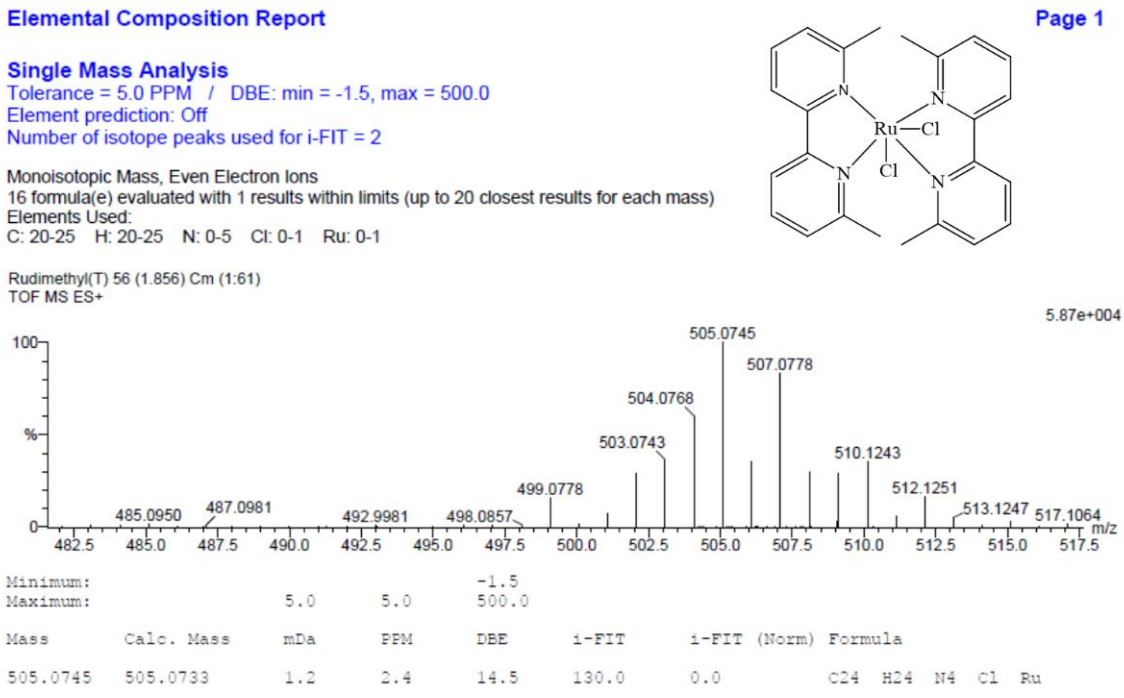

Figure SI 4.11: ESI-MS (TOF) spectrum for **Ru-5**

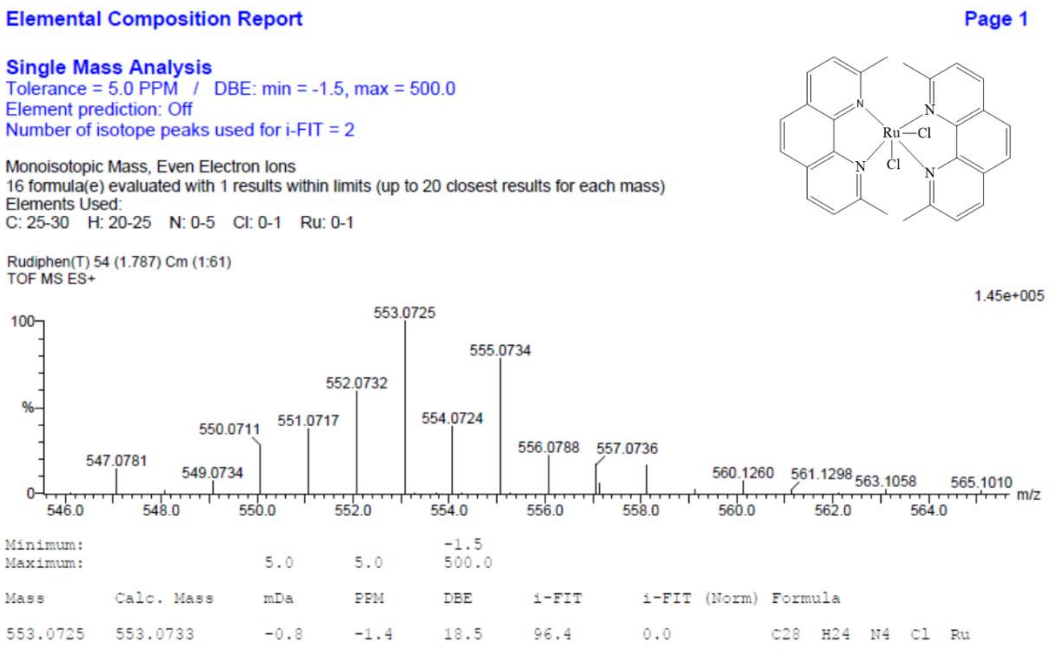

Figure SI 4.12: ESI-MS (TOF) spectrum for **Ru-6**

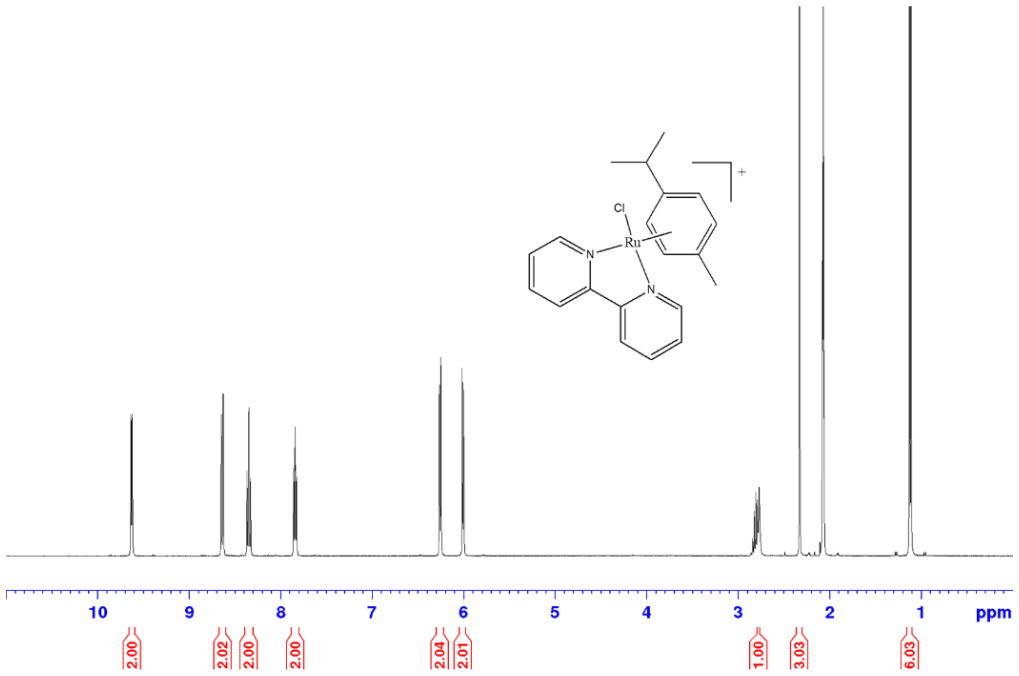

Figure SI 4.13: ^{1}H NMR (400 MHz, acetone-d_6) spectrum of ((2,2'-bipyridyl)-chloro(η^6-p-cymene)ruthenium(II) hexaflourophosphate

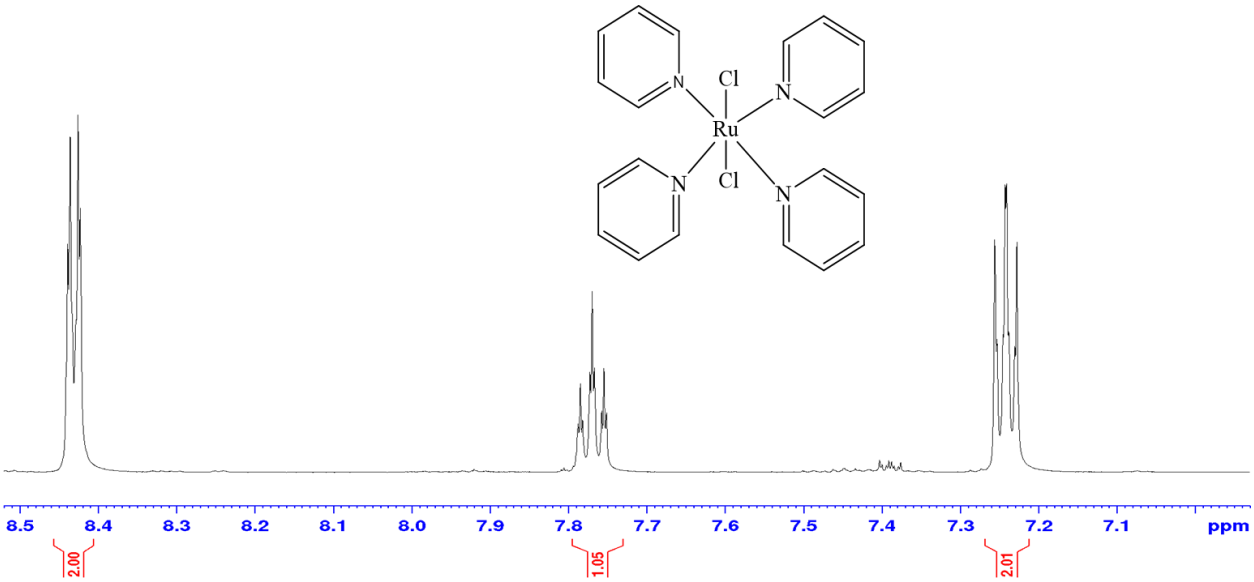

Figure SI 4.14: ^{1}H NMR (400 MHz, DMSO-d_6) of **Ru-1**

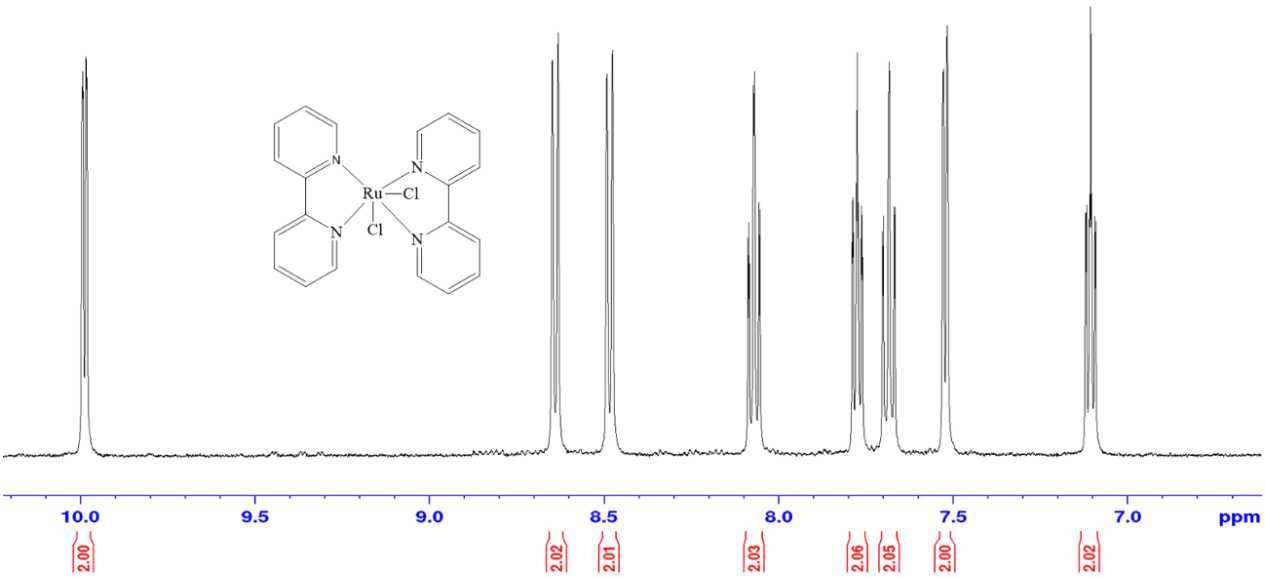

Figure SI 4.15: ^{1}H NMR (400 MHz, DMSO-d_6) of **Ru-2**

CHAPTER FIVE

The Role of Bridging Ligand on the Reactivity of η^6-*p*-cymene Ruthenium(II) Complexes: Kinetics and Mechanistic studies

Abstract

Substitution kinetics of the aqua ligands in a series of six ruthenium(II) *p*-cymene complexes by thiourea nucleophiles (thiourea, *N,N*-dimethylthiourea and *N,N,N',N'*-tetramethylthiourea) in 0.1 M $HClO_4/NaClO_4$ aqueous medium were investigated as a function of nucleophile concentration and temperature. All the reactions were performed under *pseudo*-first order conditions using stopped flow and ultraviolet-visible spectrophotometry. A single substitution step was observed in all the complexes. Dependence of observed rate constant on the nucleophilic concentration can be described by the rate law, $k_{obs} = k_2$[Nucleophile]. The reactivity of the mononuclear and binuclear complexes decreased in the order: **Ru-1** > **Ru-2** and **Ru-3** > **Ru-4** > **Ru-5** > **Ru-6,** respectively. Comparing the reactivity of the mononuclear complexes, it was found that chelation of a bipyridyl ligand to the *p*-cymene ruthenium(II) complex (**Ru-1**) significantly reduces its reactivity due to increase in steric hindrance around the metal centre and reduced electrophilicity of the complex. The binuclear complex (**Ru-3**) is more reactive than its related mononuclear complex (**Ru-2**) due to synergistic effects of the two metal centres which make the complex more electrophilic. Comparing the reactivity of the binuclear complexes, it was observed that increase in steric hindrance and decrease in electrophilicity of the complexes retard the reactivity. The inter-metallic distance was found to have a negative correlation with the reactivity of the complexes due to decrease in synergistic effects of the two metal centres as the distance increases. Computational results support the experimental results. The activation parameters ($\Delta H^{\neq} > 0$, $\Delta S^{\neq} < 0$) for all the

complexes support an associative mechanism of activation where the transition state is more ordered than the starting states. The current study has highlighted the strong dependence of the kinetic behavior of ruthenium(II) *p*-cymene complexes on the bridging ligand; therefore, variation of the rigid linker can be utilized to tune their reactivity.

5.1 Introduction

Ruthenium complexes have been explored as attractive alternatives to platinum-based complexes as anticancer agents.[1] Their attractive properties include; high selectivity for cancer cells,[2] high cellular uptake, low systemic toxicity, and the ability to mimic iron in binding biomolecules.[2a, 3] Furthermore, they exist in numerous oxidation states under physiological conditions but commonly as ruthenium(II) or ruthenium(III).[1b, 3]

The half-sandwich arene and polypridyl complexes form the most important classes of potential anticancer ruthenium(II) complexes.[1a] The half-sandwich ruthenium(II) arene complexes also known as the piano-stool ruthenium(II) complexes display a *pseudo*-octahedral geometry in which the π-bonded arene ligand occupy three coordination sites. The other three remaining coordination sites offer diverse coordination modes that can be used to modulate the properties of the complexes. The hydrophobic arene ligand facilitates diffusion of the drug through the cell membrane as well as stabilizes the metal in its 2+ oxidation state.[4] They exhibit superior anticancer activities both *in vitro* and *in vivo* even in *cisplatin* resistance cells.[1a, 5] A synergistic effect is responsible for the higher cytotoxicity observed in multinuclear complexes compared to their mononuclear analogues.[6] In biological systems, anticancer complexes encounter an array of potential deactivators such as glutathione and cysteinyl residues of protein.

These molecules play an important role in drug distribution and activity because they offer kinetic and thermodynamics competition to DNA binding.[7] In dinuclear complexes, the nature, size and electronic properties of the bridging ligands greatly influence these interactions. For instance; prolonging the size of polypridyl bridging ligand is reported to promote cellular uptake, intercalation into DNA double helix and cytotoxicity.[6a, 8]

A careful look into literature reveals that there is limited information on kinetics of ligand(s) exchange in ruthenium(II) arene complexes.[7c, 9] Detailed understanding of the factors that control the kinetics of ligand substitution around the ruthenium metal center is thus immensely important.

On the kinetics and mechanistic front, the effect of bridging ligand in square planar platinum(II) complexes is well established and depends entirely on the inherent properties of the linker. [10] For instance; increase in steric bulkiness of the bridging ligand as well as the separation distance between the metal centers dampens the reactivity of these complexes.[10a, 10b, 11] On the contrary, an increase in π acceptor character of the bridging ligand enhances reactivity of a complex by increasing its electrophilicity.[10c] A literature survey show that the role of bridging ligand in octahedral arene complexes is not explored to a greater extent and therefore there is need to establish the relationship between the bridging ligand and the lability of the leaving group in these complexes. Hydrolysis of the metal-choro bond in biological systems play a key role in the activation of metal based anticancer complexes.[11] It enhances the hydrophilicity and cellular uptake of the complex as well as increasing its anticancer efficacy.[11-12] Accordingly, all the complexes studied herein were converted into their respective aqua species.

Due to the foregoing reasons, a systematic study was undertaken on the effect of rigid bridging ligand on the substitution kinetics of ruthenium(II) *p*-cymene complexes using sulfur based nucleophiles *viz*: thiourea (Tu), *N,N*-dimethylthiourea (Dmtu) and *N,N,N',N'*-tetramethylthiourea (Tmtu). The study involved four dinuclear complexes with different π-conjugated binucleating ligands *viz*: 2,2'-bipyrimidine (**Ru-3**), 2,3-*bis*(2-pyridyl)-pyrazine (**Ru-4**), 2,3-*bis*(2-pyridyl)-quinoxaline (**Ru-5**) and 6,7-dimethyl-2,3-*bis*(2-pyridyl)quinoxaline (**Ru-6**). In addition, two mononuclear complexes, [Ru(*p*-cymene)(2,2'-bipyridine)OH_2)]$^{2+}$ (**Ru-2**) and [Ru(*p*-

cymene)$H_2O)_3]^{2+}$ (**Ru-1**) were also studied for purposes of providing insight to the role of the bridging linker. Structures of these complexes are shown in Figure 5.1.

Computational studies and ^{1}H NMR kinetics were also done to gain further insight into the substitution processes. The study has generated vital information on substitution and thermodynamic properties of ruthenium(II) *p*-cymene complexes as well as their kinetic stability.

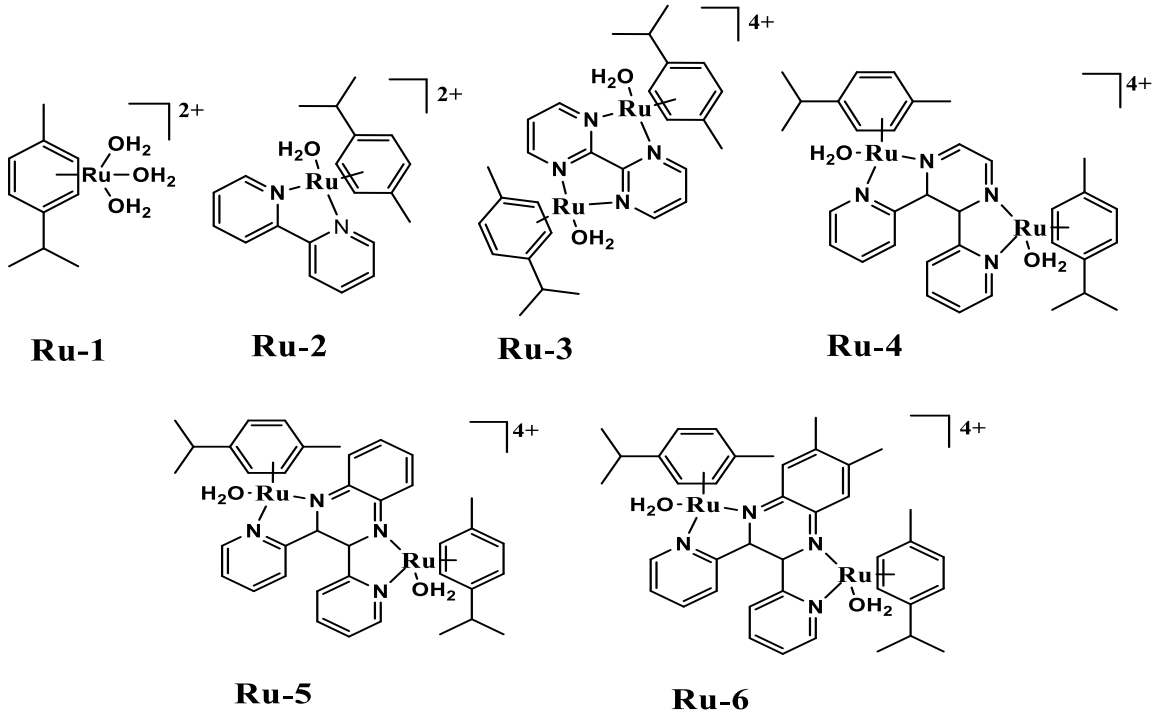

Figure 5.1: Structures of investigated ruthenium(II) complexes studied (counter ions are omitted for clarity)

5.2 Experimental

5.2.1 Materials and Procedures

All the syntheses were performed under dinitrogen atmosphere using standard Schlenk techniques. Dichloro(*p*-cymene)ruthenium(II) dimer (97%), 2,2'-bipyrimidine (95%), 2,3-*bis*(2-pyridyl)-pyrazine (98%), 6,7-dimethyl-2,3-*bis*(2-pyridyl)quinoxaline (98%), KPF_6 (98%), NH_4PF_6 (≥ 98

%), NH_4BF_4 (≥ 97%), 2,2'-bipyridyl (≥ 99%), NaOH (≥ 97%), $AgClO_4$ (99%), $NaClO_4.H_2O$ (98%), $HClO_4$ (70 wt % solution), celite(® 545), Tu (≥ 99 %), Dmtu (99%) and Tmtu (98%) were supplied by Sigma-Aldrich. 2,3-*bis*(2-pyridyl)quinoxaline was synthesized as per literature methods[13] (Supplementary Information, SI 5.1). Organic solvents were purchased from Merck (Pty) and used without further purification.

5.2.2 Synthesis of the Complexes

The complexes were synthesized according to published literature methods.[14] Synthetic procedures used, and characterization information obtained are summarized.

Triaqua(η^6-*p*-cymene)ruthenium(II) perchlorate: The complex was synthesized *in situ* by reacting dichloro(*p*-cymene)ruthenium(II) dimer (100 mg, 0.16 mmol) with 3.98 equivalents of $AgClO_4$ in 0.01 M $HClO_4$ solution. The mixture was stirred in the dark at 50℃ for 12 h. Upon cooling to room temperature, the solution was allowed to stand for 3 h and the grey AgCl precipitate therein filtered off and the filtrate refrigerated until further use.

(2,2'-bipyridine)chloro(η^6-*p*-cymene)ruthenium(II) hexaflourophosphate: A mixture of dichloro(*p*-cymene)ruthenium(II) dimer (100.0 mg, 0.16 mmol) and 2, 2'-bipyridyl (59.0 mg, 0.38 mmol) in 25 mL of methanol was stirred at room temperature for 2 h. NH_4PF_6 (57.0 mg, 0.35 mmol) in 5 mL of methanol was added to the solution and the resulting mixture stirred for further 1 h. The orange-yellow precipitate that formed was filtered off, washed with chilled methanol and diethyl ether. The product was further recrystallized by slow diffusion of diethyl ether into methanolic solution of the complex. Shiny yellow crystalline solid was obtained. Yield: 164.0 mg (90%). *Anal*. *Calc*. for $C_{20}H_{22}ClN_2PF_6Ru$; C, 42.0; H, 3.9; N, 4.9%. *Found*: C, 42.3; H, 3.8; N, 4.7%. ^{1}H NMR (400 MHz; acetone-d_6): δ (ppm) = 9.62 (d, 2H), 8.62 (d, 2H), 8.32 (td, 2H), 7.82 (td, 2H), 6.25 (d, 2H), 6.00 (d, 2H), 2.67 (hept, 1H), 2.33 (s, 3H) and 1.11 (d, 6H). ^{13}C NMR (400

MHz; acetone-d_6): δ (ppm) = 155.8, 155.0, 140.0, 127.7, 123.8, 105.2, 104.0, 86.7, 84.5, 31.1, 27.7 and 18.1. ESI-MS(TOF) (*m/z*): 427.05 $(M)^+$.

(μ$_2$-2,2'-bipyrimidyl)dichloro*bis*(η^6-*p*-cymene)diruthenium(II) hexaflourophosphate): 122.0 mg (0.2 mmol) of dichloro(*p*-cymene)ruthenium(II) dimer, 31.6 mg (0.2 mmol) of 2,2'-bipyrimidine and 77.0 mg (0.42 mmol) of KPF_6 in 20 mL methanol were stirred at room temperature for 4 h. The complex which precipitated out as a yellow solid, was filtered off, washed (3 × 10 mL) diethyl ether and dried under vacuum. Crystals were obtained by slow diffusion of diethyl ether into acetonic solution of the complex. Yield: 118.8 mg (60%). *Anal*. *Calc*. for $C_{28}H_{34}Cl_2N_4P_2F_{12}Ru_2$; C, 34.2; H, 3.8; N, 5.4%. *Found*: C, 34.0; H, 3.5; N, 5.7%. ^{1}H NMR (500 MHz; acetone-d_6): δ (ppm) = 10.15 (d, 4H), 8.40 (t, 2H), 6.49 (d, 4H), 6.26 (d, 4H), 2.89 (hept, 2H), 2.36 (s, 6H) and 1.14 (d, 12H). ^{1}C NMR (500 MHz; acetone-d_6): δ (ppm) = 163.8, 161.6, 126.9, 108.4, 105.2, 85.8, 84.1, 31.1, 21.5 and 18.1. ESI-MS (TOF) (*m/z*): 429.05 $(M)^+$.

(μ$_2$-2,3-*bis*(2-pyridyl)-pyrazine)dichloro*bis*(η^6-*p*-cymene)diruthenium(II) tetraflouroborate: A mixture of dichloro(*p*-cymene)ruthenium(II) dimer (122.0 mg, 0.2 mmol) and 2,3-*bis*(2-pyridyl)-pyrazine (46.8 mg, 0.2 mmol) in 30 mL of methanol was stirred continuously at room temperature for 6 h. The solution was filtered through celite to remove any solid impurities. 10 mL of saturated methanolic solution of NH_4BF_4 was added to the filtrate and the resulting solution kept in refrigerator for slow crystallization. After a couple of days, the brown microcrystalline solid formed was filtered, washed with methanol, diethyl ether and dried under vacuum. Yield: 129.7 mg (67%). *Anal*. *Calc*. for $C_{34}H_{38}Cl_2N_4B_2F_8Ru_2$; C, 43.0; H, 4.0 N, 5.9%. *Found*: C, 42.8; H, 3.7; N, 6.0%. ^{1}H NMR (400 MHz; DMSO-d_6): δ (ppm) = 9.66 (m, 4H), 8.80 (s, 2H), 8.21 (t, 2H), 7.96 (t, 2H), 6.42- 6.09 (m, 8H) 2.92 (hept, 2H), 2.31 (s, 6H) and 1.22 (dd, 12H). ^{13}C NMR (400 MHz;

DMSO-d_6): δ (ppm) = 158.1, 152.0, 140.7, 130.7, 130.5, 129.3, 109.8, 102.1, 88.1, 87.5, 87.4, 32.0, 22.5, 22.2 and 18.5. ESI-MS (TOF) (*m/z*): 505.08 $(M)^+$.

(μ$_2$-2,3-*bis*(2-pyridyl)quinoxaline)dichloro*bis*(η^6-*p*-cymene)diruthenium(II) hexaflourophosphate: A mixture of 122.0 mg (0.2 mmol) of dichloro(*p*-cymene)ruthenium(II) dimer, 56.8 mg (0.2 mmol) of 2,3-*bis*(2-pyridyl) quinoxaline and 77.0 mg (0.42 mmol) of NH_4PF_6 in 20 mL of methanol was refluxed for 4 h. After cooling to ambient temperature, the violet precipitate formed was filtered off, washed with (3 × 10 mL) water, 10 mL of methanol and 10 mL of diethyl ether and dried under vacuum. Dark violet shiny crystals were obtained. Yield: 185.1 mg (83%). *Anal*. *Calc*. for $C_{38}H_{40}Cl_2N_4P_2F_{12}Ru_2$; C, 40.9; H, 3.6; N, 5.0%. *Found*: C, 41.1; H, 3.7; N, 4.8%. ^{1}H NMR (500 MHz; DMSO-d_6): δ (ppm) = 9.58 (d, 2H), 8.85 (m, 2H), 8.56 (d, 2H), 8.41 (m, 2H), 8.24 (td, 2H), 8.01 (t, 2H), 6.43 (d, 2H), 6.34 (d, 2H), 6.12 (m, 4H), 2.76 (hept, 2H), 2.51 (s, 6H), 1.15 (d, 6H) and 1.02 (d, 6H). ^{13}C NMR (500 MHz; DMSO-d_6): δ (ppm) = 157.7, 153.2, 149.9, 143.0, 140.4, 136.2, 131.6, 129.6, 129.2, 109.9, 102.7, 88.6, 87.4, 86.6, 84.1, 30.9, 22.6, 21.7 and 18.0. ESI-MS (TOF) (*m/z*): 555.05 $(M)^+$.

(μ$_2$-6,7-dimethyl-2,3-*bis*(2-pyridyl)quinoxaline)dichloro*bis*(η^6-*p*-cymene)diruthenium(II) hexaflourophosphate: A methanolic solution (30 mL) containing 122.0 mg (0.2 mmol) of dichloro(*p*-cymene)ruthenium(II) dimer, 62.4 mg (0.2 mmol) of 6,7-dimethyl-2,3-*bis*(2-pyridyl) quinoxaline and 77.0 mg (0.42 mmol) of KPF_6 was refluxed for 6 h. The resulting solution was concentrated to about 5 mL under reduced pressure and upon cooling excess diethyl ether was added to precipitate the complex. The deep brown precipitate obtained was filtered off, washed with (3 × 10 mL) of *n*-pentane and dried under vacuum. Yield: 160.0 mg (70%). *Anal*. *Calc*. for $C_{40}H_{44}Cl_2N_4P_2F_{12}Ru_2$; C, 42.0; H, 3.9 N, 4.9%. *Found*: C, 41.75; H, 4.1; N, 4.7 ^{1}H NMR (400 MHz; acetone-d_6): δ (ppm) = 9.57 (d, 2H), 8.57 (d, 2H), 8.52 (s, 2H), 8.24 (t, 2H), 7.98 (t, 2H)

6.43 (d, 2H), 6.36 (d, 2H), 6.13-6.10 (m, 4H), 2.79-2.72 (m, 8H), 2.31 (s, 6H), 1.30 (d, 6H) and 1.18 (d, 6H). ^{13}C NMR (400 MHz; acetone-d_6): δ (ppm) = 157.2, 153.1, 148.7, 142.5, 140.2, 128.5, 110.5, 102.1, 88.7, 87.6, 85.8, 83.5, 48.9, 30.9, 20.3 and 17.4. ESI-MS (TOF) (*m/z*): 583.13 $(M)^+$.

5.2.3 Physical Measurements and Instrumentation

NMR spectra were acquired on Bruker Avance DPX III 400/500 MHz spectrometer fitted with 5 mm probe at 303 K. Chemical shifts expressed in parts per million (δ) were referenced to $Si(CH_3)_4$ internal standard. Electrospray ionization (ESI^+) mass spectra were recorded on a TOF micromass spectrometer. Typical NMR and MS spectra are presented in Supplementary Information (Figures SI 5.8-5.18). Microanalyses (C, H, and N) of the complexes were carried out by Thermo Scientific Flash 2000 analyzer. Cary 100 Series ultraviolet-visible spectrophotometer with Agilent technologies Cary temperature controller (± 0.05℃) was used for acid-base pH titrations and kinetic measurements. Kinetic studies of **Ru-1** was monitored using Applied Photophysics SX 20 stopped-flow reaction analyzer equipped with an online data acquisition program. The temperature of the analyzer was maintained within ± 0.1℃.

The pH of the aqueous complex solutions was determined by Jenway 4330 combined pH and conductivity meter. A glass embodied 4.5 mm diameter tip and 3.0 M NaCl solution electrode was used. The meter was calibrated with three standard buffer solutions (pH 4.0, 7.0 and 10.0) before use. p*K*a and kinetic data were processed using OriginPro 9.1® program.[15]

5.2.4 Aquation of the Complexes

Desired aqua solutions were prepared by reacting known amount of the chloro complexes with slightly less stoichiometric amount of $AgClO_4$ in 0.01 M $HClO_4$ solution. This was to ensure that no Ag^+ remained unreacted in the solution. For instance; aquation of the binuclear chloro complexes was achieved by reacting their chloro complexes with 1.98 equivalents of $AgClO_4$

while for the mononuclear complex, **Ru-2**, 0.99 equivalent of $AgClO_4$ was used. All the reactions were carried out in the dark at 50 ℃ for 48 h. The solutions were thereafter cooled to room temperature and the grey AgCl precipitate filtered off using Millipore filtration system.[16] The filtrates were refrigerated at 4 ℃ before use for p*K*a titrations and kinetic studies.

5.2.5 p*K*a Determination of the Aqua Complexes

Spectrophotometric acid-base titration of the aqua complexes with NaOH was done from pH 1 to 10/12 at 298 K. To avoid dilution effects and absorbance corrections, large complex volumes of about 500 mL were used.[17] From pH 1 to 3, small granules of crushed NaOH pellets were added stepwise while from 4 to 10/12, NaOH solutions of decreasing concentrations were added dropwise. After each addition, the complex solution was stirred for about 2 min prior to pH measurement and respective spectrum recording. For the pH measurements, 0.6 mL aliquots in glass ampules were used and discarded to avoid *in situ* contamination of the stock complex solution by Cl^- from the meter electrode while the aliquots used for absorbance measurements were returned to the stock solution. A confirmatory reverse pH titration was done using $HClO_4$ solutions in place of NaOH.

5.2.6 Kinetic Measurements

Nucleophile solutions of known concentration maintained at pH 2.0 and 0.1 M $HClO_4/NaClO_4$ ionic strength were prepared shortly before use. Likewise, the complex solutions were maintained at similar pH and ionic strength. The concentration of the aqua complexes used were; **Ru-1** (1.307 mM), **Ru-2** (0.440 mM) **Ru-3** (0.430 mM), **Ru-4** (0.103 mM) **Ru-5** (0.561 mM) and **Ru-6** (0.525 mM). Substitution studies were done under *pseudo*-first conditions in which the concentration of the nucleophile was at least 10 folds higher with respect to each leaving group in the complex. The ultraviolet-visible spectral changes of the reactions were taken to determine appropriate

wavelength to follow each reaction which was done by monitoring absorbance changes as function of time at a specific wavelength. Concentration dependence studies were performed at 25℃ while the temperature dependence reactions were studied from 20 to 40℃ at an interval of 5℃. The results recorded herein are an average of three independent runs.

5.2.7 Computational Modelling

Computational studies were performed using Gaussian 09W program package with the support of GaussView 5.0 visualization program.[18] Density functional theoretical (DFT) calculations were done using the hybrid B3LYP method at Los Alamos National Laboratory 2-double- ζ (LANL2DZ) effective core potential.[19] DFT utilizes electron density over wave-function, therefore applicable to systems with large number of electrons as it is in this study. To incorporate solvent effects, the systems were fully optimized in water environment using CPCM solvent model at overall charge of +4 and +2 for the binuclear and mononuclear complexes, respectively.

Global electrophilicity indices (ω) for the complexes were calculated from the relationship, $\omega = \mu^2/2\eta$.[20] Natural Bond Order (NBO) analysis was used to determine atomic charges of selected atoms in these complexes. [18] All the systems were optimized at singlet spin ground electronic state.

5.3 Results

5.3.1 Acid-Base Equilibria of the Aqua Complexes

The p*Ka* values of the aqua complexes were determined by fitting a single or double Boltzmann fit on a plot of absorbance versus pH at a selected wavelength. Typical ultraviolet-visible spectra obtained for the titration of **Ru-6** with NaOH is shown in Figure 5.2. The inset shows plots of absorbance versus pH at λ = 270 and 340 nm. Additional spectra are presented in the

Supplementary Information (Figures SI 5.6-5.7) while the p*K*a values are summarized in Table 5.1. All the complexes showed two or more isosbestic points signifying that changes in absorbance as a function of pH arose from an equilibrium of the aqua and hydroxo species in the solution.[10c]

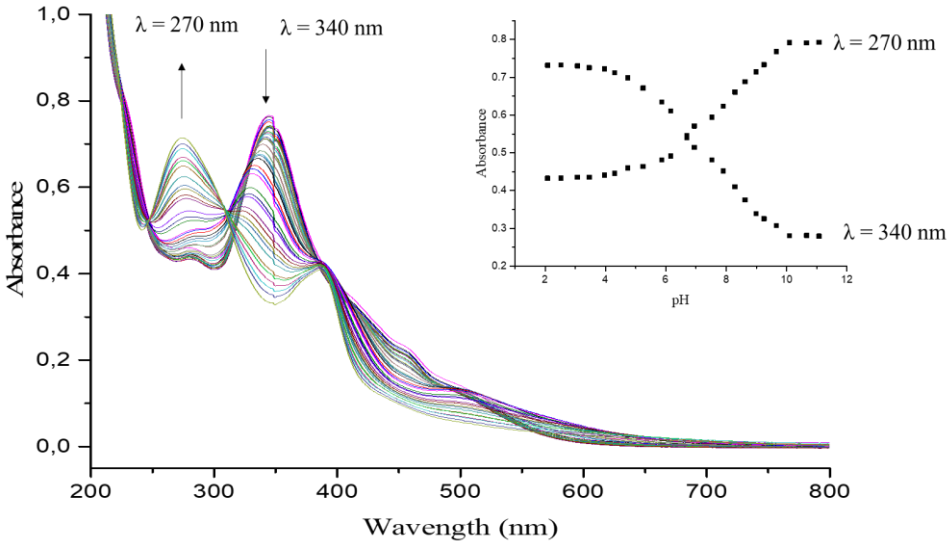

Figure 5.2: Ultraviolet-visible spectra of **Ru-6** complex recorded as a function of pH in the range 1–11 at 298 K. **Inset**: Plot of absorbance versus pH at λ = 270 and λ = 340 nm

Table 5.1: p*K*a values obtained for the deprotonation of the complexes

Complex	**Ru-1**	**Ru-2**	**Ru-3**	**Ru-4**	**Ru-5**	**Ru-6**
p*K*a$_1$	4.21 ± 0.01	7.38 ± 0.02	6.12 ± 0.05	6.29 ± 0.08	6.02 ± 0.02	6.32 ± 0.03
p*K*a$_2$	-	-	8.21 ± 0.21	8.50 ± 0.23	8.15 ± 0.32	8.91 ± 0.10

From Table 5.1, it is observed that the mononuclear complexes showed a single p*K*a value while the binuclear complexes exhibited two p*K*a values. Among the complexes studied, **Ru-1** is the most acidic as indicated by its low p*K*a value.[21] Comparing the mononuclear complex **Ru-2** and

its related binuclear complex, **Ru-3**, one notices that, the binuclear complex is more acidic due to increased positive charge and π-back-bonding of electron density from the metal centres.[10c]

The existence of two p*K*a values in the binuclear complexes signify a stepwise deprotonation of the aqua ligands as illustrated in Scheme 5.1. It is noteworthy that the p*K*a$_1$ values decrease with increase in the strength of π-acceptor ability of the bridging ligand.[17, 22] Increase in π-acceptor ability of the bridging ligand enhances the withdrawal of electrons from the metal centre leaving it depleted of negative charge, thus making the aqua ligand more acidic.[11] It is further observed that the p*K*a$_2$ value in all the binuclear complexes is at least 2 p*K*a unit higher than the p*K*a$_1$. This difference is because after the deprotonation of the first aqua ligand, the overall charge of the complex reduces from +4 to +3. This makes the second ruthenium metal center less electrophilic decreasing the tendency for another deprotonation to occur.[10b, 10c, 23] The presence of σ-donor methyl groups on the quinoxaline moiety in **Ru-6** lowers the electrophilicity of the complex by increasing the electronic density at the metal centre. This is responsible for the high basicity observed.

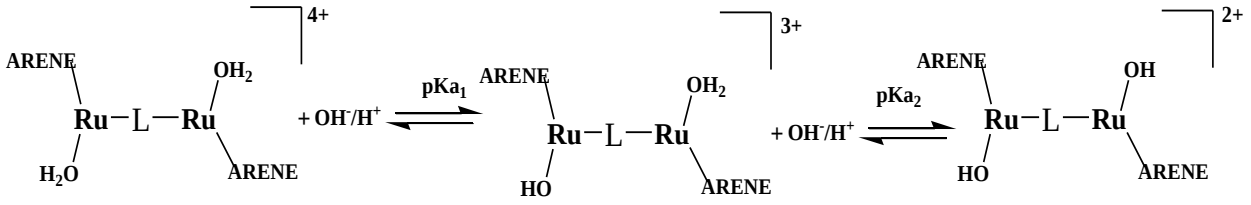

Scheme 5.1: Stepwise deprotonation of the aqua ligands in the binuclear complexes

At pH of 2.0, all the complexes exist entirely as aqua, making it an ideal pH for the kinetic investigations.

5.3.2 Computational Results

Electronic and structural properties of the complexes revealed by computational analysis are useful in understanding the reactivity trend observed. Figures 5.4 and 5.5 show the DFT-optimized structures of the frontier orbitals and their respective energy separation. Key computational data obtained is summarized in Table 5.2.

The optimized structures show that the complexes adopt a *pseudo*-octahedral geometry in which the *p*-cymene moiety is located opposite the aqua ligand to minimize steric interactions.[14a] In the binuclear complexes the two aqua ligands are *trans* to each other. In **Ru-3**, the two pyrimidinyl moiety planes are co-planar because the bridging ligand coordinates each metal centre through two equivalent nitrogen atoms. However, in the rest of the binuclear complexes each metal centre is coordinated to the bridging ligand through non-equivalent nitrogen atoms; a pyridyl and pyrazinic/quinoxalinic. The two pyridyl moieties in these binuclear complexes are not co-planar to each other. This occur in order to ameliorate the steric interactions of the hydrogen atoms at the *meta* positions in the pyridyl rings.[24] The angle between the two pyridyl moiety planes in **Ru-4**, **Ru-5** and **Ru-6** is 50.68, 56.33, and 55.54°, respectively. Figure 5.3 illustrates the non-planarity of the pyridyl moieties in **Ru-4**.

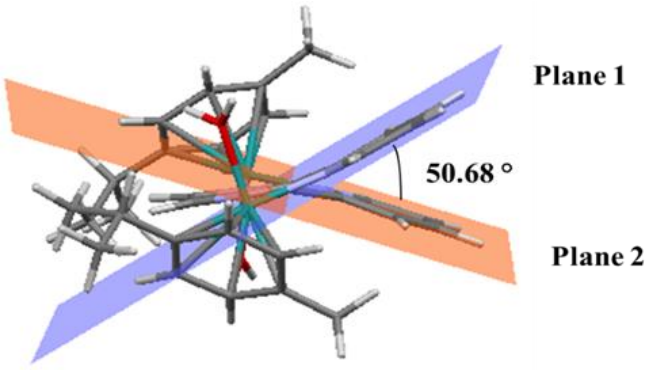

Figure 5.3: DFT-optimized structure of **Ru-4** showing the dihedral angle between the planes of the pyridyl moieties

In the chelated complexes, the HOMO is largely based on the metal centre(s) and *p*-cymene group(s) while the LUMO is largely based on the chelating ligand. The binuclear complexes have a smaller energy gap compared to the mononuclear complexes because the second metal center stabilizes the π* orbital of the ligand by lowering the HOMO–LUMO gap.[25] A look at the dπ HOMO energy of **Ru-4**, **Ru-5** and **Ru-6** reveals that it remains invariant as the bridging ligand is systematically varied. This is an indication that the bridging ligand has no effect on the relative energy of dπ HOMO. On the contrary, the π* LUMO energy is somewhat affected by the bridging ligand.[25a]

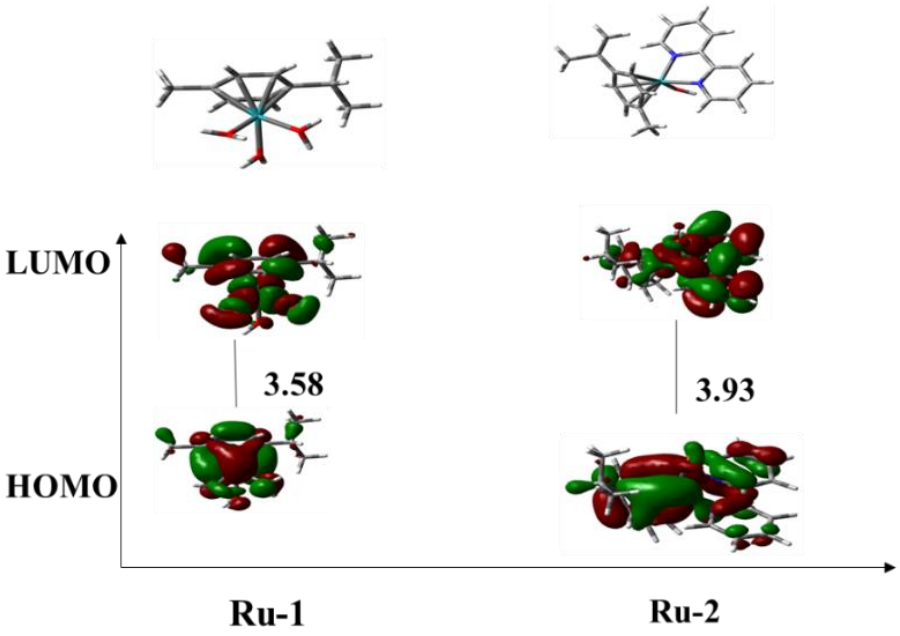

Figure 5.4: DFT-optimized frontier molecular orbitals of the mononuclear complexes

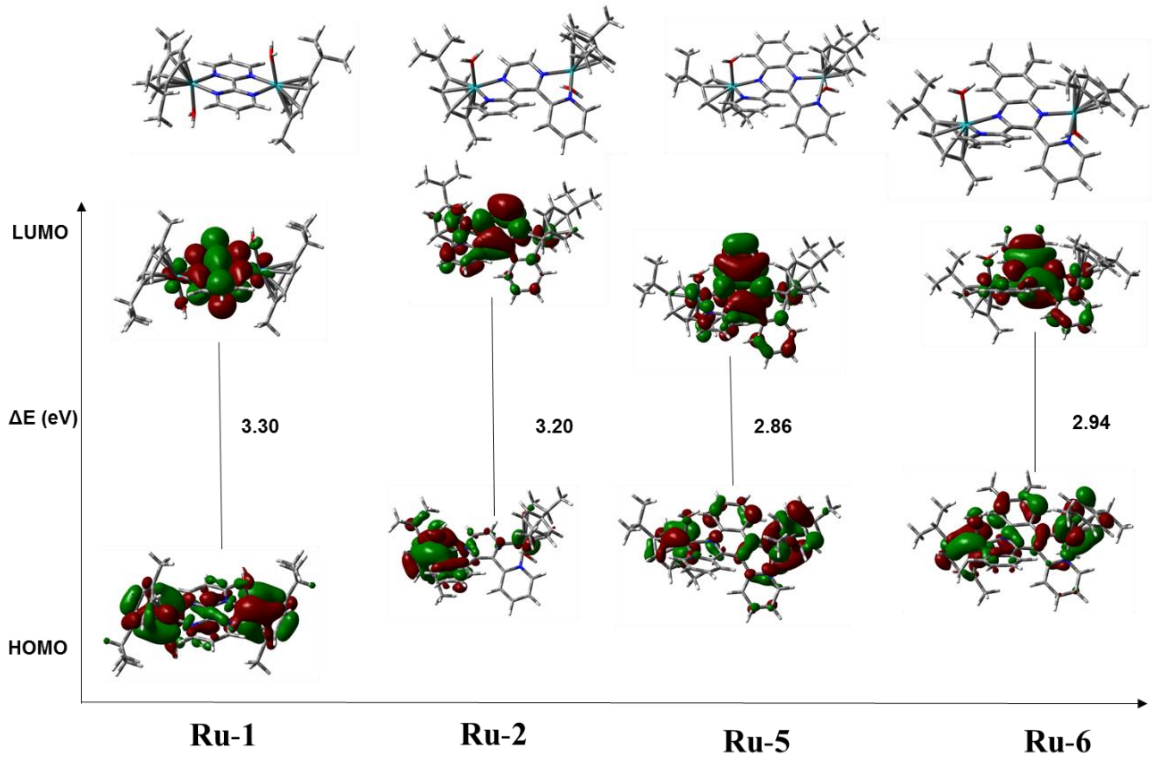

Figure 5.5: DFT-optimized frontier molecular orbitals of the binuclear complexes

Table 5.2: Summary of selected computational data for the investigated complexes

Complex	**Ru-1**	**Ru-2**	**Ru-3**	**Ru-4**	**Ru-5**	**Ru-6**
HOMO-LUMO energy						
HOMO /eV	-6.62	-6.98	-7.57	-7.18	-7.18	-7.12
LUMO /eV	-3.04	-3.05	-4.27	-3.98	-4.32	-4.18
HOMO-LUMO gap /eV	3.58	3.93	3.30	3.20	2.86	2.94
NBO charge (Ru)	0.383	0.280	0.306	0.303	0.284	0.281
Electrophilicity index (ω) /eV	6.52	6.40	10.62	9.73	11.52	10.86
Dipole moment /D	8.69	4.89	0.003	5.08	6.77	8.43
Ru-OH_2 bond length / Å	2.254	2.154	2.151	2.158	2.144	2.153
Ru-Ru distance / Å	-	-	5.66	6.88	6.95	6.96
Pyridyl Inter-planar angle /°	-	-	-	50.68	56.33	55.54

5.3.3 Kinetics Results

The substitution kinetics of aqua ligands in the six complexes was investigated with three thiourea nucleophiles with varied steric demands under *pseudo*-first order conditions. The substitution reactions occurred with concomitant change in absorbance bands. A single substitution step was observed in all the complexes. Representative spectra obtained for the reaction of the mononuclear and binuclear complexes with the nucleophiles are shown Figure 5.6 and 5.7, respectively.

Kinetic traces taken at a suitable wavelength were fitted into a single exponential function. From these exponential fits, *pseudo*-first order rate constants (k_{obs}) were computed and plotted against nucleophile concentrations. k_{obs} values and respective nucleophile concentrations are presented in the Supplementary Information (Table SI 5.1- 5.6).

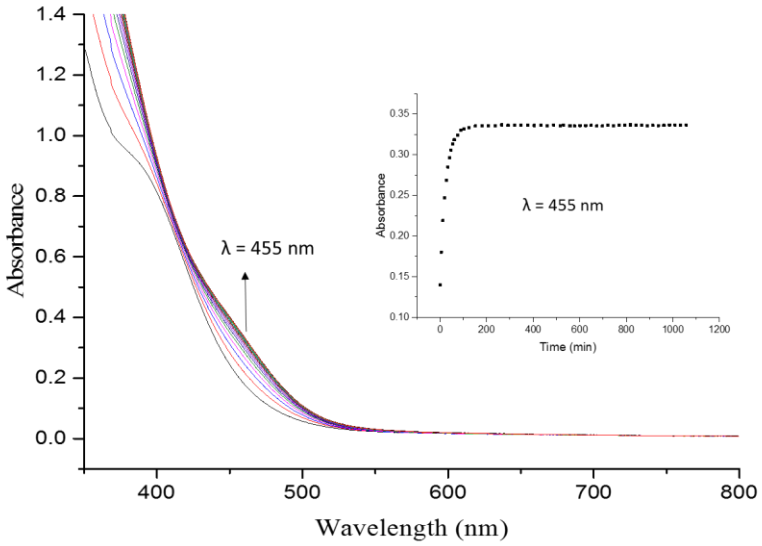

Figure 5.6: Ultraviolet-visible spectra for the reaction of **Ru-2** (0.440 mM) with Dmtu (44.0 mM) at 298 K, pH = 2.0, *I* = 0.1M $HClO_4/NaClO_4$. **Inset:** A kinetic trace at λ = 455 nm.

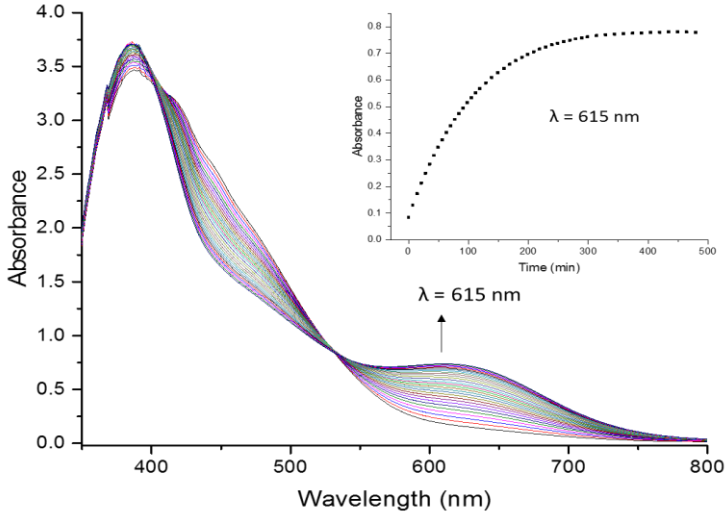

Figure 5.7: Ultraviolet-visible spectra for the reaction of **Ru-5** (0.561 mM) with Dmtu (112.2 mM) at 298 K, pH = 2.0, *I* = 0.1M $HClO_4/NaClO_4$. **Inset:** A kinetic trace at λ = 615 nm

A linear dependence of k_{obs} on the nucleophile concentration with zero intercept was exhibited by all the complexes as shown in Figure 5.8 and Supplementary Figures SI 5.1-5.2. The slope of the graph gave the second order rate constant (k_2). Therefore, the reactions can be described by equation (i)

$$k_{obs} = k_2[\text{Nucleophile}] \quad \text{(i)}$$

The k_2 values obtained are summarized in Table 5.3.

To determine the thermodynamic properties, the reactions were studied as a function of temperature from 20 to 40℃ at an interval of 5℃. Activation parameters were calculated from Eyring plots ($\ln\left(\frac{k_2}{T}\right)$ versus $\frac{1}{T}$) and the values obtained are tabulated in Table 5.3. Typical Eyring plots obtained are shown in Figure 5.9. $\ln\left(\frac{k_2}{T}\right)$ and respective $\frac{1}{T}$ values are presented in the Supplementary Information (Tables SI 5.7-5.12) while additional plots are shown in Figures SI

5.3 and 5.4 (Supplementary Information). For all the studied complexes, the activation enthalpies ($\Delta H^{\neq}$) and entropies ($\Delta S^{\neq}$) were positive and negative, respectively.

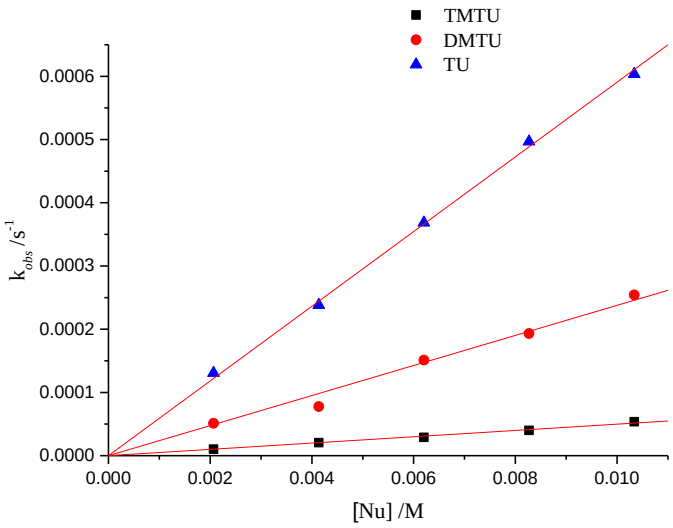

Figure 5.8: Dependence of k_{obs} on the concentration of incoming thiourea nucleophiles for the substitution of the aqua ligands in **Ru-4** at 298 K, pH = 2.0, I = 0.1 M $HClO_4/NaClO_4$

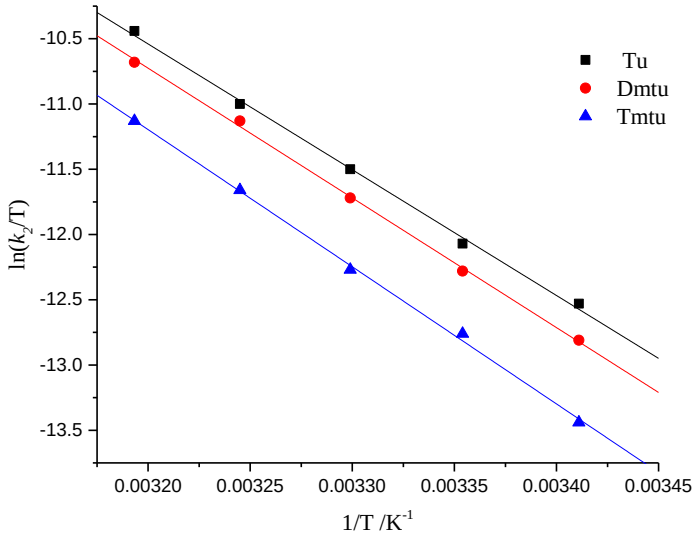

Figure 5.9: Eyring plots for the reaction of **Ru-5** with thiourea nucleophiles at different temperatures, pH = 2.0, I = 0.1 M $HClO_4/NaClO_4$

Table 5.3: Second order rate constants (k_2) and activation parameters for the displacement of aqua ligands by thiourea nucleophiles

Complex	Nu	k_2 /10^{-2} M^{-1} s^{-1}	$\Delta H^{\neq}$ /kJmol^{-1}	$\Delta S^{\neq}$ /Jmol^{-1}K^{-1}
Ru-1	**Tu**	614 ± 7	62 ± 2	-23 ± 7
	Dmtu	440 ± 6	65 ± 2	-17 ± 6
	Tmtu	314 ± 7	67 ± 2	-13 ± 7
Ru-2	**Tu**	7.77 ± 0.09	63 ± 3	-56 ± 10
	Dmtu	6.26 ± 0.10	57 ± 2	-77 ± 6
	Tmtu	2.10 ± 0.04	68 ± 1	-47 ± 4
Ru-3	**Tu**	28.71 ± 0.30	56 ± 2	-71 ± 7
	Dmtu	13.53 ± 0.30	63 ± 3	-51 ± 9
	Tmtu	1.28 ± 0.02	76 ± 2	-25 ± 8
Ru-4	**Tu**	5.91 ± 0.05	57 ± 2	-77 ± 7
	Dmtu	2.38 ± 0.08	67 ± 2	-51 ± 8
	Tmtu	0.50 ± 0.01	76 ± 3	-33 ± 9
Ru-5	**Tu**	0.17 ± 0.01	80 ± 2	-29 ± 7
	Dmtu	0.14 ± 0.01	83 ± 2	-22 ± 5
	Tmtu	0.09 ± 0.02	87 ± 2	-11 ± 6
Ru-6	**Tu**	0.12 ± 0.01	84 ± 2	-20 ± 6
	Dmtu	0.11 ± 0.01	84 ± 2	-19 ± 7
	Tmtu	0.05 ± 0.07	88 ± 2	-18 ± 6

5.3.4 ^{1}H NMR Kinetics

To gain further insight into the substitution process of the binuclear complexes, a reaction of the chloride derivative of **Ru-3** with 6 equivalents of Tu was followed by ^{1}H NMR in acetone-d_6 at 303 K. An overlay of time dependent spectra obtained is shown in Figure 5.10. To effectively monitor the reaction, an aromatic proton (H_α) adjacent to the pyrimidinic N was chosen since it

bears maximum impact of changes in the coordination at the ruthenium centre. The proton H_a for unreacted **Ru-3** derivative resonate at δ = 10.14 ppm and on reaction with Tu the peak slightly shifts downfield to δ = 10.16 ppm with its intensity progressively decreasing over time. As the intensity decreased, a new set of two peaks with $\Delta\delta \approx 0.6$ ppm resonating at δ = 9.92 ppm and δ = 9.34 ppm appeared and gradually increased in intensity maintaining an equal isomeric proportion. These results suggest the formation of two substitution products which are possibly a *trans*-product (δ = 9.92 ppm) and a *cis*-product (δ = 9.34 ppm).

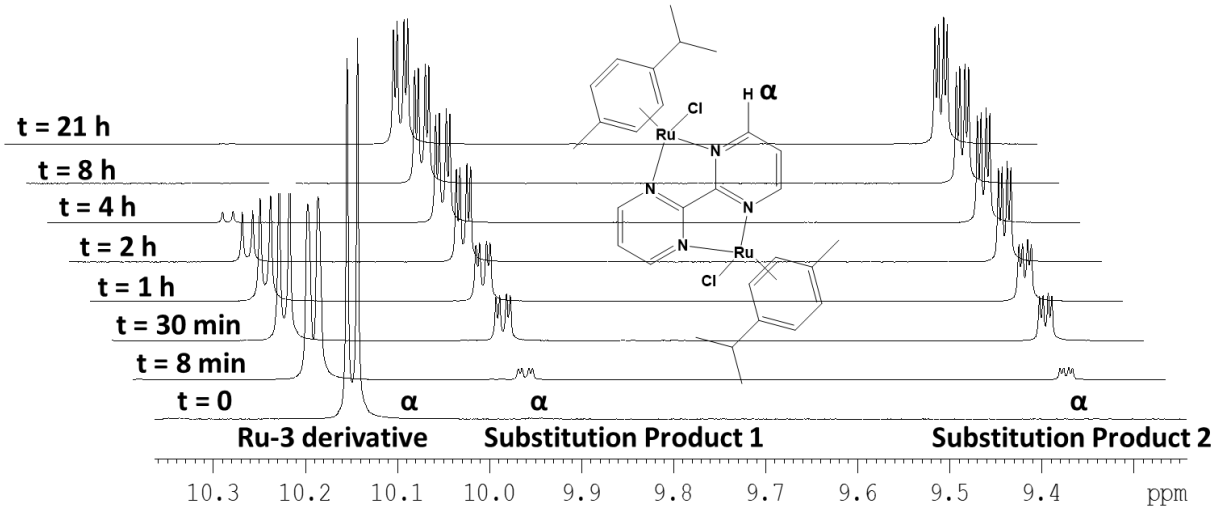

Figure 5.10: ^{1}H NMR spectral arrays for the reaction of **Ru-3** derivative with 6 equivalents of Tu in acetone-d_6 at 303 K

A close look at the spectra obtained (Supplementary Information, Figure SI 5.5) reveal a diastereotopic behavior of the *cis* conformer formed. The aromatic protons on the *p*-cymene groups in *cis* product give four sets of doublets instead of two. This shows that the two *p*-cymene groups are non-equivalent due to decreased symmetry of the complex,[26] due to coordination of more sterically bulky Tu. A plausible mechanism for the substitution reactions in the binuclear complexes is shown in Scheme 5.2.

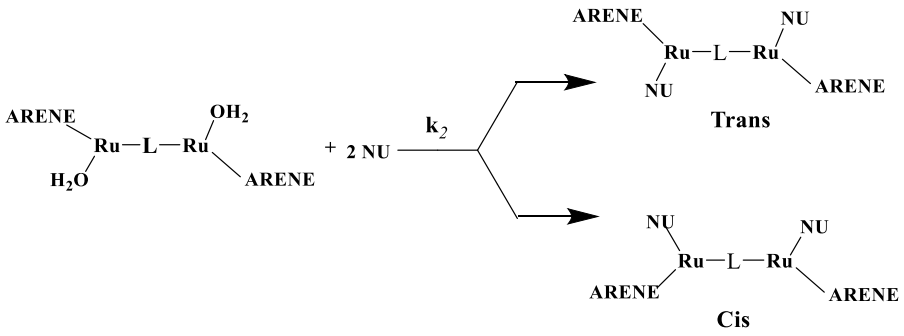

Scheme 5.2: Proposed reaction pathway for the investigated binuclear ruthenium(II) complexes

5.4 Discussion

In this study the role of the bridging ligand on the reactivity of half-sandwich ruthenium(II) complexes was investigated. The set of complexes used included two mononuclear complexes in which the ruthenium metal centre is bonded to *p*-cymene and three aqua ligands (**Ru-1**) and **Ru-2** where two aqua ligands of **Ru-1** were replaced by a bidentate 2,2'-bipyridyl chelating ligand. From **Ru-3** to **Ru-6** the bridging ligand was varied. In this discussion, the substitution reactivity of the complexes with Tu was used as a representative.

Comparing the reactivity of the two mononuclear complexes, **Ru-1** is found to be ~10^2 folds more reactive than **Ru-2**. This is attributed to differences in electronic and steric contributions of the spectator ligand(s) in the two complexes. **Ru-1** is more electrophilic than **Ru-2** as shown by the DFT-computed global electrophilicity indices (Table 5.2) and p*K*a values (Table 5.1) (*vide supra*). This is further supported by the localized charges at the metal centres as reflected by the NBO charges of 0.383 (**Ru-1**) and 0.280 (**Ru-2**). Therefore, the metal centre in **Ru-1** is more electron deficient and thus more attractive for facile nucleophilic attack. The reactivity of **Ru-1** is further enhanced by the significantly weaker Ru-OH_2 bond compared to **Ru-2** as evidenced by the bond length of 2.254 Å and 2.154 Å in **Ru-1** and **Ru-2,** respectively. This means that the aqua ligand in **Ru-2** is more strongly bonded and therefore less labile.[27] Furthermore, the 2,2'-bipyridyl

chelating ligand in **Ru-2** introduces steric hindrance around the metal centre thereby impeding the nucleophilic attack. A similar observation was made in which the presence of bipyridyl ligand in $[(\eta^6\text{-benzene})Ru(H_2O)bipyridyl]^{2+}$ retarded the rate of water exchange by 100 folds compared to $[(\eta^6\text{-benzene})Ru(H_2O)_3]^{2+}$.[4b]

Ru-3 is ten times more reactive than the closely related mononuclear analogue, **Ru-2**. This is attributed to fact the that 2,2,-bipyrimidine ligand in **Ru-3** is a stronger π-acceptor than 2,2'-bipyridyl ligand (**Ru-2)**.[28] Secondly, it also attributed to the synergistic electronic effects caused by the second metal center through the π-system of the *bis*-chelated 2,2'-bipyrimidine bridging ligand.[14a] The effect of this is stabilization of the LUMO in **Ru-3** with a concomitant narrowing of the frontier orbital energy gap.[25] Consequently, the binuclear complex becomes more electrophilic leading to decrease in electron density at the metal centre as shown by the NBO charges on the ruthenium metal. This is corroborated by the fact that **Ru-3** is 1.2 p*Ka* units more acidic than **Ru-2** (Table 5.1). Therefore, the metal centres in **Ru-3** become more susceptible to nucleophilic attack.

Despite the binuclear complexes showing two p*K*a values, a simultaneous substitution of the two aqua ligands was observed. A similar observation has also been reported in literature.[10b] The second order rate constants for the simultaneous substitution of the aqua ligands in the binuclear complexes decreased in the order; **Ru-3** > **Ru-4** > **Ru-5** > **Ru-6**. This shows that the bridging ligand plays a role in influencing the reactivity of the complexes through stereo-electronic contributions. Due to the A-A coordinative type of bridging ligand in **Ru-3**, the space around the metal centres is less restricted compared to the other binuclear complexes which have A-B coordinative type of bridging ligands. Therefore, the incoming nucleophile experiences less steric hindrance in accessing the metal centres in **Ru-3** relative to the other binuclear complexes.

Looking at global electrophilicity indices one notices that **Ru-3** is more electrophilic than **Ru-4.** This is corroborated by the local charges on the metal centre as shown by the NBO charges of 0.306 (**Ru-3)** and 0.303 (**Ru-4)**. This is because the two coordinated nitrogen atoms of the 2,2'-bipyrimidine bridge are *meta*-positioned and thus make the bridge a more effective π-acceptor than 2,3-*bis*(2-pyridyl)pyrazine.[28a] In 2,3-*bis*(2-pyridyl)pyrazine, the two pyrazinic N atoms are at *para* positions to each other which exposes the pyrazine moiety to two conflicting forces; an electron withdrawing and an electron donating effect eventually making the bridging ligand a less effective π-acceptor.[28b] The additional phenyl ring in **Ru-5** enhances the π-acceptor character of the bridging ligand by increasing the aromatic surface thus stabilizing the π* LUMO orbital causing a decrease in HOMO-LUMO gap.[29] Since the HOMO is largely based on the dπ orbital of metal, a smaller energy separation between the frontier orbitals facilitate effective π-back donation of electron density from the metal centre to the ligand which should make the complex more electrophilic.[30] This is supported by the calculated global electrophilicity index which is the highest in the series (Table 5.2). Therefore, the reactivity is expected to be enhanced but it was found to be less compared to **Ru-3** and **Ru-4**. This can be accounted for by an increase in steric hindrance around the metal centres of **Ru-5** as shown by the large dihedral angle of 56.33° between the pyridyl planes. Besides, the localized charge on the metal centres is less positive, possibly due to a superior σ-donation capability of the 2,3-*bis*(2-pyridyl)-quinoxaline because its coordination mode allows it to have both π-acceptor and σ-donor properties. The two methyl substituents in the 2,3-*bis*(2-pyridyl)-quinoxaline framework in **Ru-6** further enhances σ-donation towards the metal centres. This destabilizes the LUMO energy leading to widening of energy separation between the frontier orbitals. As a consequence, π-back-bonding of electron density decreases. The net effect is high electron density on the metal centres leading to decreased reactivity relative to **Ru-5**. This

argument is supported by cyclic voltammetric data reported in literature for related complexes. The methyl substituents in 2,3-*bis*(2-pyridyl)-quinoxaline framework were observed to shift the reduction potential of its complex to a more negative value compared to that of derivative coordinated with unsubstituted 2,3-*bis*(2-pyridyl)-quinoxaline.[25a] Therefore, the dampened reactivity in both **Ru-5** and **Ru-6** in comparison to **Ru-4**, is due to both steric and σ-induction effects.

It was observed that the Ru-Ru intermetallic separation distance (Table 5.2) in the binuclear complexes has an inverse relationship with the substitution reactivity trend. As the inter-metallic distance increases from **Ru-3** to **Ru-6**, the effective electrocommunication through the π-effect of the bridge between the metal centres diminishes, decreasing the synergistic interactions between the two metal centres and as a result the reactivity slows down accordingly.[31]

An inverse relationship is also noticed between the dipole moments, a measure of the inductive negative charge of a system,[32] and the reactivity of the binuclear complexes. This is supported by a decrease in the positive charge at the metal centres as one move from **Ru-3** to **Ru-6** as shown by the NBO charges. The progressive decrease in the positive charge at the metal centre reduces its proneness to nucleophilic attack.

The rate of substitution of the aqua ligands by these bio-relevant nucleophiles decreased as the steric bulkiness of the nucleophile increased *viz*; Tu > Dmtu > Tmtu. The activation parameters, ($\Delta H^{\neq} > 0$, $\Delta S^{\neq} < 0$) support an associative mechanism where transition state is more ordered.[33] This is further supported by the sensitivity of the k_2 values to steric bulkiness of the incoming nucleophile.[34]

5.5 Conclusions

The study has demonstrated that the reactivity of ruthenium(II) *p*-cymene aqua complexes is strongly depended on the inherent stereo-electronic properties of coordinated chelating/bridging ligand. Increase in steric hindrance around the metal centre reduces the rate of substitution in both the mononuclear and binuclear complexes by limiting attack of the metal centre by the nucleophile. The reactivity of the binuclear complexes is also influenced by the inter-metallic distance; as the distance increases the reactivity decreases due to reduced electronic communication through the π-bridge between the metal centres. Decrease in the electrophilicity of complexes and increase in electron density around metal centre was also found to retard the reactivity of the complexes. The study has also shown that two geometric isomeric substitution products are formed during the substitution reactions of the binuclear complexes. All the substitution reactions are associatively activated as shown by the negative activation entropy.

5.6 References

[1] (a) W. Han Ang, P. J. Dyson, *European Journal of Inorganic Chemistry* **2006**, *2006*, 4003-4018; (b) I. Kostova, *Current Medicinal Chemistry* **2006**, *13*, 1085-1107; (c) E. S. Antonarakis, A. Emadi, *Cancer Chemotherapy and Pharmacology* **2010**, *66*, 1-9.

[2] (a) M. Pongratz, P. Schluga, M. A. Jakupec, V. B. Arion, C. G. Hartinger, G. Allmaier, B. K. Keppler, *Journal of Analytical Atomic Spectrometry* **2004**, *19*, 46-51; (b) G. Sava, S. Zorzet, C. Turrin, F. Vita, M. Soranzo, G. Zabucchi, M. Cocchietto, A. Bergamo, S. DiGiovine, G. Pezzoni, *Clinical Cancer Research* **2003**, *9*, 1898-1905.

[3] C. S. Allardyce, P. J. Dyson, *Platinum Metals Review* **2001**, *45*, 62-69.

[4] (a) Y. K. Yan, M. Melchart, A. Habtemariam, P. J. Sadler, *Chemical Communications* **2005**, 4764-4776; (b) L. Dadci, H. Elias, U. Frey, A. Hoernig, U. Koelle, A. E. Merbach, H. Paulus, J. S. Schneider, *Inorganic Chemistry* **1995**, *34*, 306-315.

[5] (a) J. Furrer, G. Süss-Fink, *Coordination Chemistry Reviews* **2016**, *309*, 36-50; (b) M. Babak, W. Ang, *Multinuclear Organometallic Ruthenium-Arene Complexes for Cancer Therapy*, *Vol. 18*, **2018**, pp. 172-192.

[6] (a) M.-G. Mendoza-Ferri, C. G. Hartinger, R. E. Eichinger, N. Stolyarova, K. Severin, M. A. Jakupec, A. A. Nazarov, B. K. Keppler, *Organometallics* **2008**, *27*, 2405-2407; (b) M. G. Mendoza-Ferri, C. G. Hartinger, M. A. Mendoza, M. Groessl, A. E. Egger, R. E. Eichinger, J. B. Mangrum, N. P. Farrell, M. Maruszak, P. J. Bednarski, *Journal of Medicinal Chemistry* **2009**, *52*, 916-925.

[7] (a) J. Reedijk, *Proceedings of the National Academy of Sciences* **2003**, *100*, 3611-3616; (b) J. Reedijk, *Chemical Reviews* **1999**, *99*, 2499-2510; (c) F. Wang, H. Chen, J. A. Parkinson, P. d. S. Murdoch, P. J. Sadler, *Inorganic Chemistry* **2002**, *41*, 4509-4523.

[8] S. Schäfer, I. Ott, R. Gust, W. S. Sheldrick, *European Journal of Inorganic Chemistry* **2007**, *2007*, 3034-3046.

[9] (a) F. Tiba, D. Jaganyi, A. Mambanda, *Journal of Coordination Chemistry* **2010**, *63*, 2542-2560; (b) A. Rilak, R. Puchta, Ž. D. Bugarčić, *Polyhedron* **2015**, *91*, 73-83; (c) M. M. Milutinović, S. K. Elmroth, G. Davidović, A. Rilak, O. R. Klisurić, I. Bratsos, Ž. D. Bugarčić, *Dalton Transactions* **2017**, *46*, 2360-2369.

[10] (a) P. O. Ongoma, D. Jaganyi, *Dalton Transactions* **2013**, *42*, 2724-2734; (b) A. Mambanda, D. Jaganyi, *Dalton Transactions* **2012**, *41*, 908-920; (c) T. Soldatović, S. Jovanović, Ž. D. Bugarčić, R. van Eldik, *Dalton Transactions* **2012**, *41*, 876-884; (d) P. O. Ongoma, D. Jaganyi, *International Journal of Chemical Kinetics* **2013**, *45*, 676-691.

[11] A. M. Pizarro, A. Habtemariam, P. J. Sadler, in *Medicinal Organometallic Chemistry*, Springer, **2010**, pp. 21-56.

[12] M. Li, L. Lai, Z. Zhao, T. Chen, *Chemistry–An Asian Journal* **2016**, *11*, 310-320.

[13] H. A. Goodwin, F. Lions, *Journal of the American Chemical Society* **1960**, *82*, 5013-5023.

[14] (a) P. Govindaswamy, J. M. Canivet, B. Therrien, G. Süss-Fink, P. Štěpnička, J. Ludvík, *Journal of Organometallic Chemistry* **2007**, *692*, 3664-3675; (b) A. Singh, N. Singh, D. S. Pandey, *Journal of Organometallic Chemistry* **2002**, *642*, 48-57; (c) R. Lalrempuia, M. R. Kollipara, *Polyhedron* **2003**, *22*, 3155-3160; (d) B. Therrien, G. Süss-Fink, P. Govindaswamy, C. Saïd-Mohamed, *Polyhedron* **2007**, *26*, 4065-4072; (e) L. Colina-Vegas, W. Villarreal, M. Navarro, C. R. de Oliveira, A. E. Graminha, P. I. d. S. Maia, V. M. Deflon, A. G. Ferreira, M. R. Cominetti, A. A. Batista, *Journal of Inorganic Biochemistry* **2015**, *153*, 150-161; (f) L. Bíró, A. J. Godó, Z. Bihari, E. Garribba, P. Buglyó, *European Journal of Inorganic Chemistry* **2013**, *2013*, 3090-3100.

[15] OriginPro9.1, OriginLab Corporation, One Roundhouse Plaza, Suite 303, Northampton, MA 01060, United States, 2014 1800-969-7720. *www.OriginLab.com*.

[16] Ž. D. Bugarčić, B. V. Petrović, R. Jelić, *Transition Metal Chemistry* **2001**, *26*, 668-671.

[17] A. Hofmann, D. Jaganyi, O. Q. Munro, G. Liehr, R. van Eldik, *Inorganic Chemistry* **2003**, *42*, 1688-1700.

[18] M. Frisc, G. Trucks, H. Schlegel, G. Scuseria, M. Robb, J. Cheeseman, G. Scalmani, V. Barone, B. Mennucci, G. Petersson, *Gaussian Inc, Wallingford* **2010**.

[19] J. Li, L.-C. Xu, J.-C. Chen, K.-C. Zheng, L.-N. Ji, *The Journal of Physical Chemistry A* **2006**, *110*, 8174-8180.

[20] R. G. Parr, L. v. Szentpaly, S. Liu, *Journal of the American Chemical Society* **1999**, *121*, 1922-1924.

[21] D. Jaganyi, A. Hofmann, R. van Eldik, *Angewandte Chemie International Edition* **2001**, *40*, 1680-1683.

[22] A. F. Peacock, A. Habtemariam, S. A. Moggach, A. Prescimone, S. Parsons, P. J. Sadler, *Inorganic Chemistry* **2007**, *46*, 4049-4059.

[23] A. Hofmann, R. van Eldik, *Dalton Transactions* **2003**, 2979-2985.

[24] (a) C. Knorrs, H. D. Gafney, A. David Baker, C. Braunstein, T. C. Strekas, *Journal of Raman Spectroscopy* **1983**, *14*, 32-35; (b) J. Cooper, D. MacQueen, J. Petersen, D. W. Wertz, *Inorganic Chemistry* **1990**, *29*, 3701-3705.

[25] (a) S. M. Molnar, K. R. Neville, G. E. Jensen, K. J. Brewer, *Inorganica Chimica Acta* **1993**, *206*, 69-76; (b) K. J. Brewer, W. R. Murphy Jr, J. D. Petersen, *Inorganic Chemistry* **1987**, *26*, 3376-3379.

[26] A. Garci, G. Gupta, C. Dalvit, B. Therrien, *European Journal of Inorganic Chemistry* **2014**, *2014*, 5651-5661.

[27] T. Bugarcic, A. Habtemariam, R. J. Deeth, F. P. Fabbiani, S. Parsons, P. J. Sadler, *Inorganic Chemistry* **2009**, *48*, 9444-9453.

[28] (a) S. C. Rasmussen, M. M. Richter, E. Yi, H. Place, K. J. Brewer, *Inorganic Chemistry* **1990**, *29*, 3926-3932; (b) A. R. Katritzky, C. A. Ramsden, J. A. Joule, V. V. Zhdankin, *Handbook of Heterocyclic Chemistry, Vol. 10*, Elsevier, **2010**, pp. 38-60.

[29] (a) M. M. Richter, K. J. Brewer, *Inorganic Chemistry* **1993**, *32*, 5762-5768; (b) L. M. Vogler, C. Franco, S. W. Jones, K. J. Brewer, *Inorganica Chimica Acta* **1994**, *221*, 55-59.

[30] (a) T. S. Morais, T. J. Silva, F. Marques, M. P. Robalo, F. Avecilla, P. J. A. Madeira, P. J. Mendes, I. Santos, M. H. Garcia, *Journal of Inorganic Biochemistry* **2012**, *114*, 65-74; (b) V. Moreno, M. Font-Bardia, T. Calvet, J. Lorenzo, F. X. Avilés, M. H. Garcia, T. S. Morais, A. Valente, M. P. Robalo, *Journal of Inorganic Biochemistry* **2011**, *105*, 241-249.

[31] F. Baumann, A. Stange, W. Kaim, *Inorganic Chemistry Communications* **1998**, *1*, 305-308.

[32] M. Das, S. E. Livingstone, *Journal of the Chemical Society, Dalton Transactions* **1975**, 452-455.

[33] (a) T. Das, B. Bera, A. Datta, A. Ghosh, *Transition Metal Chemistry* **2009**, *34*, 247-253; (b) J. D. Atwood, *Inorganic and Organometallic Reaction Mechanisms*, 2nd edition ed., VCH Publishers, **1997**, pp. 1-18, 47-90.

[34] H. Ertürk, J. Maigut, R. Puchta, R. van Eldik, *Dalton Transactions* **2008**, 2759-2766.

SI 5 Supplementary Information

SI 5.1 Synthesis of 2,3-bis(2'-pyridyl)-quinoxaline

A mixture of 270.0 mg of *o*-phenylenediamine and 530.0 mg of 2,2'pyridil in 20 mL of ethanol was refluxed for 1 h. On cooling the ligand separated as light brown solid. It was further purified by recrystallization from ethanol. Yield (579.10 mg, 81%). *Anal. Calc*. for $C_{18}H_{12}N_4$: C, 76.0; H, 4.25; N, 19.7%. *Found*: C, 76.05; H, 4.2; N, 19.8%. ^{1}H NMR (400 MHz; DMSO-d_6); δ (ppm) = 8.29 (d, 2H), 8.24 (m, 2H), 8.02 (d, 2H), 7.97 (m, 4H), 7.37 (m, 2H). ^{13}C NMR (400 MHz; DMSO-d_6); δ (ppm) = 157.4, 152.9, 148.5, 140.7, 137.3, 131.5, 129.5, 123.3, 123.7. TOF(ESI+): 307.095 (M+ Na).

SI 5.2 Average k_{obs} values for the substitution of aqua ligands in the complexes

Table SI 5.1: Average k_{obs} (s^{-1}) for the reaction of **Ru-1** (1.307 mM) with thiourea nucleophiles

[Nu] /M	**Tu** (λ = 600 nm) k_{obs} /s^{-1}	**Dmtu** (λ = 620 nm) k_{obs} /s^{-1}	**Tmtu** (λ = 640 nm) k_{obs} /s^{-1}
0.1960	1.234	0.883	0.649
0.1568	0.938	0.676	0.499
0.1176	0.712	0.496	0.349
0.0784	0.477	0.344	0.227
0.0392	0.232	0.187	0.124

Table SI 5.2: Average k_{obs} (s^{-1}) for the reaction of **Ru-2** (0.440 mM) with thiourea nucleophiles

[Nu] /M	**Tu** (λ = 450 nm)	**Dmtu** (λ = 455 nm)	**Tmtu** (λ = 430 nm)
	k_{obs} /s^{-1}	k_{obs} /s^{-1}	k_{obs} /s^{-1}
0.0440	3.359×10^{-3}	2.860×10^{-3}	9.336×10^{-4}
0.0352	2.807×10^{-3}	2.165×10^{-3}	7.018×10^{-4}
0.0264	2.022×10^{-3}	1.505×10^{-3}	5.525×10^{-4}
0.0176	1.419×10^{-3}	1.132×10^{-3}	3.950×10^{-4}
0.0088	6.607×10^{-4}	5.610×10^{-4}	2.109×10^{-4}

Table SI 5.3: Average k_{obs} (s^{-1}) for the reaction of **Ru-3** (0.430 mM) with thiourea nucleophiles

[Nu**]**/M	**Tu** (λ = 500 nm)	**Dmtu** (λ = 500 nm)	**Tmtu** (λ = 500 nm)
	k_{obs} /s^{-1}	k_{obs} /s^{-1}	k_{obs} /s^{-1}
0.0430	1.233×10^{-2}	5.921×10^{-3}	5.433×10^{-4}
0.0344	9.868×10^{-3}	4.822×10^{-3}	4.301×10^{-4}
0.0258	7.269×10^{-3}	3.132×10^{-3}	3.312×10^{-4}
0.0172	4.938×10^{-3}	2.204×10^{-3}	2.374×10^{-4}
0.0085	2.857×10^{-3}	1.231×10^{-3}	1.280×10^{-4}

Table SI 5. 4: Average k_{obs} (s^{-1}) for the reaction of **Ru-4** (0.103 mM) with thiourea nucleophiles

[Nu]/M	**Tu** (λ = 600 nm)	**Dmtu** (λ = 620 nm)	**Tmtu** (λ = 640 nm)
	k_{obs} /s^{-1}	k_{obs} /s^{-1}	k_{obs} /s^{-1}
0.01034	6.036×10^{-4}	2.542×10^{-4}	5.359×10^{-5}
0.00827	4.967×10^{-4}	1.932×10^{-4}	4.006×10^{-5}
0.0062	3.685×10^{-4}	1.512×10^{-4}	2.902×10^{-5}
0.00413	2.384×10^{-4}	7.761×10^{-5}	2.062×10^{-5}
0.00207	1.309×10^{-4}	5.123×10^{-5}	1.032×10^{-5}

Table SI 5.5: Average k_{obs} (s^{-1}) for the reaction of **Ru-5** (0.561 mM) with thiourea nucleophiles

[Nu] /M	**Tu** (λ = 600 nm)	**Dmtu** (λ = 620 nm)	**Tmtu** (λ = 640 nm)
	k_{obs} /s^{-1}	k_{obs} /s^{-1}	k_{obs} /s^{-1}
0.1122	1.891×10^{-4}	1.595×10^{-4}	1.068×10^{-4}
0.0898	1.521×10^{-4}	1.253×10^{-4}	7.963×10^{-4}
0.0673	1.118×10^{-4}	9.317×10^{-5}	5.789×10^{-4}
0.0449	7.910×10^{-4}	6.047×10^{-5}	3.969×10^{-4}
0.0225	3.993×10^{-4}	3.246×10^{-5}	1.797×10^{-4}

Table SI 5.6: Average k_{obs} (s^{-1}) for the reaction of **Ru-6** (0.525 mM) with thiourea nucleophiles

[Nu**]** /M	**Tu** (λ = 604 nm)	**Dmtu** (λ = 604 nm)	**Tmtu** (λ = 620 nm)
	k_{obs} /s^{-1}	k_{obs} /s^{-1}	k_{obs} /s^{-1}
0.1049	1.192×10^{-4}	1.192×10^{-4}	5.152×10^{-5}
0.0839	9.725×10^{-5}	9.210×10^{-5}	4.101×10^{-5}
0.0629	7.288×10^{-5}	6.852×10^{-5}	2.914×10^{-5}
0.0419	5.004×10^{-5}	4.614×10^{-5}	2.001×10^{-5}
0.0210	2.778×10^{-5}	2.642×10^{-5}	1.072×10^{-5}

SI 5.3 Average $\ln\left(\frac{k_2}{T}\right)$ values for the substitution of aqua ligands in the investigated complexes

Table SI 5.7: Average $ln\left(\frac{k_2}{T}\right)$ obtained from the reaction of **Ru-1** with thiourea nucleophiles

T /K	$\frac{1}{T}$ /K^{-1}	$\ln\left(\frac{k_2}{T}\right)$**Tu**	$\ln\left(\frac{k_2}{T}\right)$**Dmtu**	$\ln\left(\frac{k_2}{T}\right)$**Tmtu**
293.15	0.00340	-4.351	-4.685	-4.905
298.15	0.00335	-3.982	-4.226	-4.547
303.15	0.00330	-3.583	-3.892	-4.187
308.15	0.00325	-3.167	-3.459	-3.694
313.15	0.00319	-2.811	-3.030	-3.251

Table SI 5.8: Average $ln\left(\frac{k_2}{T}\right)$ for the reaction of **Ru-2** with thiourea nucleophiles

T /K	$\frac{1}{T}$ /K^{-1}	$\ln\left(\frac{k_2}{T}\right)$**Tu**	$\ln\left(\frac{k_2}{T}\right)$**Dmtu**	$\ln\left(\frac{k_2}{T}\right)$**Tmtu**
293.15	0.00340	-8.628	-8.728	-9.954
298.15	0.00335	-8.229	-8.469	-9.563
303.15	0.00330	-7.768	-8.080	-9.122
308.15	0.00325	-7.427	-7.718	-8.683
313.15	0.00319	-7.059	-7.323	-8.245

Table SI 5.9: Average $ln\left(\frac{k_2}{T}\right)$ for the reaction of **Ru-3** with the thiourea nucleophiles

T /K	$\frac{1}{T}$ /K^{-1}	$\ln\left(\frac{k_2}{T}\right)$**Tu**	$\ln\left(\frac{k_2}{T}\right)$**Dmtu**	$\ln\left(\frac{k_2}{T}\right)$**Tmtu**
293.15	0.00340	-7.756	-8.240	-10.550
298.15	0.00335	-7.351	-7.806	-10.052
303.15	0.00330	-7.085	-7.396	-9.651
308.15	0.00325	-6.681	-6.984	-9.096
313.15	0.00319	-6.332	-6.635	-8.634

Table SI 5.10: Average $ln\left(\frac{k_2}{T}\right)$ for the reaction of **Ru-4** with thiourea nucleophiles

T /K	$\frac{1}{T}$ /K^{-1}	$\ln\left(\frac{k_2}{T}\right)$**Tu**	$\ln\left(\frac{k_2}{T}\right)$**Dmtu**	$\ln\left(\frac{k_2}{T}\right)$**Tmtu**
293.15	0.00340	-8.927	-9.794	-11.471
298.15	0.00335	-8.526	-9.412	-11.062
303.15	0.00330	-8.150	-8.905	-10.497
308.15	0.00325	-7.794	-8.501	-10.012
313.15	0.00319	-7.491	-8.091	-9.519

Table SI 5.11: Average $ln\left(\frac{k_2}{T}\right)$ for the reaction of **Ru-5** with thiourea nucleophiles

T /K	$\frac{1}{T}$ /K^{-1}	$\ln\left(\frac{k_2}{T}\right)$**Tu**	$\ln\left(\frac{k_2}{T}\right)$**Dmtu**	$\ln\left(\frac{k_2}{T}\right)$**Tmtu**
293.15	0.00340	-12.53	-12.81	-13.44
298.15	0.00335	-12.07	-12.28	-12.76
303.15	0.00330	-11.52	-11.72	-12.27
308.15	0.00325	-11.01	-11.13	-11.66
313.15	0.00319	-10.44	-10.68	-11.13

Table SI 5.12: Average $ln\left(\frac{k_2}{T}\right)$ obtained for the reaction of **Ru-6** with thiourea nucleophiles

T /K	$\frac{1}{T}$ /K^{-1}	$\ln\left(\frac{k_2}{T}\right)$**Tu**	$\ln\left(\frac{k_2}{T}\right)$**Dmtu**	$\ln\left(\frac{k_2}{T}\right)$**Tmtu**
293.15	0.00340	-12.923	-13.054	
298.15	0.00335	-12.466	-12.492	-13.321
303.15	0.00330	-11.900	-11.990	-12.841
308.15	0.00325	-11.387	-11.461	-12.313
313.15	0.00319	-10.845	-10.928	-11.656

SI 5.4 Typical plots of k_{obs} versus nucleophile concentration for the substitution of the aqua ligands by thiourea nucleophiles

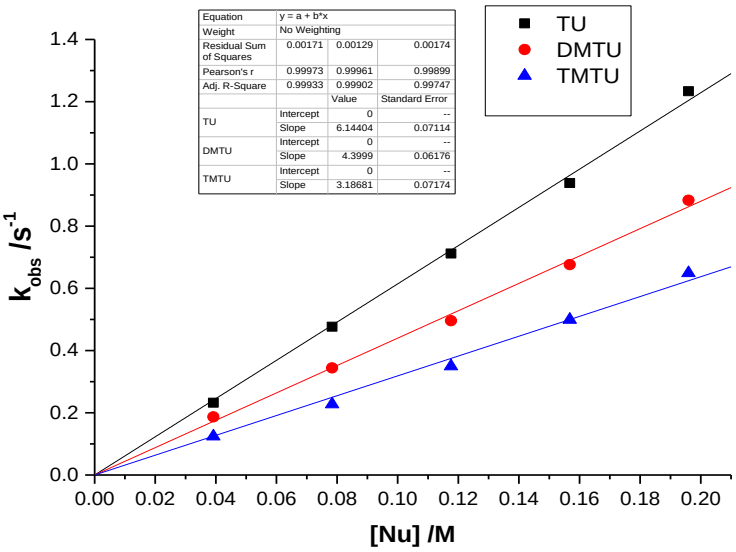

Figure SI 5.1: Dependence of k_{obs} on concentration of incoming thiourea nucleophiles for the substitution of the aqua ligands in **Ru-1** at 298 K, pH = 2.0, I = 0.1 M $HClO_4/NaClO_4$

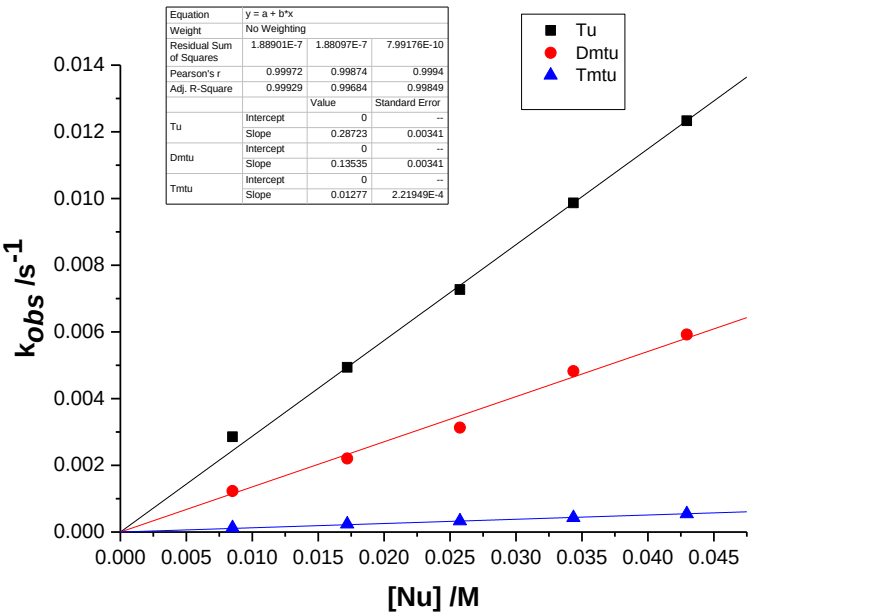

Figure SI 5.2: Dependence of k_{obs} on concentration of incoming thiourea nucleophiles for the substitution of the aqua ligands in **Ru-3** at 298 K, pH = 2.0, I = 0.1 M $HClO_4/NaClO_4$

SI 5.5 Typical Eyring plots for the substitution of the aqua ligands

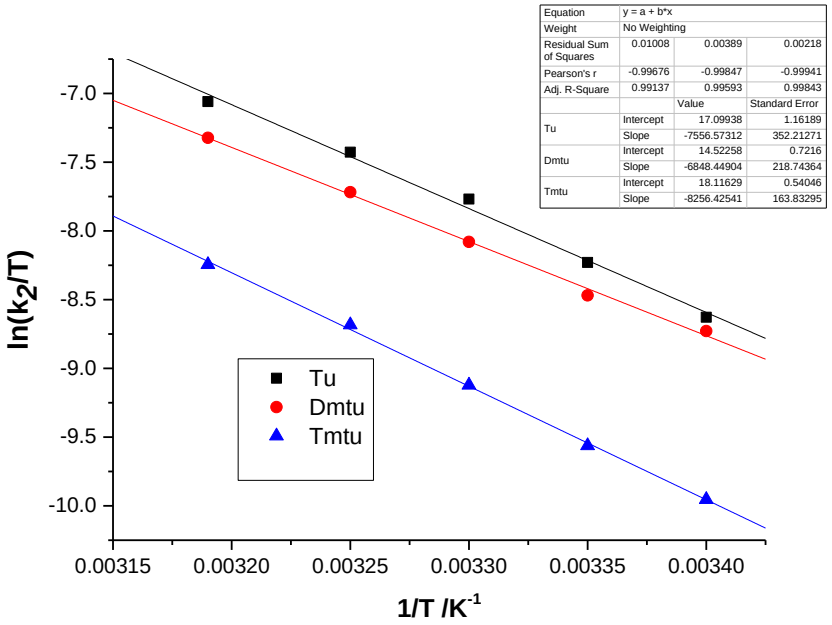

Figure SI 5.3: Eyring plots for the reaction of **Ru-2** with thiourea nucleophiles at different temperatures, pH = 2.0, *I* = 0.1 M $HClO_4/NaClO_4$

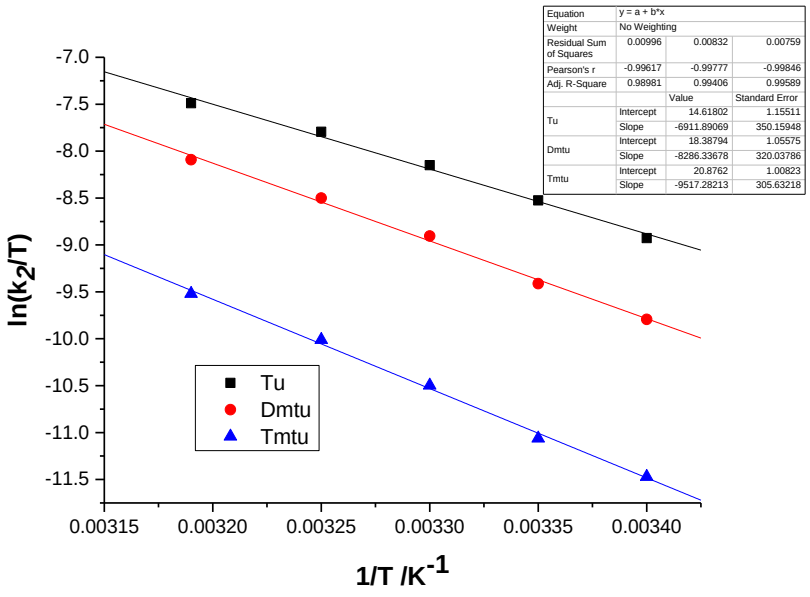

Figure SI 5.4: Eyring plots for the reaction of **Ru-4** with thiourea nucleophiles at different temperatures, pH = 2.0, *I* = 0.1 M $HClO_4/NaClO_4$

SI 5.6 ^{1}H NMR spectrum for the reaction of Ru-3 derivative with Tu

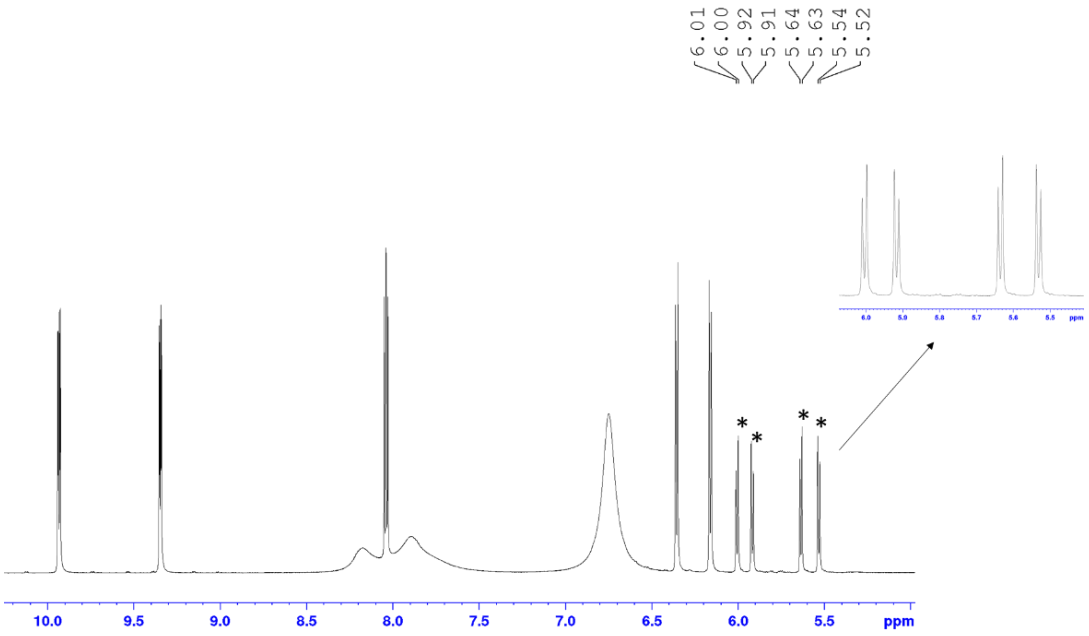

Figure SI 5.5: ^{1}H NMR spectrum of (**Ru-3 derivative +Tu**) substitution products showing peaks for aromatic protons for *p*-cymene in the *cis* product

SI 5.7 Typical ultraviolet-visible spectra for p*K*a titration of the complexes

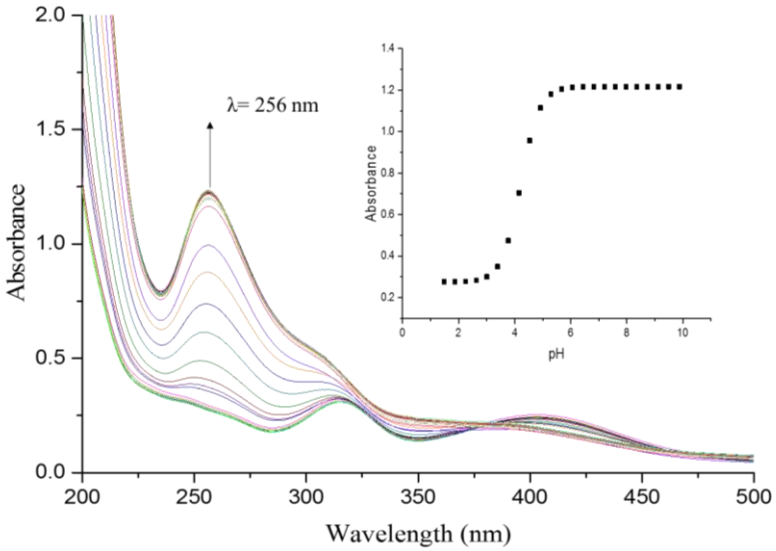

Figure SI 5.6: Ultraviolet-visible spectra of **Ru-1** complex recorded as a function of pH in the range 1–10 at 298 K. **Inset**: Plot of absorbance versus pH at λ = 256 nm

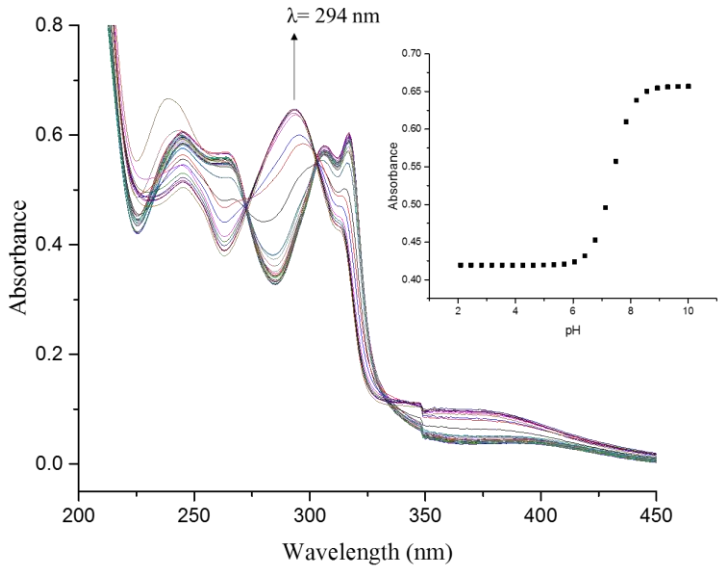

Figure SI 5.7: Ultraviolet-visible spectra of **Ru-2** complex recorded as a function of pH in the range 1–10 at 298 K. **Inset**: A plot of absorbance versus pH at λ = 294 nm

SI 5.8 Samples of MS, ^{1}H and ^{13}C NMR spectra for the studied complexes

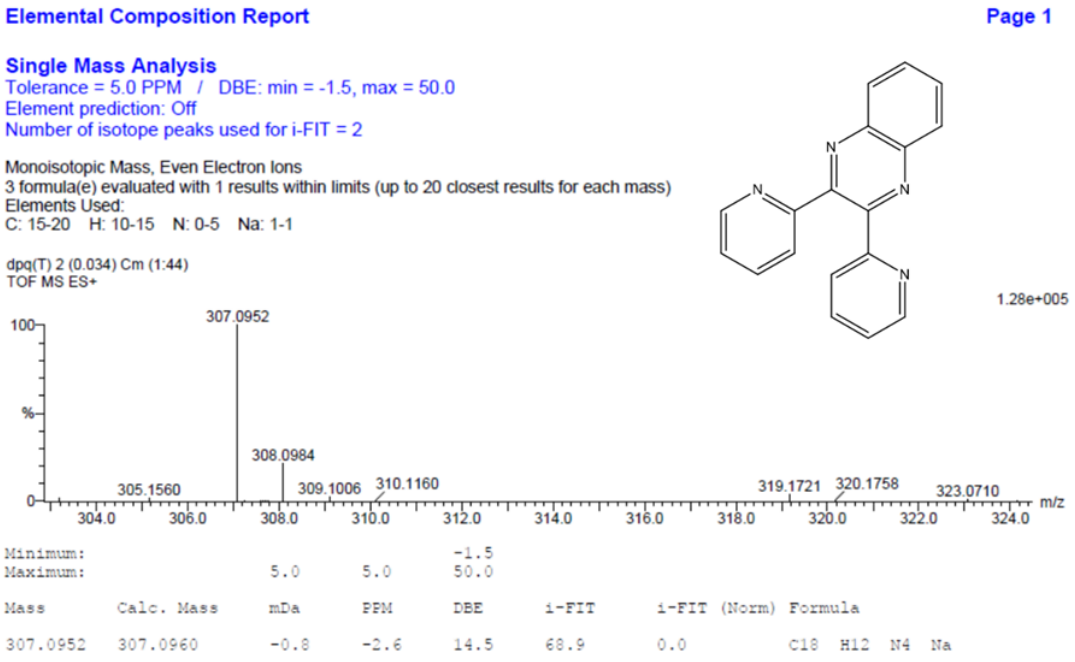

Figure SI 5.8: ESI-MS (TOF) spectrum of 2,3-bis(2'-pyridyl)-quinoxaline

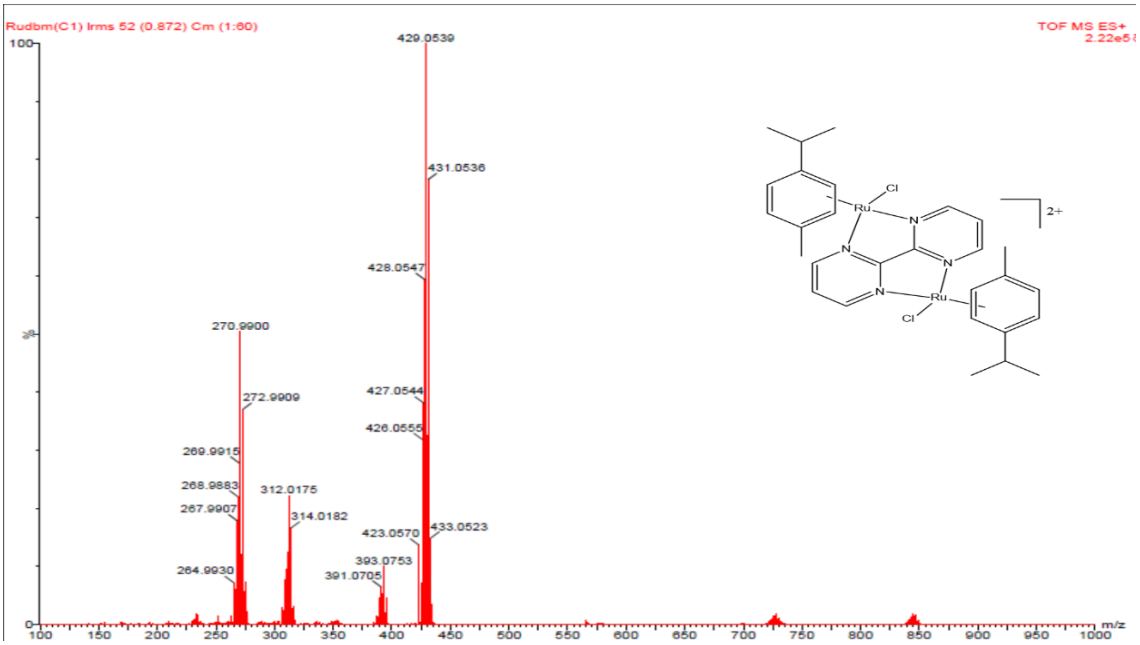

Figure SI 5.9: ESI-MS(TOF) spectrum of (μ_2-2,2'-bipyrimidyl)-dichloro-bis(η^6-*p*-cymene) diruthenium(II) hexaflourophosphate

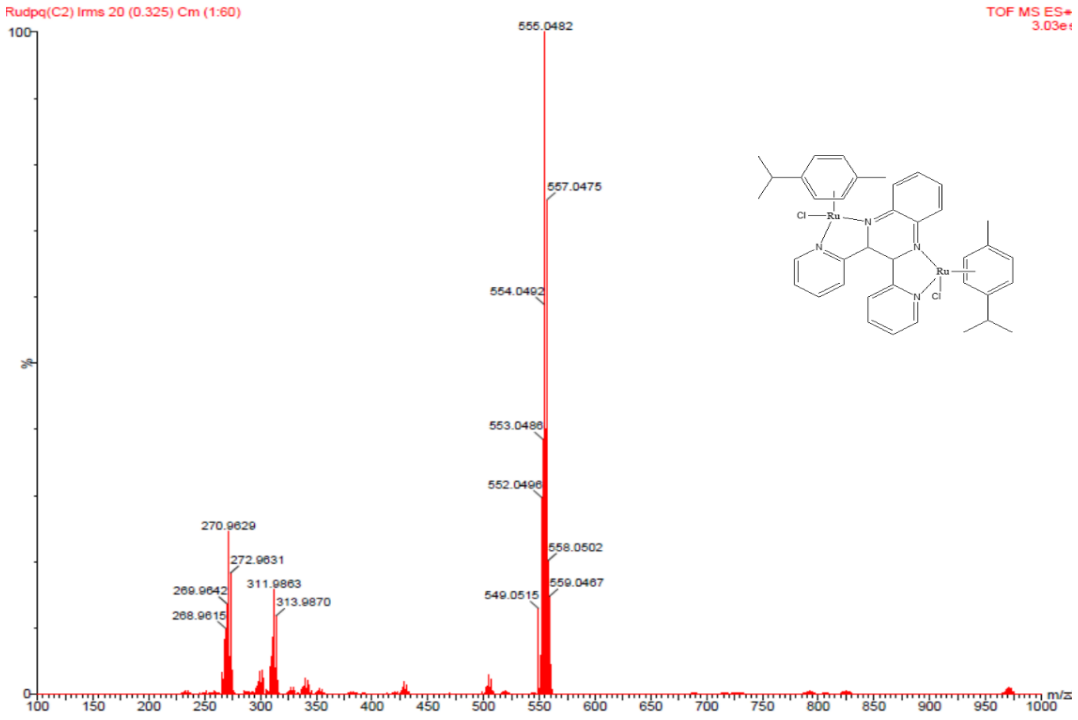

Figure SI 5.10: ESI-MS (TOF) spectrum of (μ_2-2,3-bis(2-pyridyl)quinoxaline)-dichloro-bis(*p*-cymene)diruthenium(II) hexafluorophosphate

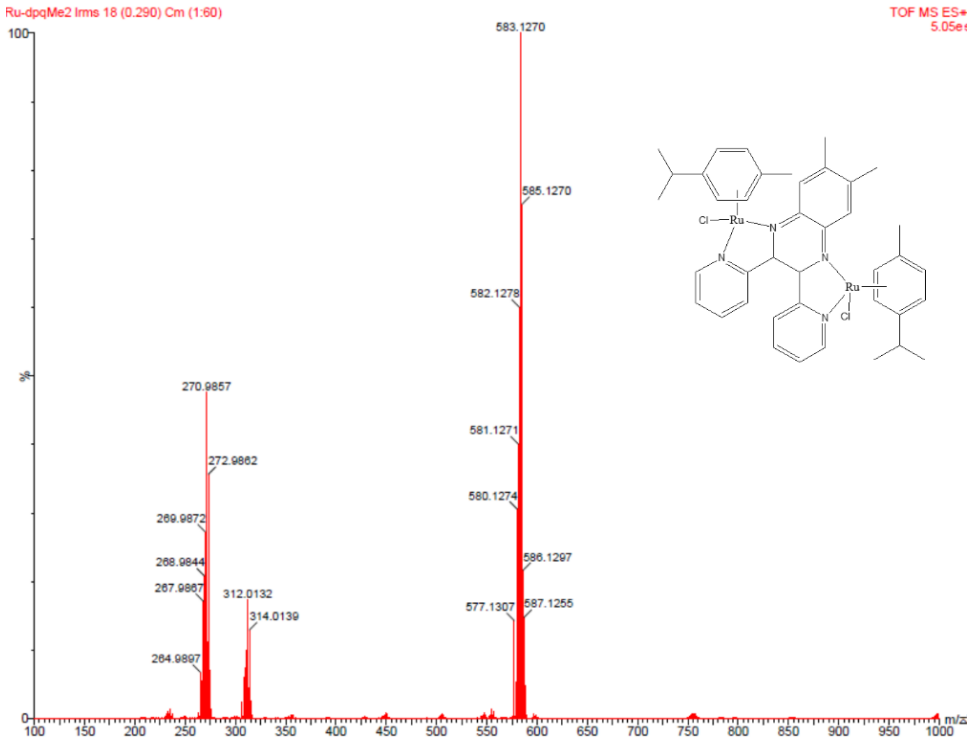

Figure SI 5.11: ESI-MS (TOF) spectrum of (μ_2-6,7-dimethyl-2,3-bis(2-pyridyl) quinoxaline)-dichloro-bis(*p*-cymene)diruthenium(II) hexaflourophosphate

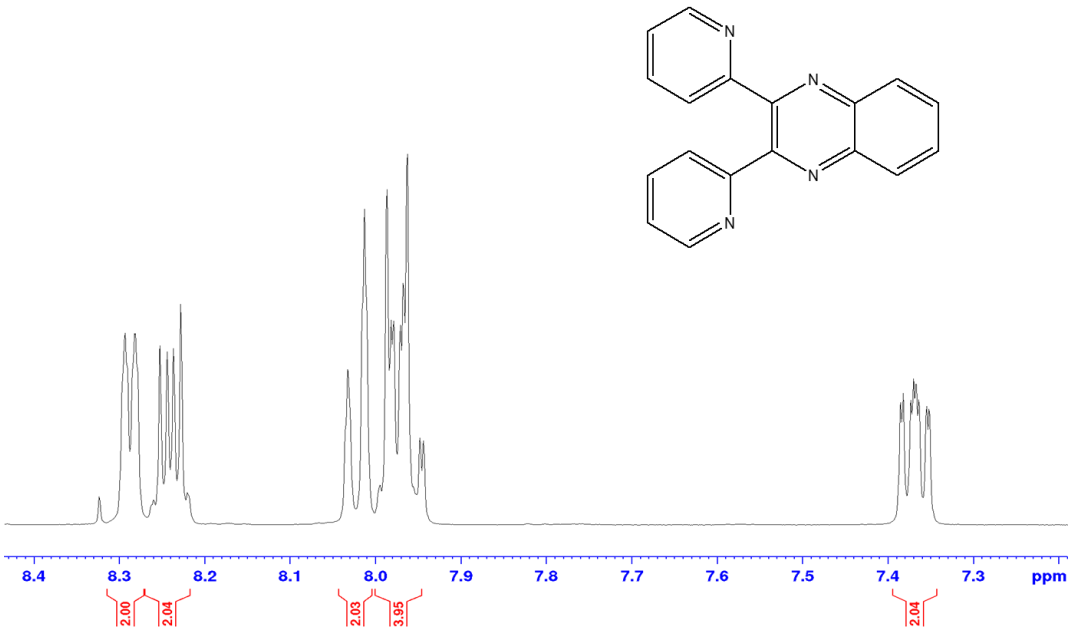

Figure SI 5.12: ^{1}H NMR (400 MHz, DMSO-d_6) spectrum of 2,3-bis(2'-pyridyl)-quinoxaline

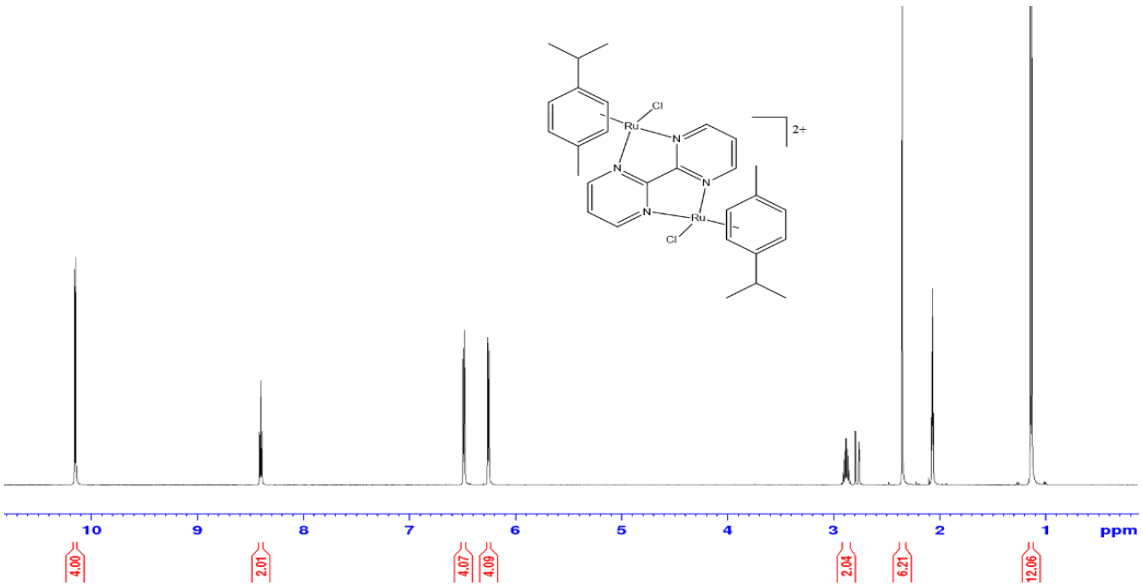

Figure SI 5.13: ^{1}H NMR (400 MHz, acetone-d_6) spectrum of (μ_2-2,2'-bipyrimidyl)-dichloro-bis(η^6-*p*-cymene)diruthenium(II) hexaflourophosphate

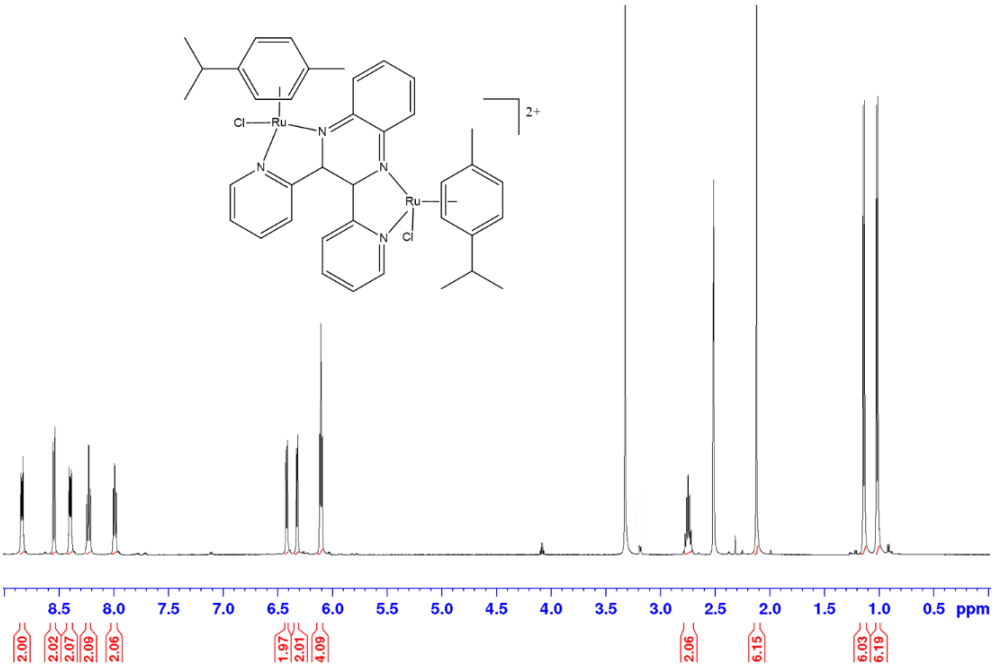

Figure SI 5.14: ^{1}H NMR (400 MHz, DMSO-d_6) spectrum of (μ_2-2,3-bis(2-pyridyl)quinoxaline)-dichloro-bis(*p*-cymene)diruthenium(II) hexafluorophosphate

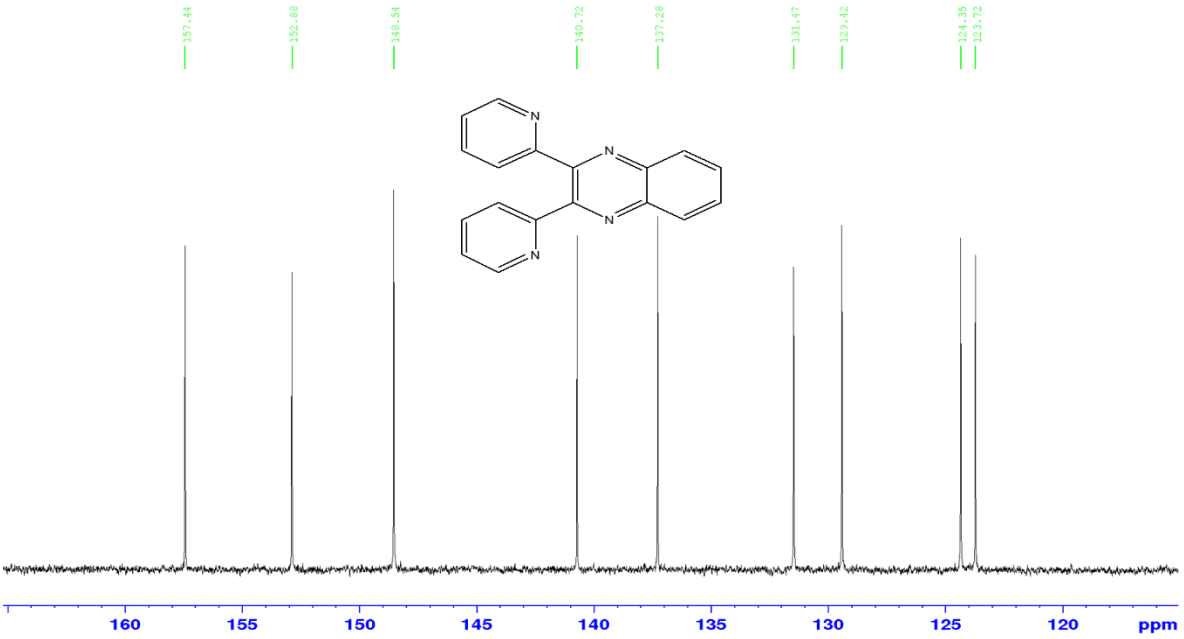

Figure SI 5.15: ^{13}C NMR (400 MHz, DMSO-d_6) spectrum of 2,3-bis(2'-pyridyl)-quinoxaline

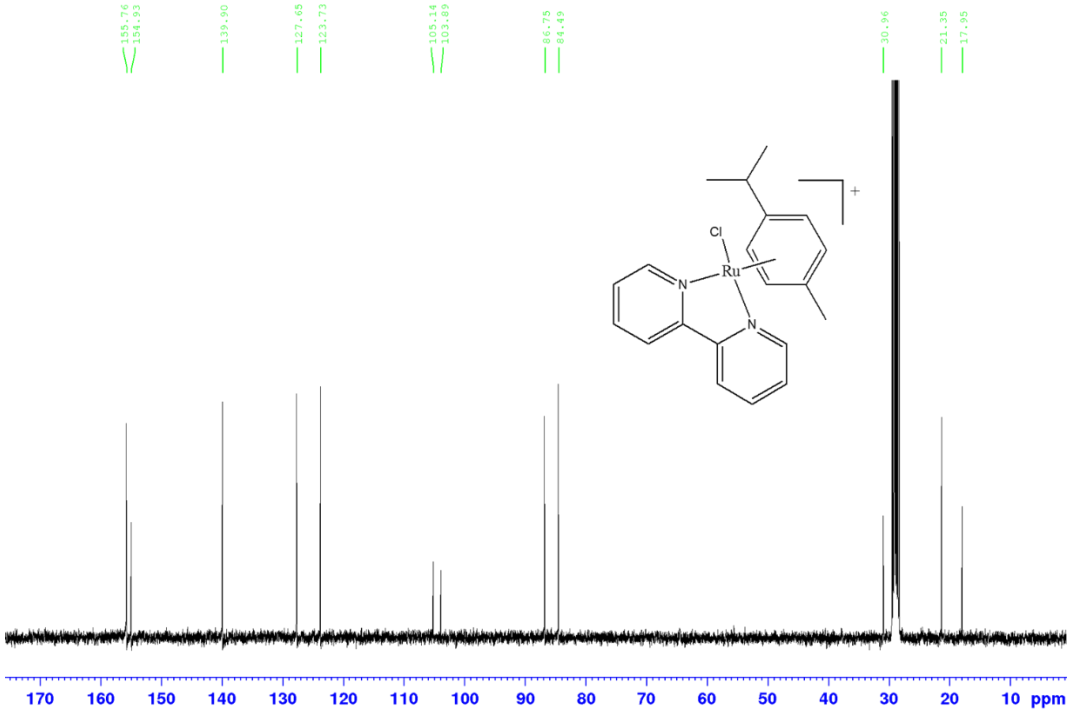

Figure SI 5.16: ^{13}C NMR (400 MHz, acetone-d_6) spectrum of (2,2'-bipyridine)-chloro(η^6-*p*-cymene)ruthenium(II) hexafluorophosphate

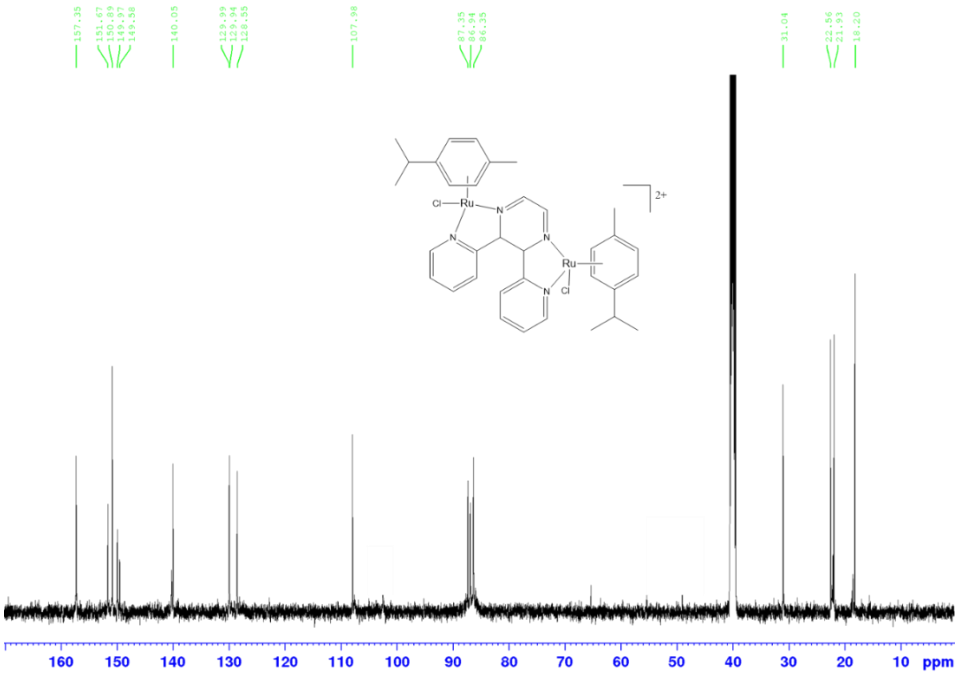

Figure SI 5.17: ^{13}C NMR (400 MHz, DMSO-d_6) spectrum of (μ_2-2,3-bis(2-pyridyl)-pyrazine)-dichloro-bis(*p*-cymene)diruthenium(II) tetrafluoroborate

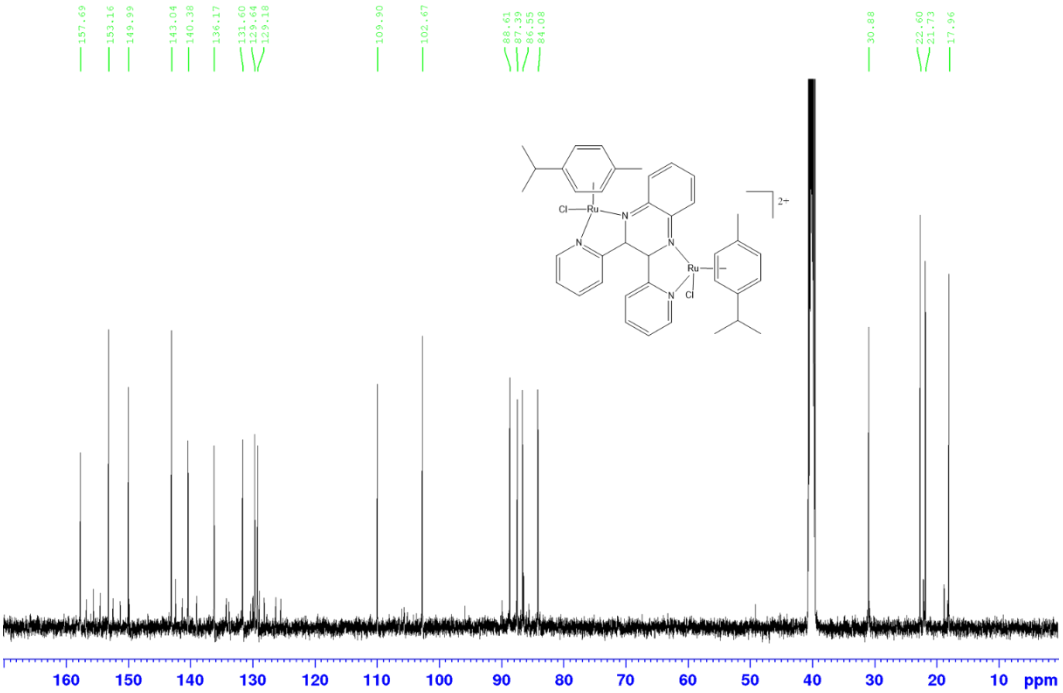

Figure SI 5.18: ^{13}C NMR (400 MHz, DMSO-d_6) spectrum of (μ_2-2,3-bis(2-pyridyl)quinoxaline)-dichloro-bis(*p*-cymene)diruthenium(II) hexafluorophosphate

CHAPTER SIX

Kinetic and Mechanistic Studies of η^6-*p*-Cymene Ruthenium (II) Complexes with α,α'-diimine Bridging Ligands

Abstract

Substitution kinetics of the aqua ligands in four binuclear ruthenium(II) *p*-cymene complexes with different α,α'-diimine bridging ligands [2-pyridyl aldazine (**Ru-1**), *p*-phenylene-bis(picoline)aldimine (**Ru-2**), *p*-biphenylene-bis(picoline) aldimine (**Ru-3**) and *p*-xylene-bis(picoline) aldimine (**Ru-4**)] was investigated as a function of nucleophile concentration and temperature under *pseudo*-first order conditions using thiourea nucleophiles of different steric demands. Ultraviolet-visible spectrophotometric technique was used to monitor the reactions. The simultaneous substitution of the aqua ligands in all the complexes obeyed the rate law, $k_{obs} = k_2$[Nucleophile]. The rates of substitution decreased in the order: **Ru-1** > **Ru-4** > **Ru-3** > **Ru-2**. The reactivity of the complexes is controlled by the inherent electronic and steric contributions of the bridging ligand. The strong π-acceptor bridging ligand is responsible for the high reactivity observed in **Ru-1** compared to the rest of the complexes. From **Ru-2** to **Ru-4**, the reactivity increases with decrease in steric congestion around the metal centres, which is positively correlated to the flexibility of the bridging ligand. The cage effect plays a role in the enhanced reactivity of **Ru-4** compared to **Ru-3** and **Ru-2.** DFT-calculated quantum chemical descriptors show that the HOMO-LUMO energy separation and chemical hardness increase from **Ru-1** to **Ru-4** with concomitant decrease in electrophilicity.

Similarly, the localized charge on the metal centres as shown by the NBO charges decrease from **Ru-1** to **Ru-4.** All the complexes showed stepwise deprotonation of the coordinated aqua ligands except **Ru-4** and the p*K*a values increased from **Ru-1** to **Ru-4** due to progressive increase in σ-donicity of the spacers. The calculated activation parameters ($\Delta H^{\neq} > 0$, $\Delta S^{\neq} < 0$) observed in all the complexes support an associative mechanism of activation.

6.1 Introduction

Medical interests in the utilization of *pseudo*-octahedral half-sandwich ruthenium(II) complexes as anticancer agents has vastly grown over the last three decades due to their amphiphilic nature brought about by the hydrophobic arene moiety and the hydrophilic metal centre.[1] The π-bonded arene ligand occupy three coordination sites; the remaining three sites offer diverse coordination modes that can be utilized for tailored anticancer agents.[1b]. The arene ligand facilitates the passive diffusion of the complex through the lipophilic cell membrane as well as stabilizing the metal centre at its +2 oxidation state.[2]

It is established that most of the active arene-based ruthenium(II) complexes contain a stable N,N-chelating ligand and a labile halide group.[3] These complexes have exhibited excellent cytotoxicity both *in vitro* and *in vivo* including activity in *cisplatin* resistant cells.[4] Their cytoxicity can be tuned by varying either the arene group or the size and electronic properties of the chelating ligand.[5] Studies have shown that increasing the π-surface area of the coordinated ligands enhance the cytotoxicity of the complexes.[6] However, changing the leaving group does not impact cytoxicity because the complexes are activated by aquation.[7] Importantly, it can also be tuned by increasing the number of metal centres which are linked together.[7-8]

Multinuclearity is an emerging approach in anticancer drug design to overcome chemo-resistance by recurring tumours.[8] Literature review show that binuclear ruthenium(II) complexes are more active than their mononuclear analogues because of synergistic effects.[9] The length of the linker between the two metal centres is found to have a positive correlation with cytoxicity of the complexes.[4b, 10] This is because lipophilicity and cellular uptake of the complexes increase with increase in the length of the spacer.[4b, 5, 10a] Therefore, the bridging ligand modulate the biological

and pharmacological properties of these complexes as well as provide steric protection to metal centres against biological non-target molecules.[11]

Extensive studies investigating the effect of the bridging ligand on substitution kinetics of square-planar platinum(II) complexes has been reported.[12] It is established that the effect of the linker on reactivity is entirely depended on the intrinsic properties therein. These include; the net σ-inductive effect of the linker, magnitude of the steric hindrance introduced by the linker, the rigidity/flexibility of the linker, [12a, 12b] the length of the linker,[12c-e] the head group that coordinates the metal centres and the symmetry of the complexes.[12b, 13] Due to synergistic or antagonistic factors, the role of a bridging ligand on the reactivity of transition metal complexes is specific to the chemistry of the complex and the bridging ligand. In addition, there is hardly as much literature about the structure-reactivity relationship on binuclear ruthenium(II) arene complexes.

In the blood stream, anticancer metallodrugs remain as chloro complexes because of the high concentration of chloride ions (about 100 Mm) therein, but once they enter the cell, where the concentration of chloride ions is low (about 3-20 mM) they undergo aquation. The activated aqua species interact with DNA as well as other biomolecules including S-donor groups that have high affinity for metal centres. These non-target molecules offer kinetic and thermodynamics competition to DNA binding and thus affecting the distribution and efficacy of the metallodrug.[14]

This study was undertaken to understand the role of non-aliphatic bridging ligands on the reactivity of ruthenium(II) *p*-cymene complexes. To achieve this, four complexes with α,α'-diimine bridging ligands; *viz*. 2-pyridyl aldazine (PAA) (**Ru-1**), *p*-phenylenebis(picoline)aldimine (PBP) (**Ru-2**), *p*-biphenylenebis(picoline)aldimine (BBP) (**Ru-3**) and *p*-xylene-bis(picoline)aldimine (XBP) (**Ru-4**) (Figure 6.1) were synthesized and characterized. Because of their biological importance, high solubility and nucleophilicity, neutral thiourea nucleophiles of

varying steric demands were used.[15] These are; thiourea (Tu), 1,3-dimethylthiourea (Dmtu) and *1,1,3,3*-tetramethylthiourea (Tmtu). Tu combines the properties of thioether and thiolate and has been used as a protection agent to minimize nephrotoxicity induced by *cisplatin* treatment.[14b] Likewise, Dmtu has been used in cytoprotection of liver and kidney against mitochondrial damage caused by *cisplatin*.[16]

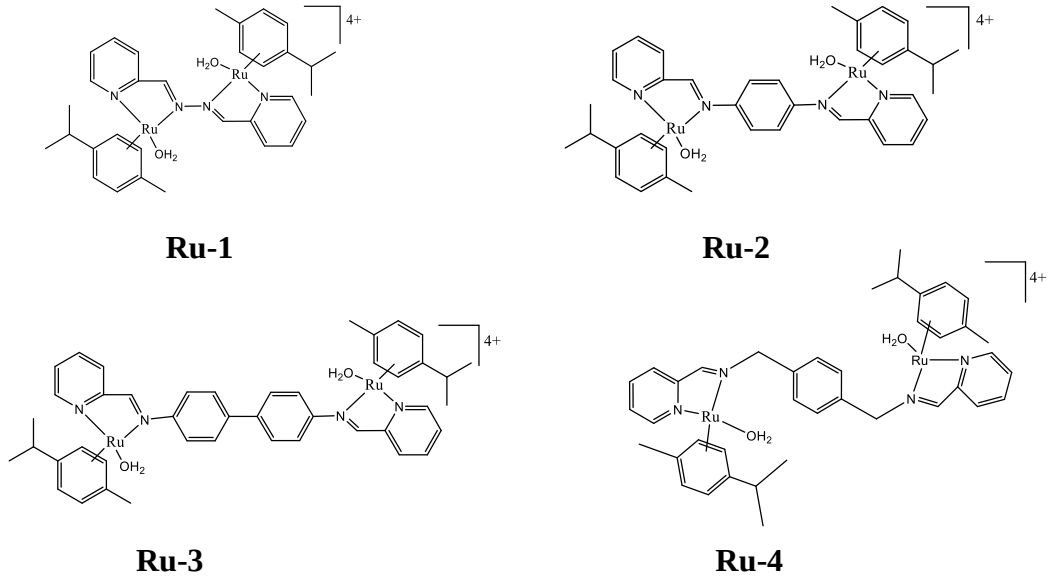

Figure 6.1: Structures of the investigated ruthenium(II) complexes (ClO_4^{2-} counter ions omitted for clarity)

Computational studies were performed using Gaussian 09W program package to assist in understanding and interpreting the experimental results obtained. Results from this study sheds light on the interactions between potential anticancer metallodrugs and deactivating molecules in biological systems.

6.2 Experimental

6.2.1 Materials and Procedures

All the syntheses were performed under dinitrogen atmosphere using standard Schlenk techniques. Benzidine (≥ 98%), 2-pyridinecarbaldehyde (99%), hydrazine hydrate solution (80% in H_2O), *p*-phenylenediamine (≥ 99%), *p*-xylenediamine (99%), dichloro(*p*-cymene)ruthenium(II) dimer (97%), $NaBF_4$ (98%), anhydrous $AgClO_4$ (97%), $NaClO_4.H_2O$ (98%), $HClO_4$ (70 wt % solution), celite (® 545), pH standard reference solutions (4.0, 7.0 and 10.0), Tu (≥ 99%), Dmtu (99%) and Tmtu (98%) were supplied by Sigma-Aldrich. Organic solvents were purchased from Merck (Pty) and used without further purification. Ultrapure deionized water from Modulab system was used in the relevant reactions. The ligands and complexes were synthesized according to published literature methods.[17]

6.2.2 Synthesis of Ligands

PAA: 30 mL of ethanolic solution containing 0.99 mL of hydrazine hydrate solution was added drop-wise to 3.55 mL of 2-pyridinecarbaldehyde in 10 mL of ethanol. As the exothermic reaction ensued, fine yellow needle-like crystalline solids appeared. The product was filtered off and recrystallized from ethanol. Yield: 2.86 g (84%). *Anal*. *Calc*. for $C_{12}H_{10}N_4$; C, 68.56; H, 4.79; N, 26.65. *Found*: C, 68.52; H, 4.89; N, 26.44. ^{1}H NMR (400 MHz, benzene-d_6): δ (ppm) = 9.11 (s, 2H), 8.55 (d, 2H), 8.21 (d, 2H), 7.10 (t, 2H), 6.69 (t, 2H). ^{13}C (400 MHz, benzene-d_6): δ (ppm) = 162.5, 153.7, 149.7, 135.7, 124.5, 121.4. ESI-MS (TOF) (*m/z*): 233.08 (M + Na).

PBP: 2-pyridinecarbaldehyde (1.323 mL) was added dropwise to a stirring ethanolic solution of *p*-phenylenediamine (0.85 g) maintained at 60℃. The mixture was refluxed for 2 h and the resulting red solution cooled to 0℃. The yellow precipitate which formed was filtered off and recrystallized from ethanol. Yield: 2.02 g (90%). *Anal*. *Calc*. for $C_{18}H_{14}N_4$; C, 75.50; H, 4.93; N,

19.57. *Found*: C, 75.40; H, 5.07; N, 19.34. ^{1}H NMR (400 MHz, DMSO-d_6): δ (ppm) = 8.75 (d, 2H), 8.68 (s, 2H), 8.19 (d, 2H), 7.97 (t, 2H), 7.54 (t, 2H), 7.47 (s, 4H). ^{13}C (400 MHz, DMSO-d_6): δ (ppm) = 160.4, 154.1, 149.7, 149.0, 137.1, 125.6, 122.3, 121.3. ESI-MS (TOF) (*m/z*): 309.11 (M + Na).

BBP: 2-pyridinecarbaldehyde (0.66 mL) was added drop by drop to a stirring ethanolic solution of benzidine (0.72 g) maintained at 60℃. The mixture was refluxed for 2 h and the resulting solution cooled to ambient temperature. The yellow crystalline solid formed was filtered off and recrystallized from ethanol. Yield: 1.18 mg (83%). *Anal*. *Calc*. for $C_{24}H_{18}N_4$; C, 79.54; H, 5.01; N, 15.46. *Found*: C, 79.48; H, 5.12; N, 15.31. ^{1}H NMR (400 MHz, benzene-d_6): δ (ppm) = 8.98 (s, 2H), 8.63 (d, 2H), 8.43 (d, 2H), 7.52 (t, 4H), 7.37 (d, 4H), 7.20 (t, 2H), 6.76 (t, 2H). ^{13}C (400 MHz, benzene-d_6): δ (ppm) = 160.8, 155.5, 150.5, 149.6, 139.1, 135.9, 124.6, 121.9, 121.2. ESI-MS (TOF) (*m/z*): 385.14 (M + Na).

XBP: 2-pyridinecarbaldehyde (1.06 mL) was added drop by drop to a stirring ethanolic solution of *p*-xylenediamine (0.86 g) maintained at 65℃. The mixture was refluxed for 3 h and the resulting solution cooled to 0 °C. The off-white precipitate formed was filtered off and recrystallized from ethanol. Yield: 1.62 g (82%). *Anal*. *Calc*. for $C_{20}H_{18}N_4$; C, 76.41; H, 5.77; N, 17.82. *Found*: C, 76.39; H, 5.51; N, 17.65. ^{1}H NMR (400 MHz, chloroform-*d*): δ (ppm) = 8.67(d, 2H), 8.51 (s, 2H), 8.08 (d, 2H), 7.74 (t, 2H), 7.34 (m, 6H), 4.90 (d, 4H). ^{13}C (400 MHz, Toluene-d_8) δ (ppm) = 162.7, 155.4, 149.1, 138.0, 135.5, 124.0, 120.6, 64.4. ESI-MS (TOF) (*m/z*): 337.14 (M + Na).

6.2.3 Synthesis of the complexes

A suspension of 1.00 mmol of dichloro(*p*-cymene)ruthenium(II) dimer in 30 mL of methanol was treated with 1.00 mmol of the ligand (PAA, PBP, BBP and XBP) and allowed to stir at room temperature for 4 h. The solution was filtered through celite to remove unreacted materials. 10 mL

of a saturated methanolic solution of $NaBF_4$ was then added to the filtrate. The resulting solution was kept in the refrigerator for slow crystallization to take place. After a couple of days, the crystalline solids formed were filtered off, washed with methanol, diethyl ether and dried under vacuum. The product was purified by recrystallization from dichloromethane/petroleum ether (40-60 V/V) solvent system.

(μ$_2$-PAA)-dichloro-*bis*(η^6-*p*-cymene)diruthenium(II) tetraflouroborate: Orange microcrystalline solid. Yield: (702 mg, 76%). *Anal*. *Calc*. for $B_2C_{32}Cl_2F_8H_{38}N_4Ru_2$; C, 41.54; H, 4.14; N, 6.05. *Found*: C, 41.16; H, 4.12; N, 5.97. ^{1}H NMR (500 MHz, DMSO-d_6): δ (ppm) = 9.71 (d, 2H), 9.37 (s, 2H), 8.67 (m, 2H), 8.48 (td, 2H), 8.06 (td, 2H), 6.50 (d, 2H), 6.23 (br, 4H), 6.09 (br, 2H), 2.80 (m, 2H), 2.31 (s, 6H), 1.12 (m, 12H). ^{13}C NMR (500 MHz, DMSO-d_6): δ (ppm) = 167.6, 157.0, 152.11, 140.8, 133.2, 130.9, 108.5, 87.5, 85.7, 83.8, 31.2, 22.9, 18.9. ESI-MS (TOF) (*m/z*): 481.07 (M^+)

(μ$_2$-PBP)-dichloro-*bis*(η^6-*p*-cymene)diruthenium(II) tetraflouroborate: Dark red crystalline solid. Yield: (689 mg, 69%). *Anal*. *Calc*. for $B_2C_{38}Cl_2F_8H_{42}N_4Ru_2$; C, 45.58; H, 4.23; N, 5.59. *Found*: C, 45.82; H, 4.33; N, 5.50. ^{1}H NMR (500 MHz, DMSO-d_6): δ (ppm) = 9.64 (d, 2H), 9.04 (d, 2H), 8.38 (t, 4H), 8.08 (d, 4H), 7.95-7.93 (m, 2H), 6.19 (t, 2H), 5.87-5.84 (m, 2H), 5.77-5.71 (m, 4H), 2.61 (hept, 2H), 2.23 (d, 6H), 1.06 (m, 12H). ^{13}C NMR (500 MHz, DMSO-d_6): δ (ppm) = 169.2, 156.6, 154.9, 152.8, 131.1, 129.7, 124.4, 106.0, 104.4, 87.1, 85.7, 31.0, 22.3, 18.9. ESI-MS (TOF) (*m/z*): 557.10 (M^+).

(μ$_2$-BBP)-dichloro-*bis*(η^6-*p*-cymene)diruthenium(II) tetrafluoroborate: Brown red solid. Yield: (641 mg, 59%) *Anal*. *Calc*. for $B_2C_{44}Cl_2F_8H_{46}N_4Ru_2$; C, 49.05; H, 4.30; N, 5.20. *Found*: C, 48.71; H, 4.34; N, 5.01. ^{1}H NMR (500 MHz, DMSO-d_6): δ (ppm) = 9.62 (d, 2H), 9.02 (s, 2H), 8.36-8.32 (m, 4H), 8.14 (dd, 4H), 8.00 (d, 4H), 7.94 (t, 2H), 6.15 (d, 2H), 5.83 (d, 2H), 5.74 (d,

2H), 5.66 (d, 2H), 2.60 (m, 2H), 2.22(s, 6H), 1.05 (d, 12H). ^{13}C NMR (500 MHz, DMSO-d_6): δ (ppm) = 168.3, 156.5, 155.0, 151.9, 140.5, 130.7, 129.5, 128.3, 123.9, 105.7, 104.0, 87.1, 86.5, 85.6, 31.0, 22.3, 18.8. ESI-MS (TOF) (*m/z*): 633.14 (M^+)

(μ$_2$-XBP)-dichloro-*bis*(η^6-*p*-cymene)diruthenium(II) tetrafluoroborate: Orange solid. Yield: (846 mg, 82%) *Anal*. *Calc*. for $B_2C_{40}Cl_2F_8H_{46}N_4Ru_2$; C, 46.67; H, 4.50; N, 5.44. *Found*: C, 46.36; H, 4.78; N, 5.38. ^{1}H NMR (500 MHz, DMSO-d_6): δ (ppm) = 9.54 (d, 2H), 8.55 (s, 2H), 8.26 (t, 2H), 8.17 (d, 2H), 7.83 (t, 2H), 7.59 (s, 4H), 6.25 (d, 2H), 6.13 (d, 2H), 5.93-5.88 (m, 4H), 5.75 (d, 2H), 5.56 (d, 2H), 2.61 (m, 2H), 2.11 (s, 6H), 1.02 (d, 6H), 0.94 (d, 6H). ^{13}C NMR (500 MHz, DMSO-d_6): δ (ppm) = 167.9, 156.4, 154.8, 140.2, 135.2, 131.0, 129.7, 128.8, 105.0, 103.9, 87.9, 84.5, 68.9, 30.9, 22.6, 21.9, 18.8. ESI-MS (TOF) (*m/z*): 585.14 (M^+).

6.2.4 Physical Measurements and Instrumentation

Bruker Avance DPX III 400/500 MHz spectrometer fitted with 5 mm probe was used to record ^{1}H and ^{13}C NMR spectra of the ligands and complexes at 30℃. All the chemical shifts were expressed in parts per million (ppm) and referenced to trimethylsilane. Electrospray ionization (ESI^+) mass spectra were recorded on a Time of Flight (TOF) Micromass spectrometer. Sample NMR and MS spectra obtained are presented in the Supplementary Information (Figure SI 6.13-6.24). Elemental analyses of C, H, and N of the samples were done using Thermo Scientific Flash 2000 analyzer. Agilent technologies Cary 100 Series ultraviolet-visible spectrophotometer equipped with a temperature control unit (accuracy of ± 0.05℃) was used for p*K*a titrations and kinetic studies. Jenway 4330 combined pH and conductivity meter with a 4.5 mm diameter microelectrode was used to determine the pH of the aqueous complexes. Before use, the electrode was calibrated with pH 4.0, 7.0 and 10.0 reference solutions. OriginPro 9.1® program was used to analyze the acid-base titration data and the kinetic data obtained.[18]

6.2.5 Aquation of the Complexes

Aqua species of the complexes were prepared by reacting a known amount of the chloro complexes with 1.99 equivalents of $AgClO_4$ in 0.01 M $HClO_4$. In all the reactions, the mixtures were stirred in the dark at 50 ℃ for 48 h. The solutions were thereafter cooled to ambient temperature, allowed to stand for at least 3 h and the grey AgCl precipitate filtered off using 0.45 μm nylon membrane.[19] The filtrates were diluted appropriately for p*K*a titrations and kinetic studies.

6.2.6 Determination of p*K*a of the Aqua Complexes

Spectrophotometric acid-base titration of the aqua complexes with NaOH was done from pH 2 to 12 at 25 ℃. Large complex volumes (about 500 mL) were used to avoid dilution effects and absorbance corrections.[20] From pH 2-3, small grains of crushed NaOH pellets were added stepwise while from 4 to 10/12, NaOH solution of decreasing concentration was added dropwise using a pasteur pipette. The titrations were done in such a way that many evenly distributed points were obtained. After each base addition, the complex solution was stirred for about 2 min prior to pH measurement and respective spectrum acquisition. For the pH measurements, about 0.6 mL aliquots in glass ampules were used and discarded to avoid contamination of the stock complex solution with chloride ions from the electrode while the aliquots used for absorbance measurements were returned back to the stock solution. A confirmatory reverse pH titration was done using $HClO_4$ solutions in place of NaOH.

6.2.7 Kinetic Measurements

Nucleophile solutions of known concentration maintained at pH 2.0 and 0.1 M $HClO_4/NaClO_4$ ionic strength were prepared shortly before use. Likewise, the complex solutions were maintained at similar pH and ionic strength. The concentration of the aqua complexes used were; **Ru-1** (0.248 mM), **Ru-2** (0.660 mM), **Ru-3** (0.144 mM), **Ru-4** (0.171 mM). Substitution reactions were

performed under *pseudo*-first order conditions in which the nucleophilic concentration was at least 20 folds higher than the concentration of the metal complex to drive the reactions to completion. The reactions were initiated by mixing equal volumes of thermally equilibrated complex and nucleophile in a tandem cuvette. The ultraviolet-visible spectral changes resulting from the reactions were recorded from 800 to 200 nm wavelength range. Concentration dependence studies were performed at a constant temperature of 25℃. On the other hand, temperature dependence of reaction rates was studied from 25 to 45℃ at an interval of 5℃. For each reaction, at least three independent runs were performed.

6.2.8 Computational Modelling

Computational calculations were performed using density functional theory (DFT) method implemented by Gaussian 09W suite of programs.[21] The structures were optimized using the hybrid Becke, 3-parameter, Lee-yang-Parr (B3LYP) at the standard Los Alamos National Laboratory 2 double ζ (LANL2DZ) basis set.[22] DFT utilizes electron density over wave-function in the determination of a system's properties. Therefore, it is applicable in these complexes with large number of electrons since electron densities are always three dimensional irrespective of the number of electrons involved.[23] LANL2DZ exploits relativistic effective core potentials (ECP) to effectively account for the inner core 28 electrons ([Ar]$3d^{10}$) in ruthenium.[24] The systems were fully optimized in aqua media using conductor-like polarizable continuum (CPCM) solvent model[25] at singlet spin ground state and an overall charge of +4.

Quantum chemical descriptors; chemical hardness (η), chemical softness (σ) and global electrophilicity indices (ω) for the complexes were calculated as described in literature.[26] Due to its high reliability Hirshfeld Population Analysis was used to determine the atomic charges in the complexes.[27]

6.3 Results

6.3.1 Acid-Base Equilibria of the Aqua Complexes

p*K*a values of the complexes were determined by fitting Boltzmann sigmoid function on the plot of absorbance versus pH at a selected wavelength. Typical ultraviolet-visible spectra obtained for the titration of **Ru-1** with NaOH is presented in Figure 6.2. The inset shows a plot of absorbance as a function of pH at λ = 290 nm. The p*K*a values obtained are collected in Table 6.1. Additional plots are presented in the Supplementary Information (Figure SI 6.5- 6.6)

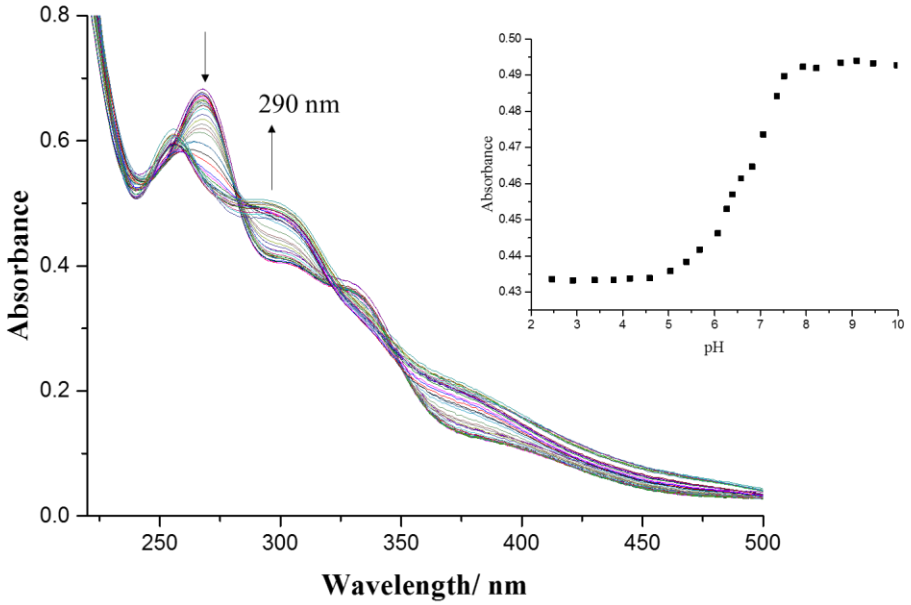

Figure 6.2: Ultraviolet-visible spectra of **Ru-1** recorded as a function of pH (2–10) at 298 K. **Inset**: A plot of absorbance versus pH at λ = 290 nm

Table 6.1: Summary of p*K*a values obtained for the deprotonation of the aqua ligands

Complex	Ru-1	Ru-2	Ru-3	Ru-4
p*K*a$_1$	6.32 ± 0.12	6.76 ± 0.03	6.85 ± 0.01	6.97 ± 0.02
p*K*a$_2$	7.23 ± 0.04	8.98 ± 0.03	10.71 ± 0.04	-

Complexes **Ru-1** to **Ru-3**, displayed a stepwise deprotonation of the aqua ligands recording a positive relationship between the p*K*a values and the length of the linker. As the separation distance increases, the charge addition between the two metal centres decreases, thus decreasing the electrophilicity of the complexes and acidity of the coordinated aqua ligands.[12b, 28] For instance; the short Ru-Ru intermetallic distance in **Ru-1** enables effective electronic communication between the two metal centres leading to an overall high acidity of the bound aqua ligands. The pK_{a_2} values obtained are at least 0.9 p*K*a units more basic than pK_{a_1}. This is because after the deprotonation of the first aqua ligand, the overall charge of the complex reduces from +4 to +3 making the second metal center less electrophilic hence diminishing the tendency for another deprotonation to occur.[12a, 12e, 29]

A single p*K*a value was observed in complex **Ru-4** signaling simultaneous deprotonation of the coordinated aqua ligands. The XBP bridging ligand in **Ru-4** is unconjugated beyond the α,α'-diimines, this causes weak interactions between the metal centres making them act independently.[12b, 17a]. The one p*K*a value obtained for **Ru-4** is supported by electrochemical reduction of a complex utilizing this ligand which showed a single broad two-electron reduction wave.[17a] Compared to the pK_{a_1} values of other complexes, the high value obtained in **Ru-4** is attributed to the methylene groups which lower the localized charge on the metal centres through inductive σ-donation.[30] As a result the basicity of the coordinated aqua ligands is enhanced.

From the acidity constants, all the complexes exist exclusively as aqua species at a pH of 2.0. Considering this, all the kinetic studies were performed at pH 2.0.

6.3.2 Computational Results

Computational modelling was carried out to gain an insight on the spatial arrangement of the ligand systems as well as electronic properties of the complexes studied. Geometry optimized structures of the complexes and their respective frontier orbitals are shown in Figure 6.3 while key computational parameters obtained are documented in Table 6.2. Figure 6.4 shows typical numbering of the nitrogen atoms in the complexes.

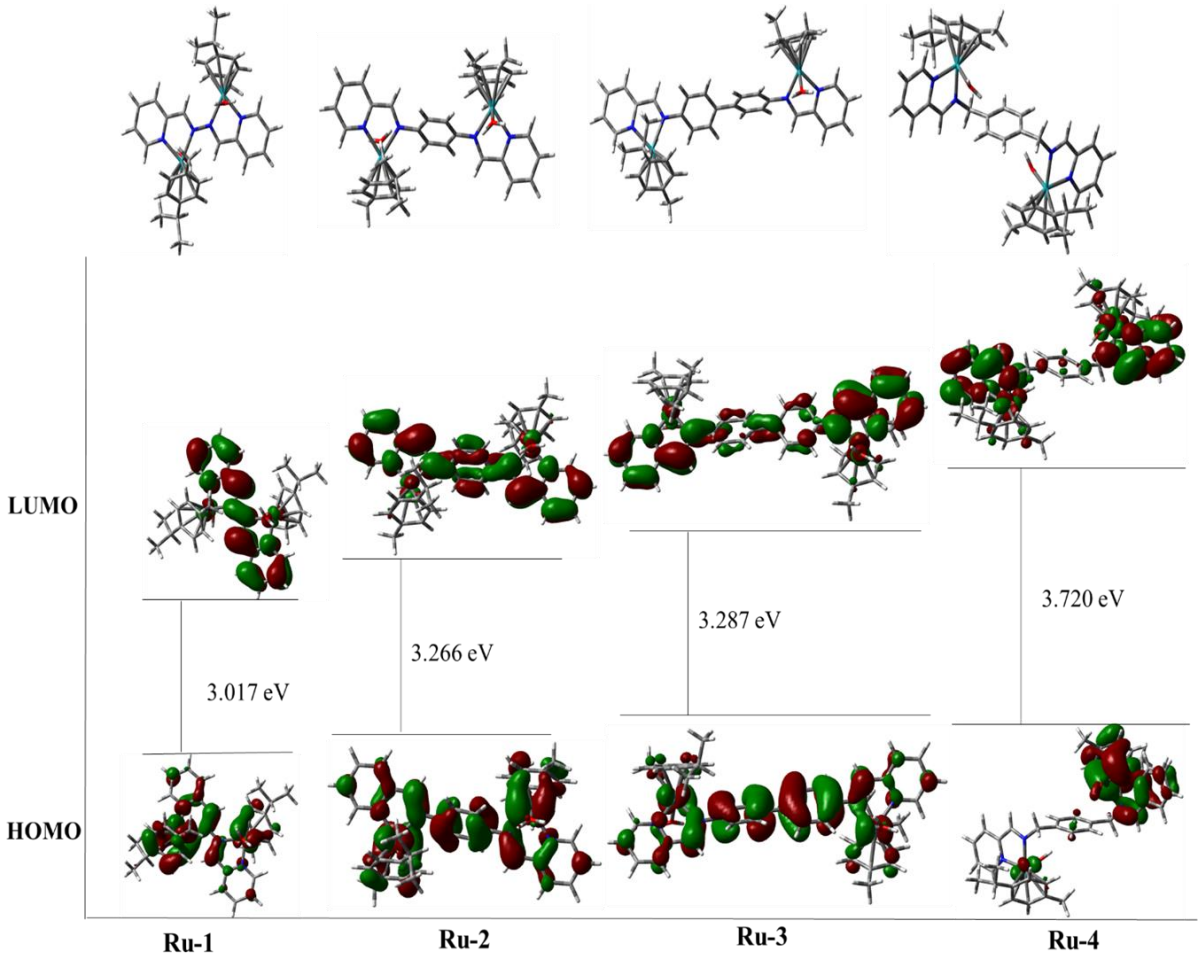

Figure 6.3: Geometry optimized structures, frontier orbitals and their respective energy gaps for the studied complexes

From the mappings of the frontier orbitals, it is observed that the HOMO in **Ru-1** is largely based on the metal centres and arene ligands. In **Ru-2** and **Ru-3**, it is spread throughout the complex with the phenyl and biphenyl spacers making substantial contributions. In **Ru-4**, the HOMO is largely concentrated on one of the two Ru-α,α'-diimine moieties and the proximate arene group. On the other hand, the LUMO is largely based on the bridging ligand with the α,α'-diimine moieties making significant contributions in **Ru-3** and **Ru-4**.

Table 6.2: Selected computational data for the optimized complexes

Complex	**Ru-1**	**Ru-2**	**Ru-3**	**Ru-4**
HOMO-LUMO energies / eV				
HOMO	-7.335	-7.038	-6.885	-7.129
LUMO	-4.318	-3.772	-3.598	-3.409
$\Delta E_{HOMO-LUMO}$	3.017	3.266	3.287	3.720
Chemical hardness (η) / eV	1.509	1.633	1.644	1.860
Chemical softness (σ) / eV^{-1}	0.663	0.612	0.608	0.538
Electrophilicity index (ω) / eV	11.252	8.945	8.358	7.463
Hirshfeld charge (Ru)	0.128	0.121	0.117	0.109
Bond Length / Å				
Ru-N2	2.146	2.090	2.088	2.083
Ru-N1	2.076	2.077	2.077	2.078
Ru-OH_2	2.148	2.152	2.154	2.157
Ru-Ru	5.314	8.783	12.873	
Diimine moiety planes separation / Å	-	0.446	-	5.473
Dihedral angle of diimine moiety planes /º	5.33	-	33.08	-

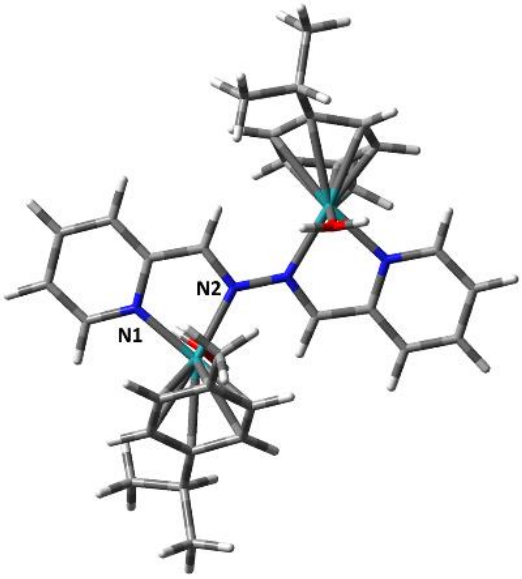

Figure 6.4: DFT-optimized structure showing numbering of the nitrogen atoms in the complexes

The planarity of the minimum energy structures obtained, shows that the two 9-atomic Ru-α,α'-diimine moieties are non-planar to one another. In complexes **Ru-1** and **Ru-3** the two moieties are tilted away from each other at a dihedral angle of 5.33º and 33.08º, respectively. The two planes in **Ru-2** and **Ru-4** are parallel to one another with a separation distance of 0.446 and 5.473 Å, respectively. Figures showing these angles and separation distances are presented in the Supplementary Information (Figure SI 6.7-6.10). The bridging ligand in **Ru-4** form two V-shaped curvatures of average θ = 112.18º as shown in Figure 6.5. This is attributed to the presence of methylene groups which enhances the flexibility of the bridging ligand.

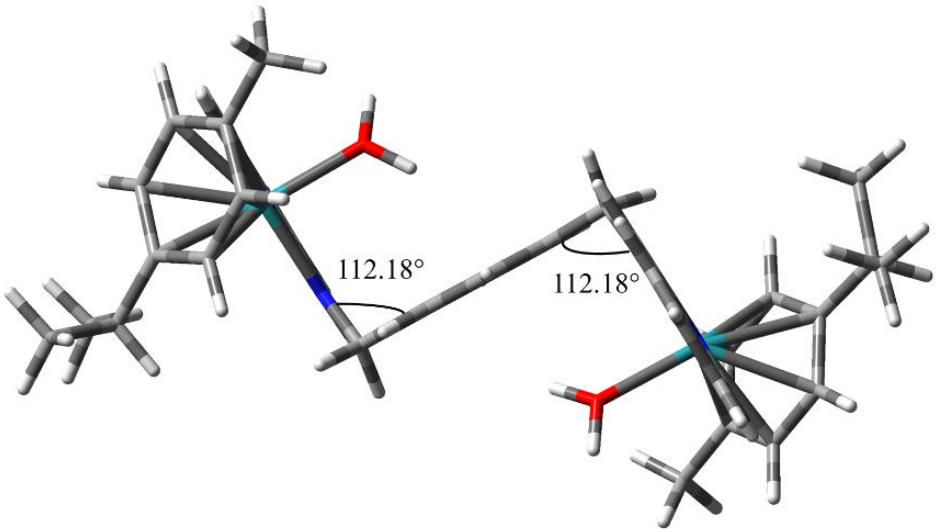

Figure 6.5: Geometry optimized structure of **Ru-4** showing the V-shaped curvatures

As revealed by the modelled structures, the phenyl ring(s) in **Ru-2** and **Ru-3** are twisted away from the mean plane of bridging ligand at an angle of 46.26º and 47.01º, respectively. In addition, the two phenyl rings in **Ru-3** are twisted in opposite direction to one another at an angle of 30.27º (Figures SI 6.11-6.12, Supplementary Information). This is attributed to steric interactions between the proximate hydrogen atoms.[31] The Ru-N1 bond length is invariant across the complexes denoting that the spacer does not affect electronic distribution in the pyridyl moieties of the complexes. On the contrary, the linker influences the Ru-N2 and Ru-OH_2 bond lengths. The shortening of Ru-N2 and elongation of Ru-OH_2 bond from **Ru-1** to **Ru-4**, shows progressive increase in the σ-donor ability of the spacers.[12b]

Inspection of the quantum chemical descriptors documented in Table 6.2, show that the LUMO energy shifts proportionately to more positive values as the linker is varied from PAA to XBP. Similarly, from **Ru-1** to **Ru-4** the HOMO-LUMO gap increase with concomitant decrease in the electrophilicity index of the complexes and localized charge on the ruthenium atoms as given by the Hirshfeld charges. The increase in chemical hardness/decrease in chemical softness as one

moves from **Ru-1** to **Ru-4**, point out to increase in the stability of the complexes as the bridging ligand is varied from PAA to XBP.[32]

6.3.3 Kinetic Results

The rate of displacement of the coordinated aqua ligands in the four complexes were investigated using thiourea based nucleophiles of varied steric demands under *pseudo*-first order conditions. The substitution reactions were monitored spectrophotometrically by following change in absorbance of the spectra at a selected wavelength as a function of time. Typical spectra obtained for the reaction of **Ru-4** with Dmtu is shown Figure 6.6.

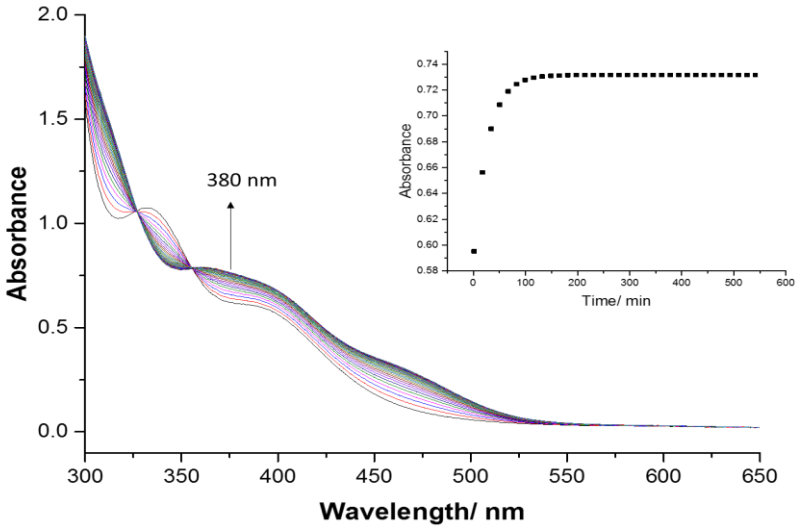

Figure 6.6: Ultraviolet-visible spectra for the reaction of **Ru-4** (0.171 mM) with Dmtu (34.2 mM) at 298 K, pH = 2.0, *I* = 0.1 M $HClO_4/NaClO_4$. **Inset**: A kinetic trace obtained at λ = 380 nm

Then kinetic traces taken at the suitable wavelength were fitted into a single exponential decay standard function to generate *pseudo*-first order rate constants (k_{obs}) using equation (i).[33]

$$A_t = A_o + (A_o - A_\infty)\exp(-k_{obs}t) \quad \text{(i)}$$

where; A_o = absorbance at the initiation of the reaction, A_t = absorbance at time t, and A_∞ = absorbance at the end of the reaction.

The k_{obs} values obtained were plotted against nucleophile concentrations. A linear dependence of k_{obs} on the nucleophile concentration was exhibited by all the reactions of the complexes. The intercept of all the plots was zero, indicating the absence of reverse or solvolysis reaction. A collection of k_{obs} values and respective nucleophile concentrations are presented in the Supplementary Information (Tables SI 6.1-6.4). Typical plots of k_{obs} versus nucleophile concentration obtained for **Ru-1** is shown in Figure 6.7. Additional plots are presented in the Supplementary Information (Figures SI 6.1-6.2). The second order rate constant (k_2) for the reactions was obtained from the slopes of the plots. The values obtained are tabulated in Table 6.3. All the concentration dependent substitution reactions can be described by the equation (ii).

$$k_{obs} = k_2[\text{Nucleophile}] \qquad \text{(ii)}$$

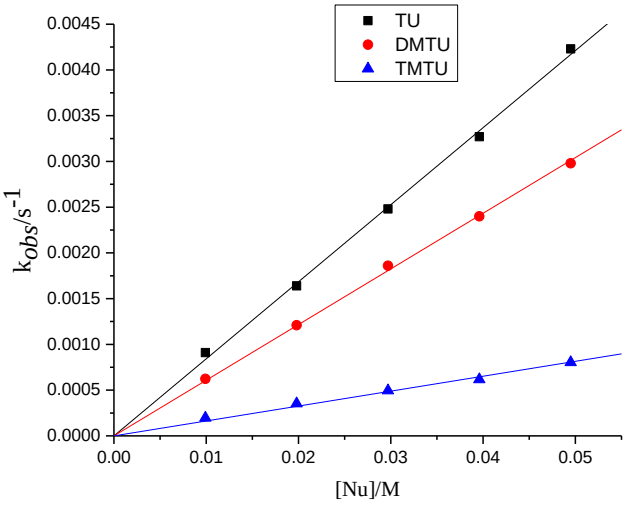

Figure 6.7: Dependence of *pseudo*-first order rate constant (k_{obs}) on the concentration of thiourea nucleophiles for the substitution of the aqua ligands in **Ru-1** at 298 K, pH = 2.0, I = 0.1 M $HClO_4/NaClO_4$

To determine the thermodynamic parameters of the substitution process, the reaction temperature was varied systematically from 25 ℃ to 45 ℃ at an interval of 5 ℃ and the respective temperature dependent k_2 calculated. The ln $\left(\frac{k_2}{T}\right)$ values obtained were plotted as a function of $\frac{1}{T}$. Activation enthalpy ($\Delta H^{\neq}$) and entropy ($\Delta S^{\neq}$) were calculated from the slope and the y-intercept, respectively using the Eyring equation (iii).[33]

$$\ln\left(\frac{k_2}{T}\right) = -\frac{\Delta H^{\neq}}{R}.\frac{1}{T} + \left(23.78 + \frac{\Delta S^{\neq}}{R}\right) \quad \text{(iii)}$$

Typical Eyring plots obtained for **Ru-4** are shown in Figure 6.8 and the values of $\Delta H^{\neq}$ and $\Delta S^{\neq}$ obtained are given in Table 6.3. Additional Eyring plots and values of ln $\left(\frac{k_2}{T}\right)$ and respective $\frac{1}{T}$ are presented in the Supplementary Information (Figures SI 6.3-6.4 and Tables SI 6.5-6.8).

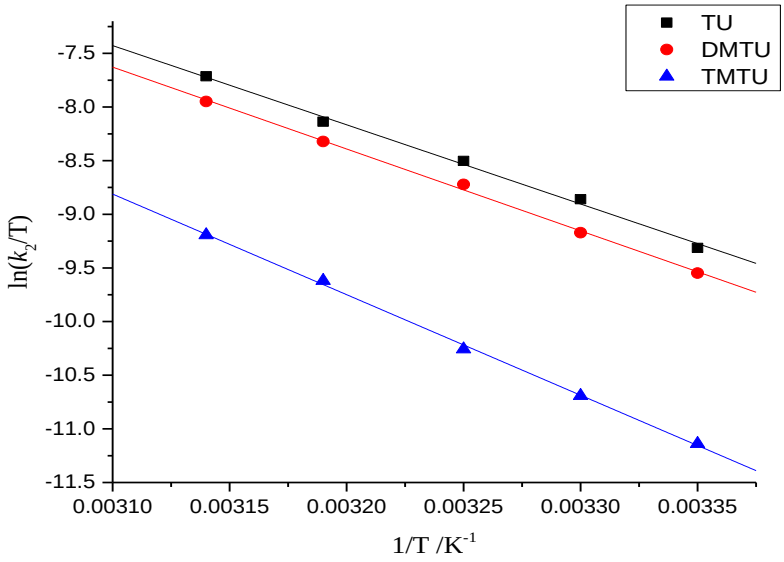

Figure 6.8: Eyring plots for the reaction of **Ru-4** with thiourea nucleophiles in the range 25 - 45 ℃, pH = 2.0, I = 0.1 M $HClO_4/NaClO_4$

Table 6.3: Summary of second order rate constants (k_2) and activation parameters

Complex	Nu	k_2 /10^{-3} M^{-1} s^{-1}	$\Delta H^{\neq}$ /kJmol^{-1}	$\Delta S^{\neq}$ /Jmol^{-1}K^{-1}
Ru-1	**Tu**	84.22 ± 0.83	59 ± 2	-68 ± 7
	Dmtu	60.83 ± 0.45	57 ± 1	-77 ± 4
	Tmtu	16.30 ± 0.38	64 ± 1	-65 ± 4
Ru-2	**Tu**	2.20 ± 0.03	60 ± 2	-95 ± 5
	Dmtu	2.89 ± 0.04	59 ± 2	-97 ± 5
	Tmtu	1.21 ± 0.01	66 ± 2	-78 ± 5
Ru-3	**Tu**	4.99 ± 0.03	62 ± 2	-80 ± 5
	Dmtu	5.41 ± 0.05	66 ± 1	-68 ± 4
	Tmtu	1.72 ± 0.03	70 ± 2	-62 ± 5
Ru-4	**Tu**	26.40 ± 0.12	59 ± 2	-69 ± 8
	Dmtu	21.95 ± 0.15	63 ± 2	-64 ± 5
	Tmtu	4.21 ± 0.04	78 ± 2	-29 ± 5

6.4 Discussion

In this study the effect of α,α'-diimine-based bridging ligands on the reactivity of low-spin d^6 binuclear ruthenium(II) *p*-cymene complexes was investigated. The bridging ligand bind the metal centres forming two 5-membered stable chelate rings. The electron donating aliphatic substituents on the *p*-cymene ligand fortifies the Ru-*p*-cymene bonds, making the *p*-cymene ligand unfavourable to substitution.[34] In all the complexes, a single substitution step was observed indicating that the two coordinated aqua ligands were simultaneously displaced by the thiourea nucleophiles. With Tu as the entering group, the k_2 values decreased in the order; **Ru-1** (0.084 $M^{-1}s^{-1}$) > **Ru-4** (0.026 $M^{-1}s^{-1}$) > **Ru-3** (0.005 $M^{-1}s^{-1}$) > **Ru-2** (0.002 $M^{-1}s^{-1}$). Similarly, the other two nucleophiles followed the same trend. The differences in reactivity observed is attributed to stereo-electronic properties brought about by the coordinated bridging ligand.

A comparison of reactivity reference to **Ru-1** show that this complex is at least 3 times more reactive than the other complexes which is attributable mainly to its strong π-acceptor 2-pyridyl aldazine bridging ligand.[17a, 35] This is evident from the computational results which show that the frontier molecular orbitals are well stabilized and the energy gap between them is narrower compared to the rest of the systems. Therefore, **Ru-1** is more electrophilic due to effective π-back-donation from the dπ orbitals largely based on metal ion to the stabilized π* orbital of the bridging ligand.[20] Moreover, the short Ru-Ru intermetallic distance (5.314 Å**)** in **Ru-1** promotes effective electronic communication between the metal centres, thus strengthening the π-back-bonding effects through enhanced electron density delocalization.[35] The metal centres are thus deprived of electron density making them more positively charged as shown by a large Hirshfeld charge of 0.128. This makes them more attractive for facile nucleophilic attack. The low p*K*a values in **Ru-1** documented in table 6.1 corroborate this argument.

When spacers; phenyl (**Ru-2**), biphenyl (**Ru-3**) and xylyl (**Ru-4**) are placed between α,α'-diimine moieties, the complexes become progressively less electrophilic because of destabilization of the LUMO orbitals with concomitant widening of the HOMO-LUMO energy gap.[36] This reduces the ability of the bridging ligand to withdraw electrons from the metal centres as indicated by diminution of the local charges on the metal centres from **Ru-1** to **Ru-4**. As shown by the modelled structures, the bridging ligands in **Ru-2**, **Ru-3** and **Ru-4** are distorted. For instance; the phenyl ring(s) in **Ru-2** and **Ru-3** are twisted out of the mean plane of the bridging ligand at a dihedral angle of 46.26º and 47.01º, respectively. These distortions further compromises the π-acceptor abilities of the bridging ligands hence reducing the electrophilicity of the complexes.[37]

The observed differences in quantum chemical descriptors as the linker is varied is validated by preceding studies utilizing these ligands.[17a, 38] Characteristic metal to ligand charge transfer

($t_2g \rightarrow \pi^*$) bands show a hypsochromic shift as the bridging ligand is changed from PAA to XBP. This signals an increase in the HOMO-LUMO gap and therefore the energy required to effect electronic promotion increases accordingly. Likewise, the anodic reduction potentials of related complexes show a consistent shift to more negative values as the ligand is varied from PAA to XBP as result of the destabilization of the π* LUMO orbital. Therefore, the electron withdrawing ability of the ligands decreases from PAA to XBP.

This would lead the reactivity to decrease from **Ru-2** to **Ru-4.** However, the opposite trend was observed and this is due to a progressive decrease in steric hindrance in the vicinity of the metal centres as the bridging ligand is varied from PBP to XBP.[12a, 39] A change of the bridge from **Ru-2** to **Ru-4** restricts the metal centres of the latter complexes to geometric orientations that reduce the steric congestion around the metal centres. This is demonstrated by the variance in the non-planarity topography of two Ru-α,α'-diimine moieties for the complexes. The metal centres in **Ru-2** are the most sterically hindered by the bridging ligand and the arene groups because of the relatively short Ru-Ru intermetallic distance (8.783 Å) and the limited ability to rotate as shown by the minute inter-plane distance (0.446 Å) between the planes of the Ru-α,α'-diimine moiety. [17c] As the spacer is changed from phenyl (**Ru-2**) to biphenyl (**Ru-3**), the distance between the metal centres increases to 12.873 Å and the flexibility of the bridging ligand slightly increases.[40] This causes the two Ru-α,α'-diimine moieties to tilt away from each other at dihedral angle of 33.08º. As a result, the steric hindrance around the metal centres is alleviated, making the metal centres more exposed for nucleophilic attack.

When compared to **Ru-2** and **Ru-3**, incoming nucleophiles experience less steric hindrance in attacking the metal centres in **Ru-1.** This is because of the absence of a spacer between the azine nitrogen atoms in **Ru-1** unlike in **Ru-2** and **Ru-3.** Importantly, **Ru-1** has a rotational freedom

around the N-N single bond that further alleviates possible steric hindrance, while in **Ru-2** and **Ru-3** such possibility is minimal due to increased rigidity of the bridging ligands therein.[17c]

In **Ru-4** due to the high flexibility of the bridging ligand, the metal centres are aligned along two parallel vectors resulting in a large separation distance (5.473 Å) between the planes of the Ru-α,α'-diimine moieties. This significantly reduces the steric shielding around the metal centres making them more accessible for nucleophilic attack.

Furthermore, its optimized structure (Figure 6.5) suggest a solvent assisted entrapment of the incoming nucleophiles through the cage effect at its proximate V-shaped cavities.[41] The entrapped molecules promote effective collisions with the metal centres thereby enhancing the reactivity of the complex. The cage effect has been reported to enhance the reactivity of dinuclear platinum complexes.[12a, 12b]

A look at the Ru-OH_2 bond lengths show an increasing trend as the Hirshfeld charges on the metal centre decrease from **Ru-1** to **Ru-4**.This due to progressive increase in electron density at the metal centres through inductive donation from the spacers.[28] Therefore, the *trans*-influence of the xylyl spacer as depicted by the elongated Ru-OH_2 bond and the markedly low atomic charge on the ruthenium centres in **Ru-4** makes the substitution of the aqua ligands in **Ru-4** easier compared to **Ru-3** and **Ru-2**.[12a, 28]

Further, the trend of reactivity for these binuclear complexes is in agreement with those reported from other studies which have shown that increase in steric hinderance caused by the chelating ligand decrease the reactivity of arene ruthenium(II) complexes.[2b, 42]

It is expected that, the reactivity of the three nucleophiles should follow the trend Tu > Dmtu > Tmtu due to increasing bulkiness of the nucleophiles. However, in **Ru-2** and **Ru-3**, the more

sterically hindered Dmtu reacts faster that Tu. This is due to inductive effect brought about by the two methyl substituents in Dmtu which donate electron density to the sulfur atom increasing the basicity of the nucleophile.[20, 43] Despite the metal centres in **Ru-2** and **Ru-3** being more sterically hindered, the high basicity of Dmtu enable it to overcome steric shielding. In Tmtu, the four methyl substituents retards its approach towards the metal centres causing transition state destabilization leading to high activation enthalpy which slows down the reactivity.[44]

The negative value of $\Delta S^{\neq}$ and the low positive values of $\Delta H^{\neq}$ suggest an associative mechanism of activation.[33] The negative activation entropy also imply a more ordered transition state compared to the starting conditions and the final products.[45] An associative mechanism of activation has been reported in other arene-based ruthenium(II) complexes.[2b, 46]

6.5 Conclusions

The present study has demonstrated that the reactivity of binuclear ruthenium(II) *p*-cymene complexes with α,α'-diimine bridging ligands is controlled by the inherent steric and electronic factors associated with the bridging ligand. The high reactivity in **Ru-1** compared to the other complexes is ascribed to the strong π-acceptor properties of 2-pyridyl aldazine bridging ligand which enhances the electrophilicity of the complex, hence making the metal centres more attractive for facile nucleophilic attack. The other complexes have electron donor spacers between the azine nitrogen atoms of their bridging ligands which compromise their π-acceptor properties, thus lowering their electrophilicity. This is supported by the computational results which indicate that the HOMO-LUMO gap and chemical hardness are least in **Ru-1** and increase progressively from **Ru-2** to **Ru-4.** Furthermore, the coordinated aqua ligands in **Ru-1** are the most acidic as indicated by the low p*K*a values. Therefore, the metal centres in **Ru-1** are more attractive for nucleophilic attack than in the other complexes. In complexes **Ru-2, Ru-3** and **Ru-4,** the reactivity is inversely

correlated to the steric hindrance in the vicinity of the metal centres. Increased flexibility of the ligand reduces steric congestion around the metal centre hence increasing the reactivity of the complexes. In **Ru-4**, the presence of the two V-shaped curvatures proximate to the metal centres facilitate entrapment of the incoming nucleophile through the cage effect leading to more effective collisions with the metal centres. The reactions proceed through an associative mechanism.

6.6 References

[1] (a) L. Dale, J. Tocher, T. Dyson, D. Edwards, D. Tocher, *Anti-Cancer Drug Design* **1992**, *7*, 3-14; (b) P. J. Dyson, *Chimia International Journal for Chemistry* **2007**, *61*, 698-703.

[2] (a) Y. K. Yan, M. Melchart, A. Habtemariam, P. J. Sadler, *Chemical Communications* **2005**, 4764-4776; (b) L. Dadci, H. Elias, U. Frey, A. Hoernig, U. Koelle, A. E. Merbach, H. Paulus, J. S. Schneider, *Inorganic Chemistry* **1995**, *34*, 306-315.

[3] R. E. Morris, R. E. Aird, P. del Socorro Murdoch, H. Chen, J. Cummings, N. D. Hughes, S. Parsons, A. Parkin, G. Boyd, D. I. Jodrell, *Journal of Medicinal Chemistry* **2001**, *44*, 3616-3621.

[4] (a) M. Melchart, P. J. Sadler, *Bioorganometallics: Biomolecules, Labeling, Medicine* **2006**, 39-64; (b) M.-G. Mendoza-Ferri, C. G. Hartinger, R. E. Eichinger, N. Stolyarova, K. Severin, M. A. Jakupec, A. A. Nazarov, B. K. Keppler, *Organometallics* **2008**, *27*, 2405-2407.

[5] S. Schäfer, I. Ott, R. Gust, W. S. Sheldrick, *European Journal of Inorganic Chemistry* **2007**, *2007*, 3034-3046.

[6] R. Aird, J. Cummings, A. Ritchie, M. Muir, R. Morris, H. Chen, P. Sadler, D. Jodrell, *British Journal of Cancer* **2002**, *86*, 1652-1657.

[7] M. G. Mendoza-Ferri, C. G. Hartinger, A. A. Nazarov, R. E. Eichinger, M. A. Jakupec, K. Severin, B. K. Keppler, *Organometallics* **2009**, *28*, 6260-6265.

[8] C. G Hartinger, A. D Phillips, A. A Nazarov, *Current Topics in Medicinal Chemistry* **2011**, *11*, 2688-2702.

[9] H. Chen, J. A. Parkinson, O. Nováková, J. Bella, F. Wang, A. Dawson, R. Gould, S. Parsons, V. Brabec, P. J. Sadler, *Proceedings of the National Academy of Sciences* **2003**, *100*, 14623-14628.

[10] (a) A. Romerosa, T. Campos-Malpartida, C. Lidrissi, M. Saoud, M. Serrano-Ruiz, M. Peruzzini, J. A. Garrido-Cárdenas, F. García-Maroto, *Inorganic Chemistry* **2006**, *45*, 1289-1298; (b) M. Auzias, B. Therrien, G. Süss-Fink, P. Štěpnička, W. H. Ang, P. J. Dyson, *Inorganic Chemistry* **2008**, *47*, 578-583; (c) L. K. Batchelor, E. Păunescu, M. n. Soudani, R. Scopelliti, P. J. Dyson, *Inorganic Chemistry* **2017**, *56*, 9617-9633.

[11] S. D. Brown, K. D. Trotter, O. B. Sutcliffe, J. A. Plumb, B. Waddell, N. E. Briggs, N. J. Wheate, *Dalton Transactions* **2012**, *41*, 11330-11339.

[12] (a) A. Mambanda, D. Jaganyi, *Dalton Transactions* **2012**, *41*, 908-920; (b) A. Mambanda, D. Jaganyi, S. Hochreuther, R. van Eldik, *Dalton Transactions* **2010**, *39*, 3595-3608; (c) H. Ertürk, A. Hofmann, R. Puchta, R. van Eldik, *Dalton Transactions* **2007**, 2295-2301; (d) P. A. Wangoli, G. Kinunda, *New Journal of Chemistry* **2018**, *42*, 214-227; (e) T. Soldatović, S. Jovanović, Ž. D. Bugarčić, R. van Eldik, *Dalton Transactions* **2012**, *41*, 876-884.

[13] A. Shaira, D. Jaganyi, *Journal of Coordination Chemistry* **2015**, *68*, 3013-3031.

[14] (a) J. Reedijk, *Proceedings of the National Academy of Sciences* **2003**, *100*, 3611-3616; (b) J. Reedijk, *Chemical Reviews* **1999**, *99*, 2499-2510; (c) F. Wang, H. Chen, J. A. Parkinson, P. d. S. Murdoch, P. J. Sadler, *Inorganic Chemistry* **2002**, *41*, 4509-4523; (d) P. Pil, *Encyclopedia of Cancer* **1997**, *1*, 391-410.

[15] W. C. Schiessl, N. K. Summa, C. F. Weber, S. Gubo, C. Dücker-Benfer, R. Puchta, N. J. van Eikema Hommes, R. van Eldik, *Zeitschrift für Anorganische und Allgemeine Chemie* **2005**, *631*, 2812-2819.

[16] (a) N. A. G. dos Santos, N. M. Martins, C. Curti, M. d. L. P. Bianchi, A. C. dos Santos, *Chemico-Biological Interactions* **2007**, *170*, 177-186; (b) N. Santos, C. C. Bezerra, N. Martins, C. Curti, M. Bianchi, A. Santos, *Cancer Chemotherapy and Pharmacology* **2008**, *61*, 145-155.

[17] (a)M.-A. Haga, K. Koizumi, *Inorganica Chimica Acta* **1985**, *104*, 47-50; (b) D. A. Edwards, G. M. Hoskins, M. F. Mahon, K. C. Malloy, G. R. Rudolph, *Polyhedron* **1998**, *17*, 2321-2326; (c) A. Singh, M. Chandra, A. N. Sahay, D. S. Pandey, K. K. Pandey, S. M. Mobin, M. C. Puerta, P. Valerga, *Journal of Organometallic Chemistry* **2004**, *689*, 1821-1834.

[18] OriginPro9.1, OriginLab Corporation, One Roundhouse Plaza,Suite 303, Northampton, MA 01060, United States, *2014 1800-969-7720. www.OriginLab.com.*

[19] Ž. D. Bugarčić, B. V. Petrović, R. Jelić, *Transition Metal Chemistry* **2001**, *26*, 668-671.

[20] A. Hofmann, D. Jaganyi, O. Q. Munro, G. Liehr, R. van Eldik, *Inorganic Chemistry* **2003**, *42*, 1688-1700.

[21] M. Frisc, G. Trucks, H. Schlegel, G. Scuseria, M. Robb, J. Cheeseman, G. Scalmani, V. Barone, B. Mennucci, G. Petersson, *Gaussian Inc, Wallingford* **2010**.

[22] J. Li, L.-C. Xu, J.-C. Chen, K.-C. Zheng, L.-N. Ji, *The Journal of Physical Chemistry A* **2006**, *110*, 8174-8180.

[23] V. Gupta, *Principles and Applications of Quantum Chemistry*, Elsevier Inc., London, UK, **2015**, pp. 156-175.

[24] M. Okamura, M. Yoshida, R. Kuga, K. Sakai, M. Kondo, S. Masaoka, *Dalton Transactions* **2012**, *41*, 13081-13089.

[25] M. Cossi, G. Scalmani, N. Rega, V. Barone, *The Journal of Chemical Physics* **2002**, *117*, 43-54.

[26] (a) R. G. Parr, L. v. Szentpaly, S. Liu, *Journal of the American Chemical Society* **1999**, *121*, 1922-1924; (b) R. G. Pearson, *Inorganica Chimica Acta* **1992**, *198*, 781-786; (c) I. M. Wekesa, D. Jaganyi, *Dalton Transactions* **2014**, *43*, 2549-2558; (d) R. G. Pearson, *Journal of Molecular Structure: THEOCHEM* **1992**, *255*, 261-270.

[27] (a) F. L. Hirshfeld, *Theoretical Chemistry Accounts: Theory, Computation, and Modeling (Theoretica Chimica Acta)* **1977**, *44*, 129-138; (b) E. R. Davidson, S. Chakravorty, *Theoretical Chemistry Accounts: Theory, Computation, and Modeling (Theoretica Chimica Acta)* **1992**, *83*, 319-330.

[28] H. Ertürk, R. Puchta, R. van Eldik, *European Journal of Inorganic Chemistry* **2009**, *2009*, 1331-1338.

[29] A. Hofmann, R. van Eldik, *Dalton Transactions* **2003**, 2979-2985.

[30] S. Hochreuther, R. Puchta, R. van Eldik, *Inorganic chemistry* **2011**, *50*, 8984-8996.

[31] A. Streitwieser, C. H. Heathcock, E. M. Kosower, P. J. Corfield, *Introduction to Organic Chemistry, Vol. 643*, Macmillan New York, New York, **1992**.

[32] C. A. Mebi, *Journal of Chemical Sciences* **2011**, *123*, 727-731.

[33] J. D. Atwood, *Inorganic and Organometallic Reaction Mechanisms*, 2nd edition ed., VCH Publishers, **1997**, pp. 1-18, 47-90.

[34] B. Therrien, *Coordination Chemistry Reviews* **2009**, *253*, 493-519.

[35] S. Radisavljević, A. Đ. Kesić, S. Jovanović, B. Petrović, *Transition Metal Chemistry* **2018**, *43*, 331-338.

[36] A. Mambanda, D. Jaganyi, in *Advances in Inorganic Chemistry, Vol. 70*, Elsevier, **2017**, pp. 243-276.

[37] J. D. Knoll, B. A. Albani, C. B. Durr, C. Turro, *The Journal of Physical Chemistry A* **2014**, *118*, 10603-10610.

[38] S. Chakraborty, P. Munshi, G. K. Lahiri, *Polyhedron* **1999**, *18*, 1437-1444.

[39] P. Hormnirun, E. L. Marshall, V. C. Gibson, R. I. Pugh, A. J. White, *Proceedings of the National Academy of Sciences* **2006**, *103*, 15343-15348.

[40] F. Cherioux, J. Coraux, V. Muller, L. Magaud, N. Bendiab, M. Den Hertog, O. Leynaud, W. Hourani, S. Lamare, D. Kamaruddin, *Chemistry-A European Journal* **2017**, *23*, 10969-10973.

[41] U. Fekl, R. van Eldik, C. Richardson, W. T. Robinson, *Inorganic chemistry* **2001**, *40*, 3247-3251.

[42] K. Purkait, S. Chatterjee, S. Karmakar, A. Mukherjee, *Dalton Transactions* **2016**, *45*, 8541-8555.

[43] Ž. D. Bugarčić, J. Bogojeski, B. Petrović, S. Hochreuther, R. van Eldik, *Dalton Transactions* **2012**, *41*, 12329-12345.

[44] G. K. Rauth, D. Das, C. Sinha, K. Bag, A. Mahapatra, *Transition Metal Chemistry* **2002**, *27*, 639-645.

[45] (a) M. A. A. K.Ghosh, B. K.Bera, S. Mallick, S. Mondal, P. Karmakar, *Inorganic Chemistry: An Indian Journal* **2010**, *5*, 176-183; (b) T. Das, B. Bera, A. Datta, A. Ghosh, *Transition Metal Chemistry* **2009**, *34*, 247-253.

[46] A. Rilak, B. Petrović, S. Grgurić-Šipka, Ž. Tešić, Ž. D. Bugarčić, *Polyhedron* **2011**, *30*, 2339-2344.

SI 6 Supplementary Information

SI 6.1 Average k_{obs} values for the simultaneous substitution of aqua ligands in the investigated complexes

Table SI 6.1: Average k_{obs} (s^{-1}) for the reaction of **Ru-1** (0.248 mM) with thiourea nucleophiles

[Nu] /M	**Tu** (λ = 370 nm) k_{obs} /s^{-1}	**Dmtu** (λ = 370 nm) k_{obs} /s^{-1}	**Tmtu** (λ = 385 nm) k_{obs} /s^{-1}
0.0495	4.23×10^{-3}	2.98×10^{-3}	8.04×10^{-4}
0.0396	3.27×10^{-3}	2.40×10^{-3}	6.17×10^{-4}
0.0297	2.48×10^{-3}	1.86×10^{-3}	4.95×10^{-4}
0.0198	1.64×10^{-3}	1.21×10^{-3}	3.53×10^{-4}
0.0099	9.11×10^{-4}	6.23×10^{-4}	1.97×10^{-4}

Table SI 6.2: Average k_{obs} (s^{-1}) for the reaction of **Ru-2** (0.660 mM) with thiourea nucleophiles

[Nu] /M	**Tu** (λ = 515 nm) k_{obs} /s^{-1}	**Dmtu** (λ = 515 nm) k_{obs} /s^{-1}	**Tmtu** (λ = 515 nm) k_{obs} /s^{-1}
0.1319	2.852×10^{-4}	3.711×10^{-4}	1.570×10^{-4}
0.1055	2.359×10^{-4}	3.108×10^{-4}	1.276×10^{-4}
0.0792	1.731×10^{-4}	2.322×10^{-4}	9.909×10^{-5}
0.0528	1.234×10^{-4}	1.594×10^{-4}	6.680×10^{-5}
0.0264	6.128×10^{-5}	8.545×10^{-5}	3.142×10^{-5}

Table SI 6.3: Average k_{obs} (s^{-1}) for the reaction of **Ru-3** (0.144 mM) with thiourea nucleophiles

[Nu] /M	**Tu** (λ = 310 nm) k_{obs} /s^{-1}	**Dmtu** (λ = 310 nm) k_{obs} /s^{-1}	**Tmtu** (λ = 330 nm) k_{obs} /s^{-1}
0.0288	1.454×10^{-4}	1.562×10^{-4}	5.112×10^{-5}
0.0231	1.136×10^{-4}	1.223×10^{-4}	3.901×10^{-5}
0.0173	8.643×10^{-5}	9.452×10^{-5}	2.871×10^{-5}
0.0115	5.662×10^{-5}	6.548×10^{-5}	2.013×10^{-5}
0.0058	2.914×10^{-5}	3.064×10^{-5}	8.386×10^{-6}

Table SI 6.4: Average k_{obs} (s^{-1}) for the reaction of **Ru-4** (0.171 mM) with thiourea nucleophiles

[Nu] /M	**Tu** (λ = 376 nm) k_{obs} /s^{-1}	**Dmtu** (λ = 380 nm) k_{obs} /s^{-1}	**Tmtu** (λ = 372 nm) k_{obs} /s^{-1}
0.0342	9.010×10^{-4}	7.543×10^{-4}	1.439×10^{-4}
0.0273	7.150×10^{-4}	6.028×10^{-4}	1.157×10^{-4}
0.0205	5.515×10^{-4}	4.362×10^{-4}	8.843×10^{-5}
0.0137	3.611×10^{-4}	3.045×10^{-4}	5.458×10^{-5}
0.00683	1.821×10^{-4}	1.498×10^{-4}	2.724×10^{-5}

SI 6.2 Average $\ln\left(\frac{k_2}{T}\right)$ values for the simultaneous substitution of aqua ligands in the investigated complexes

Table SI 6.5: Average $ln\left(\frac{k_2}{T}\right)$ for the reaction of **Ru-1** with thiourea nucleophiles

T /K	$\frac{1}{T}$ /K^{-1}	$\ln\left(\frac{k_2}{T}\right)$ **Tu**	$\ln\left(\frac{k_2}{T}\right)$ **Dmtu**	$\ln\left(\frac{k_2}{T}\right)$ **Tmtu**
298.15	0.00335	-8.234	-8.509	-9.814
303.15	0.00330	-7.801	-8.151	-9.401
308.15	0.00325	-7.432	-7.822	-8.99
313.15	0.00319	-7.050	-7.438	-8.554
318.15	0.00314	-6.725	-7.042	-8.200

Table SI 6.6: Average $ln\left(\frac{k_2}{T}\right)$ for the reaction of **Ru-2** with thiourea nucleophiles

T /K	$\frac{1}{T}$ /K^{-1}	$\ln\left(\frac{k_2}{T}\right)$**Tu**	$\ln\left(\frac{k_2}{T}\right)$ **Dmtu**	$\ln\left(\frac{k_2}{T}\right)$ **Tmtu**
298.15	0.00335	-11.824	-11.522	-12.381
303.15	0.00330	-11.424	-11.179	-12.048
308.15	0.00325	-11.125	-10.884	-11.628
313.15	0.00319	-10.676	-10.394	-11.106
318.15	0.00314	-10.285	-10.047	-10.735

Table SI 6.7: Average $ln\left(\frac{k_2}{T}\right)$ for the reaction of **Ru-3** with thiourea nucleophiles

T /K	$\frac{1}{T}$ /K^{-1}	$\ln\left(\frac{k_2}{T}\right)$ **Tu**	$\ln\left(\frac{k_2}{T}\right)$ **Dmtu**	$\ln\left(\frac{k_2}{T}\right)$ **Tmtu**
298.15	0.00335	-10.997	-10.907	-12.099
303.15	0.00330	-10.631	-10.537	-11.712
308.15	0.00325	-10.193	-10.113	-11.253
313.15	0.00319	-9.801	-9.678	-10.797
318.15	0.00314	-9.395	-9.236	-10.309

Table SI 6.8: Average $ln\left(\frac{k_2}{T}\right)$ for the reaction of **Ru-4** with thiourea nucleophiles

T /K	$\frac{1}{T}$ /K^{-1}	$\ln\left(\frac{k_2}{T}\right)$ **Tu**	$\ln\left(\frac{k_2}{T}\right)$ **Dmtu**	$\ln\left(\frac{k_2}{T}\right)$ **Tmtu**
298.15	0.00335	-9.313	-9.548	-11.139
303.15	0.00330	-8.859	-9.172	-10.692
308.15	0.00325	-8.503	-8.721	-10.257
313.15	0.00319	-8.137	-8.321	-9.619
318.15	0.00314	-7.714	-7.949	-9.194

SI 6.3 Typical plots of k_{obs} versus nucleophile concentration for the studied reactions

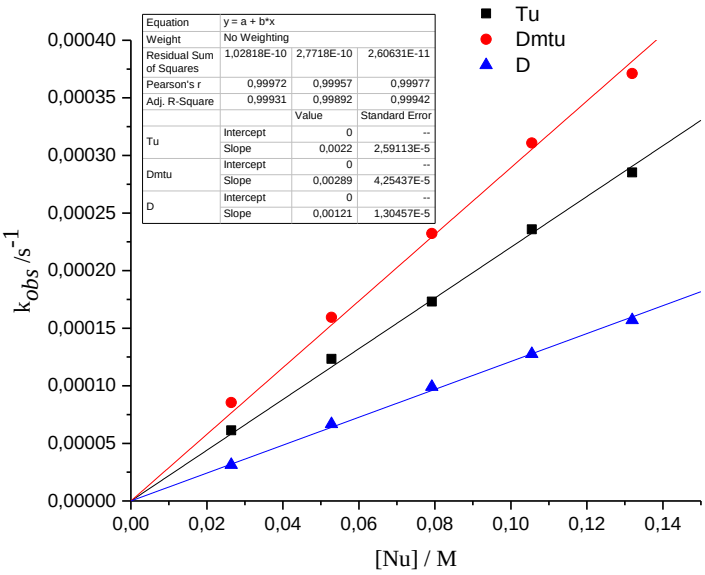

Figure SI 6.1: Dependence of k_{obs} on concentration of incoming thiourea nucleophiles for the substitution of the aqua ligands in **Ru-2** at 298 K, pH = 2.0, I = 0.1 M $HClO_4/NaClO_4$

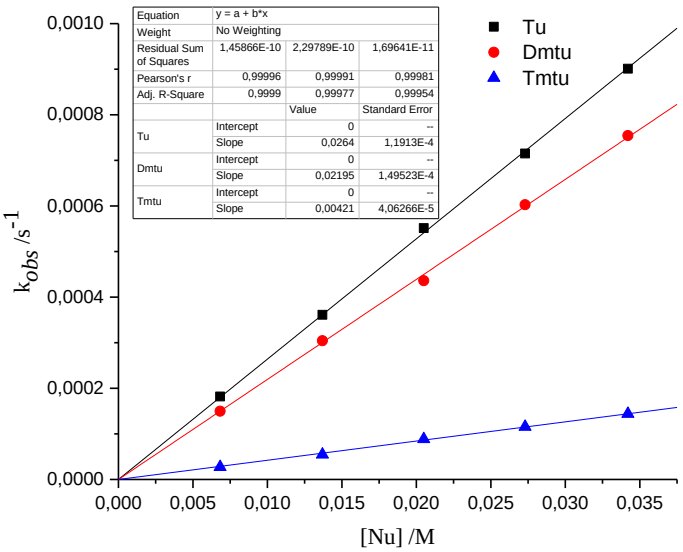

Figure SI 6.2: Dependence of k_{obs} on concentration of incoming thiourea nucleophiles for the substitution of the aqua ligands in **Ru-4** at 298 K, pH = 2.0, I = 0.1 M $HClO_4/NaClO_4$

SI 6.4 Typical Eyring plots for the substitution of the aqua ligands

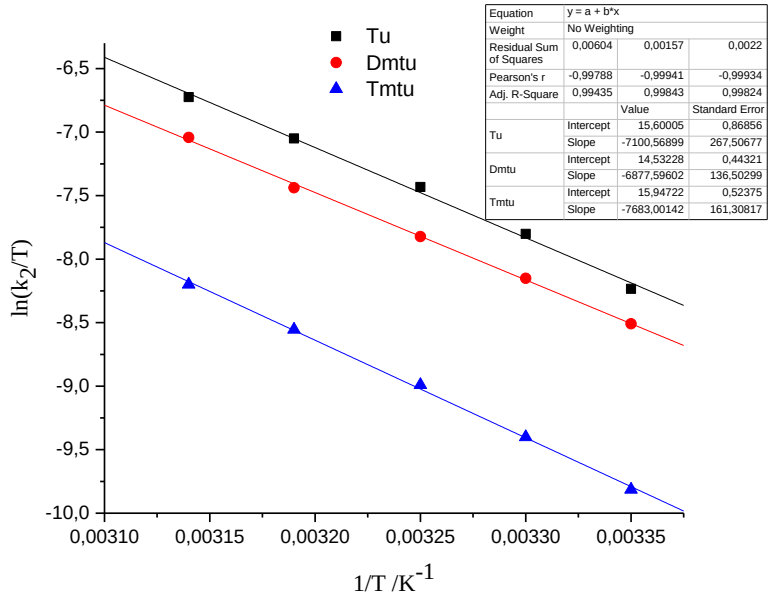

Figure SI 6.3: Eyring plots for the reaction of **Ru-1** with thiourea nucleophiles at different temperatures, pH = 2.0, I = 0.1 M $HClO_4/NaClO_4$

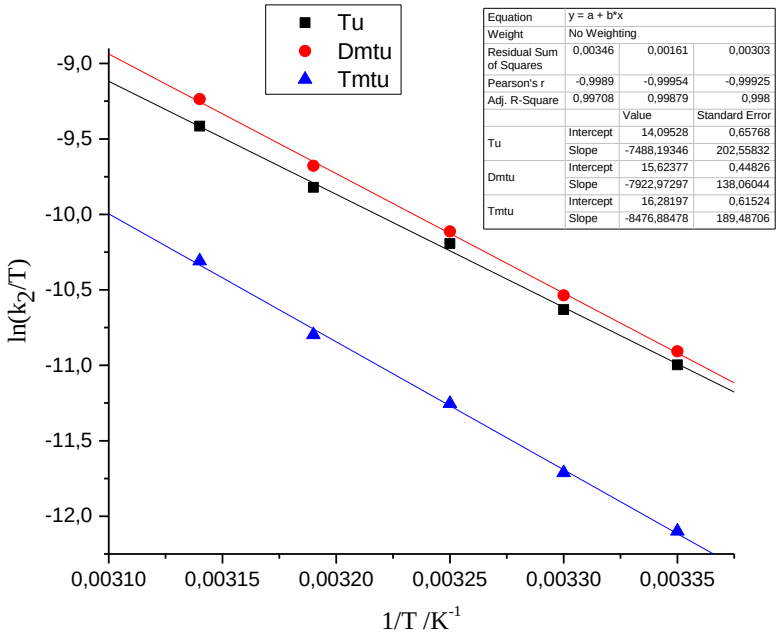

Figure SI 6.4: Eyring plots obtained for the reaction of **Ru-3** with thiourea nucleophiles at different temperatures, pH = 2.0, I = 0.1 M $HClO_4/NaClO_4$

SI 6.5 Typical ultraviolet-visible spectra for the pKa titration of the complexes

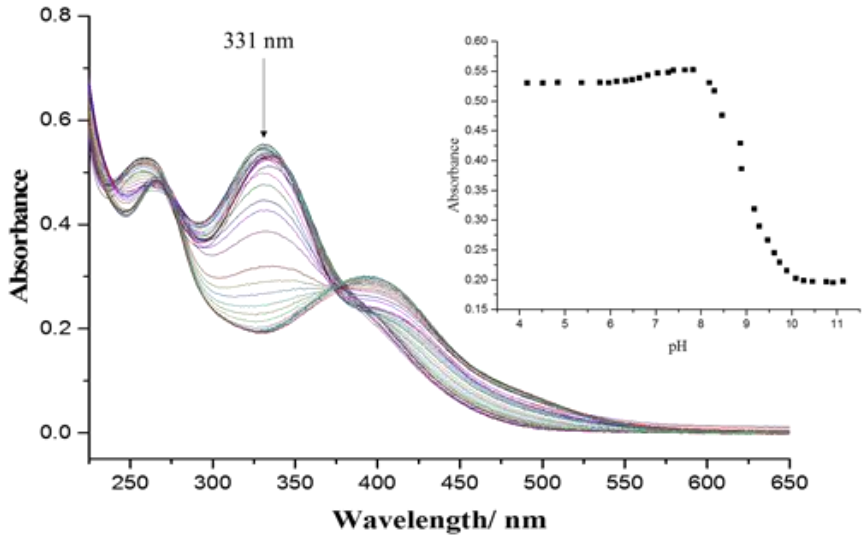

Figure SI 6.5: Ultraviolet-visible spectra of **Ru-2** complex recorded as a function of pH in the range 1–12 at 298 K. **Inset**: Plot of absorbance versus pH at λ = 256 nm

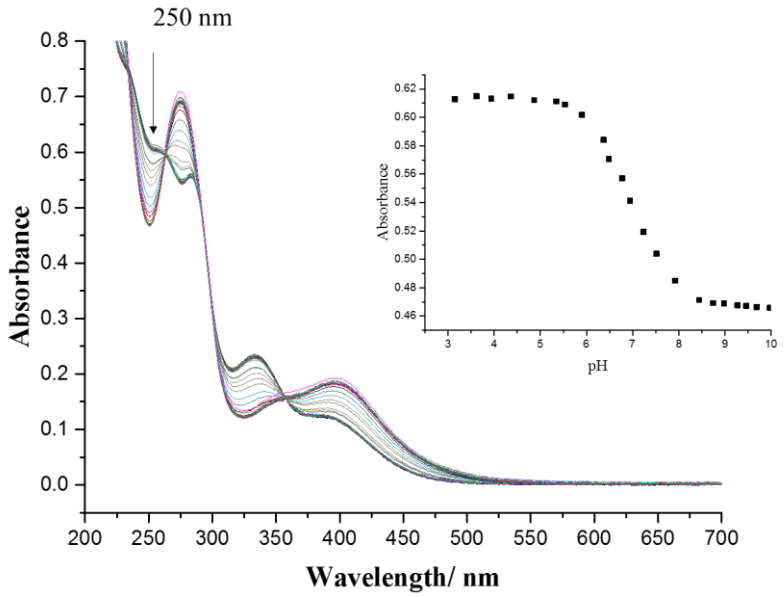

Figure SI 6.6: Ultraviolet-visible spectra of **Ru-4** complex recorded as a function of pH in the range 1–10 at 298 K. **Inset**: Plot of absorbance versus pH at λ = 250 nm

SI 6.6 Additional DFT-optimized structures of the studied complexes

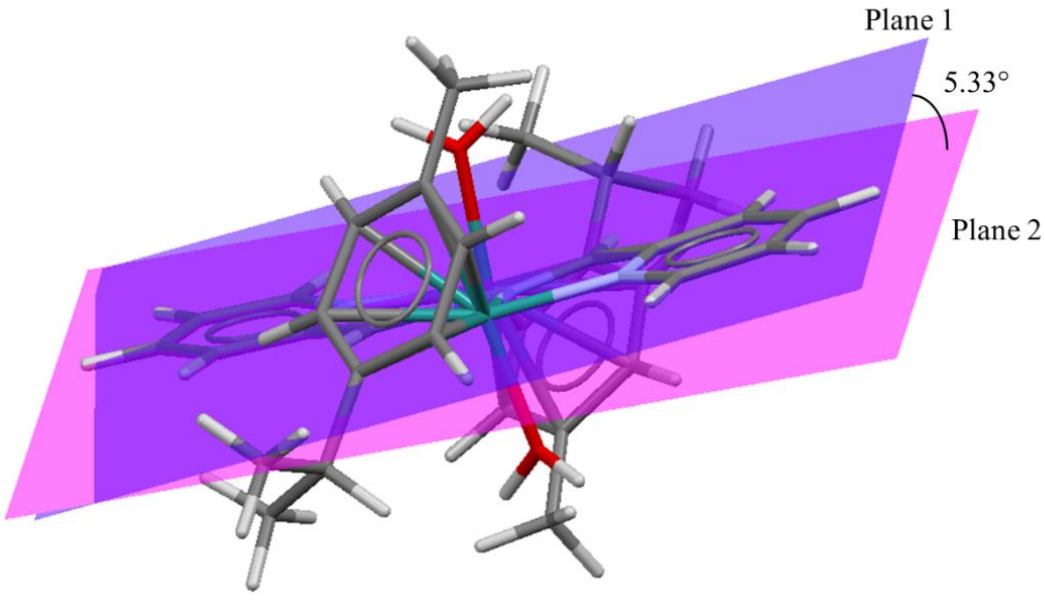

Figure SI 6.7: DFT-optimized structure of **Ru-1** showing the dihedral angle of between the planes of the α,α'-diimine moieties

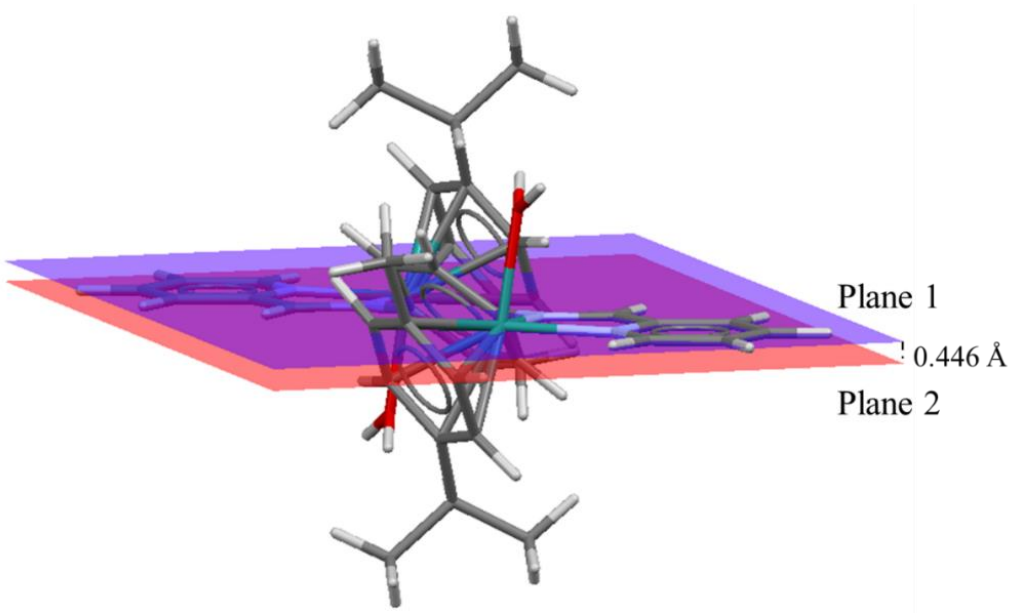

Figure SI 6.8: DFT-optimized structure of **Ru-2** showing the distance between the α,α'-diimine moiety planes

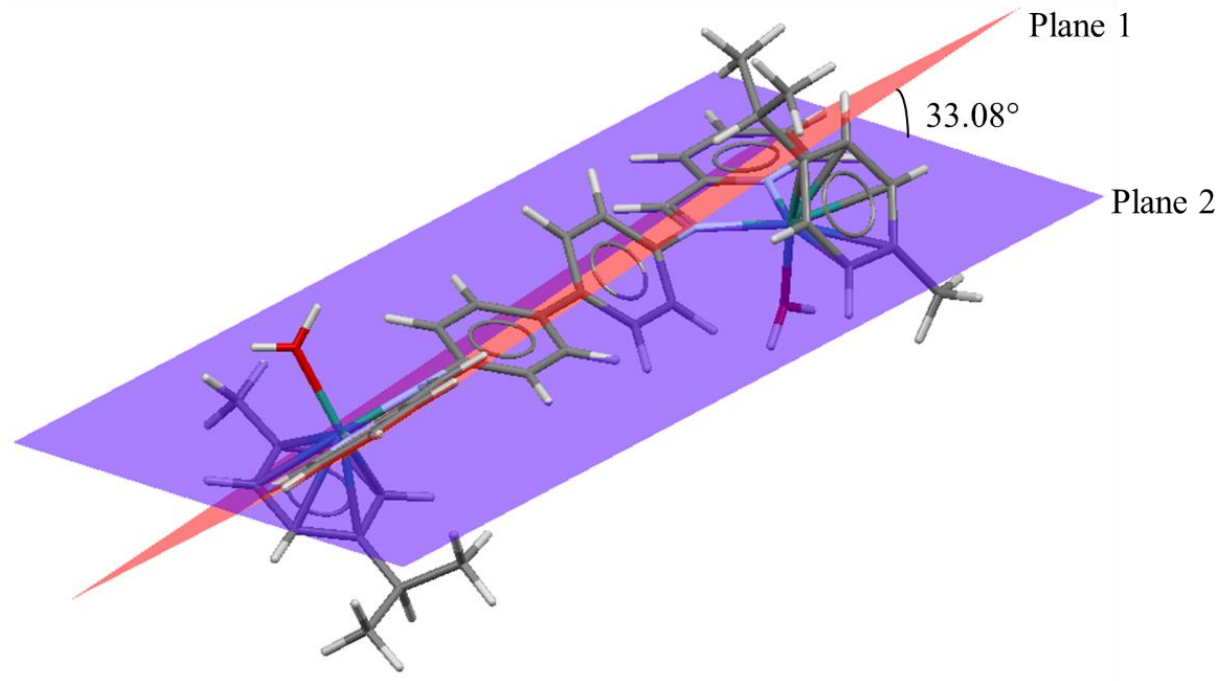

Figure SI 6.9: DFT-optimized structure of **Ru-3** showing the dihedral angle between the α,α'-diimine moiety planes

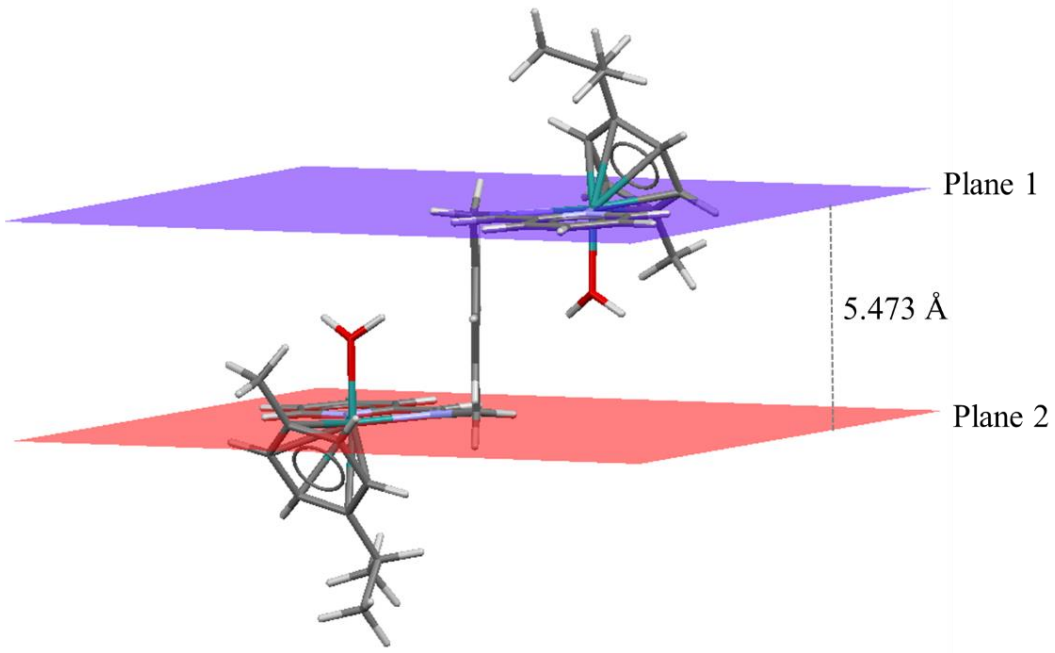

Figure SI 6.10: DFT-optimized structure of **Ru-4** showing the dihedral angle between the α,α'-diimine moiety planes

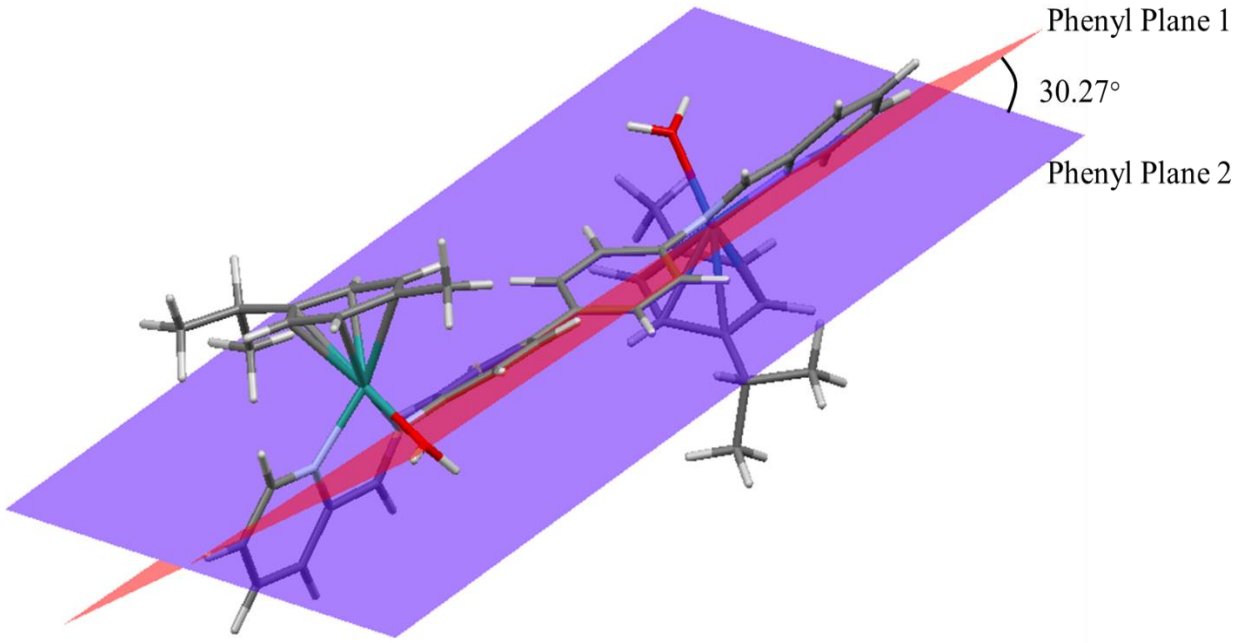

Figure SI 6.11: DFT-optimized structure of **Ru-3 s**howing the dihedral angle between the phenyl planes

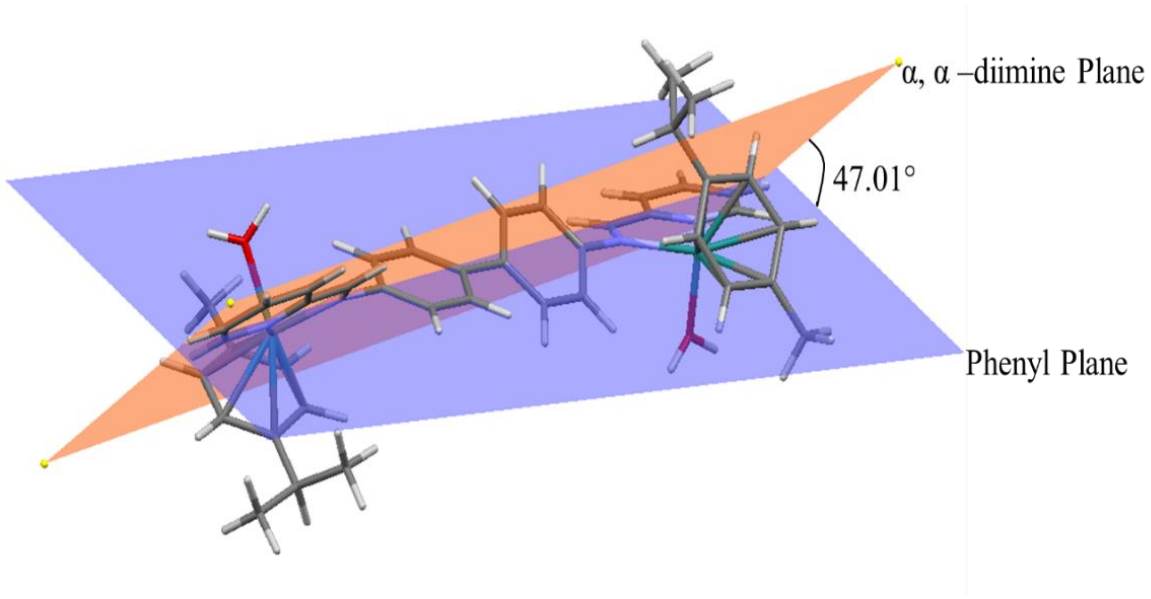

Figure SI 6.12: DFT-optimized structure of **Ru-3 s**howing the dihedral angle between the α,α'-diimine plane and phenyl planes

SI 6.7 Samples of MS, ^{1}H and ^{13}C NMR spectra for the ligands and complexes

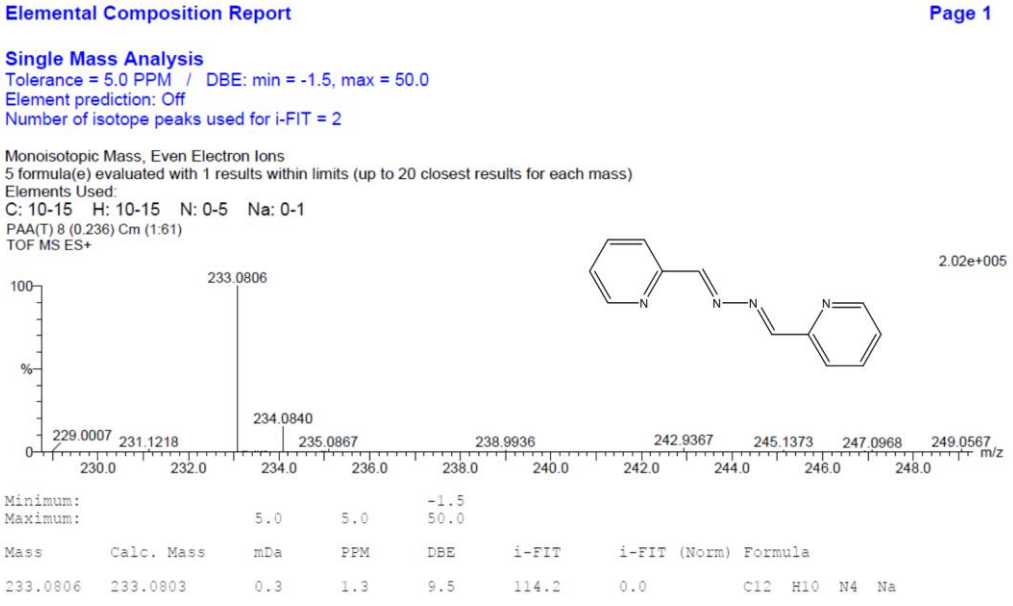

Figure SI 6.13: ESI-MS (TOF) spectrum for 2-pyridine aldazine

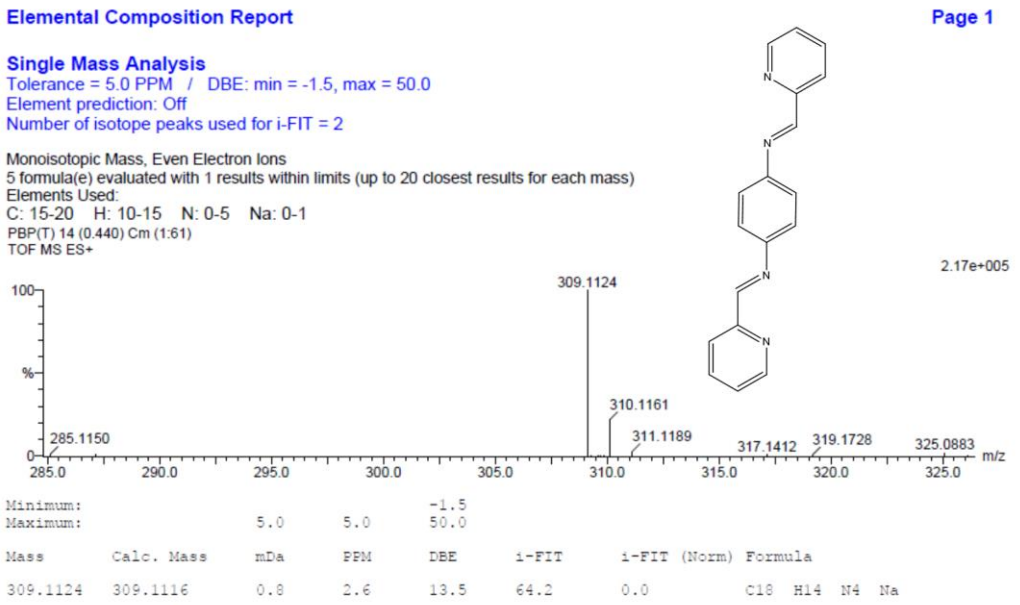

Figure SI 6.14: ESI-MS (TOF) spectrum for *p*-phenylene-bis(picoline)-aldimine (PBP)

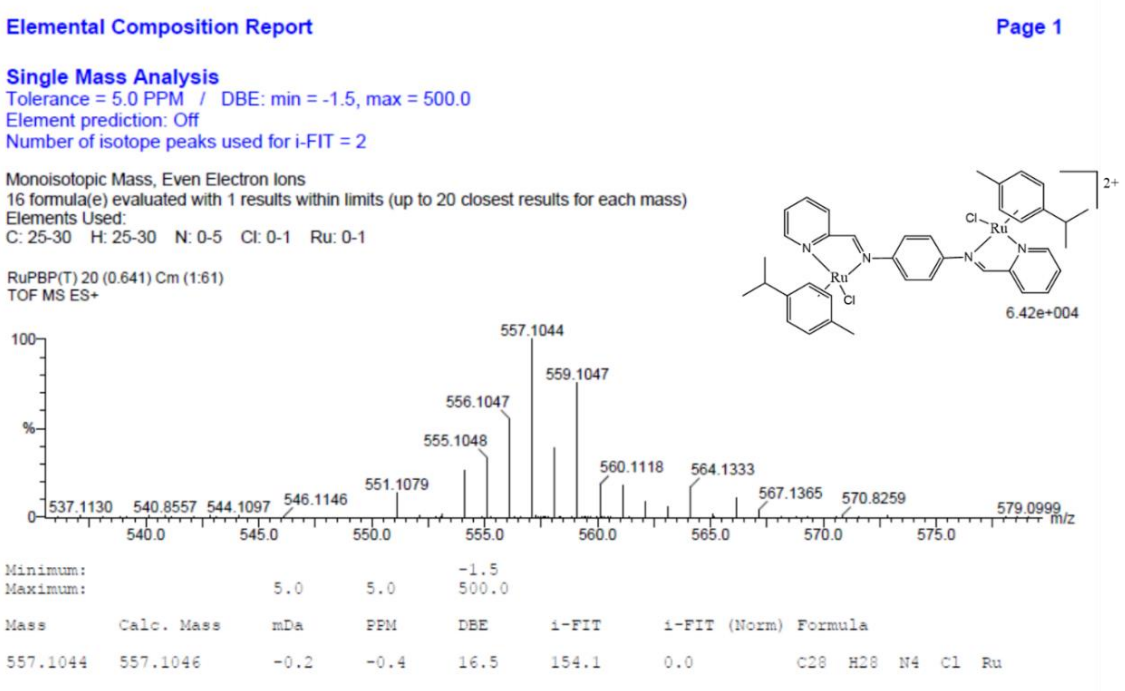

Figure SI 6.15: ESI-MS (TOF) spectrum (μ_2-PBP)-dichloro-bis(η^6-*p*-cymene)diruthenium(II) tetrafluoroborate

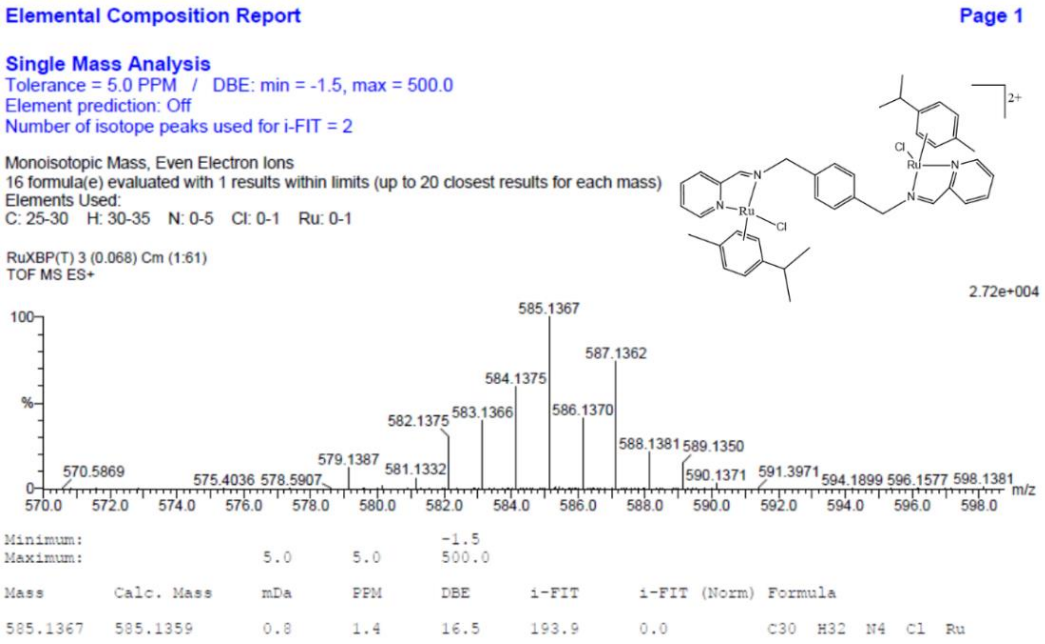

Figure SI 6.16: ESI-MS (TOF) spectrum (μ_2-XBP)-dichloro-bis(η^6-*p*-cymene)diruthenium(II) bis(tetrafluoroborate)

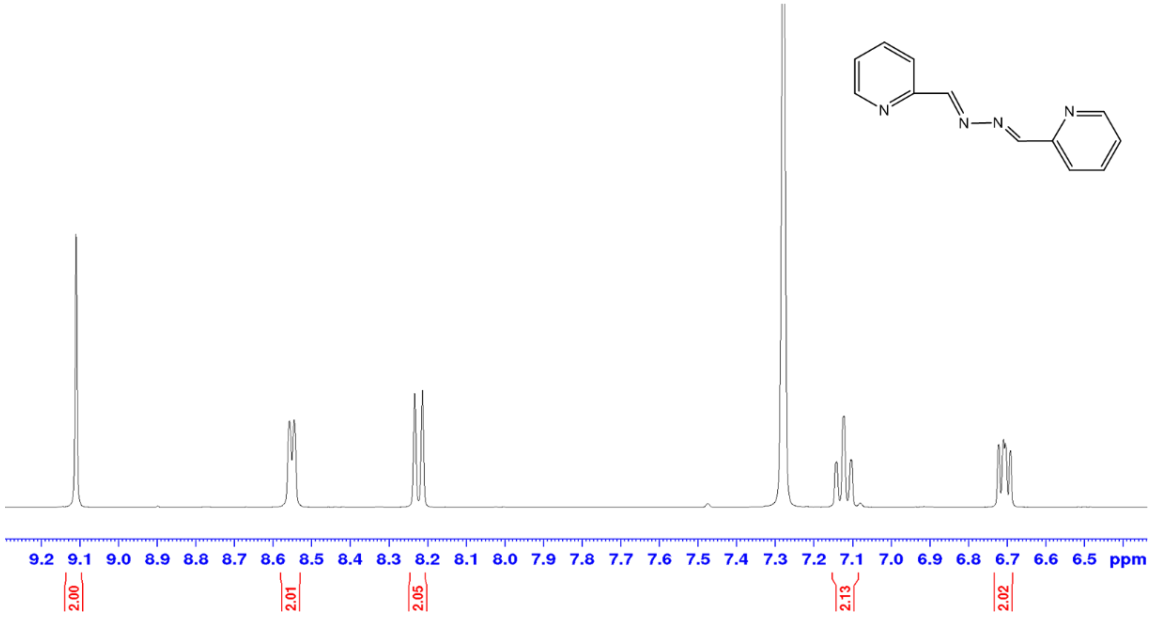

Figure SI 6.17: ^{1}H NMR (400 MHz, benzene-d_6) of spectrum of 2-pyridine aldazine

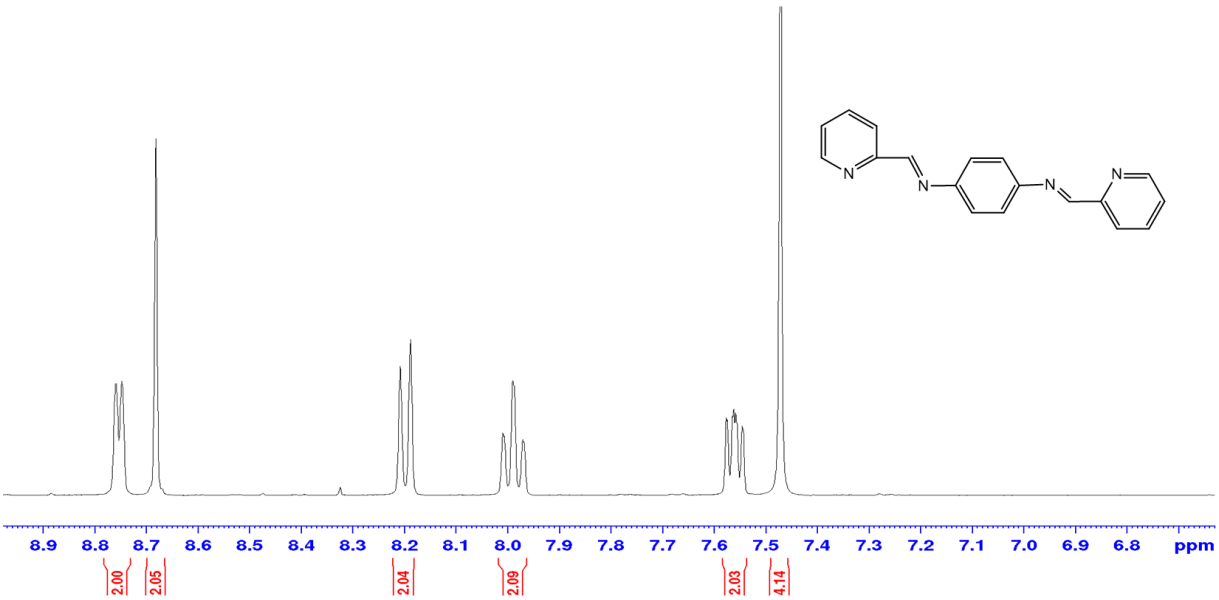

Figure SI 6.18: ^{1}H NMR (400 MHz, DMSO-d_6) spectrum of *p*-phenylene-bis(picoline)-aldimine (PBP)

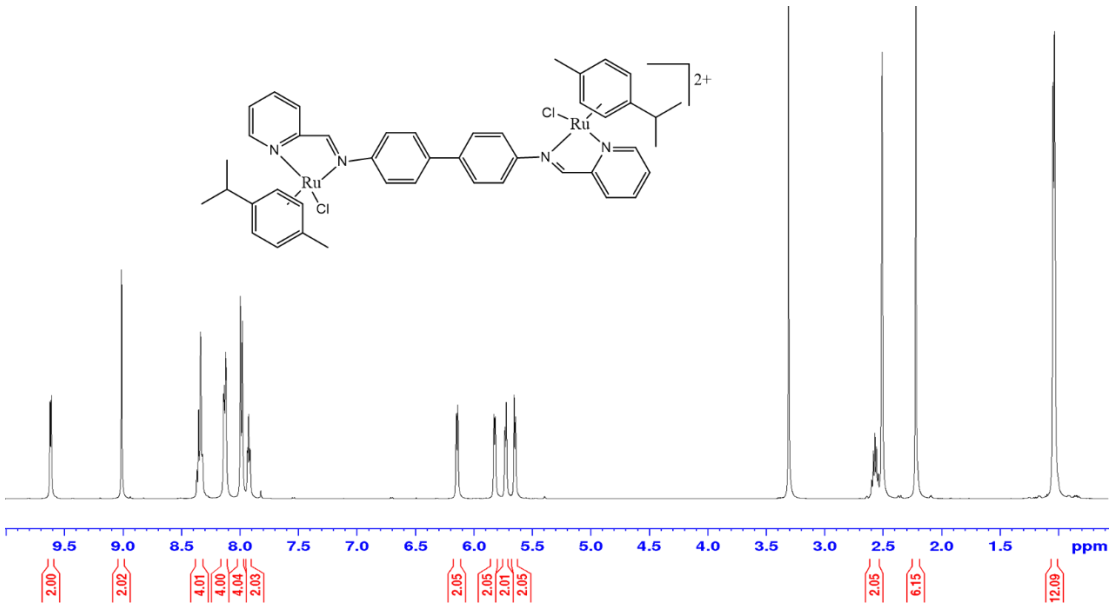

Figure SI 6.19: ^{1}H NMR (500 MHz, DMSO-d_6) spectrum of (μ_2-BBP)-dichloro-bis(η^6-*p*-cymene)diruthenium(II) tetrafluoroborate

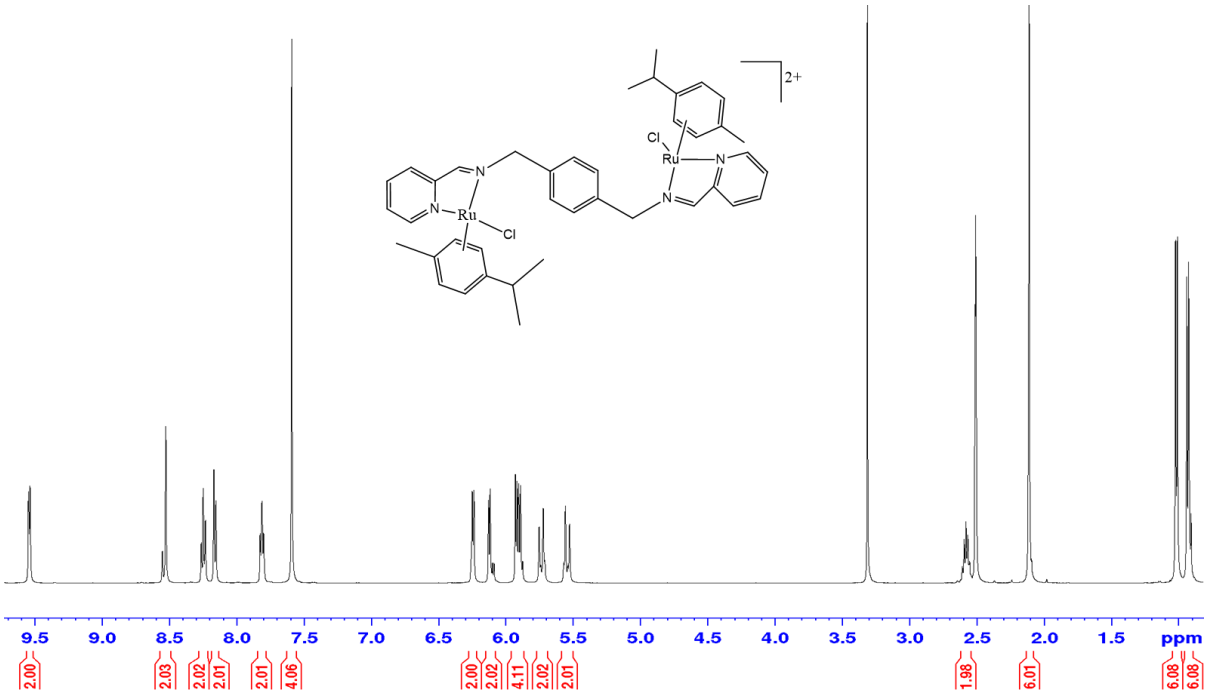

Figure SI 6.20: ^{1}H NMR (500 MHz, DMSO-d_6) spectrum of (μ_2-XBP)-dichloro-bis(η^6-*p*-cymene)diruthenium(II) tetrafluoroborate

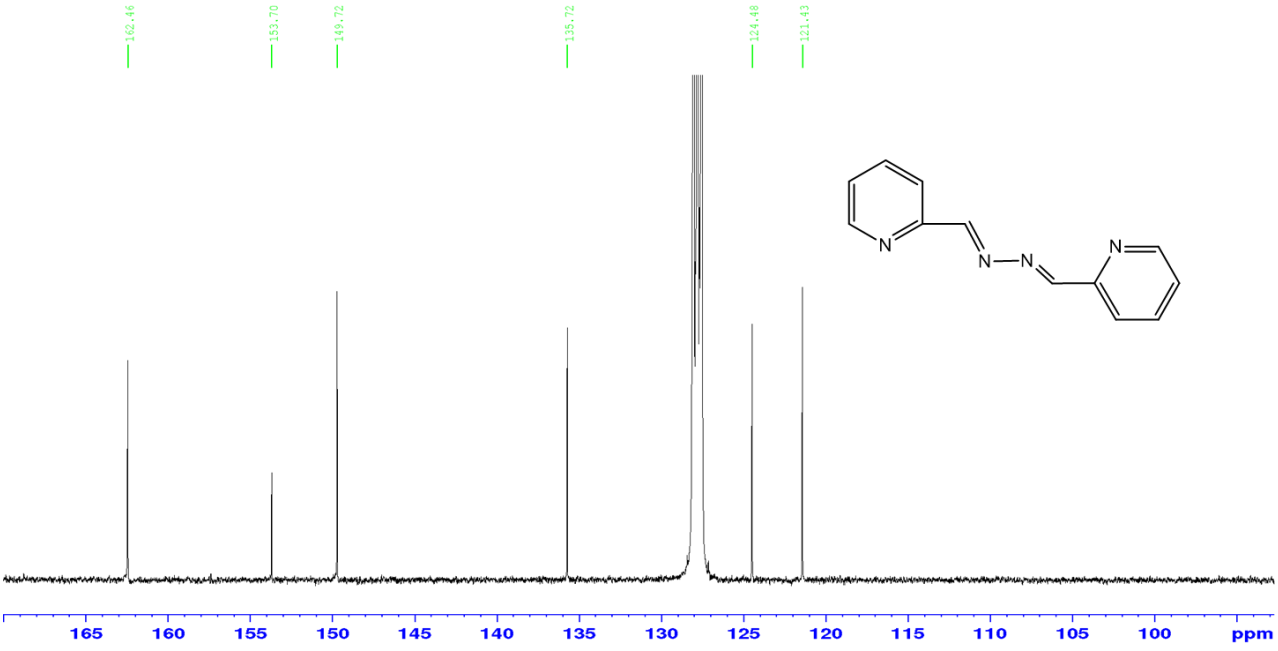

Figure SI 6.21: ^{13}C NMR (400 MHz, benzene-d_6) spectrum of 2-pyridine aldazine

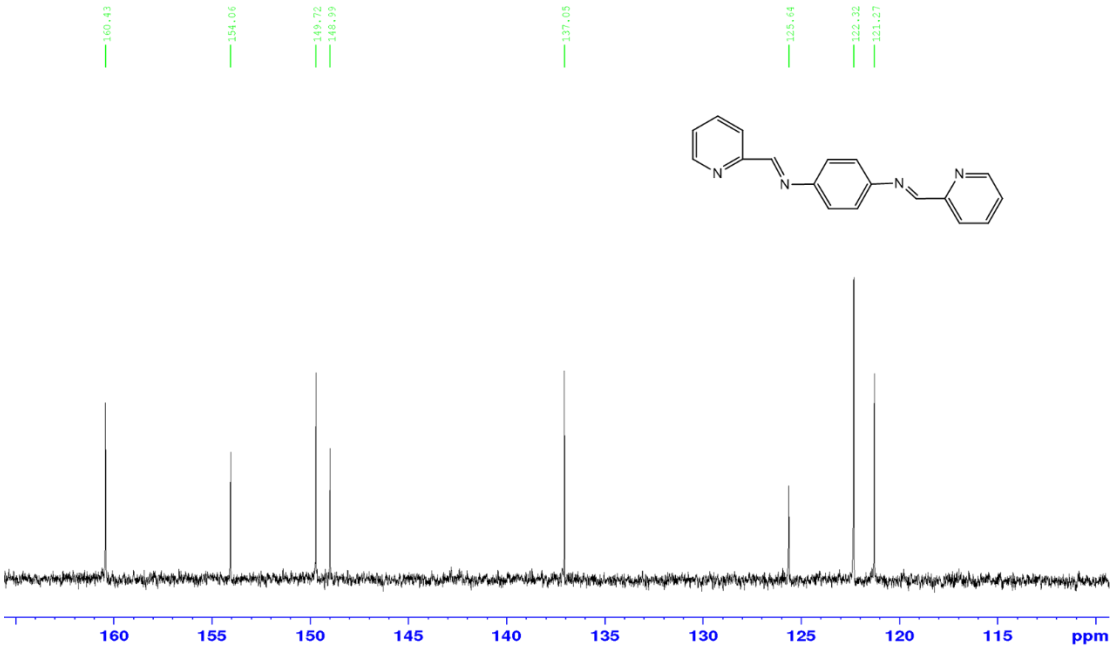

Figure SI 6.22: ^{13}C NMR (400 MHz, DMSO-d_6) spectrum of *p*-phenylene-bis(picoline)-aldimine (PBP)

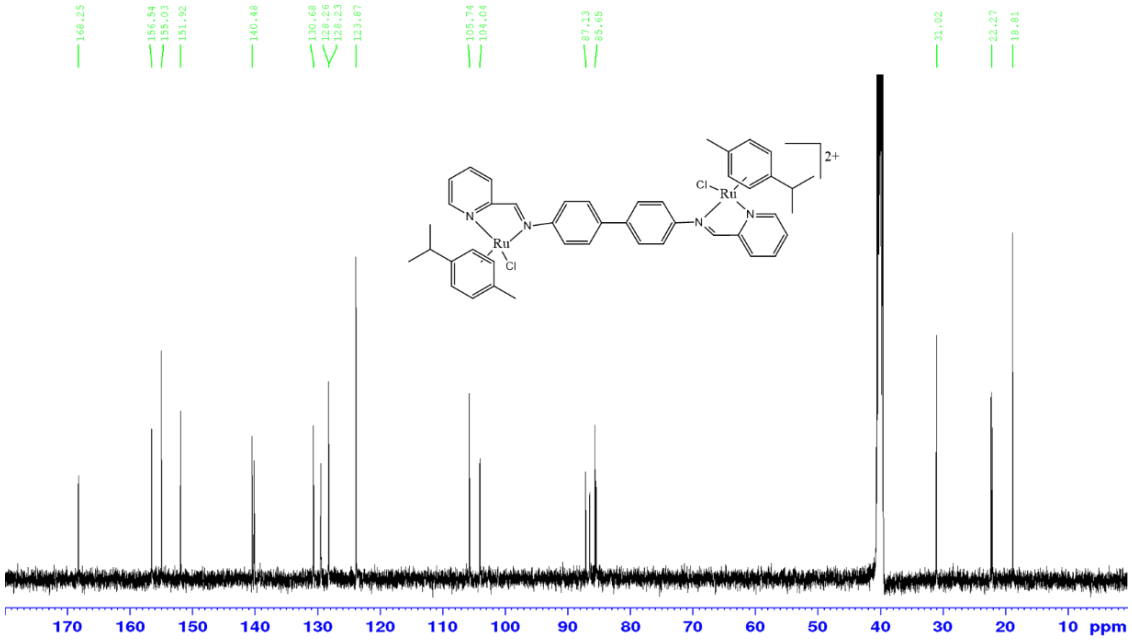

Figure SI 6.23: ^{13}C NMR (500 MHz, DMSO-d_6) spectrum of (μ_2-BBP)-dichloro-bis(η^6-*p*-cymene)diruthenium(II) tetrafluoroborate

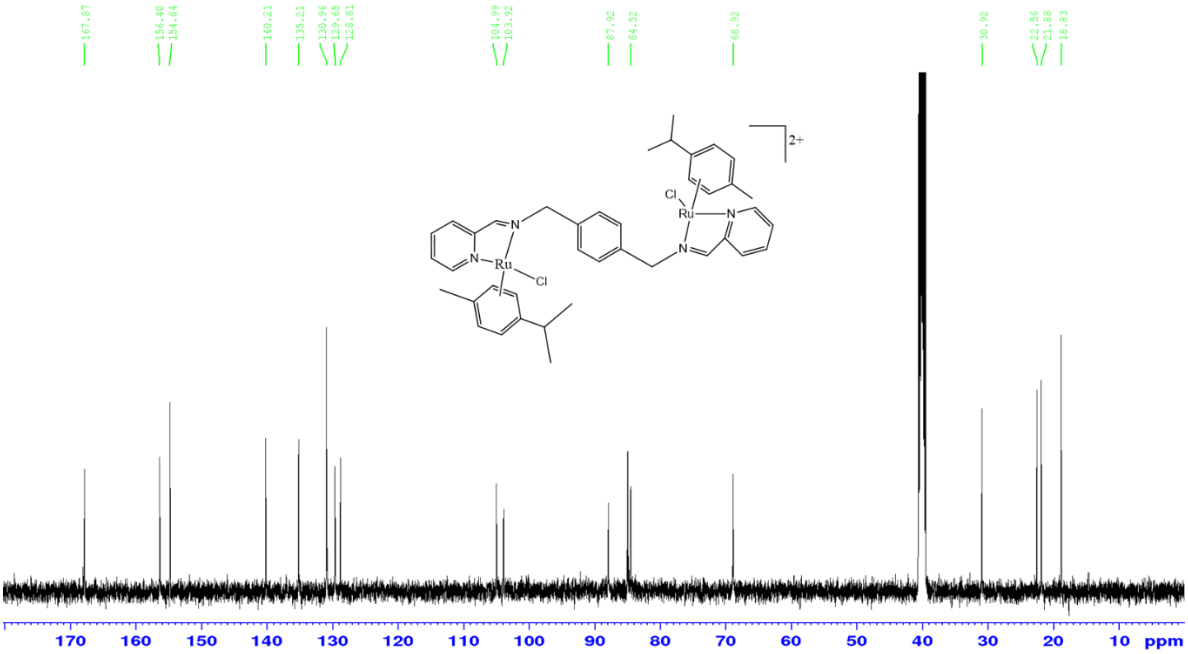

Figure SI 6.24: ^{13}C NMR (500 MHz, DMSO-d_6) spectrum of (μ_2-XBP)-dichloro-bis(η^6-*p*-cymene)diruthenium(II) tetrafluoroborate

CHAPTER SEVEN

Summary and Future Prospects

7.1 Summary

The aim of this work was to investigate the kinetic behavior of ruthenium(II) complexes as affected by different ligand systems around the metal centre. Biorelevant nucleophiles of varied steric requirements (thiourea, *N*,*N*-dimethylthiourea and *N,N,N',N'*-tetramethylthiourea) were used to model the interaction of these potential anticancer agents with sulfur containing proteins in biological systems. The rate of substitution was studied as a function of both concentration and temperature under *pseudo*-first order conditions using stopped-flow and ultraviolet-visible spectrophotometric techniques. Computational studies using density functional theory were carried out to gain insight into the structural and electronic properties of these complexes.

Chapter One: Introduction is the introductory chapter where the development of metallotherapeutic agents from *cisplatin* to ruthenium-based agents is summarized. This chapter mentions platinum-based metallodrugs that are globally or regional approved for utilization in anticancer therapy as well the challenges faced during their use. It highlights the interests in the development of ruthenium based anticancer agents. It concludes by outlining the rationale of the work as well the aims of this study.

Chapter Two: Literature Review. It presents the kinetic and mechanistic theoretical aspects pertinent to the study of substitution reactions. The theory, substitution reactions and kinetics is reviewed as well as factors that affect the rate of substitution reactions in transition metal complexes. Commonly used techniques in kinetic studies are also discussed.

The experimental work is reported and discussed in **Chapter Three** to **Six**

In **Chapter Three**, the role of π-extension of the auxiliary ligand on the substitution kinetics of mono aqua terpyridyl based complexes is reported. A series of four complexes were studied as shown in Figure 7.1.

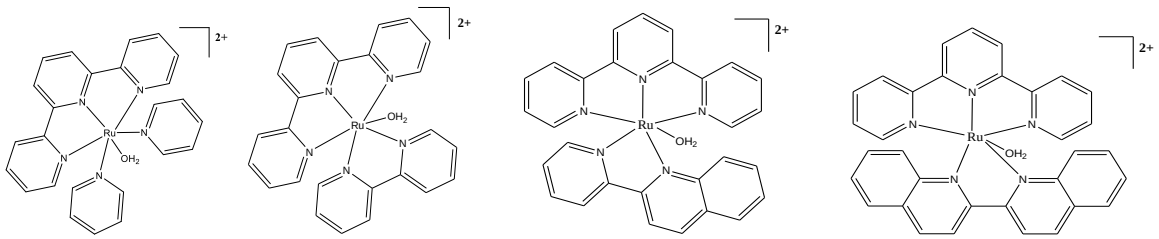

Ru-1 **Ru-2** **Ru-3** **Ru-4**

Figure 7.1: Structures of the investigated ruthenium(II) complexes

The rate of substitution of the aqua ligands in the complexes followed the order; **Ru-4** > **Ru-3** > **Ru-1** > **Ru-2**. It was observed that the reactivity of the complexes with bidentate N^N auxiliary ligand (**Ru-2** to **Ru-4**) increased with increase in π-conjugated surface area of the auxiliary ligand. As the π-aromatic area increase, the LUMO of the complexes is stabilized reducing the energy gap between the frontier orbitals. This facilitates effective π-back-bonding of electron density from the metal centre to the ligands making the complexes more electrophilic. Consequently, the metal centre becomes more prone facile nucleophilic attack. This trend in reactivity is supported by p*K*a values and DFT-calculated parameters. **Ru-1** is more reactive than **Ru-2** despite **Ru-2** being more electrophilic. This is because replacing the two *trans* pyridine ligands in **Ru-1** with a chelating bipyridyl ligand (**Ru-2**), increases the steric hindrance around the metal centre impeding nucleophilic attack. The crystal structure of $[Ru(terpy)(bipy)Tu)](ClO_4)_2$ reveal that the substitution product formed is stable and the oxidation state (+2) of the metal centre is maintained after reaction.

In **chapter four**, the effects of π-back-bonding and *trans*-effect on the reactivity of ruthenium(II) polypridyl complexes with two chloro leaving groups are reported (Figure 7.2).

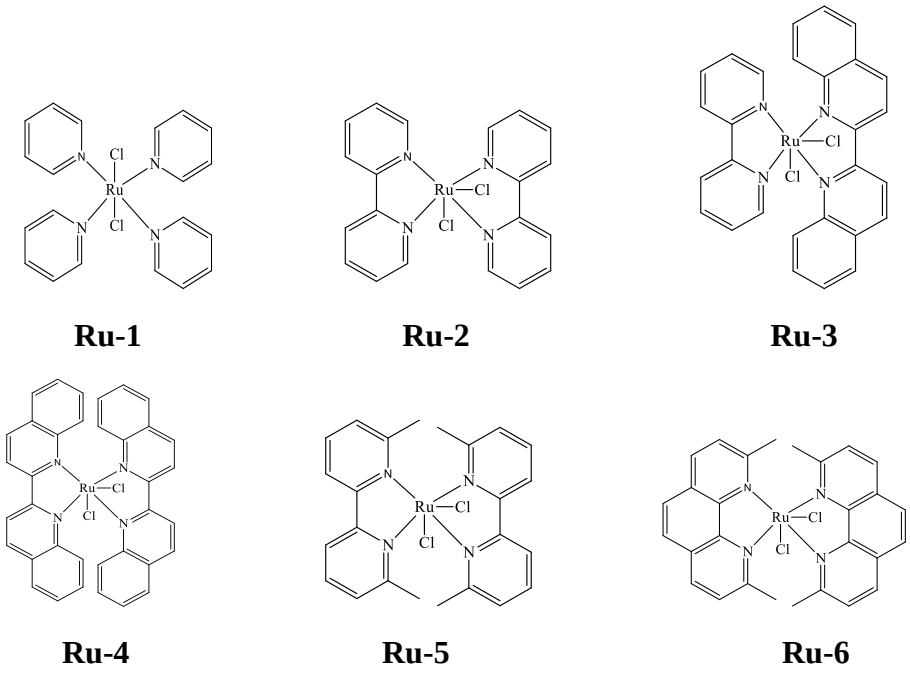

Figure 7.2: Structures of investigated ruthenium(II) complexes

The simultaneous substitution of the chloro ligands decreased in the order; **Ru-3** > **Ru-4** > **Ru-2** > **Ru-1** and **Ru-5** > **Ru-6** > **Ru-2**. In the first set of complexes (**Ru-1** to **Ru-4**), the DFT results show that the separation energy between the frontier orbitals decreased from **Ru-1** to **Ru-4** while the trend in electrophilicity indices is the opposite. This shows that the π-back-bonding of the electron density to the dπ* orbital based on the ligands increase as one moves from **Ru-1** to **Ru-4** and therefore susceptibility of the metal centre to nucleophilic attack increase in the same order. Despite **Ru-4** being more electrophilic, it is less reactive than **Ru-3.** This is so because the two biquinoline ligands in **Ru-4** form banana-shaped curvatures that limit the space around the metal thereby increasing steric hindrance to the incoming nucleophile. In the second set of complexes (**Ru-2, Ru-5** and **Ru-6**) it was observed that the global electrophilicity indices and reactivity have

an inverse relationship. This means that σ-*trans* effect of the coordinated ligand is responsible for the reactivity trend observed. An increase in π-acceptor ability of the influencing ligand reduces the σ-*trans* effect. This is responsible for the lower reactivity of **Ru-6** compared to **Ru-5**. The crystal structure of *trans*-$[Ru(bipy)_2(Tmtu)_2](ClO_4)_2$ show that the stereochemistry of the complex and oxidation state (+2) of the metal centre is maintained after reaction with sulfur-based nucleophiles.

In **Chapter Five**, the role of the bridging ligand on the reactivity of *p*-cymene ruthenium(II) complexes is reported. The mononuclear and dinuclear complexes investigated are given in Figure 7.3.

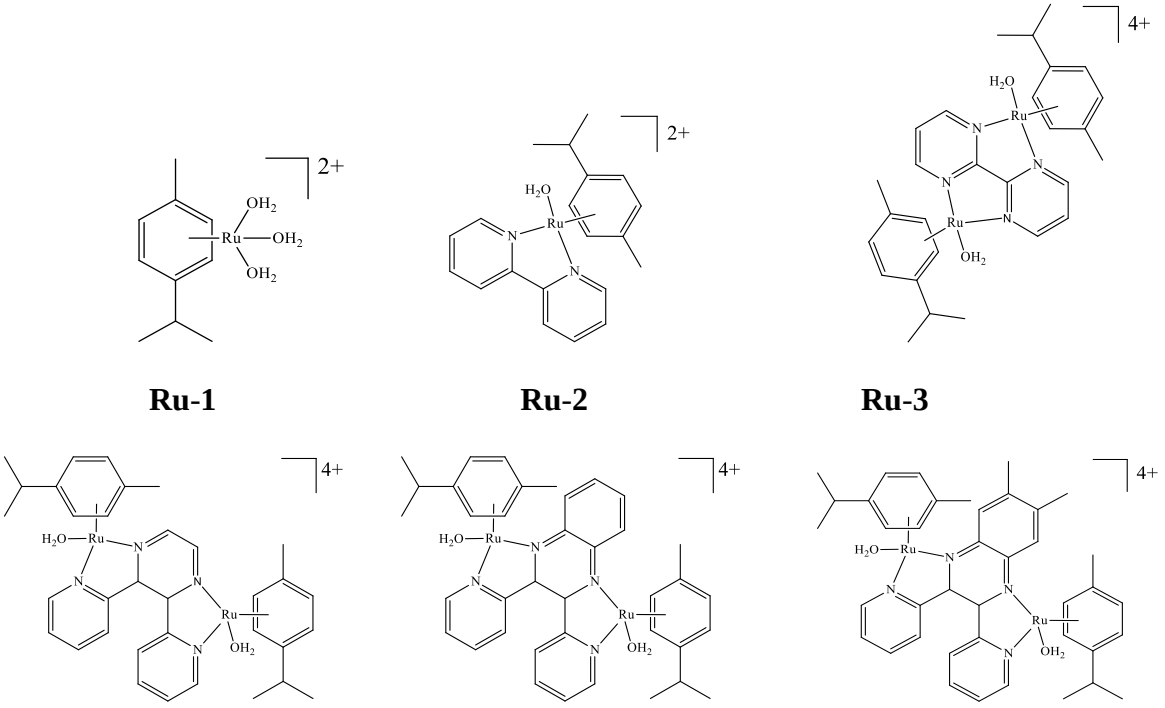

Ru-1 **Ru-2** **Ru-3**

Ru-4 **Ru-5** **Ru-6**

Figure 7.3: Structures of the investigated ruthenium(II) complexes

The simultaneous substitution of the aqua ligands in the binuclear complexes decreased in the order; **Ru-3** > **Ru-4** > **Ru-5** > **Ru-6**. This trend is attributed to stereo-electronic factors associated with the bridging ligand. The incoming nucleophile experience less steric hindrance in attacking the metal centre in complex **Ru-3** compared to the rest of the binuclear complexes. In addition, as supported by DFT calculated data, complex **Ru-3** is more electrophilic than complex **Ru-4**. In **Ru-5** the steric hindrance posed to the incoming nucleophile is higher due to increased non-planarity of the pyridyl moieties therein. The methyl substituents in **Ru-6** decreases the electrophilicity of the complex further retarding its reactivity. It was also observed that during the substitution reactions of the binuclear complexes, two products are formed simultaneously. The high reactivity of complex **Ru-1** compared to **Ru-2** is attributed to its high electrophilicity as shown from the DFT calculated index and its lower p*K*a value. Besides, the bipyridyl ligand increases the steric hindrance around the metal centre in **Ru-2**. Complex **Ru-3** is more reactive compared to its related mononuclear complex (**Ru-2**) due to synergistic effects of the two metal centres which make the dinuclear complex more electrophilic therefore more susceptible to nucleophilic attack.

In **chapter six**, the role of α,α'-diimine bridging ligand is reported. The spacer between the α,α'-diimine moieties was varied (Figure 7.4).

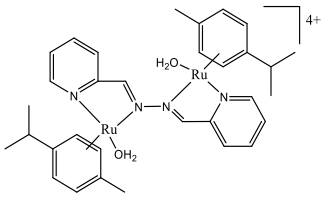

Ru-1

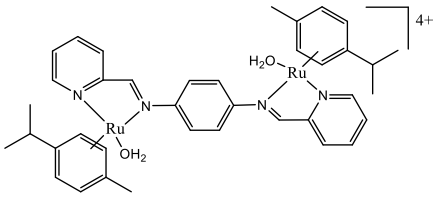

Ru-2

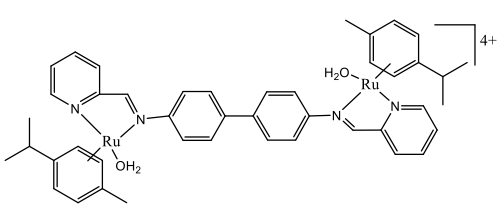

Ru-3

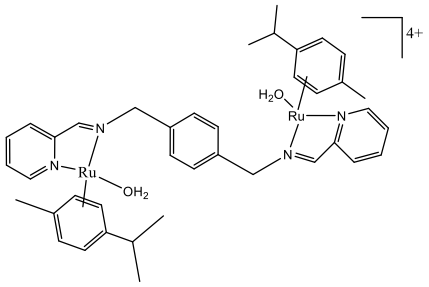

Ru-4

Figure 7.4: Structures of the investigated ruthenium(II) complexes

The simultaneous substitution of the aqua ligands in the complexes decreased in the order; **Ru-1** > **Ru-4** > **Ru-3** > **Ru-2**. The high reactivity of **Ru-1** compared to the other complexes is due to the strong π-acceptor bridging ligand (2-pyridyl aldazine) therein which enhances π-back-bonding of the electron density from the metal to the ligand. This is supported by both DFT-calculated parameters such as global electrophilicity indices and HOMO-LUMO gap and experimentally measured p*K*a values. For the rest of the complexes, the reactivity decreases with increase in steric crowding around the metal centre due to hampered nucleophilic attack. In addition to decreased steric hinderance around the metal centre, the bridging ligand in **Ru-4** forms two V-shaped curvatures that possibly facilitate the interaction between the nucleophile and the metal centre though the cage effect.

The activation parameters obtained in all the studies ($\Delta H^{\neq} > 0$, $\Delta S^{\neq} < 0$) support an associative mechanism.

7.2 Future Prospects

From the results obtained in **Chapter Three** and **Four**, it would be important to establish the effect of electron-donating/withdrawing groups on the *para* and *ortho* positions of the auxiliary ligands in terpyridine based ruthenium(II) complexes. A proposed study is shown in Figure 7.5. These complexes can be synthesized according to reported literature methods.[1]

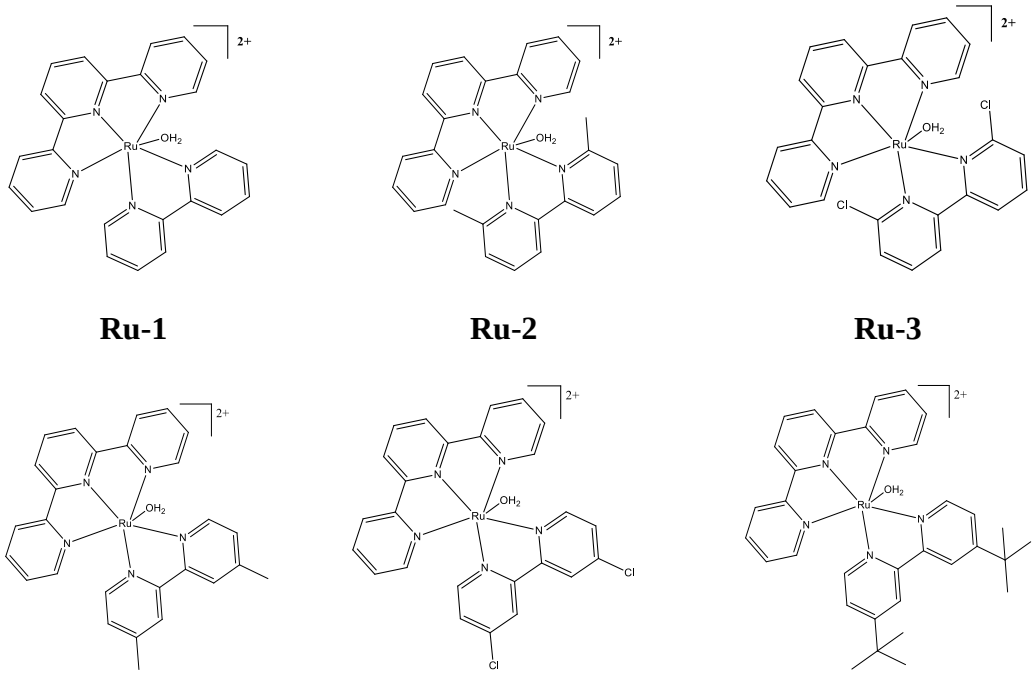

Figure 7.5: Effects of electron-donating/withdrawing groups on the reactivity of ruthenium(II) complexes

Arene-based ruthenium(II) complexes remain a favorite in the search of ruthenium-based chemotherapeutic agents.[2] Therefore, more research on the kinetic behavior of arene based ruthenium(II) complexes as affected by different ligands should be done. An example of a possible scheme is shown in Figure 7.6. These complexes can be synthesized according to reported literature methods.[3]

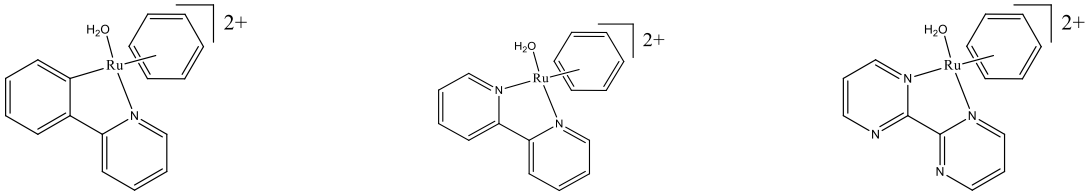

Ru-1 **Ru-2** **Ru-3**

Figure 7.6: A proposed scheme based on arene-ruthenium(II) complexes

To fully understand the anticancer potential of the studied complexes, DNA and protein binding studies should be done. Efforts should be made to understand the transport mechanisms and toxicity profiles in biological systems of these potential antineoplastic agents.

7.3 References

[1] (a) B. P. Sullivan, J. M. Calvert, T. J. Meyer, *Inorganic Chemistry* **1980**, *19*, 1404-1407; (b) K. J. Takeuchi, M. S. Thompson, D. W. Pipes, T. J. Meyer, *Inorganic Chemistry* **1984**, *23*, 1845-1851; (c) A. Bahreman, B. Limburg, M. A. Siegler, E. Bouwman, S. Bonnet, *Inorganic chemistry* **2013**, *52*, 9456-9469; (d) C.-M. Che, C. Ho, T.-C. Lau, *Journal of the Chemical Society, Dalton Transactions* **1991**, 1901-1907; (e) Y. Mulyana, G. Collins, R. Keene, *Journal of Inclusion Phenomena and Macrocyclic Chemistry* **2011**, *71*, 371-379; (f) D. J. Wasylenko, C. Ganesamoorthy, B. D. Koivisto, M. A. Henderson, C. P. Berlinguette, *Inorganic Chemistry* **2010**, *49*, 2202-2209; (g) T. P. Brewster, W. Ding, N. D. Schley, N. Hazari, V. S. Batista, R. H. Crabtree, *Inorganic Chemistry* **2011**, *50*, 11938-11946.

[2] (a) A. Levina, A. Mitra, P. A. Lay, *Metallomics* **2009**, *1*, 458-470; (b) G. S. Smith, B. Therrien, *Dalton Transactions* **2011**, *40*, 10793-10800; (c) B. S. Murray, M. V. Babak, C. G. Hartinger, P. J. Dyson, *Coordination Chemistry Reviews* **2016**, *306*, 86-114.

[3] (a) O. Saavedra-Díaz, R. Cerón-Camacho, S. Hernández, A. D. Ryabov, R. Le Lagadec, *European Journal of Inorganic Chemistry* **2008**, *2008*, 4866-4869; (b) D. A. Freedman, J. K. Evju, M. K. Pomije, K. R. Mann, *Inorganic Chemistry* **2001**, *40*, 5711-5715; (c) S. Betanzos-Lara, O. Novakova, R. J. Deeth, A. M. Pizarro, G. J. Clarkson, B. Liskova, V. Brabec, P. J. Sadler, A. Habtemariam, *Journal of Biological Inorganic Chemistry* **2012**, *17*, 1033-1051.